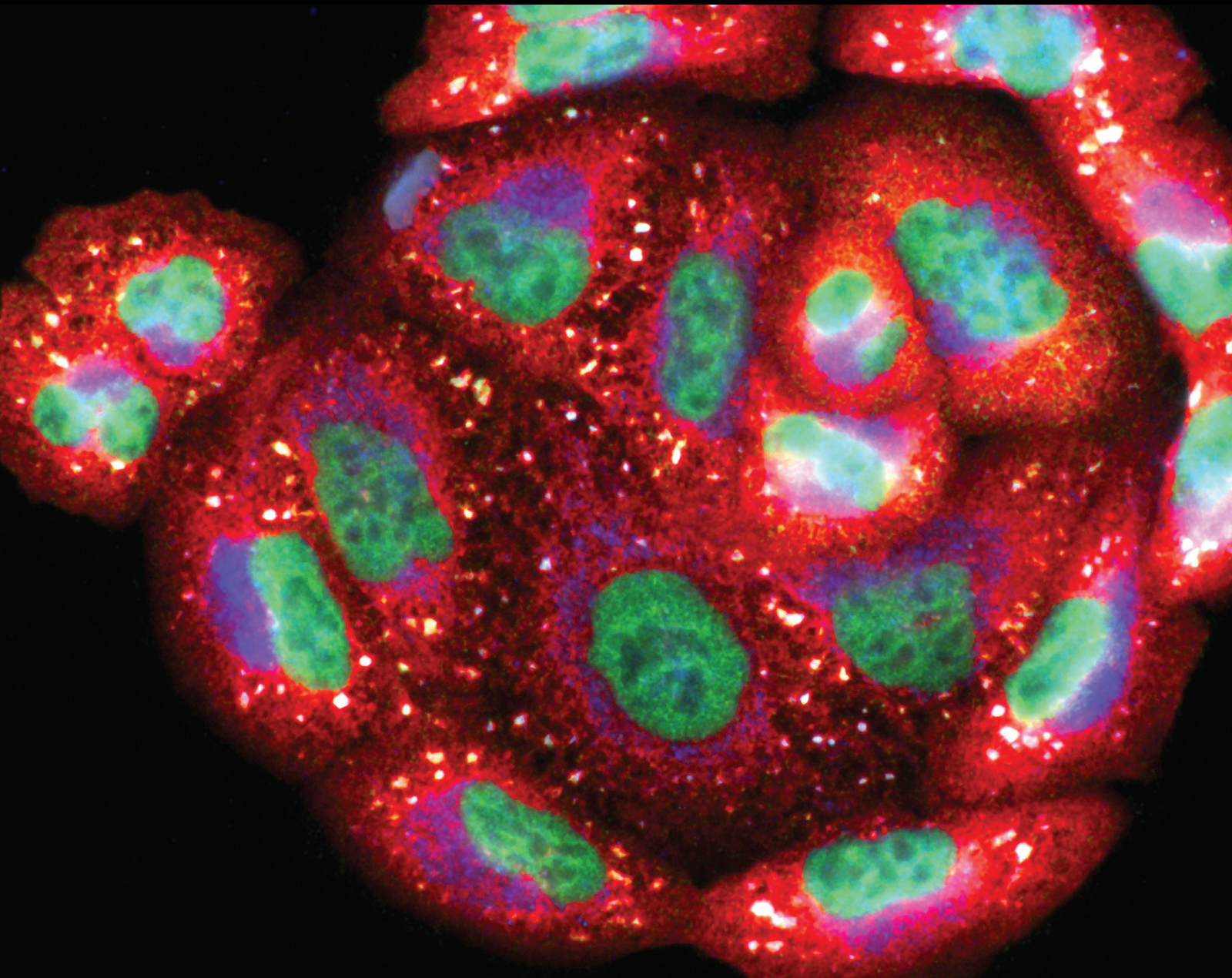


Oxidative Stress and Autoimmunity: Causes and Consequences

Lead Guest Editor: Ivan Srejovic

Guest Editors: Olga Pechanova, Chunying Li, and Miodrag Lukic





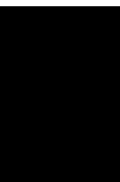
Oxidative Stress and Autoimmunity: Causes and Consequences

Oxidative Medicine and Cellular Longevity

Oxidative Stress and Autoimmunity: Causes and Consequences

Lead Guest Editor: Ivan Srejovic

Guest Editors: Olga Pechanova, Chunying Li, and
Miodrag Lukic



Copyright © 2022 Hindawi Limited. All rights reserved.

This is a special issue published in "Oxidative Medicine and Cellular Longevity" All articles are open access articles distributed under the Creative Commons Attribution License, which permits unrestricted use, distribution, and reproduction in any medium, provided the original work is properly cited.

Chief Editor

Jeannette Vasquez-Vivar, USA

Associate Editors

Amjad Islam Aqib, Pakistan
Angel Catalá , Argentina
Cinzia Domenicotti , Italy
Janusz Gebicki , Australia
Aldrin V. Gomes , USA
Vladimir Jakovljevic , Serbia
Thomas Kietzmann , Finland
Juan C. Mayo , Spain
Ryuichi Morishita , Japan
Claudia Penna , Italy
Sachchida Nand Rai , India
Paola Rizzo , Italy
Mithun Sinha , USA
Daniele Vergara , Italy
Victor M. Victor , Spain

Academic Editors

Ammar AL-Farga , Saudi Arabia
Mohd Adnan , Saudi Arabia
Ivanov Alexander , Russia
Fabio Altieri , Italy
Daniel Dias Rufino Arcanjo , Brazil
Peter Backx, Canada
Amira Badr , Egypt
Damian Bailey, United Kingdom
Rengasamy Balakrishnan , Republic of Korea
Jiaolin Bao, China
Ji C. Bihl , USA
Hareram Birla, India
Abdelhakim Bouyahya, Morocco
Ralf Braun , Austria
Laura Bravo , Spain
Matt Brody , USA
Amadou Camara , USA
Marcio Carcho , Portugal
Peter Celec , Slovakia
Giselle Cerchiaro , Brazil
Arpita Chatterjee , USA
Shao-Yu Chen , USA
Yujie Chen, China
Deepak Chhangani , USA
Ferdinando Chiaradonna , Italy

Zhao Zhong Chong, USA
Fabio Ciccarone, Italy
Alin Ciobica , Romania
Ana Cipak Gasparovic , Croatia
Giuseppe Cirillo , Italy
Maria R. Ciriolo , Italy
Massimo Collino , Italy
Manuela Corte-Real , Portugal
Manuela Curcio, Italy
Domenico D'Arca , Italy
Francesca Danesi , Italy
Claudio De Lucia , USA
Damião De Sousa , Brazil
Enrico Desideri, Italy
Francesca Diomede , Italy
Raul Dominguez-Perles, Spain
Joël R. Drevet , France
Grégory Durand , France
Alessandra Durazzo , Italy
Javier Egea , Spain
Pablo A. Evelson , Argentina
Mohd Farhan, USA
Ioannis G. Fatouros , Greece
Gianna Ferretti , Italy
Swaran J. S. Flora , India
Maurizio Forte , Italy
Teresa I. Fortoul, Mexico
Anna Fracassi , USA
Rodrigo Franco , USA
Juan Gambini , Spain
Gerardo García-Rivas , Mexico
Husam Ghanim, USA
Jayeeta Ghose , USA
Rajeshwary Ghosh , USA
Lucia Gimeno-Mallench, Spain
Anna M. Giudetti , Italy
Daniela Giustarini , Italy
José Rodrigo Godoy, USA
Saeid Golbidi , Canada
Guohua Gong , China
Tilman Grune, Germany
Solomon Habtemariam , United Kingdom
Eva-Maria Hanschmann , Germany
Md Saquib Hasnain , India
Md Hassan , India









Tim Hofer , Norway
John D. Horowitz, Australia
Silvana Hrelia , Italy
Dragan Hrnčić, Serbia
Zebo Huang , China
Zhao Huang , China
Tariq Hussain , Pakistan
Stephan Immenschuh , Germany
Norsharina Ismail, Malaysia
Franco J. L. , Brazil
Sedat Kacar , USA
Andleeb Khan , Saudi Arabia
Kum Kum Khanna, Australia
Neelam Khaper , Canada
Ramoji Kosuru , USA
Demetrios Kouretas , Greece
Andrey V. Kozlov , Austria
Chan-Yen Kuo, Taiwan
Gaocai Li , China
Guoping Li , USA
Jin-Long Li , China
Qiangqiang Li , China
Xin-Feng Li , China
Jialiang Liang , China
Adam Lightfoot, United Kingdom
Christopher Horst Lillig , Germany
Paloma B. Liton , USA
Ana Lloret , Spain
Lorenzo Loffredo , Italy
Camilo López-Alarcón , Chile
Daniel Lopez-Malo , Spain
Massimo Lucarini , Italy
Hai-Chun Ma, China
Nageswara Madamanchi , USA
Kenneth Maiese , USA
Marco Malaguti , Italy
Steven McAnulty, USA
Antonio Desmond McCarthy , Argentina
Sonia Medina-Escudero , Spain
Pedro Mena , Italy
V́ctor M. Mendoza-Núñez , Mexico
Lidija Milkovic , Croatia
Alexandra Miller, USA
Sara Missaglia , Italy

Premysl Mladenka , Czech Republic
Sandra Moreno , Italy
Trevor A. Mori , Australia
Fabiana Morroni , Italy
Ange Mouithys-Mickalad, Belgium
Iordanis Mourouzis , Greece
Ryoji Nagai , Japan
Amit Kumar Nayak , India
Abderrahim Nemmar , United Arab Emirates
Xing Niu , China
Cristina Nocella, Italy
Susana Novella , Spain
Hassan Obied , Australia
Pál Pacher, USA
Pasquale Pagliaro , Italy
Dilipkumar Pal , India
Valentina Pallottini , Italy
Swapnil Pandey , USA
Mayur Parmar , USA
Vassilis Paschalis , Greece
Keshav Raj Paudel, Australia
Ilaria Peluso , Italy
Tiziana Persichini , Italy
Shazib Pervaiz , Singapore
Abdul Rehman Phull, Republic of Korea
Vincent Pialoux , France
Alessandro Poggi , Italy
Zsolt Radak , Hungary
Dario C. Ramirez , Argentina
Erika Ramos-Tovar , Mexico
Sid D. Ray , USA
Muneeb Rehman , Saudi Arabia
Hamid Reza Rezvani , France
Alessandra Ricelli, Italy
Francisco J. Romero , Spain
Joan Roselló-Catafau, Spain
Subhadeep Roy , India
Josep V. Rubert , The Netherlands
Sumbal Saba , Brazil
Kunihiro Sakuma, Japan
Gabriele Saretzki , United Kingdom
Luciano Saso , Italy
Nadja Schroder , Brazil













Anwen Shao , China
Iman Sherif, Egypt
Salah A Sheweita, Saudi Arabia
Xiaolei Shi, China
Manjari Singh, India
Giulia Sita , Italy
Ramachandran Srinivasan , India
Adrian Sturza , Romania
Kuo-hui Su , United Kingdom
Eisa Tahmasbpour Marzouni , Iran
Hailiang Tang, China
Carla Tatone , Italy
Shane Thomas , Australia
Carlo Gabriele Tocchetti , Italy
Angela Trovato Salinaro, Italy
Rosa Tundis , Italy
Kai Wang , China
Min-qi Wang , China
Natalie Ward , Australia
Grzegorz Wegrzyn, Poland
Philip Wenzel , Germany
Guangzhen Wu , China
Jianbo Xiao , Spain
Qiongming Xu , China
Liang-Jun Yan , USA
Guillermo Zalba , Spain
Jia Zhang , China
Junmin Zhang , China
Junli Zhao , USA
Chen-he Zhou , China
Yong Zhou , China
Mario Zoratti , Italy

Contents

Psoriasis between Autoimmunity and Oxidative Stress: Changes Induced by Different Therapeutic Approaches

Marija V. Medovic , Vladimir Lj. Jakovljevic , Vladimir I. Zivkovic , Nevena S. Jeremic , Jovana N. Jeremic , Sergey B. Bolevich , Ana B. Ravic Nikolic , Vesna M. Milicic , and Ivan M. Srejavic 
Review Article (17 pages), Article ID 2249834, Volume 2022 (2022)



Melissa officinalis L. Supplementation Provides Cardioprotection in a Rat Model of Experimental Autoimmune Myocarditis

Nevena D. Draginic , Vladimir L. Jakovljevic , Jovana N. Jeremic , Ivan M. Srejavic , Marijana M. Andjic , Marina R. Rankovic, Jasmina Z. Sretenovic , Vladimir I. Zivkovic , Biljana T. Ljubic , Slobodanka L. Mitrovic , Stefani S. Bolevich , Sergey B. Bolevich , and Isidora M. Milosavljevic 
Research Article (12 pages), Article ID 1344946, Volume 2022 (2022)



The Attenuation of Chronic Ulcerative Colitis by (R)-salbutamol in Repeated DSS-Induced Mice

Liangjun Deng , Haihua Guo, Shanping Wang , Xiaoming Liu, Yue Lin, Rui Zhang, and Wen Tan 
Research Article (20 pages), Article ID 9318721, Volume 2022 (2022)




GPX4-Regulated Ferroptosis Mediates S100-Induced Experimental Autoimmune Hepatitis Associated with the Nrf2/HO-1 Signaling Pathway

Lujian Zhu, Dazhi Chen, Yin Zhu, Tongtong Pan, Dingchao Xia, Tingchen Cai, Hongwei Lin, Jing Lin, Xiaozhi Jin, Faling Wu, Sijie Yu, Kailu Zhu, Lanman Xu , and Yongping Chen 
Research Article (16 pages), Article ID 6551069, Volume 2021 (2021)




Hydrogen-Rich Water Ameliorates Murine Chronic Graft-versus-Host Disease through Antioxidation

Liren Qian , Jiaxin Liu, Weina Ma, Yu Liu, Xiaona Wang, and Daihong Liu 
Research Article (8 pages), Article ID 1165928, Volume 2021 (2021)

The Efficacy of Antioxidative Stress Therapy on Oxidative Stress Levels in Rheumatoid Arthritis: A Systematic Review and Meta-analysis of Randomized Controlled Trials

Liuting Zeng , Ganpeng Yu , Kailin Yang , Jun Li, Wensa Hao, and Hua Chen 
Research Article (30 pages), Article ID 3302886, Volume 2021 (2021)

YAP-Dependent Induction of CD47-Enriched Extracellular Vesicles Inhibits Dendritic Cell Activation and Ameliorates Hepatic Ischemia-Reperfusion Injury

Zenan Yuan, Linsen Ye, Xiao Feng, Tian Zhou, Yi Zhou, Shuguang Zhu, Changchang Jia, Haibo Li, Dongbo Qiu, Kun Li, Wei Liu, Yang Li, Hui Tang, Guoying Wang, Qi Zhang, Yang Yang , Guihua Chen , and Hua Li 
Research Article (15 pages), Article ID 6617345, Volume 2021 (2021)

Review Article

Psoriasis between Autoimmunity and Oxidative Stress: Changes Induced by Different Therapeutic Approaches

Marija V. Medovic ^{1,2} **Vladimir Lj. Jakovljevic** ^{3,4} **Vladimir I. Zivkovic** ³
Nevena S. Jeremic ⁵ **Jovana N. Jeremic** ⁵ **Sergey B. Bolevich** ⁴
Ana B. Ravic Nikolic ^{1,2} **Vesna M. Milicic** ^{1,2} and **Ivan M. Srejsovic** ³

¹Department of Dermatovenerology, University of Kragujevac, Faculty of Medical Sciences, Svetozara Markovica 69, 34000 Kragujevac, Serbia

²University Clinical Center Kragujevac, Zmaj Jovina 30, 34000 Kragujevac, Serbia

³Department of Physiology, University of Kragujevac, Faculty of Medical Sciences, Svetozara Markovica 69, 34000 Kragujevac, Serbia

⁴I.M. Sechenov First Moscow State Medical University, Department of Human Pathophysiology, Moscow, Russian Federation, Trubetskaya Str. 2, 119992 Moscow, Russia

⁵Department of Pharmacy, University of Kragujevac, Faculty of Medical Sciences, Svetozara Markovica 69, 34000 Kragujevac, Serbia

Correspondence should be addressed to Vladimir Lj. Jakovljevic; drvladakbg@yahoo.com

Received 22 October 2021; Accepted 15 February 2022; Published 11 March 2022

Academic Editor: Dragan Hrnčić

Copyright © 2022 Marija V. Medovic et al. This is an open access article distributed under the Creative Commons Attribution License, which permits unrestricted use, distribution, and reproduction in any medium, provided the original work is properly cited.

Psoriasis is defined as chronic, immune-mediated disease. Regardless of the development of new therapeutic approaches, the precise etiology of psoriasis remains unknown and speculative. The aim of this review was to systematize the results of previous research on the role of oxidative stress and aberrant immune response in the pathogenesis of psoriasis, as well as the impact of certain therapeutic modalities on the oxidative status in patients with psoriasis. Complex immune pathways of both the innate and adaptive immune systems appear to be major pathomechanisms in the development of psoriasis. Oxidative stress represents another important contributor to the pathophysiology of disease, and the redox imbalance in psoriasis has been reported in skin cells and, systemically, in plasma and blood cells, and more recently, also in saliva. Current immune model of psoriasis begins with activation of immune system in susceptible person by some environmental factor and loss of immune tolerance to psoriasis autoantigens. Increased production of IL-17 appears to be the most prominent role in psoriasis pathogenesis, while IL-23 is recognized as master regulator in psoriasis having a specific role in cross bridging the production of IL-17 by innate and acquired immunity. Other proinflammatory cytokines, including IFN- γ , TNF- α , IL-1 β , IL-6, IL-22, IL-26, IL-29, or IL-36, have also been reported to play important roles in the development of psoriasis. Oxidative stress can promote inflammation through several signaling pathways. The most noticeable and most powerful antioxidative effects exert various biologics compared to more convenient therapeutic modalities, such as methotrexate or phototherapy. The complex interaction of redox, immune, and inflammatory signaling pathways should be focused on further researches tackling the pathophysiology of psoriasis, while antioxidative supplementation could be the solution in some refractory cases of the disease.

1. Introduction

Psoriasis was firstly described in detail by Robert Willan, founder of dermatology as a medical specialty [1]. The prevalence of psoriasis varies from 0.51% to 11.43% in adults,

making psoriasis one of the most important global health problems [2]. According to the World Health Organization, psoriasis is classified as one of the most serious noninfectious diseases, due to complications that develop during the course of the disease and affection of multiple organ

systems [3, 4]. Psoriasis is defined as chronic, inflammatory, recurrent, incurable, and noncontagious disease, characterized by sharply demarcated erythematous skin lesions with overlying silver hyperkeratotic plaques, accompanied by systemic manifestations [3].

1.1. Clinical Presentation of Psoriasis. The most distinctive characteristic of psoriasis are well-defined, symmetric, raised skin lesions most commonly located on the knees, elbows, scalp, and trunk [5]. Such clinical presentation is a characteristic for plaque psoriasis or psoriasis vulgaris, the most common form of psoriasis, but psoriasis also may appear as guttate, pustular (von Zumbusch psoriasis) or erythrodermic psoriasis (Figure 1). Skin changes are usually accompanied by pruritus, itching, pain, cracking, bleeding, and flaking of the skin. Furthermore, psoriasis is recognized as a risk factor for many pathological conditions, including cardiovascular diseases, gastrointestinal disorders, malignant tumors, infections, and mood disorders [6]. The most common comorbidity of psoriasis is psoriatic arthritis, usually defined as heterogeneous inflammatory arthritis which affects joints and enthesal tissues [7]. Such interconnection of psoriasis and the variety of comorbidities probably arises from, on the one hand, complex etiological and pathophysiological basis of the disease, and on the other hand, the fact that psoriasis remains unrecognized and untreated for a long period [8, 9].

Psoriasis vulgaris is generally equally present among the sexes, but it develops somewhat earlier in women than in men [3]. The severity of psoriasis is usually classified using Psoriasis Area and Severity Index (PASI) and Body Surface Area (BSA) [10]. Due to the common association of psoriasis and psoriatic arthritis, several screening questionnaires are performed for early recognition of psoriatic arthritis, such as Psoriasis and Arthritis Screening Questionnaire (PASQ), Psoriasis Epidemiology Screening Tool (PEST), and Toronto Psoriatic Arthritis Screen (ToPAS) [11].

1.2. Main Pathophysiological Features of Psoriasis. Psoriasis is defined as chronic, immune-mediated disease. Regardless of the development of new therapeutic approaches, the precise etiology of psoriasis remains unknown and speculative. Complex immune pathways of both the innate and adaptive immune systems appear to be pathophysiological basis in the development of psoriasis [12, 13]. Furthermore, epidemiological investigations indicated the importance of genetic component in the development of psoriasis [14]. Firstly, it was noticed that psoriasis concordance is higher in monozygotic twins [15]. Recent genetic studies identified almost 60 psoriasis susceptibility loci which could interfere with the development of psoriasis [14]. Various environmental factors, such as stress, mechanical trauma, and streptococcal infections are considered to trigger and not cause the disease. In predisposed persons, various factors may provoke the onset of disease or exacerbation of existing symptoms.

Due to the complex pathophysiological mechanisms that affect various tissues and organs, psoriasis may be defined as a systemic disorder with the predominant skin representation. Cutaneous psoriatic manifestations occur as a result

of disruption of skin homeostasis due to immune-mediated aberrant differentiation of keratinocytes [12]. Interleukin-(IL-) 23 and IL-17 are recognized as key immune mediators that mediate not only the development of skin lesions but also the occurrence of psoriasis-associated comorbidities [3]. Skin lesions, followed by extracutaneous comorbidities and chronic course of the disease, significantly affect the quality of life of the psoriasis-suffering patients resulting in the development of anxiety and depression [16].

Psoriasis is a chronic, incurable disease, so treatment of psoriasis can reduce skin lesions, but not provide a complete cure. The psoriatic therapy varies depending on the surface of affected skin—PASI [17]. The most effective therapeutics in psoriasis treatment are biologic therapies, recently developed drugs that target some immune pathway. Drugs from this group act in different ways and target diverse cytokines: tumor necrosis factor α (TNF- α) (adalimumab, certolizumab pegol, etanercept, and infliximab), IL-12/IL-23p40 (ustekinumab), IL-17A (ixekizumab, secukinumab), IL-17 receptor (brodalumab), and IL-23p19 (guselkumab, risankizumab, and tildrakizumab) [18] (Table 1). Biologics are usually used in severe cases of psoriasis. Mild disease is treated with topical preparations combined with phototherapy, and moderate psoriasis is treated with immunomodulatory therapy.

Reactive oxygen species (ROS) represent important regulators of immune response [19]. The imbalance in production and elimination of ROS results in oxidative stress and, consequently, oxidative damage of various cellular structures. Proinflammatory processes involved in the development of autoimmune disorders are combined with increased production of ROS and oxidative stress. Redox imbalance in psoriasis exists both in skin cells and, systemically, in plasma and blood cells [20]. Thus, ROS and oxidative stress appear to be an important step in the psoriasis pathophysiological cascade. The aim of this review is to show the relationship between redox balance and applied therapy in patients suffering from psoriasis.

1.3. Autoimmune Nature of Psoriasis. The main feature of autoimmune disorders is destruction of healthy tissues by the host immune system upon misidentification and recognition of its own tissue structures as foreign. The results of the immunological studies in the recent decades showed involvement of both innate and acquired immunity and importance of T cells in pathogenesis of psoriasis [21–23]. T helper (Th) cells are classified as Th1 cells, which predominantly secrete TNF- α , interferon- (IFN-) γ , and IL-2, and Th2 cells, which secrete IL-4, IL-5, IL-10, and IL-13 [24]. Determination of naïve T cells toward Th1 or Th2 subpopulation depends on the stimulation by IL-12, which mediates Th1 differentiation, or IL-2, which mediates Th2 differentiation [25]. Due to increased levels of TNF- α and IL-12 in psoriatic lesions, psoriasis is defined as Th1-mediated disease [26]. IL-23 is another important cytokine in the development of psoriasis because it shifts the differentiation of naïve T cells toward proinflammatory Th17 cells [27]. These findings are the backbone of the development of new therapeutic approaches such as biologic therapies. Apart from T cells, as



FIGURE 1: Continued.

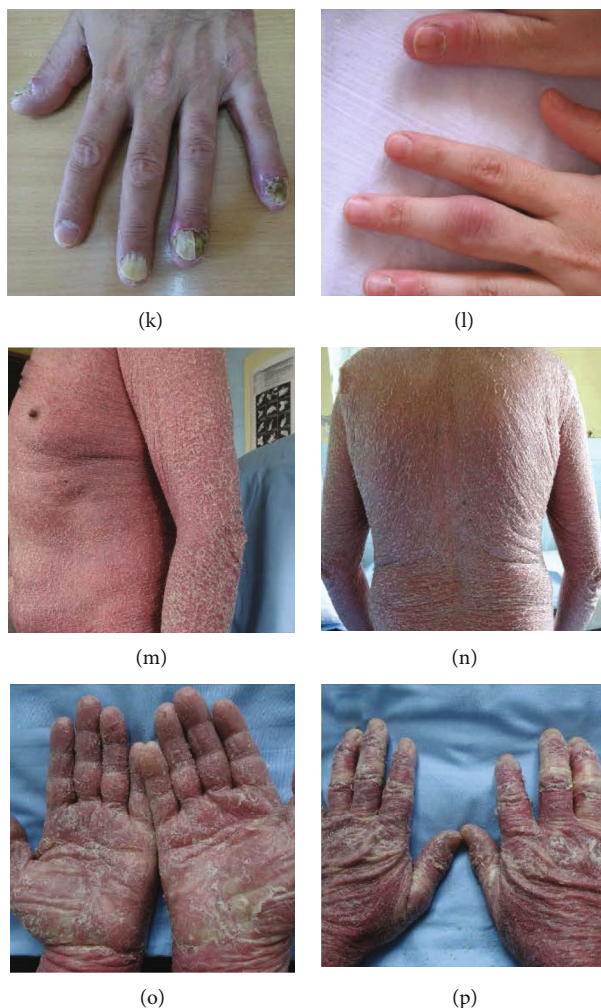


FIGURE 1: Clinical manifestations of psoriasis. Psoriasis vulgaris manifested through typical erythematous plaques with silvery scales of various sizes from guttate lesions through nummular to giant lumbar plaque (a). Psoriasis vulgaris and guttate psoriasis (b, d). Generalized psoriasis (c, h, i). Inverse psoriasis (g). Psoriatic lesions on the feet and hands (e, f, j, k), including psoriatic nail dystrophy (f, k) and psoriatic arthritis (l). Erythrodermic psoriasis, erythema, and squamous cover 90% of the skin (m, n, o, p). Pictures presented are part of the private collection of Vesna M. Milicic and Ana B. Ravic Nikolic.

TABLE 1: Biologics in psoriasis treatment.

Name of the drug	Biological target
Ustekinumab	IL-12 and IL-23—p40 subunit
Guselkumab	
Tildrakizumab	IL-23—p19 subunit
Risankizumab	
Secukinumab	
Ixekizumab	IL-17
Bimekizumab	
Brodalumab	IL-17 receptor
Etanercept	
Infliximab	
Adalimumab	TNF- α
Certolizumab pegol	
Golimumab	

representatives of acquired immunity, neutrophils, dendritic antigen presenting cells (APCs), and Natural Killer T (NKT) cells in pathogenesis of psoriasis play an important role [28]. One of the first described histopathological hallmarks of psoriasis was Munro's microabscesses containing neutrophils [29]. Increased neutrophil activity in psoriatic plaques results in increased ROS production [30] (Figure 2, Table 2). ROS act as stimulators of dendritic APCs to present antigens to T cells, which further stimulate proliferation of keratinocytes [29]. ROS also have a role of second messengers in inflammatory signaling cascades involving activation of mitogen-activated protein kinase (MAPK), nuclear factor-kappa B (NF- κ B). NKT cells encompass heterologous cells which share some features of the natural killer (NK) and T cells. In psoriatic patients, NKT cells interact with other components of immune system, thereby supporting the creation of proinflammatory environment. Subset of NKT cells, NKT17 cells, can produce IL-17, and they are found in many tissues, among others in the skin, but their

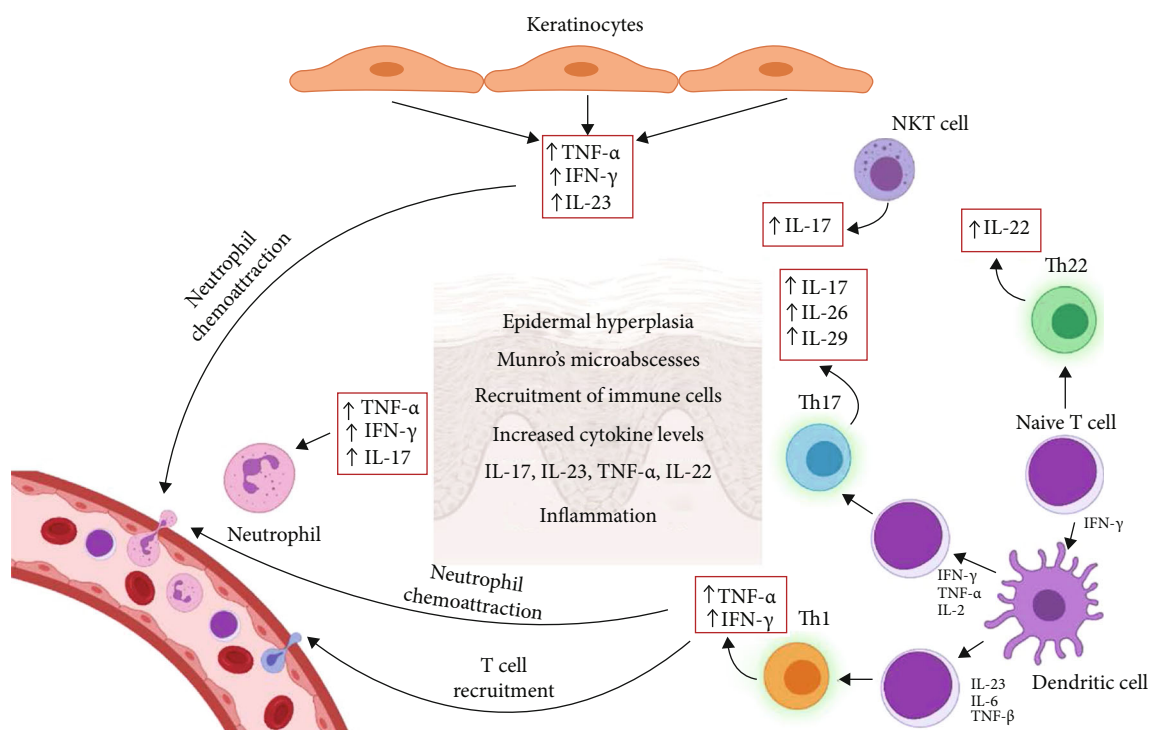


FIGURE 2: Immune response in psoriasis. Complex interaction of various parts of innate (dendritic cells, NKT cells, and neutrophils) and acquired immunity (T cells) in pathophysiology of psoriasis. IFN: interferon; IL: interleukin; NKT: natural killer T; Th: T-helper cell; TGF: transforming growth factor; TNF: tumour necrosis factor.

TABLE 2: Main articles included in the summary of signaling cascades shown in Figure 2.

Article	Main findings
Marble et al. <i>J Dermatol Sci.</i> 2007; 48(2):87-101. [26]	CD11c + dendritic cells, CD68+ macrophages and TNF- α + cells are increased in psoriatic lesions
Ten Bergen et al. <i>Scand J Immunol.</i> 2020; 92(4):e12946. [27]	TNF- α /IL-23/IL-17 axis appears to have central role in the pathophysiology of psoriasis
Bos et al. <i>Br J Dermatol.</i> 2005; 152(6):1098-107. [28]	Activation of innate immunity, represented by the activity of NKT cells, dendritic cells, neutrophils, and keratinocytes, is crucial in pathogenesis of psoriasis.
Chiang et al. <i>Front Immunol.</i> 2019; 10:2376. [29]	The abundant presence of neutrophils in the psoriatic skin lesions and formation of Munro's microabscesses serves as a typical histopathologic hallmark of psoriasis.
Kim and Krueger. <i>Dermatol Clin.</i> 2015; 33(1):13-23. [13]	Keratinocytes appear to be important regulators of immune responses, involved in increased production of TNF- α or IFN- γ in psoriasis.
Hawkes et al. <i>J Immunol.</i> 2018; 201(6):1605-1613. [34]	Psoriasis is characterized by the presence of multiple T lymphocyte subsets (Th1, Th17, and Th22).
Stephen-Victor et al. <i>PLoS Pathog.</i> 2016; 12(6):e1005624 [37]	Th17 cells, besides IL-17, produce TNF- α , IL-26, and IL-29, which further stimulate release of proinflammatory mediators.
Wang et al. <i>J Cell Mol Med.</i> 2019; 23(12):7926-7932. [38]	
Levin and Gottlieb. <i>J Am Acad Dermatol.</i> 2014; 70(3):555-61. [46]	IL-23 is recognized as a key regulator in psoriasis due to specific role in cross bridging the production of IL-17 by innate and acquired immunity.
Langrish et al. <i>Immunol Rev.</i> 2004; 202:96-105. [47]	

role in the pathogenesis of psoriasis is not fully understood [31, 32].

Keratinocytes play an important role in physiological orchestration of innate and acquired immune responses in the skin due to various pathological stimuli. Injured keratinocytes may produce TNF- α and IFN- γ [13]. TNF- α induces increased neutrophil accumulation in injured skin, and IFN- γ increases recruitment of Th1 cells. Psoriatic plaques contain increased number of T lymphocytes which produce IFN- γ , IL-17, and IL-22, labeled as Th1, Th17, and Th22 cells, respectively [13].

Dendritic APCs may have a crucial role in pathogenesis of psoriasis due to the activation of T cells and production of various proinflammatory cytokines. Population of skin dendritic cells include epidermal dendritic cells (Langerhans cells) and dermal dendritic cells (myeloid and plasmacytoid dendritic cells). CD11c is recognized as the correct marker of myeloid dendritic cells, while blood dendritic cell antigen (BDCA) is used for identification of different human subsets of dendritic cells [33]. Myeloid CD11c⁺BDCA-1⁻ dermal dendritic cells are recognized as proinflammatory dendritic cells which induce activation and clonal expansion of CD4⁺ and CD8⁺ T cells and their stimulation in the production of IFN- γ , IL-17, and IL-22 [34]. Furthermore, it was shown that content of CD11c⁺BDCA-1⁻ dermal dendritic cells is increased in psoriatic lesion, but their number is significantly reduced upon effective therapeutic approach [35].

The current immune model of psoriasis begins with the activation of immune system in susceptible persons by some environmental factor and a loss of immune tolerance to psoriasis autoantigens [34]. TNF- α and IFN- γ , secreted by dendritic cells, induce polarization and expansion of IL-17 and IL-22 secreting T cells (Th17 and Th22 cells), resulting in significant increase of the IL-17 and IL-22 production (Figure 2, Table 2). IL-17 is recognized as the key cytokine in the development of psoriasis. There are six isoforms of IL-17 (IL-17A–IL-17F), whereby IL-17A has the most prominent role in psoriasis pathogenesis [36]. Th17 cells, besides IL-17, produce TNF- α , IL-26, and IL-29. IL-17A, alone or synergistically with TNF- α , induces the release of proinflammatory molecules from keratinocytes and enhances aberrant proliferation of keratinocytes leading to epidermal hyperplasia. Increased production of IL-26 and IL-29 by Th17 stimulate further release of proinflammatory mediators which recruit Th1 cells into psoriatic skin lesions [37, 38]. Increased production of IL-17 results in increased secretion of IL-19, IL-22, and IL-36 which also contribute to the development of epidermal hyperplasia [39, 40]. IL-22 in psoriatic lesions is secreted not only by CD4⁺ and CD8⁺ T cells known as Th22 and Tc22 cells but also by Th17, mast cells, and others [41]. IL-22 enhances migration of keratinocytes, increases epidermal thickness, decreases keratinocyte differentiation, and stimulates secretion of various molecules which act as chemokines, neutrophil chemoattractants [41]. IL-22 proinflammatory action is weaker than IL-17, but IL-22 mainly acts synergistically with IL-17 and TNF- α . Dendritic cells also secrete IL-23 which acts via the IL-23 receptor located on naïve T cells and promotes their differentiation into Th17 [42]. IL-23 belongs to the IL-12 cyto-

kine family. It is a composite cytokine containing two subunits IL-23p19 and IL-12p40 [43]. Acting together with TNF- α , IL-1 β , and IL-6, IL-23 stimulates the differentiation of Th17 and Tc17 cells and the conversion of regulatory T cells (T_{reg}) into Th17 cells [44]. After the differentiation of naïve T cells to Th17 cells due to various stimuli such as transforming growth factor (TGF)- β and IL-6, the presence of IL-23 is necessary to maintain the Th17 phenotype [25, 45]. Binding of IL-23 to its receptor on Th17 cells initiates signaling pathway, which results in the facilitation of IL-17 expression and increased levels of IL-17A in plasma [46]. Besides the action of IL-23 on T cells and induction of them to produce IL-17, thus provoking the inflammatory autoimmune response (acquired immunity), it can also stimulate the production of IL-17 by NK cells and neutrophils (innate immunity) [47, 48]. Thus, IL-23 is recognized as a master regulator in psoriasis having a specific role in cross bridging the production of IL-17 by innate and acquired immunity. The administration of IL-23 in mice induced epidermal hyperplasia and increased expression of both IL-17A and IL-22 [49]. Psoriasis is defined as Th17-mediated disease, but results of a growing number of studies indicate the central role of IL-23 in the development of psoriasis due to its effects on sustention of cytotoxic Th17 cells and production of IL-17 and IL-22 (Figure 2, Table 2). Altogether, various parts of acquired and innate immune system create complex signaling pathways in the development of psoriasis.

1.4. Oxidative Stress in Pathogenesis of Psoriasis. Oxidative stress is usually defined as an imbalance between the production of ROS or reactive nitrogen species (RNS) and antioxidative capacity. Decreased antioxidative ability may be the consequence of decreased activity of antioxidative enzymes (such as superoxide dismutase (SOD), catalase (CAT), and glutathione peroxidase (GPx)) or/and decreased concentration of scavenging antioxidants, both endogenous (reduced glutathione (GSH)) and exogenous (vitamin C, vitamin E, carotenoids, and others). At low, physiological concentrations, ROS/RNS have important roles as signaling molecules in regulatory cascades of different biological processes, but excess ROS/RNS and consequent oxidative stress induce oxidation of various cellular structures (DNA, lipids, and proteins) leading to cell death [50, 51].

The skin and thus keratinocytes are continuously exposed to various external stressful stimuli, including ultraviolet (UV) radiation of the sun, and oxygen from the air. It is assumed that more than 50% of skin damage induced by UV radiation is mediated by ROS/RNS [52]. Furthermore, different toxic substances, as well as their metabolites, directly or indirectly initiate the production of various prooxidative molecules in keratinocytes [53]. Oxidative stress can promote inflammation through several signaling pathways including NF- κ B, mitogen-activated protein kinases (MAPKs), and STAT3 (Signal Transducer and Activator of Transcription 3) [54]. MAPKs represent a family of serine-threonine protein kinases encompassing several members: extracellular signal-regulated kinases (ERKs), c-Jun N-terminal kinases (JNKs), and the p38 MAPKs [55]. Increased presence of ROS and impaired antioxidative

potential directly induce increased activation of NF- κ B [56]. Immunohistochemical analysis of psoriatic skin lesions showed increased levels of phosphorylated ERK1/2 and p38 MAPK [57, 58]. It was shown that propranolol induced psoriasis-like skin inflammation through increase of oxidative stress as well as NF- κ B and MAPK p38 activation and subsequent secretion of IL-23 [59]. Results of this research confirmed the crucial role of oxidative stress in IL-23/IL-17 axis of Th17-related psoriasis-like skin inflammation (Figure 3, Table 3). ROS produced in the skin also act as chemoattractant for neutrophils and, furthermore, increased number of neutrophils combined with high levels of ROS may result in the activation of neutrophils and further increase of ROS production [60, 61]. Augmented inflammatory response further facilitates production of ROS and decreases already weakened antioxidative capacity which makes psoriasis a chronic inflammatory disease [62].

The nuclear factor erythroid 2-related factor 2 (Nrf2) is redox-sensitive transcription factor involved in the regulation of keratinocyte proliferation and expression of keratin [63]. There are ambiguous data regarding the role of Nrf2 in pathogenesis of psoriasis. Lee et al. pointed out increased oxidative damage in psoriatic skin lesions combined with decreased expression of Nrf2, while dimethyl fumarate, as an Nrf2 activator, upregulated Nrf2 levels in HaCaT keratinocyte cell line and promoted growth inhibition and apoptosis [64]. The authors assumed that the increased production of ROS and oxidative stress interfere with dysregulation of the Nrf2 signaling cascade. Another study also showed a decrease of ROS and increase of nuclear accumulation of Nrf2 after the application of antioxidant, followed by the reduction of vascular endothelial growth factor (VEGF) and the reduction of keratinocyte proliferation in a similar experimental model [65]. On the other hand, Yang et al. presented increased nuclear-localized Nrf2 in psoriatic epidermis compared to normal skin [63]. Increased expression of Nrf2 was linked with higher expression of psoriasis-related keratins K6, K16, and K17. Furthermore, it was shown that IL-17 and IL-22 enhance the proliferation of psoriasis-related keratins via Nrf2 signaling. It appears that redox signaling and Nrf2 poses divergent functions in the development of psoriasis, probably due to the cellular localization of Nrf2; however, many questions are to be answered further.

Several studies indicated an increased risk for the psoriasis occurrence in persons with polymorphisms of specific genes that are related to the regulation of redox balance (Figure 3, Table 3). Asefi et al. indicated an increased risk for the development of psoriasis in persons bearing 55M allele for paraoxonase 1 (PON1) [66]. PON1 is hydrolytic enzyme bound to high-density lipoprotein (HDL), able to break down lipid peroxides. It is assumed that enzymatic activity of PON1 is crucial for protective effect of HDL. The PON1 55M allele in psoriatic patients was found to be associated with higher malondialdehyde (MDA) levels, apolipoprotein B, and lipoprotein (a), suggesting interference of oxidative stress and disturbances in lipid metabolism in the pathogenesis of psoriasis [66]. Another study also revealed lower PON1 activity in psoriasis-suffering patients due to

PON1 polymorphism related to decreased antioxidative activity and different lipid levels [67]. Glutathione S-transferases (GSTs) are a group of enzymes involved in catalytic regulation of the conjugation of GSH to various substrates, thus providing protection against various detrimental factors including oxidative stress and inflammation. Some polymorphisms of GST genes were significantly more common in patients with psoriasis compared to the healthy population [68]. Furthermore, null polymorphisms for GSTs were related to increased sensitivity psoralen-ultraviolet A (PUVA) photochemotherapy [69]. The activity of SOD also appears to be an important factor in the development of psoriasis. Knock out (KO) of extracellular SOD in mice induced more intense IL-23-mediated skin inflammation characterized with elevated accumulation of CD4⁺ T cells, CD11b⁺ macrophages, and CD11c⁺ dendritic cells accompanied by increased expression of proinflammatory cytokines [70]. Naïve CD4⁺ T cells were more differentiated into the Th17 cell in extracellular SOD KO mice compared to the wild type (WT) controls. The previous study showed decreased activity of SOD and CAT in erythrocytes of psoriatic patients [71]. Levels of MDA were higher in these patients, combined with decreased activity of antioxidative enzymes. An interplay between various components of the immune system, ROS/RNS, and antioxidative system creates intertwined signaling pathways.

Analyzing the differences in various pro- and antioxidants in stimulated and unstimulated saliva of psoriatic patients and healthy individuals, it was shown that several prooxidative markers were increased in patients with plaque psoriasis [72]. Contrary to the previous study [71], antioxidative enzymes were significantly higher not only in saliva but also in erythrocytes, of psoriatic patients compared to healthy control [72]. The same authors also showed significantly higher levels of TNF- α , IFN- γ , and IL-2, nitric oxide (NO), and nitrotyrosine in saliva of psoriatic patients compared to healthy individuals [73]. Furthermore, it was shown that various inflammation-related proteins and microbiota were changed in saliva of psoriatic patients [74, 75]. Thus, oxidative stress biomarkers, such as total oxidative status or oxidative stress index, as well as inflammatory markers could be considered as diagnostic tool in psoriasis.

1.5. Therapeutic Approaches in Psoriasis. Various treatments have been used for psoriasis patients, from topical medications that contain corticosteroids, retinoid derivatives, synthetic vitamin D3 analogues, tar, or anthralin to systemic drugs with a different mechanism of action. However, all therapeutic modalities have transient curative effects, and it is also difficult to predict the occurrence of exacerbations and determine which drug delays their occurrence most effectively. Most of the therapeutics used in psoriasis curation are not suitable for a long-term use due to serious side effects and high costs [54]. Until recently, drugs such as methotrexate, acitretin, cyclosporine, dexamethasone, and salicylic acid were most commonly used in psoriasis treatment. Many of these drugs have limited clinical efficacy due to different shortcomings including low absorption capacity, inconsistent drug release, low target tissue

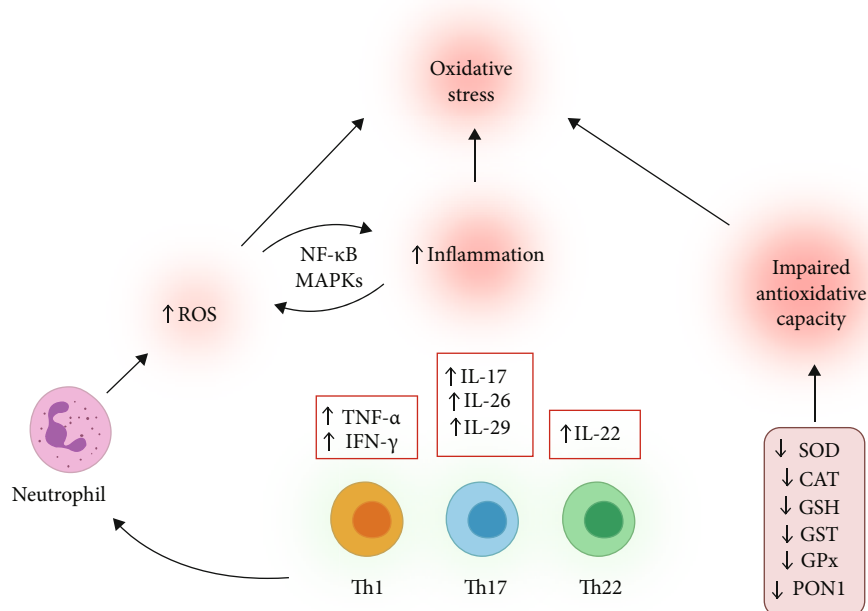


FIGURE 3: Mechanisms involved in increasing oxidative stress in psoriasis and interactions between oxidative stress and inflammation. IFN: interferon; IL: interleukin; MAPKs: mitogen-activated protein kinases, NF- κ B: nuclear factor kappa B; ROS: reactive oxygen species; Th: T-helper cell; TNF: tumour necrosis factor.

TABLE 3: Papers included in the summary of signaling cascades shown in Figure 3.

Article	Main findings
Lai et al. Redox Rep. 2018; 23(1):130-135. [54]	ROS induces proliferation and differentiation of Th17/Th1/Th22 cells.
Johansen et al. Br J Dermatol. 2005; 152(1):37-42. [57]	Activity of the MAPKs and ERK1/2 is increased in psoriatic skin.
Müller et al. Autophagy. 2020; 16(8):1380-1395. [59]	ROS are important mediators in IL23A secretion via NF- κ B and MAPK pathways.
Zhou et al. Free Radic Biol Med. 2009; 47(7):891-905. [62]	Increased inflammation facilitates production of ROS and decreases already weakened antioxidative capacity
Srivastava et al. Indian J Dermatol Venereol Leprol. 2018; 84(1):39-44. [68]	Polymorphisms in the GST genes may result in increased production of ROS that could influence the pathogenesis of psoriasis.
Lee et al. J Invest Dermatol. 2013; 133(3):732-741. [70]	SOD deficiency resulted in more severe IL-23-mediated psoriasis-like skin inflammation.
Drewa et al. Med Sci Monit. 2002; 8(8):BR338-43. [71]	SOD and CAT activities were significantly lower in psoriatic patients.

selectivity, and retention of drug molecules in the target tissue, as well as various adverse reactions [76].

Groundbreaking shifts in psoriasis therapy were achieved with the introduction of drugs that target key immune cascades in the pathogenesis of psoriasis. Biologic therapies or biologics represent progress in the treatment of psoriatic patients in the last decade, due to improved efficacy and tolerability of the drugs and consequently improved quality of life of the patients [77]. Novel biological

drugs, which target TNF- α , the p40 subunit of IL-12 and IL-23, or IL-17 receptors, are effective in treating psoriasis and reducing the PASI score [78] (Table 1). Interestingly, inhibition of IL-1, IL-6, or IFN- γ failed to achieve a significant clinical effect in psoriasis [79]. TNF- α inhibitors include etanercept, infliximab, adalimumab, certolizumab pegol, and golimumab [80]. Inhibitors of IL-17 include secukinumab, ixekizumab, and bimekizumab, while brodalumab is inhibitor of IL-17 receptor [80]. Inhibition of 12p40 subunit,

which is common for IL-12 and IL-23, represents the mechanism of action of ustekinumab and briakinumab, while guselkumab, tildrakizumab, and risankizumab are specific human antibodies targeting the p19 subunit of IL-23, thus blocking the biologic activity of IL-23 [80, 81].

Due to considerable prevalence of psoriasis in general population, as well as comorbidities related to psoriasis, new therapeutic modalities are constantly being investigated. In patients with severe cases of psoriasis in which established therapeutic procedures did not give desired results, the application of cell therapy is being examined, which includes the hematopoietic stem cell transplantation (HSCT) and mesenchymal stromal cell (MSC) [82, 83]. In addition to the fact that mesenchymal cell therapy brings the possibility of a complete recovery of patients with psoriasis, there are also a number of possible adverse effects that reduce the aspiration for their use. The possible adverse effects of cell therapy include neoplastic proliferation, graft versus host reaction, localized skin reactions, and a lack of efficacy [82]. Botulinum toxin has also been shown to be an effective drug in treatment of plaque-type psoriasis [84]. Hydrogen sulfide (H_2S) is recognized as important mediator of various physiological processes and a crucial antioxidative molecule. Due to the disturbed redox balance in psoriasis, therapeutic value of H_2S should be investigated [85]. Antioxidative support to applied antipsoriatic drugs could be an important factor in the reduction of keratinocyte proliferation and remission of the disease [65, 86, 87].

1.6. Effects of Biologic Therapeutics on Oxidative Stress

1.6.1. Effects of IL-12 and IL-23 Inhibitors on Oxidative Stress. Ustekinumab and briakinumab bind to the p40 subunit which is common to IL-12 and IL-23 preventing the interaction of these cytokines with their receptors. Both drugs are fully human monoclonal antibodies. Ustekinumab was approved by the US Food and Drug Administration (FDA) and the European Medicines Agency (EMA) in 2009 for treatment of mild to severe cases of psoriasis, while all clinical trials for briakinumab were discontinued due to the increased risk for myocardial infarction, cerebrovascular accident, and cardiac death [88, 89].

There are very limited data regarding the effects of ustekinumab on redox balance in patients with psoriasis. In a randomized clinical trial, the effects of ustekinumab (IL-12/IL-23 inhibitor), etanercept (TNF- α inhibitor), or cyclosporine were compared regarding the heart function and oxidative stress in patients with psoriasis [90]. After the four-month treatment, the MDA level in patients treated with ustekinumab was significantly decreased compared to TNF- α inhibition, where it was unchanged, or cyclosporine, where it was even increased. Another antioxidative effect of anti-IL-23 antibody was shown in experimental cerebral ischemia [91]. The application of anti-IL-23 antibody decreased the production of ROS and MDA levels in the serum and brain. The antioxidative mechanism achieved by blocking of IL-23 in this experimental model involved targeting the immune specific Janus kinase 2- (JAK2-) STAT3 pathway. Clinical efficacy of IL-12 and IL-23 blockade (ustekinumab) is presented in Figure 4.

1.6.2. Effects of IL-17A Inhibitors on Oxidative Stress. Antioxidative effect of IL-17 inhibition was first reported in a 42-year-old Caucasian woman suffering from plaque psoriasis [92]. One month after secukinumab therapy, plasma levels of lipid measured as thiobarbituric acid reactive substances (TBARS) were significantly decreased, while total antioxidant capacity was significantly improved. It was also noticed that neutrophils, monocytes, and lymphocytes decreased the production of ROS. In three murine experimental models of psoriasis-like skin disease, levels of IL-17A correlated with the severity of the disease and vascular dysfunction [93]. Treatment with anti-IL-17A antibody efficiently eradicated cutaneous lesions and decreased peripheral oxidative stress in two (CD11c-IL-17A^{ind/ind} mice and mice with imiquimod induced psoriasis) assessed the models of psoriasis. Interestingly, in the experimental model of severe psoriasis using K14-IL-17A^{ind/+} mice, neither skin lesions nor peripheral oxidative stress was improved [93]. Another study compared the effects of secukinumab (IL-17A inhibitor), cyclosporine, or methotrexate (MTX) treatment on the left ventricular function and oxidative stress in patients with psoriasis [94]. Secukinumab exerted most beneficial effects on the improvement of the left ventricular function and the decrease of MDA and protein carbonyl as markers of oxidative stress. On the other hand, MTX did not change the measured parameters for oxidative stress, while cyclosporine even caused them to increase [90]. The results of the Eding et al. showed that MutT Homolog 1 (MTH1) levels were increased in skin lesions of imiquimod-induced psoriatic mice [95]. Inhibition of MTH1 resulted in both decrease of ROS and oxidative stress and IL-17-mediated inflammation. Assessing the effect of IL-17A overexpression in CD4-IL-17A^{ind/+} mice, it was shown that IL-17A overexpression was accompanied by increased peripheral ROS/RNS levels, as well as increased ROS/RNS production by spleen CD11b⁺ cells [97]. Increased production of IL-17A, followed by an increase in oxidative stress, resulted in endothelial dysfunction and vascular damage. Clinical efficiency of IL-17 inhibition (secukinumab) is shown in Figure 5.

1.6.3. Effects of TNF α Blockers on Oxidative Stress. TNF- α alone does not elicit a significant response to keratinocytes. However, in combination with IL-17A and other cytokines, TNF- α is a significant element of the cytokine milieu in psoriasis. Powerful synergism between TNF- α and IL-17A enhances the effects of IL-17A. In addition, it leads to increased expression of IL-17R by keratinocytes [97]. TNF- α inhibitors (etanercept, adalimumab, and infliximab) are human fusion proteins used in treatment psoriasis. Aiming to investigate the effects of infliximab, as TNF- α blocker, on redox balance of psoriatic patients, Barygina and coworkers have measured various oxidative stress biomarkers in plasma and white blood cells [98]. After six-month infliximab treatment, plasma levels of MDA and protein carbonyl content were decreased, while the activity of NADPH oxidase was decreased compared to untreated patients. The most significant limitation of this study is the very small number of patients, given that only 29 patients in total were

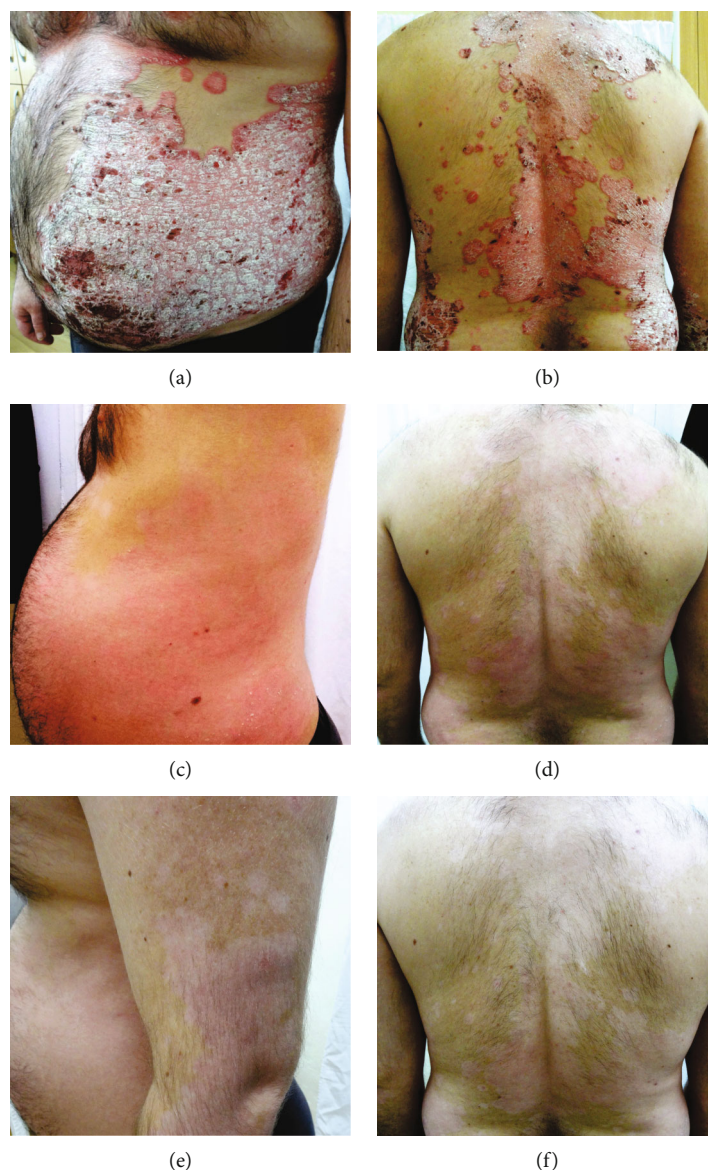


FIGURE 4: Clinical efficacy of IL-12 and IL-23 blockade (ustekinumab). Patient before starting therapy (a, b), after 8 weeks from the introduction of the IL-12/IL-23 blocker (c, d), and after 16 weeks after the introduction of the IL-12/IL-23 blocker (e, f). Pictures presented are part of the private collection of Vesna M. Milicic and Ana B. Ravic Nikolic.

included. In another study dealing with the role of etanercept, another TNF- α inhibitor, the authors measured plasma, total antioxidative capacity, and PON1 activity [99]. Etanercept application for 24 weeks significantly improved total antioxidative capacity and PON1 activity combined with reduction of inflammatory markers (C-reactive protein). Oxidative stress was also reduced by etanercept in experimental peritonitis [100]. Inhibition of TNF- α by adalimumab, human monoclonal antibody against TNF- α , showed significant reduction of oxidative stress in experimental model of vascular dementia [100]. Comparing the effects of ustekinumab, etanercept, or cyclosporine on oxidative stress in psoriasis-suffering patients, ustekinumab exerted most powerful antioxidative effect [92].

Overall, it can be concluded that all biologics exert antioxidative capacity but novel study comparing the antioxi-

dative effects of biologics of different mechanism of action should offer new insights into interfering networks of oxidative stress, immune response, and inflammation.

1.7. Effects of Immunomodulatory Therapy on Oxidative Stress. Methotrexate (MTX) is a well-established drug for systemic treatment of psoriasis due to its antiproliferative, immunosuppressive, and anti-inflammatory properties. Its exact underlining mechanisms are not fully elucidated [102]. The antiproliferative effects of MTX are based on inhibitory effect on folate-dependent enzymes, such as dihydrofolate reductase, resulting in decreased synthesis of DNA and reduced cell proliferation [103]. Immunosuppressive and anti-inflammatory ability of MTX are a consequence of increased adenosine release, decreased release of proinflammatory cytokines (TNF- α and IL-1), favored apoptosis

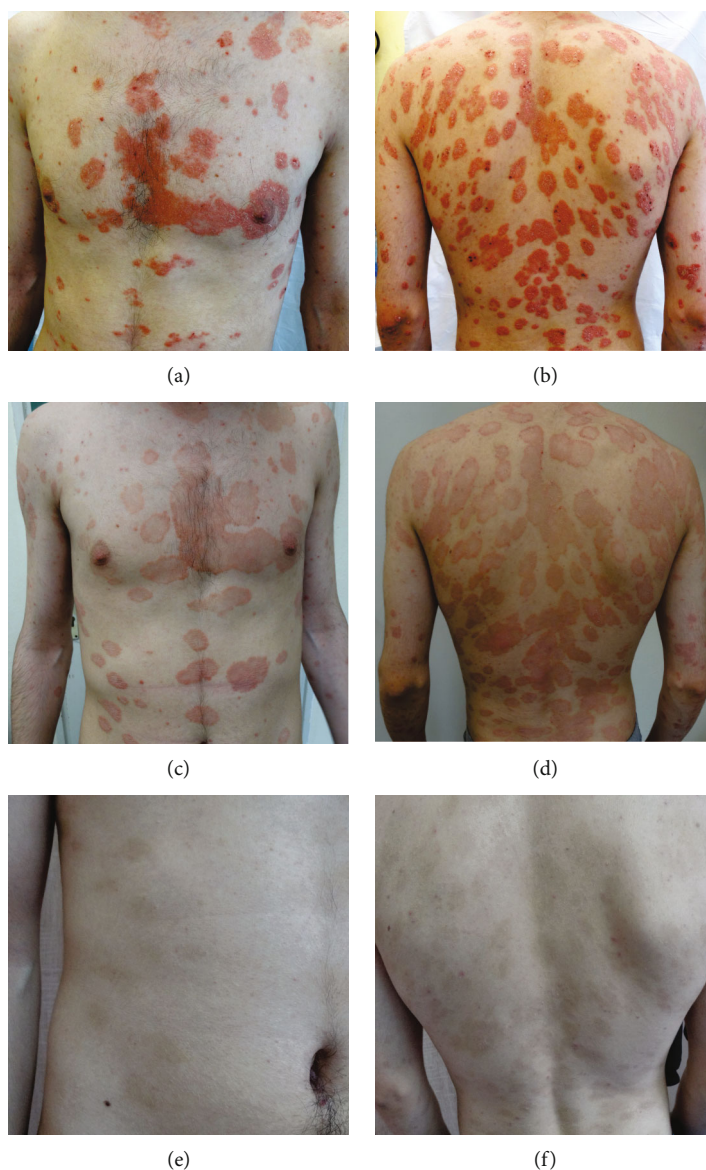


FIGURE 5: Clinical efficacy of IL-17A blockade (secukinumab). Patient before starting therapy (a, b), after 8 weeks from the introduction of the IL-17A blocker (c, d), and after 16 weeks after the introduction of the IL-17A blocker (e, f). Pictures presented are part of the private collection of Vesna M. Milicic and Ana B. Ravic Nikolic.

of activated T cells, and decreased chemotaxis of neutrophils [103].

A twelve-week MTX treatment in psoriatic patients induced augmentation of oxidative stress, reflected through increased levels of MDA and reduction of nitrate/nitrite, SOD, and CAT activity and TAS in the plasma [104]. The authors proposed that increased ROS and decreased NO production, combined with increased caspase-3 expression, represent the mechanism of MTX-mediated induction of apoptosis. Experimental study in an isolated hepatocytes rat confirmed prooxidative effects of MTX [105]. Antioxidants decreased ROS availability and reduced MTX-induced cytotoxicity. MTX also induced mitochondria swelling, decrease of ATP and GSH amount, and release of cytochrome c. The assessment of expression of isoenzymes of GST and cytochrome (CYP) families showed that expression

was increased in patients with psoriasis compared to healthy controls [106]. After 12-week MTX treatment, the expression of these enzymes, important in regulation of redox balance, did not change significantly, although there was marked clinical improvement. Prooxidative effects of MTX were shown in other tissues and organs. In the MTX treated rats, the levels of GSH, SOD, and CAT testicular were significantly decreased, combined with increased DNA and tissue damage [107]. MTX also showed prooxidative features in liver and neural tissues due to decreased activity of SOD, CAT, or GPx [108, 109].

Conversely, the results of several studies implicated antioxidative effects of MTX. Zimmerman et al. showed that MTX inhibits the generation of MAA-protein adducts, formed by MDA and acetaldehyde interaction [110]. MAA-protein adducts have high immunogenic and

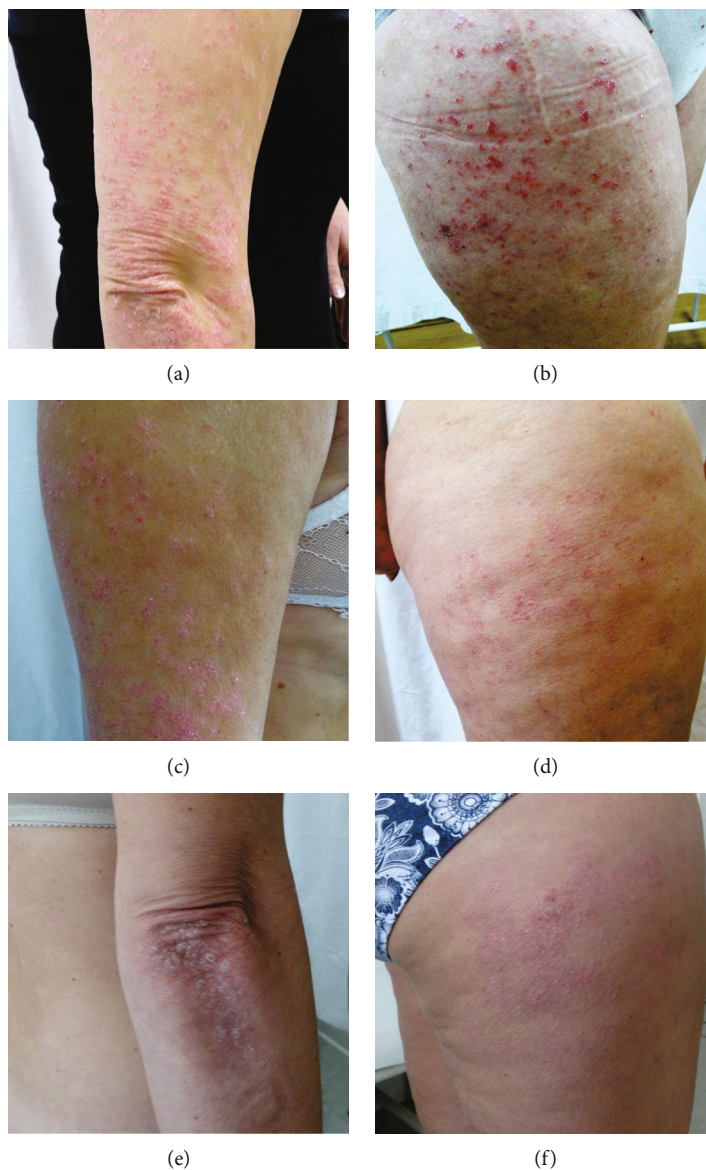


FIGURE 6: Clinical efficacy of methotrexate (MTX). Patient before starting therapy (a, b), after 8 weeks from the introduction of the MTX (15 mg per week) (c, d), and after 16 weeks after the introduction of the MTX (15 mg per week) (e, f). Pictures presented are part of the private collection of Vesna M. Milicic and Ana B. Ravic Nikolic.

prooxidative potential, so they are not only markers of oxidative stress, but also play an active role in the development of immune disorders. MTX significantly reduced the production of MAA-protein adducts as well as the level of free radicals *in vitro*. The reduction of free radicals and antioxidative action of MTX was achieved by the ability of MTX to directly scavenge O_2^- . Another study on the effects of 24 weeks of MTX therapy on oxidative stress showed antioxidative properties of MTX in psoriatic patients [111]. The levels of MDA significantly decreased, while TAS markedly increased after MTX therapy in psoriatic patients. Comparing to healthy controls the oxidative stress was higher in psoriatic patients both at the beginning and at the end of the MTX therapy protocol.

Analyzing results of different studies, it can be concluded that MTX has somewhat contradictory impact on redox bal-

ance. This could be the consequence of its prooxidative and proapoptotic effects, and on the other hand, of decreased production of ROS through inhibition of inflammation-mediated pathways [112]. Clinical efficacy MTX is shown in Figure 6.

1.8. Effects of UVB and PUVA Therapy on Oxidative Stress. Phototherapy is often used in the treatment of skin diseases. It is a type of light therapy that mimics the effects of exposure to sunlight. Established phototherapies in psoriatic patients include PUVA radiation (psoralen in combination with UVA radiation) and narrow-band UVB (NB-UVB) [113]. The phototherapeutic procedures are usually effective in psoriasis treatment, but due to potential side-effects, including carcinogenesis, it can be used only for short-term treatment of the disease [113]. Increased ROS production

during PUVA therapy, due to psoralen sensitization and UVA exposure, increases already increased levels of superoxide anion radical (O_2^-) and forms the basis of photocarcinogenesis [114].

Production of ROS due to PUVA therapy may cause oxidative damage to various macromolecules. The analysis of the PUVA effects on oxidative damage of DNA showed that suberythemal dose induced increased urinary extraction of 8-Oxo-2'-deoxyguanosine (8-oxo-dG) as a marker of DNA oxidation [115]. 8-oxo-dG in urine reached the peak 4 days after PUVA irradiation. *In vitro* study on HaCaT keratinocyte cell line also showed increased 8-oxo-dG production after exposure to therapeutic doses of PUVA and NB-UVB [116].

In the 12-week follow-up study, oxidative stress biomarkers, TBARS, and total antioxidant status (TAS) were significantly improved due to NB-UVB and PUVA therapy [117]. PUVA treatment appears to be more effective in the reduction of oxidative stress comparing to NB-UVB. The reduction of oxidative stress markers was connected with the reduction of inflammation. A study of similar design also showed the reduction of oxidative stress biomarkers, TBARS and TAS, after 12-week long PUVA and NB-UVB therapy [118]. Short-term increase of ROS production upon PUVA treatment, combined with the reduction of inflammation, could improve antioxidative potential and thus prolonged PUVA treatment results in the reduction of oxidative stress.

2. Conclusion

Oxidative stress and the aberrant immune response remain two crucial pathophysiological mechanisms in psoriasis. Their interdependence and interconnectedness represent the key to understanding etiopathogenesis of psoriasis. A large number of factors that can influence the development of psoriasis, from genetic predisposition to lifestyle, make the tangle of causes and consequences still insufficiently understood. Novel therapeutic options, primarily biological therapy, have significantly improved the quality of life of patients with psoriasis. However, the success of the applied therapy seems to depend on the reduction of both the proinflammatory and prooxidative components of the disease. The most noticeable and most powerful antioxidative effects exert various biologics compared to more convenient therapeutic modalities, such as methotrexate or phototherapy. Intersections of redox, immune, and inflammatory signaling pathways should be the focus of further researches dealing with pathophysiology of psoriasis, while antioxidative supplementation could be the solution in some refractory cases of the disease.

Conflicts of Interest

The authors declare that they have no conflicts of interest.

Acknowledgments

The authors would like to thank Mr. Dusan Tomasevic for technical support. Figures 2 and 3 are created using BioRen-

der. This work was supported by grant from the Faculty of Medical Sciences, University of Kragujevac, Serbia (project no. JP 27/20).

References

- [1] F. S. Glickman, "Lepra, psora, psoriasis," *Journal of the American Academy of Dermatology*, vol. 14, no. 5, pp. 863–866, 1986.
- [2] I. M. Michalek, B. Loring, and S. M. John, "A systematic review of worldwide epidemiology of psoriasis," *Journal of the European Academy of Dermatology and Venereology*, vol. 31, no. 2, pp. 205–212, 2017.
- [3] C. E. M. Griffiths, A. W. Armstrong, J. E. Gudjonsson, and J. N. W. N. Barker, "Psoriasis," *Lancet*, vol. 397, no. 10281, pp. 1301–1315, 2021.
- [4] W. H. Boehncke and M. P. Schön, "Psoriasis," *Lancet*, vol. 386, no. 9997, pp. 983–994, 2015.
- [5] E. Muñoz-Aceituno, L. Martos-Cabrera, M. C. Ovejero-Benito, A. Reolid, F. Abad-Santos, and E. Daudén, "Pharmacogenetics update on biologic therapy in psoriasis," *Medicina (Kaunas, Lithuania)*, vol. 56, no. 12, p. 719, 2020.
- [6] J. Takeshita, S. Grewal, S. M. Langan et al., "Psoriasis and comorbid diseases: epidemiology," *Journal of the American Academy of Dermatology*, vol. 76, no. 3, pp. 377–390, 2017.
- [7] A. Ogdie and P. Weiss, "The epidemiology of psoriatic arthritis," *Rheumatic Diseases Clinics of North America*, vol. 41, no. 4, pp. 545–568, 2015.
- [8] E. J. Horn, K. M. Fox, V. Patel, C. F. Chiou, F. Dann, and M. Lebwohl, "Are patients with psoriasis undertreated? Results of National Psoriasis Foundation survey," *Journal of the American Academy of Dermatology*, vol. 57, no. 6, pp. 957–962, 2007.
- [9] A. W. Armstrong, A. D. Robertson, J. Wu, C. Schupp, and M. G. Lebwohl, "Undertreatment, treatment trends, and treatment dissatisfaction among patients with psoriasis and psoriatic arthritis in the United States: findings from the National Psoriasis Foundation surveys, 2003-2011," *JAMA Dermatology*, vol. 149, no. 10, pp. 1180–1185, 2013.
- [10] U. Mrowietz, K. Kragballe, K. Reich et al., "Definition of treatment goals for moderate to severe psoriasis: a European consensus," *Archives of Dermatological Research*, vol. 303, no. 1, pp. 1–10, 2011.
- [11] P. J. Mease, D. D. Gladman, P. Helliwell et al., "Comparative performance of psoriatic arthritis screening tools in patients with psoriasis in European/North American dermatology clinics," *Journal of the American Academy of Dermatology*, vol. 71, no. 4, pp. 649–655, 2014.
- [12] G. Tonel and C. Conrad, "Interplay between keratinocytes and immune cells—recent insights into psoriasis pathogenesis," *The International Journal of Biochemistry & Cell Biology*, vol. 41, no. 5, pp. 963–968, 2009.
- [13] J. Kim and J. G. Krueger, "The immunopathogenesis of psoriasis," *Dermatologic Clinics*, vol. 33, no. 1, pp. 13–23, 2015.
- [14] F. Capon, "The genetic basis of psoriasis," *International Journal of Molecular Sciences*, vol. 18, no. 12, article 2526, 2017.
- [15] D. L. Duffy, L. S. Spelman, and N. G. Martin, "Psoriasis in Australian twins," *Journal of the American Academy of Dermatology*, vol. 29, no. 3, pp. 428–434, 1993.
- [16] C. Ohata, Y. Kanai, K. Murotani, H. Kitabayashi, and S. Imafuku, "Difference in health-related quality of life

- between anxiety and depressive symptoms in Japanese patients with plaque psoriasis: the ProLOGUE study,” *Journal of the European Academy of Dermatology and Venereology*, vol. 36, pp. e57–e59, 2022.
- [17] K. A. Papp and M. G. Lebwohl, “Onset of action of biologics in patients with moderate-to-severe psoriasis,” *Journal of Drugs in Dermatology*, vol. 17, no. 3, pp. 247–250, 2017.
- [18] S. K. Mahil, M. C. Ezejimofor, L. S. Exton et al., “Comparing the efficacy and tolerability of biologic therapies in psoriasis: an updated network meta-analysis,” *The British Journal of Dermatology*, vol. 183, no. 4, pp. 638–649, 2020.
- [19] Z. Yang, Z. Min, and B. Yu, “Reactive oxygen species and immune regulation,” *International Reviews of Immunology*, vol. 39, no. 6, pp. 292–298, 2020.
- [20] E. Ambrożewicz, P. Wójcik, A. Wroński et al., “Pathophysiological alterations of redox signaling and endocannabinoid system in granulocytes and plasma of psoriatic patients,” *Cell*, vol. 7, no. 10, article 159, 2018.
- [21] J. R. Bjerke, “In situ characterization and counting of mononuclear cells in lesions of different clinical forms of psoriasis,” *Acta Dermato-Venereologica*, vol. 62, no. 2, pp. 93–100, 1982.
- [22] H. Hammar, S. Q. Gu, A. Johannesson, K. G. Sundkvist, and P. Biberfeld, “Subpopulations of mononuclear cells in microscopic lesions of psoriatic patients. Selective accumulation of suppressor/cytotoxic T cells in epidermis during the evolution of the lesion,” *The Journal of Investigative Dermatology*, vol. 83, no. 6, pp. 416–420, 1984.
- [23] S. L. Gottlieb, P. Gilleaudeau, R. Johnson et al., “Response of psoriasis to a lymphocyte-selective toxin (DAB₃₈₉IL-2) suggests a primary immune, but not keratinocyte, pathogenic basis,” *Nature Medicine*, vol. 1, no. 5, pp. 442–447, 1995.
- [24] T. Biedermann, M. Röcken, and J. M. Carballido, “TH1 and TH2 lymphocyte development and regulation of TH cell-mediated immune responses of the skin,” *The Journal of Investigative Dermatology. Symposium Proceedings*, vol. 9, no. 1, pp. 5–14, 2004.
- [25] M. J. Gooderham, K. A. Papp, and C. W. Lynde, “Shifting the focus – the primary role of IL-23 in psoriasis and other inflammatory disorders,” *Journal of the European Academy of Dermatology and Venereology*, vol. 32, no. 7, pp. 1111–1119, 2018.
- [26] D. J. Marble, K. B. Gordon, and B. J. Nickoloff, “Targeting TNF α rapidly reduces density of dendritic cells and macrophages in psoriatic plaques with restoration of epidermal keratinocyte differentiation,” *Journal of Dermatological Science*, vol. 48, no. 2, pp. 87–101, 2007.
- [27] L. L. Ten Bergen, A. Petrovic, A. Krogh Aarebrot, and S. Appel, “The TNF/IL-23/IL-17 axis—head-to-head trials comparing different biologics in psoriasis treatment,” *Scandinavian Journal of Immunology*, vol. 92, no. 4, article e12946, 2020.
- [28] J. D. Bos, M. A. de Rie, M. B. Teunissen, and G. Piskin, “Psoriasis: dysregulation of innate immunity,” *The British Journal of Dermatology*, vol. 152, no. 6, pp. 1098–1107, 2005.
- [29] C. C. Chiang, W. J. Cheng, M. Korinek, C. Y. Lin, and T. L. Hwang, “Neutrophils in psoriasis,” *Frontiers in Immunology*, vol. 10, article 2376, 2019.
- [30] S. A. Belambri, L. Rolas, H. Raad, M. Hurtado-Nedelec, P. M. Dang, and J. El-Benna, “NADPH oxidase activation in neutrophils: role of the phosphorylation of its subunits,” *European Journal of Clinical Investigation*, vol. 48, article e12951, Suppl 2, 2018.
- [31] N. Milosavljevic, M. Gazdic, B. Simovic Markovic et al., “Mesenchymal stem cells attenuate acute liver injury by altering ratio between interleukin 17 producing and regulatory natural killer T cells,” *Liver Transplantation*, vol. 23, no. 8, pp. 1040–1050, 2017.
- [32] S. Bagchi, Y. He, H. Zhang et al., “CD1b-autoreactive T cells contribute to hyperlipidemia-induced skin inflammation in mice,” *The Journal of Clinical Investigation*, vol. 127, no. 6, pp. 2339–2352, 2017.
- [33] L. C. Zaba, J. Fuentes-Duculan, N. J. Eungdamrong et al., “Psoriasis is characterized by accumulation of immunostimulatory and Th1/Th17 cell-polarizing myeloid dendritic cells,” *The Journal of Investigative Dermatology*, vol. 129, no. 1, pp. 79–88, 2009.
- [34] J. E. Hawkes, B. Y. Yan, T. C. Chan, and J. G. Krueger, “Discovery of the IL-23/IL-17 signaling pathway and the treatment of psoriasis,” *Journal of Immunology*, vol. 201, no. 6, pp. 1605–1613, 2018.
- [35] L. M. Johnson-Huang, M. A. Lowes, and J. G. Krueger, “Putting together the psoriasis puzzle: an update on developing targeted therapies,” *Disease Models & Mechanisms*, vol. 5, no. 4, pp. 423–433, 2012.
- [36] Y. Iwakura, H. Ishigame, S. Saijo, and S. Nakae, “Functional specialization of interleukin-17 family members,” *Immunity*, vol. 34, no. 2, pp. 149–162, 2011.
- [37] E. Stephen-Victor, H. Fickenscher, and Bayry, J., “IL-26: an emerging proinflammatory member of the IL-10 cytokine family with multifaceted actions in antiviral, antimicrobial, and autoimmune responses,” *PLoS Pathogens*, vol. 12, no. 6, article e1005624, 2016.
- [38] J. M. Wang, A. F. Huang, W. D. Xu, and L. C. Su, “Insights into IL-29: emerging role in inflammatory autoimmune diseases,” *Journal of Cellular and Molecular Medicine*, vol. 23, no. 12, pp. 7926–7932, 2019.
- [39] E. Witte, G. Kokolakis, K. Witte et al., “IL-19 is a component of the pathogenetic IL-23/IL-17 cascade in psoriasis,” *The Journal of Investigative Dermatology*, vol. 134, no. 11, pp. 2757–2767, 2014.
- [40] Q. Jiang, G. Yang, F. Xiao et al., “Role of Th22 cells in the pathogenesis of autoimmune diseases,” *Frontiers in Immunology*, vol. 12, article 688066, 2021.
- [41] A. Chiricozzi, P. Romanelli, E. Volpe, G. Borsellino, and M. Romanelli, “Scanning the immunopathogenesis of psoriasis,” *International Journal of Molecular Sciences*, vol. 19, no. 1, article 179, 2018.
- [42] L. Zhou, I. I. Ivanov, R. Spolski et al., “IL-6 programs T_H-17 cell differentiation by promoting sequential engagement of the IL-21 and IL-23 pathways,” *Nature Immunology*, vol. 8, no. 9, pp. 967–974, 2007.
- [43] D. M. Floss, J. M. Moll, and J. Scheller, “IL-12 and IL-23-close relatives with structural homologies but distinct immunological functions,” *Cell*, vol. 9, no. 10, article 2184, 2020.
- [44] H. J. Bovenschen, P. C. van de Kerkhof, P. E. van Erp, R. Woestenenk, I. Joosten, and H. J. Koenen, “Foxp3+ regulatory T cells of psoriasis patients easily differentiate into IL-17A-producing cells and are found in lesional skin,” *The Journal of Investigative Dermatology*, vol. 131, no. 9, pp. 1853–1860, 2011.













- [45] N. J. Wilson, K. Boniface, J. R. Chan et al., "Development, cytokine profile and function of human interleukin 17-producing helper T cells," *Nature Immunology*, vol. 8, no. 9, pp. 950–957, 2007.
- [46] A. A. Levin and A. B. Gottlieb, "Specific targeting of interleukin-23p19 as effective treatment for psoriasis," *Journal of the American Academy of Dermatology*, vol. 70, no. 3, pp. 555–561, 2014.
- [47] C. L. Langrish, B. S. McKenzie, N. J. Wilson, R. de Waal Malefyt, R. A. Kastelein, and D. J. Cua, "IL-12 and IL-23: master regulators of innate and adaptive immunity," *Immunological Reviews*, vol. 202, no. 1, pp. 96–105, 2004.
- [48] Y. A. Rodriguez-Rosales, J. D. Langereis, M. A. J. Gorris et al., "Immunomodulatory aged neutrophils are augmented in blood and skin of psoriasis patients," *The Journal of Allergy and Clinical Immunology*, vol. 148, no. 4, pp. 1030–1040, 2021.
- [49] H. L. Rizzo, S. Kagami, K. G. Phillips, S. E. Kurtz, S. L. Jacques, and A. Blauvelt, "IL-23-mediated psoriasis-like epidermal hyperplasia is dependent on IL-17A," *Journal of Immunology*, vol. 186, no. 3, pp. 1495–1502, 2011.
- [50] B. Halliwell, "Biochemistry of oxidative stress," *Biochemical Society Transactions*, vol. 35, no. 5, pp. 1147–1150, 2007.
- [51] B. Halliwell, "Free radicals and antioxidants: updating a personal view," *Nutrition Reviews*, vol. 70, no. 5, pp. 257–265, 2012.
- [52] E. F. Bernstein, D. B. Brown, M. D. Schwartz, K. Kaidbey, and S. M. Ksenzenko, "The polyhydroxy acid gluconolactone protects against ultraviolet radiation in an in vitro model of cutaneous photoaging," *Dermatologic Surgery*, vol. 30, no. 2, pp. 189–196, 2004.
- [53] T. Bitto and C. Nishigori, "Impact of reactive oxygen species on keratinocyte signaling pathways," *Journal of Dermatological Science*, vol. 68, no. 1, pp. 3–8, 2012.
- [54] R. Lai, D. Xian, X. Xiong, L. Yang, J. Song, and J. Zhong, "Proanthocyanidins: novel treatment for psoriasis that reduces oxidative stress and modulates Th17 and Treg cells," *Redox Report*, vol. 23, no. 1, pp. 130–135, 2018.
- [55] J. M. Kyriakis and J. Avruch, "Mammalian MAPK signal transduction pathways activated by stress and inflammation: a 10-year update," *Physiological Reviews*, vol. 92, no. 2, pp. 689–737, 2012.
- [56] K. N. Schmidt, P. Amstad, P. Cerutti, and P. A. Baeuerle, "The roles of hydrogen peroxide and superoxide as messengers in the activation of transcription factor NF- κ B," *Chemistry & Biology*, vol. 2, no. 1, pp. 13–22, 1995.
- [57] C. Johansen, K. Kragballe, M. Westergaard, J. Henningsen, K. Kristiansen, and L. Iversen, "The mitogen-activated protein kinases p38 and ERK1/2 are increased in lesional psoriatic skin," *The British Journal of Dermatology*, vol. 152, no. 1, pp. 37–42, 2005.
- [58] X. J. Yu, C. Y. Li, H. Y. Dai et al., "Expression and localization of the activated mitogen-activated protein kinase in lesional psoriatic skin," *Experimental and Molecular Pathology*, vol. 83, no. 3, pp. 413–418, 2007.
- [59] G. Müller, C. Lübow, and G. Weindl, "Lysosomotropic beta blockers induce oxidative stress and IL23A production in Langerhans cells," *Autophagy*, vol. 16, no. 8, pp. 1380–1395, 2020.
- [60] J. Pleńkowska, M. Gabig-Cimińska, and P. Mozolewski, "Oxidative stress as an important contributor to the pathogenesis of psoriasis," *International Journal of Molecular Sciences*, vol. 21, no. 17, article 6206, 2020.
- [61] N. Vorobjeva, A. Prikhodko, I. Galkin et al., "Mitochondrial reactive oxygen species are involved in chemoattractant-induced oxidative burst and degranulation of human neutrophils in vitro," *European Journal of Cell Biology*, vol. 96, no. 3, pp. 254–265, 2017.
- [62] Q. Zhou, U. Mrowietz, and M. Rostami-Yazdi, "Oxidative stress in the pathogenesis of psoriasis," *Free Radical Biology & Medicine*, vol. 47, no. 7, pp. 891–905, 2009.
- [63] L. Yang, X. Fan, T. Cui, E. Dang, and G. Wang, "Nrf2 promotes keratinocyte proliferation in psoriasis through up-regulation of keratin 6, keratin 16, and keratin 17," *The Journal of Investigative Dermatology*, vol. 137, no. 10, pp. 2168–2176, 2017.
- [64] Y. J. Lee, J. H. Bae, S. G. Kang et al., "Pro-oxidant status and Nrf2 levels in psoriasis vulgaris skin tissues and dimethyl fumarate-treated HaCaT cells," *Archives of Pharmacological Research*, vol. 40, no. 9, pp. 1105–1116, 2017.
- [65] W. Wang and H. Wang, "Astilbin reduces ROS accumulation and VEGF expression through Nrf2 in psoriasis-like skin disease," *Biological Research*, vol. 52, no. 1, p. 49, 2019.
- [66] M. Asefi, A. Vaisi-Raygani, F. Bahrehmand et al., "Paraoxonase 1 (PON1) 55 polymorphism, lipid profiles and psoriasis," *The British Journal of Dermatology*, vol. 167, no. 6, pp. 1279–1286, 2012.
- [67] A. A. Hernández-Collazo, O. Pérez-Méndez, V. López-Olmos et al., "Association between rs662 (A > G) and rs854560 (A > T) polymorphisms in PON1 gene and the susceptibility for psoriasis in mestizo population of Western Mexico," *Molecular Biology Reports*, vol. 48, no. 1, pp. 183–194, 2021.
- [68] D. S. L. Srivastava, V. K. Jain, P. Verma, and J. P. Yadav, "Polymorphism of glutathione S-transferase M1 and T1 genes and susceptibility to psoriasis disease: a study from North India," *Indian Journal of Dermatology, Venereology and Leprology*, vol. 84, no. 1, pp. 39–44, 2018.
- [69] S. H. Ibbotson, R. S. Dawe, A. T. Dinkova-Kostova et al., "Glutathione S-transferase genotype is associated with sensitivity to psoralen-ultraviolet A photochemotherapy," *The British Journal of Dermatology*, vol. 166, no. 2, pp. 380–388, 2012.
- [70] Y. S. Lee, I. S. Cheon, B. H. Kim, M. J. Kwon, H. W. Lee, and T. Y. Kim, "Loss of extracellular superoxide dismutase induces severe IL-23-mediated skin inflammation in mice," *The Journal of Investigative Dermatology*, vol. 133, no. 3, pp. 732–741, 2013.
- [71] G. Drewa, E. Krzyżyńska-Malinowska, A. Woźniak et al., "Activity of superoxide dismutase and catalase and the level of lipid peroxidation products reactive with TBA in patients with psoriasis," *Medical Science Monitor*, vol. 8, no. 8, article BR338-343, 2002.
- [72] A. Skutnik-Radziszewska, M. Maciejczyk, K. Fejfer et al., "Salivary antioxidants and oxidative stress in psoriatic patients: can salivary total oxidant status and oxidative status index be a plaque psoriasis biomarker?," *Oxidative Medicine and Cellular Longevity*, vol. 2020, Article ID 9086024, 12 pages, 2020.
- [73] A. Skutnik-Radziszewska, M. Maciejczyk, I. Flisiak et al., "Enhanced inflammation and nitrosative stress in the saliva and plasma of patients with plaque psoriasis," *Journal of Clinical Medicine*, vol. 9, no. 3, article 745, 2020.

- [74] G. Ganzetti, A. Campanati, A. Santarelli et al., "Salivary interleukin-1 β : oral inflammatory biomarker in patients with psoriasis," *The Journal of International Medical Research*, vol. 44, 1_suppl, pp. 10–14, 2016.
- [75] D. Belström, J. M. Eiberg, C. Enevold et al., "Salivary microbiota and inflammation-related proteins in patients with psoriasis," *Oral Diseases*, vol. 26, no. 3, pp. 677–687, 2020.
- [76] P. Gisondi, F. Bellinato, M. Bruni, G. De Angelis, and G. Girolomoni, "Methotrexate vs secukinumab safety in psoriasis patients with metabolic syndrome," *Dermatologic Therapy*, vol. 33, no. 6, article e14281, 2020.
- [77] P. Biswasroy, D. Pradhan, B. Kar, G. Ghosh, and G. Rath, "Recent advancement in topical nanocarriers for the treatment of psoriasis," *AAPS PharmSciTech*, vol. 22, no. 5, p. 164, 2021.
- [78] J. W. Marson, M. L. Snyder, and M. G. Lebwohl, "Newer therapies in psoriasis," *The Medical Clinics of North America*, vol. 105, no. 4, pp. 627–641, 2021.
- [79] M. A. Richard, J. P. Lacour, M. P. Konstantinou et al., "Secukinumab efficacy in reducing the severity and the psychosocial impact of moderate-to-severe psoriasis as assessed by the simplified psoriasis index: results from the IPSI-PSO study," *Journal of the European Academy of Dermatology and Venereology*, vol. 35, no. 3, pp. 677–684, 2021.
- [80] J. Baliwag, D. H. Barnes, and A. Johnston, "Cytokines in psoriasis," *Cytokine*, vol. 73, no. 2, pp. 342–350, 2015.
- [81] F. M. Ghazawi, F. Mahmood, L. Kircik et al., "A review of the efficacy and safety for biologic agents targeting IL-23 in treating psoriasis with the focus on tildrakizumab," *Frontiers in Medicine*, vol. 8, article 702776, 2021.
- [82] A. Ruggiero, G. Fabbrocini, E. Cinelli, S. S. Ocampo Garza, E. Camela, and M. Megna, "Anti-interleukin-23 for psoriasis in elderly patients: guselkumab, risankizumab and tildrakizumab in real-world practice," *Clinical and Experimental Dermatology*, vol. 47, no. 3, 2021.
- [83] A. A. B. Eita, A. M. Zaki, and S. A. Mahmoud, "Serum 8-isoprostane levels in patients with resistant oral lichen planus before and after treatment with lycopene: a randomized clinical trial," *BMC Oral Health*, vol. 21, no. 1, article 343, 2021.
- [84] Y. Chen, Q. Yu, Y. Hu, and Y. Shi, "Current research and use of mesenchymal stem cells in the therapy of autoimmune diseases," *Current Stem Cell Research & Therapy*, vol. 14, no. 7, pp. 579–582, 2019.
- [85] J. Abou-Rahal, L. Abdullah, M. Kurban, and O. Abbas, "Letter to the editor regarding the article"Rossi A, Magri F, Michelini S, et al. New onset of alopecia areata in a patient with SARS-COV-2 infection: Possible pathogenetic correlations?," *Journal of Cosmetic Dermatology*, vol. 20, no. 7, article 2004, 2021.
- [86] Q. Xiao, L. Xiong, J. Tang, L. Li, and L. Li, "Hydrogen sulfide in skin diseases: a novel mediator and therapeutic target," *Oxidative Medicine and Cellular Longevity*, vol. 2021, Article ID 6652086, 11 pages, 2021.
- [87] F. Guarneri, L. Bertino, G. Pioggia, M. Casciaro, and S. Gangemi, "Therapies with antioxidant potential in psoriasis, vitiligo, and lichen planus," *Antioxidants (Basel)*, vol. 10, no. 7, article 1087, 2021.
- [88] A. Winiarska-Mieczan, T. Mieczan, and G. Wójcik, "Importance of redox equilibrium in the pathogenesis of psoriasis-impact of antioxidant-rich diet," *Nutrients*, vol. 12, no. 6, article 1841, 2020.
- [89] L. Puig, "The role of IL 23 in the treatment of psoriasis," *Expert Review of Clinical Immunology*, vol. 13, no. 6, pp. 525–534, 2017.
- [90] P. Traczewski and L. Rudnicka, "Briakinumab for the treatment of plaque psoriasis," *BioDrugs*, vol. 26, no. 1, pp. 9–20, 2012.
- [91] I. Ikonomidis, E. Papadavid, G. Makavos et al., "Lowering interleukin-12 activity improves myocardial and vascular function compared with tumor necrosis factor- α antagonism or cyclosporine in psoriasis," *Circulation. Cardiovascular Imaging*, vol. 10, no. 9, article e006283, 2017.
- [92] L. Fan and L. Zhou, "Anti-IL-23 exerted protective effects on cerebral ischemia-reperfusion injury through JAK2/STAT3 signaling pathway," *Molecular Biology Reports*, vol. 48, no. 4, pp. 3475–3484, 2021.
- [93] M. Becatti, M. L. Urban, G. Taurisano et al., "Secukinumab reduces plasma oxidative stress in psoriasis: a case-based experience," *Dermatologic Therapy*, vol. 31, no. 5, article e12675, 2018.
- [94] R. Schüler, A. Brand, S. Klebow et al., "Antagonization of IL-17A attenuates skin inflammation and vascular dysfunction in mouse models of psoriasis," *The Journal of Investigative Dermatology*, vol. 139, no. 3, pp. 638–647, 2019.
- [95] G. Makavos, I. Ikonomidis, I. Andreadou et al., "Effects of interleukin 17A inhibition on myocardial deformation and vascular function in psoriasis," *The Canadian Journal of Cardiology*, vol. 36, no. 1, pp. 100–111, 2020.
- [96] C. Bivik Eding, I. Köhler, D. Verma et al., "MTH1 inhibitors for the treatment of psoriasis," *The Journal of Investigative Dermatology*, vol. 141, no. 8, pp. 2037–2048.e4, 2021.
- [97] R. Schüler, P. Efentakis, J. Wild et al., "T cell-derived IL-17A induces vascular dysfunction via perivascular fibrosis formation and dysregulation of \cdot NO/cGMP signaling," *Oxidative Medicine and Cellular Longevity*, vol. 2019, Article ID 6721531, 15 pages, 2019.
- [98] M. Noack, A. Beringer, and P. Miossec, "Additive or synergistic interactions between IL-17A or IL-17F and TNF or IL-1 β depend on the cell type," *Frontiers in Immunology*, vol. 10, p. 1726, 2019.
- [99] V. V. Barygina, M. Becatti, G. Soldi et al., "Altered redox status in the blood of psoriatic patients: involvement of NADPH oxidase and role of anti-TNF- α therapy," *Redox Report*, vol. 18, no. 3, pp. 100–106, 2013.
- [100] T. Bacchetti, A. Campanati, G. Ferretti, O. Simonetti, G. Liberati, and A. M. Offidani, "Oxidative stress and psoriasis: the effect of antitumor necrosis factor- α inhibitor treatment," *The British Journal of Dermatology*, vol. 168, no. 5, pp. 984–989, 2013.
- [101] Y. Yildirim, E. G. Cellad, A. V. Kara et al., "Effect of intraperitoneal etanercept on oxidative stress in rats with peritonitis," *Oxidative Medicine and Cellular Longevity*, vol. 2016, Article ID 9418468, 6 pages, 2016.
- [102] J. J. Xu, S. Guo, R. Xue et al., "Adalimumab ameliorates memory impairments and neuroinflammation in chronic cerebral hypoperfusion rats," *Aging (Albany NY)*, vol. 13, no. 10, pp. 14001–14014, 2021.
- [103] M. Czarnecka-Operacz and A. Sadowska-Przytocka, "The possibilities and principles of methotrexate treatment of psoriasis - the updated knowledge," *Postepy Dermatologii Alergologii*, vol. 31, no. 6, pp. 392–400, 2014.
- [104] G. Piskin, V. M. Heydendael, M. A. de Rie, J. D. Bos, and M. B. Teunissen, "Cyclosporin A and methotrexate are

- equally effective in reducing T cell numbers in psoriatic skin lesions but have no consistent effect on IFN-gamma and IL-4 expression in psoriatic skin in situ," *Archives of Dermatological Research*, vol. 294, no. 12, pp. 559–562, 2003.
- [105] T. Elango, H. Dayalan, P. Gnanaraj, H. Malligarjunan, and S. Subramanian, "Impact of methotrexate on oxidative stress and apoptosis markers in psoriatic patients," *Clinical and Experimental Medicine*, vol. 14, no. 4, pp. 431–437, 2014.
- [106] A. Al Maruf, P. J. O'Brien, P. Naserzadeh, R. Fathian, A. Salimi, and J. Pourahmad, "Methotrexate induced mitochondrial injury and cytochrome c release in rat liver hepatocytes," *Drug and Chemical Toxicology*, vol. 41, no. 1, pp. 51–61, 2018.
- [107] O. Akbulak, A. S. Karadag, N. Akdeniz et al., "Evaluation of oxidative stress via protein expression of glutathione S-transferase and cytochrome p450 (CYP450) isoenzymes in psoriasis vulgaris patients treated with methotrexate," *Cutaneous and Ocular Toxicology*, vol. 37, no. 2, pp. 180–185, 2018.
- [108] S. G. Felemban, M. A. Aldubayan, A. H. Alhowail, and I. S. Almami, "Vitamin B17 ameliorates methotrexate-induced reproductive toxicity, oxidative stress, and testicular injury in male rats," *Oxidative Medicine and Cellular Longevity*, vol. 2020, Article ID 4372719, 11 pages, 2020.
- [109] M. Roghani, H. Kalantari, M. J. Khodayar et al., "Alleviation of liver dysfunction, oxidative stress and inflammation underlies the protective effect of ferulic acid in methotrexate-induced hepatotoxicity," *Drug Design, Development and Therapy*, vol. Volume 14, pp. 1933–1941, 2020.
- [110] J. U. Welbat, S. Naewla, W. Pannangrong, A. Sirichoat, A. Aranarochana, and P. Wigmore, "Neuroprotective effects of hesperidin against methotrexate-induced changes in neurogenesis and oxidative stress in the adult rat," *Biochemical Pharmacology*, vol. 178, article 114083, 2020.
- [111] M. C. Zimmerman, D. L. Clemens, M. J. Duryee et al., "Direct antioxidant properties of methotrexate: inhibition of malondialdehyde-acetaldehyde-protein adduct formation and superoxide scavenging," *Redox Biology*, vol. 13, pp. 588–593, 2017.
- [112] D. Boda, C. Negrei, F. Nicolescu, and C. Balalau, "Assessment of some oxidative stress parameters in methotrexate treated psoriasis patients," *Farmácia*, vol. 62, pp. 704–710, 2014.
- [113] A. García-Sánchez, A. G. Miranda-Díaz, and E. G. Cardona-Muñoz, "The role of oxidative stress in physiopathology and pharmacological treatment with pro- and antioxidant properties in chronic diseases," *Oxidative Medicine and Cellular Longevity*, vol. 2020, Article ID 2082145, 16 pages, 2020.
- [114] A. Mei-Yen Yong, L. Juay Kang Hng, E. Tan Yu Yuan, S. Woo Jia Qian, and C. Tan Lixian, "Targeted and localized phototherapy for atopic dermatitis and psoriasis: an eight-year experience in a tertiary dermatological centre in Singapore," *Photodermatology, Photoimmunology & Photomedicine*, vol. 37, no. 6, pp. 571–574, 2021.
- [115] P. Filipe, I. Emerit, A. Alaoui Youssefi et al., "Oxyradical-mediated clastogenic plasma factors in psoriasis: increase in clastogenic activity after PUVA," *Photochemistry and Photobiology*, vol. 66, no. 4, pp. 497–501, 1997.
- [116] M. S. Cooke, M. D. Evans, K. Patel et al., "Induction and Excretion of Ultraviolet-Induced 8-Oxo-2'-deoxyguanosine and Thymine Dimers In Vivo : Implications for PUVA," *The Journal of Investigative Dermatology*, vol. 116, no. 2, pp. 281–285, 2001.
- [117] H. Orimo, Y. Tokura, R. Hino, and H. Kasai, "Formation of 8-hydroxy-2'-deoxyguanosine in the DNA of cultured human keratinocytes by clinically used doses of narrowband and broadband ultraviolet B and psoralen plus ultraviolet A," *Cancer Science*, vol. 97, no. 2, pp. 99–105, 2006.
- [118] S. Coimbra, H. Oliveira, F. Reis et al., "Psoriasis therapy and cardiovascular risk factors," *American Journal of Clinical Dermatology*, vol. 11, no. 6, pp. 423–432, 2010.
- [119] S. Coimbra, H. Oliveira, F. Reis et al., "Erythroid disturbances before and after treatment of Portuguese psoriasis vulgaris patients: a cross-sectional and longitudinal study," *American Journal of Clinical Dermatology*, vol. 13, no. 1, pp. 37–47, 2012.

Research Article

Melissa officinalis L. Supplementation Provides Cardioprotection in a Rat Model of Experimental Autoimmune Myocarditis

Nevena D. Draginic ^{1,2} Vladimir L. Jakovljevic ^{2,3} Jovana N. Jeremic ¹
Ivan M. Srejavic ³ Marijana M. Andjic ¹ Marina R. Rankovic,¹ Jasmina Z. Sretenovic ³
Vladimir I. Zivkovic ³ Biljana T. Ljubic ⁴ Slobodanka L. Mitrovic ⁵
Stefani S. Bolevich ⁶ Sergey B. Bolevich ² and Isidora M. Milosavljevic ¹

¹Department of Pharmacy, Faculty of Medical Sciences, University of Kragujevac, 34000 Kragujevac, Serbia

²Department of Human Pathology, First Moscow State Medical University I.M. Sechenov, Moscow, Russia

³Department of Physiology, Faculty of Medical Sciences, University of Kragujevac, 34000 Kragujevac, Serbia

⁴Department of Genetics, Faculty of Medical Sciences, University of Kragujevac, 34000 Kragujevac, Serbia

⁵Department of Pathology, Faculty of Medical Sciences, University of Kragujevac, 34000 Kragujevac, Serbia

⁶Department of Pathophysiology, 1st Moscow State Medical University IM Sechenov, Moscow, Russia

Correspondence should be addressed to Vladimir L. Jakovljevic; drvladakbg@yahoo.com

Received 19 October 2021; Accepted 9 February 2022; Published 28 February 2022

Academic Editor: Abdur Rauf

Copyright © 2022 Nevena D. Draginic et al. This is an open access article distributed under the Creative Commons Attribution License, which permits unrestricted use, distribution, and reproduction in any medium, provided the original work is properly cited.

Due to existing evidence regarding antioxidant and anti-inflammatory effects of *Melissa officinalis* extracts (MOEs), this study was aimed at investigating the potential of ethanolic MOE to prevent the development of myocarditis and its ability to ameliorate the severity of experimental autoimmune myocarditis (EAM) by investigating MOE effects on *in vivo* cardiac function, structure, morphology, and oxidative stress parameters. A total of 50 7-week-old male *Dark Agouti* rats were enrolled in the study and randomly allocated into the following groups: CTRL, nontreated healthy rats; EAM, nontreated rats with EAM; MOE50, MOE100, and MOE200, rats with EAM treated with either 50, 100, or 200 mg/kg of MOE for 3 weeks *per os*. Myocarditis was induced by immunization of the rats with porcine myocardial myosin (0.5 mg) emulsion on day 0. Cardiac function and dimensions of the left ventricle (LV) were assessed via echocardiography. Additionally, the blood pressure and heart rate were measured. On day 21, rats were sacrificed and the hearts were isolated for further histopathological analyses (H/E and Picrosirius red staining). The blood samples were collected to determine oxidative stress parameters. The EAM group characteristically showed greater LV wall thickness and lower ejection fraction ($50.33 \pm 7.94\%$ vs. $84.81 \pm 7.74\%$) and fractional shortening compared to CTRL ($p < 0.05$). MOE significantly improved echocardiographic parameters (EF in MOE200 $81.44 \pm 5.51\%$) and also reduced inflammatory infiltrate (by 88.46%; $p < 0.001$) and collagen content (by 76.39%; $p < 0.001$) in the heart tissues, especially in the MOE200 group compared to the EAM group. In addition, MOEs induced a significant decrease of prooxidants production (O_2^- , H_2O_2 , and TBARS) and improved antioxidant defense system via increase in GSH, SOD, and CAT compared to EAM, with medium and high dose being more effective than low dose ($p < 0.05$). The present study suggests that ethanolic MOEs, especially in a 200 mg/kg dose, improve cardiac function and myocardial architecture, possibly via oxidative stress mitigation, thus preventing heart remodeling, development of dilated cardiomyopathy, and subsequent heart failure connected with EAM. MOEs might be considered as a potentially helpful adjuvant therapy in patients with autoimmune myocarditis.

1. Introduction

Myocarditis is an inflammatory heart disease characterized by nonischemic inflammatory infiltrates in the heart tissue associated with necrosis and/or degeneration of cardiomyocytes. Several entities have been identified as the causes of myocarditis, such as viral or bacterial infections, drugs or toxin usage, and autoimmune processes. Acute myocardial inflammation may progress to subacute and chronic phases and ultimately lead to tissue remodeling, fibrosis, myocardium architecture damage, and depressed contractile function [1]. Autoimmune myocarditis, also known as *giant cell* myocarditis, is associated with poor prognosis since it often leads to dilated cardiomyopathy (DCM) in chronic stages. It is also estimated that one-third of autoimmune myocarditis cases develop heart failure, and almost 40% of all heart failures in the population under 40 is actually associated with autoimmune myocarditis. In addition, autoimmune myocarditis tends to be unrecognized in patients with DCM, until *post mortem* histopathological analyses, as its clinical presentation varies widely [2].

Taking into account that current therapeutic options for myocarditis are limited to symptomatic treatment for arrhythmias and heart failure and that no effective therapeutic strategy has been developed yet [2], the search for novel efficient therapeutic options is necessary. The most commonly used animal model of *giant cell* autoimmune myocarditis is EAM on rodents, which allows investigation of the mechanisms involved in this pathology, as well as testing of novel treatments [2–4]. The usage of natural products in the treatment of cardiovascular disease is gaining popularity owing to their safety, fewer side effects, and lower costs. In recent years, preclinical and clinical research has been focused on identifying innovative phytomedicines, including plant extracts with high anti-inflammatory and antioxidant potential, and especially on identifying active components responsible for cardioprotection [5, 6].

Melissa officinalis L. (*Lamiaceae*), also known as lemon balm, is a perennial herb belonging to lemon scent, mint family of plants. It has been widely used in traditional medicine for centuries, mainly because of its beneficial effects on the nervous system, including anxiety symptoms and palpitation relieving, mild sedative, and hypnotic effects. In addition, a plethora of pharmacological activities of lemon balm have been described: hypoglycemic, hepatoprotective, antibacterial, anti-inflammatory, antioxidant, antiviral, antispasmodic, neuroprotective, and cytotoxic effects. Literature data also suggests its beneficial effects on the cardiovascular system such as antiarrhythmic and vasorelaxant properties and protective effects in myocardial ischemia-reperfusion injury [7–9]. These cardiovascular effects of MOEs are connected to their antioxidant potential and free radical scavenging properties. Polyphenolic compounds particularly rosmarinic acid, as the major component, but also cinnamic, protocatechuic, caffeic, ferulic, and ellagic acids; flavonoids (quercetin, luteolin, apigenin, catechin, epicatechin, and rutin); and triterpenoids ursolic and oleanolic acids are highlighted as the active compounds responsible for MOE antioxidant potential. Additionally, anti-inflammatory potential

of MOEs has been proven in the carrageenan-induced paw edema model, which may be very useful in EAM [10, 11]. It is suggested that modulation of immune response by MOEs is achieved by strong anti-inflammatory potential of rosmarinic acid and triterpenoids.

Up until now, the beneficial effects of bioactive plant compounds such as curcumin, quercetin, apigenin, berberine, resveratrol, oleanolic acid, catechin, and epigallocatechin have been confirmed in EAM model [12–14]. Several mechanisms mediate these beneficial effects, including modulation of oxidative stress, suppression of apoptosis and fibrosis, and modulation of the immune response and cytokine concentration [5, 6, 15–17]. Nonetheless, the effects of MOEs in this pathology are entirely unexplored.

Considering proven antioxidant and anti-inflammatory effects of MOEs, we aimed to investigate the potential of ethanolic MOE to prevent the development of myocarditis and its ability to ameliorate the severity of EAM by investigating MOEs effects on *in vivo* cardiac function, structure, morphology, and oxidative stress parameters.

2. Materials and Methods

2.1. Ethical Standards. All experimental procedures involving laboratory animals used in this research were approved by Ethics Committee for experimental animal well-being of the Faculty of Medical Sciences, University of Kragujevac (Kragujevac, Serbia) No. 01-10171. Furthermore, all the experimental procedures were performed according to European Directive 2010/63/EU for the welfare of laboratory animals, number and principles of Good Laboratory Practice (GLP) (86/609/EEC). Additionally, experiments were carried out following the European Union Directive 86/609/EES for the Protection of the Vertebrate Animals used for Experimental and other Scientific Purposes and the principles of ethics.

2.2. Plant Material and Plant Extraction. For the purposes of this research, dried leaves of *Melissa officinalis* L. (*Lamiaceae*) purchased from *Bilje Borca, LLC* (Belgrade, Serbia) were used. The dried plant material was pulverized with a mill (*IKA A11, Germany*) and stored in well-sealed paper bags at room temperature until the extract was made. The ethanolic MOE was obtained under the reflux of the solvent. This method involves extraction at the boiling point of the solvent (70% ethanol). The extraction was performed for 2.5 hours, after which the mixture was filtered through gauze and left at room temperature to spontaneously precipitate ballast substances. Finally, the obtained liquid extract was filtered (*Whatman, No. 1*), while we used a rotary vacuum evaporator (*RV05 basic IKA, Germany*) at 40°C, 90 rpm, and 250 mbar vacuum to obtain dry extract, which was stored in dark glass vials at +4°C until administration [18].

2.3. Animals. The study involved a total of 50 seven-week-old male *Dark Agouti* (DA) rats, weighing 150 ± 20 g at the beginning of the experiment, purchased from the Military Medical Academy Animal House, Belgrade. Firstly, animals were acclimatized for two weeks and kept in polyethylene

cages (4 per cage) under standardized controlled environmental conditions ($22 \pm 2^\circ\text{C}$ and a 12 h light/dark cycle). Free access to standard food (9% fat, 20% protein, and 53% starch) and water (*ad libitum*) was provided for all animals.

2.4. Induction of Experimental Autoimmune Myocarditis. Calcium-activated myosin from the porcine heart (Sigma-Aldrich, Munich, Germany) was dissolved in 0.01 M phosphate-buffered saline (PBS) in one tube and emulsified with an equal volume of complete Freund's adjuvant (FCA) supplemented with Mycobacterium tuberculosis (strain H37 RA; Difco Laboratories, Detroit, MI) at a concentration of 10 mg/ml mixed in a separate tube. The suspensions from both tubes were then mixed, vortexed, and transferred to a syringe. The suspension was then homogenized by moving the content back and forth between the two syringes for 60 min. The final volume of the suspension was drawn into a 1 ml sterile syringe with Luer-Lock tip and connected to a 26G needle. The suspension was prepared *ex tempore* on the day of immunization. On day 0, the rats were injected subcutaneously into both rear hind footpads with 0.1 ml of final emulsion (0.05 ml per footpad), yielding an immunizing dose of 0.25 mg/body of cardiac myosin per rat. The CFA emulsified with PBS was applied to the control group [19].

2.5. Study Design. The rats ($n = 50$) were randomly allocated into five different groups: CTRL, healthy nontreated rats; EAM, nontreated rats with myocarditis; and MOE50, MOE100, and MOE200, rats with myocarditis treated with three different doses (50 mg/kg, 100 mg/kg, and 200 mg/kg) of ethanolic MOEs. Treatment involved daily *per os* application (every day at the same time) of MOE dissolved in distilled water, *ex tempore* (volume of 300 μl approximately). All animals were weighed during the protocol to adjust the MOE dose according to the rats' body weight.

2.6. Hw/Bw and Sw/Bw Ratios. The rat's body weight was measured directly before *in vivo* functional analysis. Afterward, the rats were sacrificed and the hearts and spleens were isolated and measured in order to calculate relative heart weight (Hw) and spleen weight (Sw) to body weight (Hw/Bw and Sw/Bw) ratios.

2.7. Blood Pressure and Heart Rate Measurement. The systolic and diastolic blood pressures (SBP and DBP) and heart rate (HR) were measured by a tail-cuff noninvasive method BP system (Rat Tail Cuff Method Blood Pressure Systems (MRBP-R), IITC Life Science Inc., Los Angeles, CA, USA) twice, first at the beginning of the experimental protocol (day 0) in order to check the homogeneity of the animals, when no difference was found, and then after accomplishing the 3-week protocol before sacrificing the animals (day 21) [20].

2.8. Echocardiographic Analyses. Transthoracic echocardiography was performed to assess the effects of MOE on *in vivo* cardiac function and the development of autoimmune myocarditis. The procedure was repeated twice, first at the beginning (day 0) to check the homogeneity of the animals and

their health, when no difference was found, and then at the end of the experimental protocol (day 21) before sacrificing the animals. The animals were anesthetized with mixture of ketamine (75 mg/kg) and xylazine (5 mg/kg) intraperitoneally. Echocardiograms were performed using a Hewlett-Packard Sonos 5500 (Andover, MA, USA) sector scanner equipped with a 15.0 MHz phased-array transducer as in our previous research [20]. From the parasternal long-axis view in 2-dimensional mode, and M-mode cursor was positioned perpendicularly to the interventricular septum and posterior wall of the left ventricle (LV) at the papillary muscle level and M-mode images were obtained. The following parameters were measured: interventricular septal wall thickness at end-diastole (IVSd), LV internal dimension at end-diastole (LVIDd), LV posterior wall thickness at end-diastole (LVPWd), interventricular septal wall thickness at end-systole (IVSs), LV internal diameter at end-systole (LVIDs), and LV posterior wall thickness at end-systole (LVPWs) were recorded with M-mode. Fractional shortening percentage (FS%) was calculated from the M-mode LV diameters using the equation $[(LVIDd - LVIDs)/LVIDd] \times 100\%$, where LVIDd is left ventricular end diastolic diameter and LVIDs is left ventricular end-systolic diameter. Ejection fraction (EF%) was calculated according to the Teichholz formula [21], where LVEDV represents LV end-diastolic volume, while LVESV represents LV end-systolic volume.

$$EF = 100 \times \frac{(LVEDV - LVESV)}{LVEDV} \quad (1)$$

$$= \frac{(7 \times LVIDs)}{(2.4 \times LVIDs)} LVEDV = \frac{(7 \times LVIDd)}{(2.4 \times LVIDd)}$$

2.9. Biochemical Analyses-Oxidative Stress Parameters. After completing the 3-week protocol, all animals were anesthetized by short ketamine and xylazine narcosis and sacrificed by decapitation. The blood samples were collected to determine oxidative stress parameters spectrophotometrically (Shimadzu UV 1800 spectrophotometer, Kyoto, Japan). The blood samples were centrifuged in order to separate the plasma and obtain red blood cell (RBC) lysate suspension by washing isolated separated RBCs 3 times with ice cold saline. The following prooxidant parameters were determined from plasma samples: superoxide anion radical (O_2^-), hydrogen peroxide (H_2O_2), nitrites (NO_2^-), and index of lipid peroxidation measured as thiobarbituric acid reactive substances (TBARS). Antioxidant protection parameters were determined from erythrocyte lysate samples: the activity of catalase (CAT) and superoxide-dismutase (SOD) and the level of reduced glutathione (GSH).

2.9.1. Determination of Prooxidants (O_2^- , H_2O_2 , NO_2^- , and TBARS). The quantification of superoxide anion radical was based on the reaction of O_2^- with nitro blue tetrazolium (NBT). The protocol included mixing of 50 μl of plasma samples and 950 μl of assay mixture, followed by measuring on 550 nm in triplicate every 60 s [22].

The hydrogen peroxide (H_2O_2) determination method was based on the oxidation of phenol red with horseradish peroxidase enzyme. 200 μl of plasma sample was mixed with

800 μl of PRS (phenol red solution) and 10 μl POD (horse-radish peroxidase (1:20)). Measuring was performed at 610 nm [22].

Nitric oxide (NO) level was assessed indirectly by measuring nitrite concentration, since NO decomposes rapidly forming an equal amount of nitrite products. First, 100 μl of PCA (perchloric acid), 400 μl of 20 mM ethylenediaminetetraacetic acid (EDTA), and 200 μl of the plasma sample were mixed, put on the ice for 15 min, and centrifuged for 15 min at 6000 rpm. After separating the supernatant, 220 μl K_2CO_3 was added. Measuring was performed at 550 nm [22].

Index of lipid peroxidation in the plasma samples was estimated indirectly by measuring TBARS. First, TBA extract was made by mixing 800 μl sample and 400 μl trichloroacetic acid (TCA), which was then put on ice for 10 min and centrifuged for 15 min at 6000 rpm. Next, 1% TBA (thiobarbituric acid) in 0.05 NaOH was incubated with the obtained sample at 100°C for 15 min and after 10 min measured at wavelength of 530 nm [22].

2.9.2. Determination of Antioxidants (SOD, CAT, and GSH). Obtained lysates containing about 50 g Hb/l were used to determine antioxidant enzyme activity. CAT buffer, sample, and 10 mM H_2O_2 were used for CAT determination. Detection was performed at 360 nm [22]. SOD activity was evaluated by the epinephrine method. Lysate sample was first mixed with carbonate buffer, and then epinephrine was added. Detection was performed at 470 nm. The amount of SOD and CAT was expressed as U/g Hb $\times 103$ [23, 24]. The reduced glutathione (GSH) level was determined by GSH oxidation with 5,5-dithiobis-6,2-nitrobenzoic acid. GSH extract was made by mixing 100 μl 0.1% EDTA, 400 μl lysate, and 750 μl precipitation solution (1.67 g metaphosphoric acid, 0.2 g EDTA, 30 g NaCl, and filled with distilled water to 100 ml). This was followed by mixing in the vortex machine and extraction on cold ice (15 min) and centrifugation at 4000 rpm (10 min). Distilled water was used as a blank probe. The level of GSH was measured at 420 nm and expressed as nanomoles per milliliter of RBCs [22].

2.10. Histological Analyses of the Heart. The isolated hearts were measured and then cut into two halves so that the left and right halves of the heart were available for further histological analysis. The hearts were then fixed in 4% neutral paraformaldehyde, dehydrated in increasing alcohol concentrations (70%, 96%, and 100%), cleared in xylene, immersed in paraffin, and prepared for further analysis. 5 μm thick serial sections were stained by the H/E (hematoxylin/eosin) method for the purpose of morphometric analysis of cells and verification of morphological changes and by the Picrosirius red staining for collagen detection. Images of heart tissue sections were taken on an *Olympus BX51 light microscope*. Morphometric analysis of cardiomyocytes (longitudinal section diameter as well as cross-sectional area) was performed in the *Axiovision image analysis program* (Zeiss, USA), where 100-120 cells per animal were analyzed [25]. The cell infiltrate density and the collagen content were analyzed using *Image Pro-Plus programs* (Media Cybernetics,

USA). The analysis of cell infiltrate density and the collagen content was performed on 10 sections, of the total number of serial sections of the heart, with every 20th section of heart tissue analyzed, i.e., the distance between the analyzed plates was 100 μm . The results are presented as percentages. It is important to emphasize that no cell infiltrate was verified in the control group, and the value for infiltrate density was presented as 0%.

2.11. Statistical Analyses. IBM SPSS 20.0 was used for statistical data processing for Windows. The Kolmogorov-Smirnov and Shapiro-Wilk tests, histogram, and normal QQ plot tests were used to examine the normality of the distribution. Data are expressed as mean value (\bar{X}) \pm standard deviation (SD) and analyzed by one-way analysis of variance (ANOVA), followed by the Bonferroni test. A value of $p < 0.05$ was considered significant.

3. Results

3.1. Effects of MOE on Hw/Bw and Sw/Bw Ratios. Immunized nontreated EAM rats and rats treated with a low dose of MOE (MOE50) were shown to have significantly increased heart weights and Hw/Bw ratio compared to the healthy CTRL group ($p < 0.01$). Additionally, medium and high doses of MOE (groups MOE100 and MOE200) significantly lowered heart weights and Hw/Bw ratio compared to both EAM and MOE50 groups ($p < 0.05$). The EAM group also showed a significantly increased Sw and Sw/Bw ratio compared to CTRL, while MOE100 and MOE200 significantly lowered these two parameters. The Sw/Bw ratio reduction was the most prominent in the MOE200 group (Table 1).

3.2. Effects of MOE on Hemodynamic Parameters. Three weeks post-immunization, significantly elevated HR was observed in the EAM group compared to CTRL, while treatment with extract induced a significant HR reduction in all three dose regimens compared to EAM. Additionally, medium and high doses of extract in combination with EAM induced a significant HR reduction compared to CTRL. Systolic blood pressure was shown to be lowered in the MOE200 group compared to the CTRL, EAM, and MOE50 groups ($p < 0.05$), while no significant differences in this parameter were noticed between other groups. Also, no significant changes in DBP were observed between groups (Table 2).

Significantly decreased ejection fraction was observed in immunized EAM and MOE50 rats compared to CTRL animals (50.33% and 53.89% vs. 84.82%, $p < 0.01$), while treatment with MOE100 and MOE200 (72.47% and 81.44%) markedly improved EF after 3-week supplementation compared to both the EAM and MOE50 groups. Only the highest dose MOE200 succeeded in normalizing EF to levels similar to CTRL values. A similar trend was observed in the FS parameter, which was significantly lower in EAM rats relative to CTRL, while all three doses of MOE led to an increment of FS compared to the EAM group ($p < 0.05$). The EAM group was also associated with LVPWd and LVPWs thickening compared to healthy rat hearts, all three

TABLE 1: Effects of MOEs on body weight (Bw), heart weight (Hw), heart weight/body weight ratio (Hw/Bw ratio), spleen weight (Sw), and spleen weight/body weight ratio (Sw/Bw ratio). CTRL: control group; EAM: experimental autoimmune myocarditis group; MOE50, MOE100, and MOE200: groups of rats treated with either 50, 100, or 200 mg/kg of *Melissa officinalis* extract. Statistical significance at the level of $p < 0.05$ * compared to CTRL, # compared to EAM, and † compared to MOE50. Data are expressed mean \pm standard deviation.

	CTRL	EAM	MOE50	MOE100	MOE200
Bw (g)	215.29 \pm 5.71	212 \pm 14.97	195.88 \pm 9.34	189 \pm 10.06	194.25 \pm 6.14
Hw (mg)	777.14 \pm 34.50	1014.47 \pm 110.89*	937.50 \pm 88.28*	760.23 \pm 67.17 [#]	782.34 \pm 29.73 [#]
Sw (mg)	403.29 \pm 23.61	447.57 \pm 15.08*	398.13 \pm 23.90	351.38 \pm 30.89 [#]	335.12 \pm 15.57 [#]
Hw/Bw ratio (mg/g)	3.61 \pm 0.24	4.81 \pm 0.80*	4.80 \pm 0.60*	4.02 \pm 0.33 [#]	4.10 \pm 0.27 [#]
Sw/Bw ratio (mg/g)	1.87 \pm 0.08	2.12 \pm 0.17*	2.04 \pm 0.20	1.86 \pm 0.14 [#]	1.71 \pm 0.07 [#]

TABLE 2: Effects of MOEs on systolic (SBP), diastolic blood pressure (DBP), and heart rate (HR). CTRL: control group; EAM: experimental autoimmune myocarditis group; MOE50, MOE100, and MOE200: groups of rats treated with either 50, 100, or 200 mg/kg of *Melissa officinalis* extract. Statistical significance at the level of $p < 0.05$ * compared to CTRL, # compared to EAM, and † compared to MOE50. Data are expressed means \pm standard deviation.

	CTRL	EAM	MOE50	MOE100	MOE200
SBP (mmHg)	133.60 \pm 7.60	133.25 \pm 6.13	124.75 \pm 5.85	121.00 \pm 5.72	113.80 \pm 4.95 ^{*#}
DBP (mmHg)	81.40 \pm 4.93	78.75 \pm 6.08	79.25 \pm 8.42	80.00 \pm 5.35	68.60 \pm 4.95
HR (beats/min)	367.60 \pm 17.62	453.75 \pm 40.54*	373.50 \pm 18.73 [#]	333.00 \pm 11.22 ^{*#}	332.60 \pm 25.46 ^{*#}

doses of MOE led to reduction of these parameters, while MOE200 seemed to normalize these values to levels similar to control ones (Figure 1 and Table 3).

3.3. Effects of MOE on Oxidative Stress Parameters. Three weeks post-induction of EAM, significantly higher release of all measured prooxidant markers (O_2^- , H_2O_2 , NO_2^- , and TBARS) was observed in EAM rats compared to the CTRL group ($p < 0.05$). However, treatment with MOE in all three doses succeeded in significantly decreasing the level of TBARS and NO_2^- ($p < 0.05$) compared to EAM, with no effect on the level of hydrogen peroxide. The level of superoxide anion radical was significantly lowered only by medium and high dose MOE100 and MOE200 compared to EAM. In addition, the highest and medium dose of the applied extract showed a more dominant effect on O_2^- , NO_2^- , and TBARS compared to MOE50 (Figure 2). Regarding antioxidants, significantly lower activity of antioxidant enzymes CAT and SOD and the level of GSH were observed in the EAM group ($p < 0.05$), while MOE treatment improved antioxidant protection via an increase in all three parameters compared to EAM ($p < 0.05$). Medium and high doses of MOE significantly improved all three parameters compared to EAM and MOE50. Additionally, medium and high dose of MOE significantly improved SOD and GSH compared to the CTRL group ($p < 0.05$). No differences were observed between the MOE200 and MOE100 groups in all 3 measured parameters ($p > 0.05$). Low-dose MOE50 improved SOD and CAT compared to EAM to a lesser extent than MOE100 and MOE200 (Figure 3).

3.4. Effects of MOE on Myocardium Structure

3.4.1. Hematoxylin-Eosin Staining. The preserved myocardial structure was observed in the CTRL group of rats. H-

E-stained sections of the EAM group of rats confirmed the presence of severe myocarditis characterized by massive inflammatory cell infiltration, destruction of myocardial fibers, swelling of cardiomyocytes, interstitial edema, and increased sarcoplasmic eosinophilia. However, MOE treatment especially MOE200 improved cardiac structure after 3-week treatment. EAM heart tissue sections showed a significant presence of inflammatory infiltrate compared to CTRL healthy hearts. Inflammatory infiltrate consisted of different leukocytes including mononuclear cells, polymorphonuclear neutrophils and multinucleated giant cells, which mainly infiltrated the epicardium of the ventricular wall. Namely, all three doses of MOE (MOE50, MOE100, and MOE200) significantly reduced inflammatory infiltrate density (by 44.38%, 71.37%, and 88.46%) compared to the EAM group (Figure 4). Additionally, significant differences between different doses of MOE were observed, and a dose-dependent effect was noticed ($p < 0.01$).

3.4.2. Picosirius Red Staining. Analysis of Picosirius red staining in the heart tissue section revealed higher amount of fibrosis in the EAM group, while MOE treatment, especially MOE200, significantly decreased fibrosis compared to EAM, MOE50, and MOE100. Experimental autoimmune myocarditis (EAM group) induced significant almost three-fold increase (by 261.31%) in collagen content compared to the CTRL group of healthy rat hearts ($p < 0.01$), while 3-week MOE treatment succeeded to diminish these changes. All three doses of MOE significantly reduced the elevated collagen content compared to EAM rats (MOE50 by 50.23%, MOE100 by 61.39%, and MOE200 by 76.39%) with the most prominent effect noticed in the MOE200 group which normalized the collagen content to CTRL values.

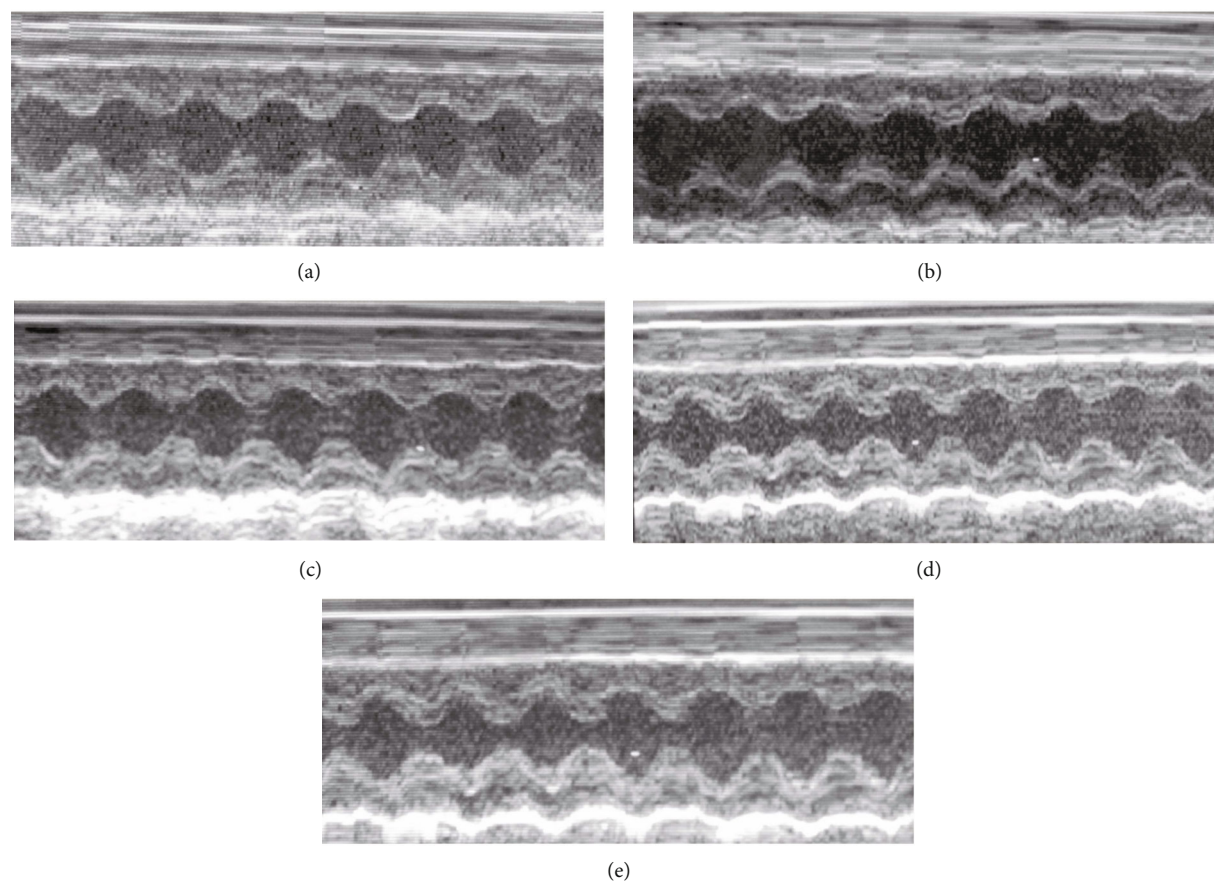


FIGURE 1: Representative M-mode echocardiograms. (a) CTRL, (b) EAM, (c) MOE50, (d) MOE100, and (e) MOE200. CTRL: control group; EAM: rats with experimental autoimmune myocarditis; MOE50, MOE100, and MOE200: groups of rats treated with either 50, 100, or 200 mg/kg of *M. officinalis* extract.

TABLE 3: Effects of MOEs on echocardiographic parameters: interventricular septal wall thickness at end-systole and end-diastole (IVSs and IVSd), left ventricular internal diameter at end-systole and end-diastole (LVIDs and LVIDd), left ventricular posterior wall thickness at end-systole and end-diastole (LVPWs and LVPWd), fractional shortening (FS), and ejection fraction (EF). CTRL: control group; EAM: experimental autoimmune myocarditis group; MOE50, MOE100, and MOE200: groups of rats treated with either 50, 100, or 200 mg/kg of *Melissa officinalis* extract. Statistical significance at the level of $p < 0.05^*$ compared to CTRL, $^\#$ compared to EAM, $^\$$ compared to MOE50, and § compared to MOE100. Data are expressed means \pm standard deviation.

	CTRL	EAM	MOE50	MOE100	MOE200
IVSd (cm)	0.150 \pm 0.039	0.174 \pm 0.035	0.145 \pm 0.032	0.148 \pm 0.018	0.140 \pm 0.012
LVIDd (cm)	0.452 \pm 0.059	0.433 \pm 0.027	0.450 \pm 0.056	0.477 \pm 0.046	0.516 \pm 0.033
LVPWd (cm)	0.152 \pm 0.027	0.193 \pm 0.029 [*]	0.179 \pm 0.015 [#]	0.169 \pm 0.024 ^{#\\$}	0.160 \pm 0.007 ^{#\\$}
IVSs (cm)	0.175 \pm 0.073	0.162 \pm 0.020	0.141 \pm 0.012	0.160 \pm 0.033	0.154 \pm 0.017
LVIDs (cm)	0.228 \pm 0.041	0.338 \pm 0.030	0.262 \pm 0.034	0.301 \pm 0.036	0.285 \pm 0.046
LVPWs (cm)	0.160 \pm 0.020	0.199 \pm 0.047 [*]	0.179 \pm 0.029 [#]	0.171 \pm 0.024 ^{#\\$}	0.161 \pm 0.007 ^{#\\$}
FS (%)	49.19 \pm 8.89	21.88 \pm 4.55 [*]	41.59 \pm 6.24 [#]	38.92 \pm 4.31 [#]	44.96 \pm 5.81 ^{#\\$}
EF (%)	84.81 \pm 7.74	50.33 \pm 7.94 [*]	53.89 \pm 4.85 [*]	72.47 \pm 8.48 ^{#\\$}	81.44 \pm 5.51 ^{#\\$}

Also, a dose-dependent effect of MOE treatment on collagen content was noticed ($p < 0.05$) (Figure 5).

3.5. Effects of MOE on Heart Morphometric Parameters. Both cross-section area and longitudinal diameters of cardiomyo-

cytes were significantly elevated in the EAM group of rats compared to the CTRL group ($p < 0.01$). However, MOE treatment significantly decreased these two parameters compared to the EAM group. Medium and high dose of MOE showed superior effects compared to a low dose of MOE

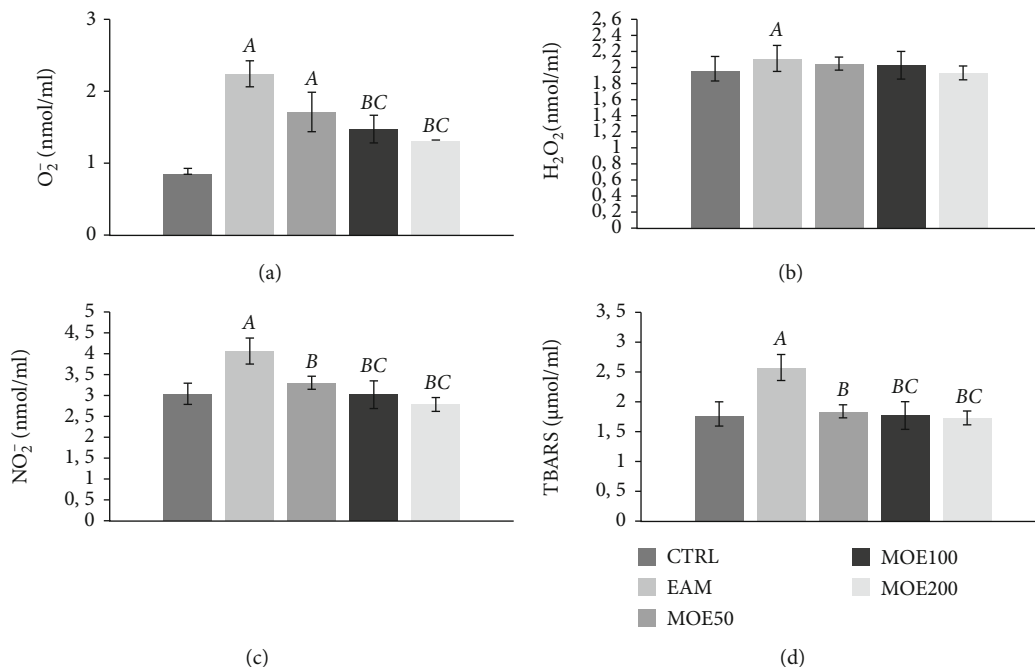


FIGURE 2: Effects of MOE on prooxidant parameters. (a) Superoxide anion radical (O_2^-), (b) hydrogen peroxide (H_2O_2), (c) nitrites (NO_2^-), and (d) index of lipid peroxidation measured as thiobarbituric acid reactive substances (TBARS). CTRL: control group; EAM: rats with experimental autoimmune myocarditis; MOE50, MOE100, and MOE200: groups of rats treated with either 50, 100, or 200 mg/kg of *Melissa officinalis* extract. Data are presented as means \pm standard deviation. Statistical significance at the level $p < 0.05$: A, compared to CTRL; B, compared to EAM; C, compared to MOE50; D, compared to MOE100; and E, compared to MOE200.

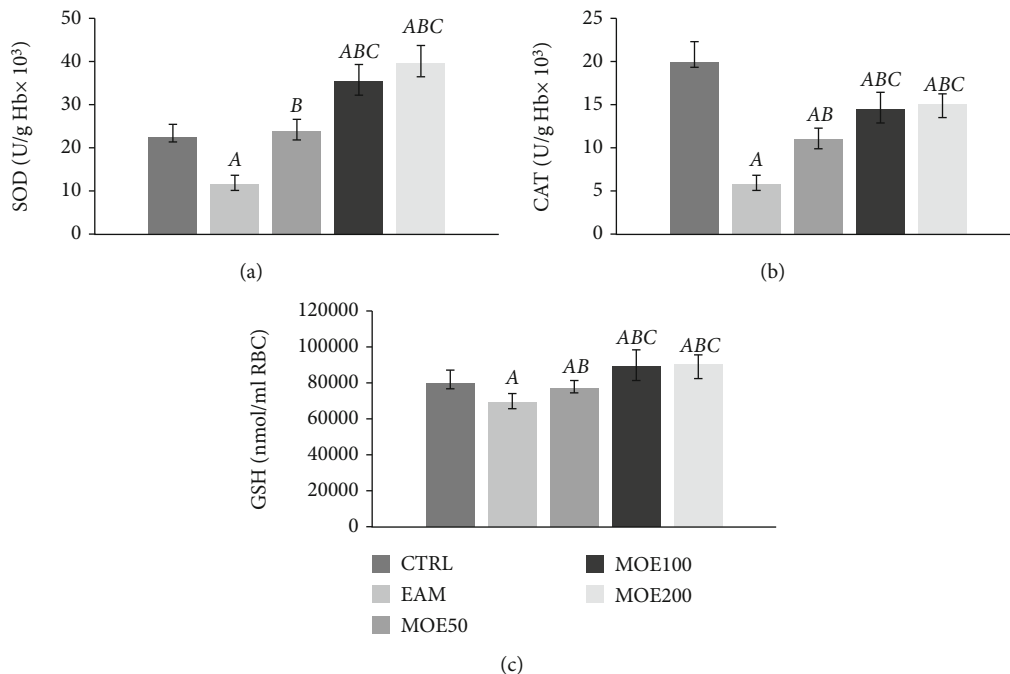


FIGURE 3: Effects of MOE on antioxidant parameters. (a) Superoxide dismutase (SOD), (b) catalase (CAT), and (c) reduced glutathione (GSH). CTRL: control group; EAM: rats with experimental autoimmune myocarditis; MOE50, MOE100, and MOE200: groups of rats treated with either 50, 100, or 200 mg/kg of *Melissa officinalis* extract. Data are presented as means \pm standard deviation. Statistical significance at the level $p < 0.05$: A, compared to CTRL; B, compared to EAM; C, compared to MOE50; D, compared to MOE100; and E, compared to MOE200.

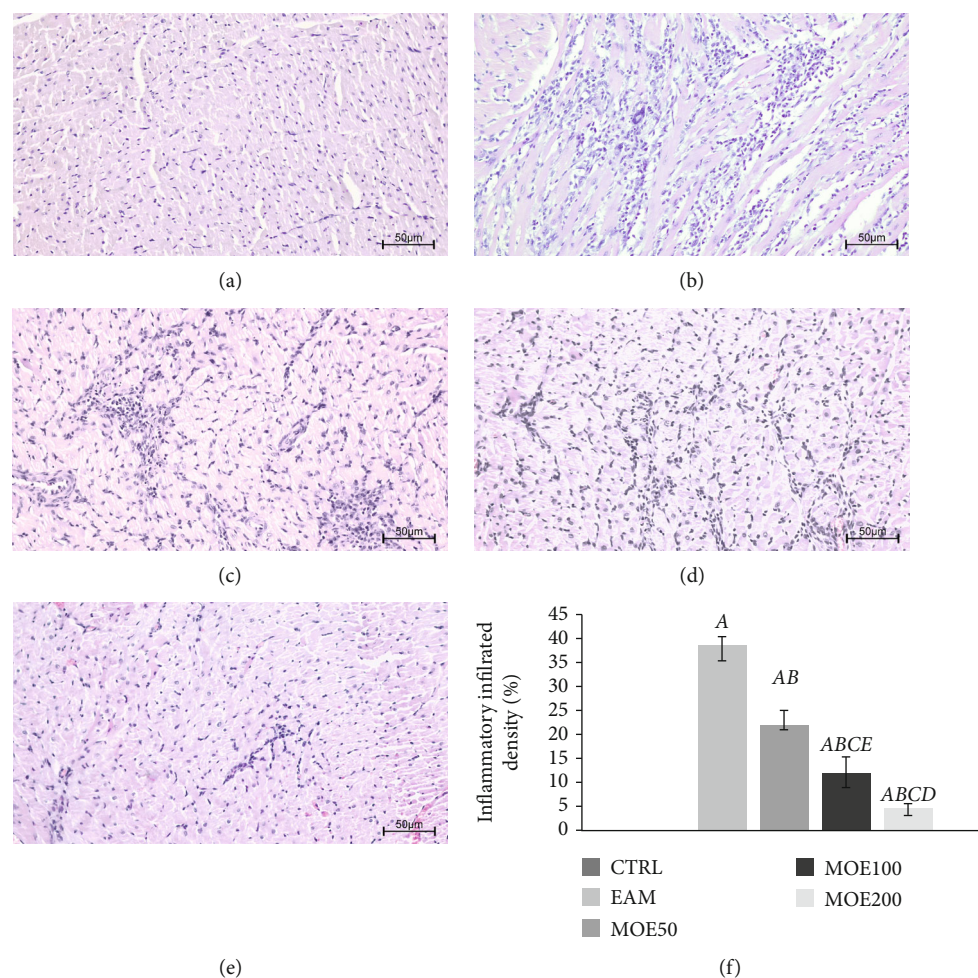


FIGURE 4: Representative heart tissue sections of H/E staining. Magnification 20x scale bar = 50 μm . (a) CTRL: control group; (b) EAM: experimental autoimmune myocarditis group; (c) MOE50: rats with EAM treated with *M. officinalis* extract in 50 mg/kg; (d) MOE100: rats with EAM treated with *M. officinalis* extract in 100 mg/kg; and (e) MOE200: rats with EAM treated with *M. officinalis* extract in 200 mg/kg. (f) Effects of MOE on heart inflammatory infiltrate density. Data are presented as means \pm standard deviation. Statistical significance at the level $p < 0.05$: A, compared to CTRL; B, compared to EAM; C, compared to MOE50; D, compared to MOE100; and E, compared to MOE200.

(MOE50 group) ($p < 0.01$). No differences in the measured parameters were noticed between MOE100 and MOE200 (Figure 6).

4. Discussion

Experimental autoimmune myocarditis in rats is associated with severe changes in the myocardial architecture including massive inflammatory cell infiltration and impaired cardiac function ultimately leading to heart remodeling and dilated cardiomyopathy (DCM). The pathophysiology of this disease is very complex and not fully elucidated yet. However, it is known that excessive ROS production and subsequent oxidative stress induce the release of inflammatory cytokines and chemokines included in leukocytes' migration to the heart tissue. Additionally, oxidative stress may cause cardiomyocyte damage by necrosis or apoptosis [2]. DCM involves the dilatation of the ventricles, which may impair systolic function [1]. Irreversible fiber damage, fibrosis, and finally heart failure may occur as the consequence of systolic dys-

function, leaving the heart transplantation as the only therapeutic option [26]. Even though there is evidence on natural products being useful in EAM pathology [5, 6], to the best of our knowledge, this is currently the first study dealing with the effects of *M. officinalis* in autoimmune myocarditis.

Hemodynamic measurements implicated that the EAM group was associated with a severe drop of ejection fraction (EF) and fractional shortening (FS), LV wall thickening, and increased heart rate. With morphometric changes, heart enlargement by increased Hw/Bw ratio, and cardiomyocyte cross section area and longitudinal diameter increment in EAM rats, all of the above-mentioned indicates disturbed heart function and the beginning of characteristic myocarditis induced DCM. Similar findings are presented in other studies using the EAM model [27, 28]. MOE treatment, especially MOE200, succeeded in improving myocardial function by normalizing EF and FS values and decreasing LVPW and preventing development of left ventricular remodeling and the progression to heart failure following myocarditis. However, recent data suggest that autoimmune

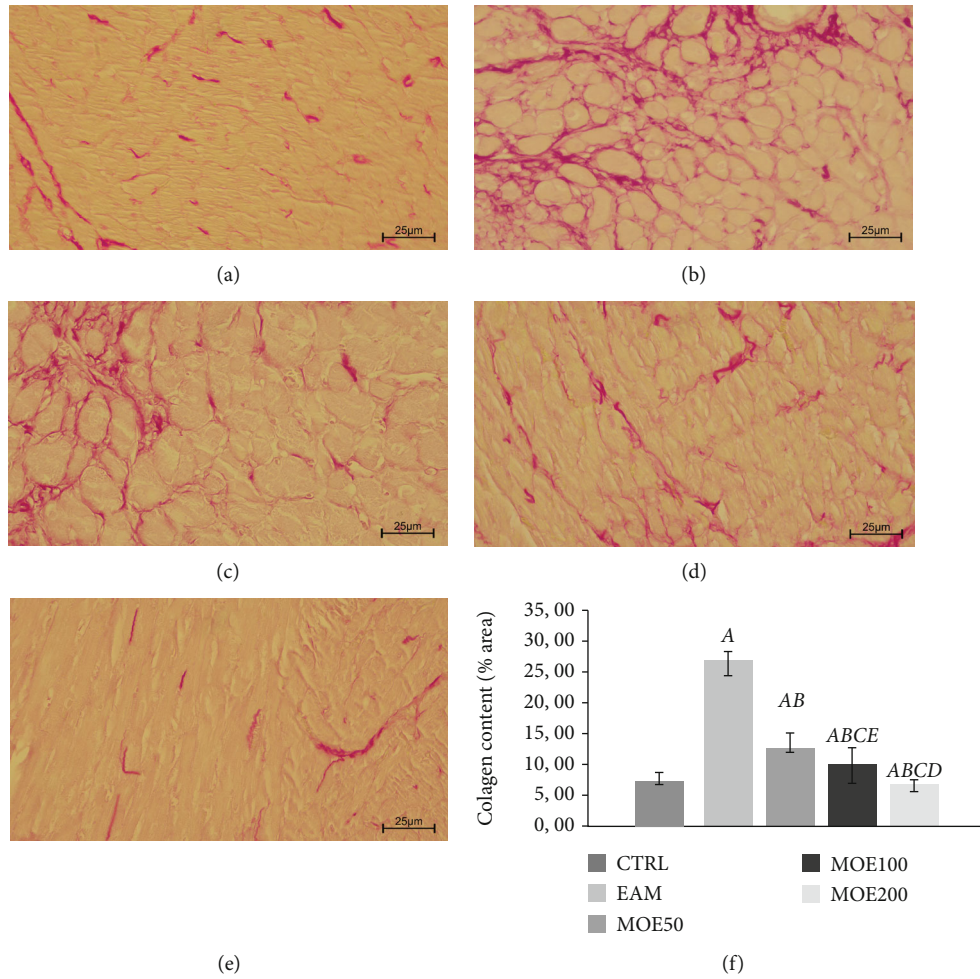


FIGURE 5: Representative heart tissue sections of Picosirius red staining. Magnification 40x scale bar = 25 μm. (a) CTRL: control group; (b) EAM: experimental autoimmune myocarditis group; (c) MOE50: rats with EAM treated with *M. officinalis* extract in 50 mg/kg; (d) MOE100: rats with EAM treated with *M. officinalis* extract in 100 mg/kg; and (e) MOE200: rats with EAM treated with *M. officinalis* extract in 200 mg/kg. (f) Effects of MOE on collagen content in heart tissue. Data are presented as means ± standard deviation. Statistical significance at the level $p < 0.05$: A, compared to CTRL; B, compared to EAM; C, compared to MOE50; D, compared to MOE100; and E, compared to MOE200.

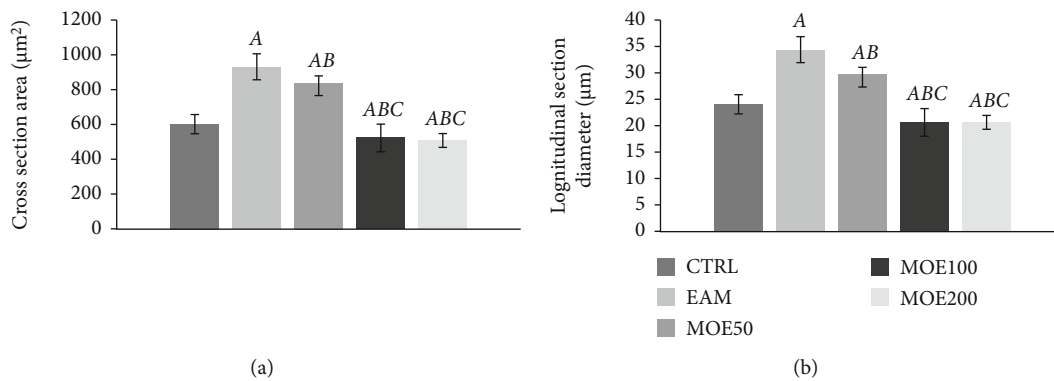


FIGURE 6: Effects of MOE treatment on morphometric parameters. CTRL: control group; EAM: experimental autoimmune myocarditis group; MOE50, MOE100, and MOE200: rats with EAM treated with *M. officinalis* extract in either 50 mg/kg, 100 mg/kg, or 200 mg/kg. Data are presented as means ± standard deviation. Statistical significance at the level $p < 0.05$: A, compared to CTRL; B, compared to EAM; C, compared to MOE50; D, compared to MOE100; and E, compared to MOE200.

myocarditis is not always associated with systolic dysfunction and that there are cases of myocarditis with preserved EF [29]. Furthermore, markedly increased heart rate in EAM was lowered by MOE treatment, which can be ascribed to Melissa's proven ability to act as an antiarrhythmic agent via activation of cardiac M_2 receptors, blockage of Ca^{2+} and K^+ channels, and slowing ventricular conductivity [9, 30, 31]. However, we did not observe any changes in the blood pressure of EAM rats unlike others [23]. Nevertheless, MOE200 showed hypotensive effects which can be explained by the previously described vasorelaxant effect of MOE involving Ca^{2+} blockage, nitric oxide pathway, but also prostacyclin and EDHF pathways [15, 24].

In our study, induction of EAM was confirmed histopathologically by characteristic severe inflammatory infiltration and fibrosis of the heart tissues which is in line with other studies using the EAM rat model [14, 27, 32]. Interestingly 3-week treatment with MOEs markedly improved myocardial architecture and decreased inflammatory infiltrate density in a dose-dependent manner, with most pronounced improvement in the MOE200 group. Also, MOE treatment decreased collagen content, suggesting again that MOE200 can prevent myocarditis-induced fibrosis and subsequent heart remodeling [27]. Mentioned effects achieved by MOE administration are most likely connected to its strong anti-inflammatory properties proved *in vivo* in the carrageenan-induced paw edema model [11], but also in other models of cardiovascular diseases [17, 33]. Even though MOEs have not been investigated in EAM pathology, achieved myocarditis ameliorating properties may be associated with synergistic action of its compounds, especially rosmarinic acid and other phenolic acids; triterpenoids oleanolic and ursolic acids; and flavonoids quercetin, rutin, myricetin, catechin, and epigallocatechin. Rosmarinic acid, the most abundant compound of MOEs, is proved to be a very potent anti-inflammatory agent per se, as demonstrated in different models of autoimmune inflammatory disease such as rheumatoid arthritis, colitis, and atopic dermatitis. Possible mechanisms of this action are decreased COX-2 expression and decreased proinflammatory cytokines IL-1, IL-6, and TNF- α release [34]. Also, in myocardial I/R injury conditions, rosmarinic acid has been shown to suppress proinflammatory cytokine expression as well and ameliorate heart damage by activating PPAR- γ and downregulating NF- κ B-mediated pathways [35]. Quercetin is also an important flavonoid component of MOE that may have contributed to its EAM ameliorating effects in our study, since it is shown that quercetin (20 mg/kg) may protect the heart from the damage in EAM conditions, via suppression of proinflammatory TNF- α and IL-17 and upregulation of anti-inflammatory cytokine IL-10 [14]. This study also used the *Dark Agouti* strain of rats, making it more comparable to our study. Other authors suggest that even in 10 mg/kg quercetin can protect the heart from EAM-induced damage via modulation of MAPK signaling cascade, more precisely by suppressing the myocardial endothelin-1 and also the mitogen-activated protein kinases (MAPK) [36]. Potent anti-inflammatory properties of quercetin have also been confirmed in other autoimmune dis-

eases [37, 38]. Another flavonoid component of MOEs, catechin, was also shown to exert protective effects in the EAM rat model by decreasing cardiac remodeling, inflammatory infiltrate, and fibrosis possibly via decreased expression of NF- κ B and ICAM-1 [27].

An important aspect in the pathophysiology of autoimmune myocarditis is the link between inflammation and excessive ROS production, otherwise oxidative stress, which we also evaluated in this study. Three weeks post-immunization, the EAM group was associated with a significant release of prooxidants O_2^- , H_2O_2 , NO_2^- , and TBARS and impaired antioxidant defense system (decreased SOD, CAT, and GSH). This is consistent with earlier studies that reported various oxidative stress marker elevations in this disease, such as superoxide anion [36], lipid peroxidation products MDA and 4-hydroxynonenal, and TBARS [39, 40]. MOE treatment showed dose-dependent drop in the release of prooxidants O_2^- , TBARS, and NO_2^- , with strong antioxidant effect and free scavenging properties of this plant and its phenolic compounds being the most responsible for this effect. Various studies showed MOEs' ability to decrease oxidative stress in different cardiovascular models, even when using shorter time of exposition (7 or 14 days) than in this study [7, 33, 39]. We found that MOE treatment improves the systemic antioxidant status of EAM rats. The results of other studies support this finding, since there is evidence that MOEs can improve antioxidant capacity, mostly via SOD increment in models of LAD *in vivo* regional I/R injury and doxorubicin-induced cardiotoxicity. Additionally, *in vitro* investigations on MOEs confirmed its strong free radical scavenging properties on DPPH, ABTS, O_2^- , and NO_2^- radicals, but also iron (II) chelating activity of that potentiates its antioxidant properties [41, 42]. Besides mentioned antioxidant effects of MOEs, it is important to emphasize that rosmarinic acid, dominant phenolic component of this plant, per se possesses strong effect in mitigating oxidative stress in different disorders [43]. The antioxidant power of rosmarinic acid is mainly based on its ability to stabilize membranes and stop free radical movement, thus preventing oxidation of the membranes [44].

Thus, oxidative stress ameliorating effect of the applied MOE treatment may also be one of the main mechanisms of autoimmune myocarditis improvement achieved by MOEs.

5. Conclusion

In the light of these findings, the present study suggests that ethanolic MOEs improve cardiac function and myocardial architecture and mitigate oxidative stress, thus preventing heart remodeling, DCM, and subsequent heart failure connected with human giant cell myocarditis and EAM. However, the most prominent reduction of cardiac inflammatory infiltration, fibrosis, and oxidative stress with preservation of ejection fraction has been observed with the highest dose of MOE, 200 mg/kg. This study is the first to provide evidence on *M. officinalis* effects in cardiac autoimmunity. However, additional experiments and future investigations are necessary and should help in revealing

the exact mechanism of action of MOEs in EAM pathology. MOEs should be considered as a potentially helpful adjuvant therapy in patients with autoimmune myocarditis.

Data Availability

The data used to support the findings of this study are available from the corresponding author upon request.

Conflicts of Interest

The authors declare that they have no conflict of interest regarding the publication of this paper.

Acknowledgments

The authors would like to express gratitude to the Faculty of Medical Sciences, University of Kragujevac for Grant No. JP 26/20.

References

- [1] W. Bracamonte-Baran and D. Čiháková, "Cardiac autoimmunity: myocarditis," *Advances in Experimental Medicine and Biology*, vol. 1003, pp. 187–221, 2017.
- [2] J. Suzuki, M. Ogawa, R. Watanabe et al., "Autoimmune giant cell myocarditis: clinical characteristics, experimental models and future treatments," *Expert Opinion on Therapeutic Targets*, vol. 15, no. 10, pp. 1163–1172, 2011.
- [3] P. Błyszczuk, "Myocarditis in humans and in experimental animal models," *Frontiers in Cardiovascular Medicine*, vol. 6, p. 64, 2019.
- [4] J. M. Myers, D. Fairweather, S. A. Huber, and M. W. Cunningham, "Autoimmune myocarditis, valvulitis, and cardiomyopathy," *Current Protocols in Immunology*, vol. 101, no. 1, 2013.
- [5] B. Javadi and A. Sahebkar, "Natural products with anti-inflammatory and immunomodulatory activities against autoimmune myocarditis," *Pharmacological Research*, vol. 124, pp. 34–42, 2017.
- [6] A. Enayati, M. Banach, T. Jamialahmadi, and A. Sahebkar, "Protective role of nutraceuticals against myocarditis," *Bio-medicine & Pharmacotherapy*, vol. 146, 2021.
- [7] S. Joukar, H. Asadipour, M. Sheibani, H. Najafipour, and S. Dabiri, "The effects of *Melissa officinalis* (lemon balm) pretreatment on the resistance of the heart to myocardial injury," *Pharmaceutical Biology*, vol. 54, no. 6, pp. 1005–1013, 2016.
- [8] Z. Akhondali, M. Dianat, and M. Radan, "Negative chronotropic and antidysrhythmic effects of hydroalcoholic extract of lemon balm (*Melissa officinalis* L.) on CaCl₂-induced arrhythmias in rats," *Electronic Physician*, vol. 7, no. 1, pp. 971–976, 2015.
- [9] S. Joukar and H. Asadipour, "Evaluation of *Melissa officinalis* (lemon balm) effects on heart electrical system," *Research in Cardiovascular Medicine*, vol. 4, no. 2, p. 6, 2015.
- [10] J. T. Lin, Y. C. Chen, Y. C. Lee, C. W. Rolis-Hou, F. L. Chen, and D. J. Yang, "Antioxidant, anti-proliferative and cyclooxygenase-2 inhibitory activities of ethanolic extracts from lemon balm (*Melissa officinalis* L.) leaves," *LWT*, vol. 49, no. 1, pp. 1–7, 2012.
- [11] Y. Birdane, M. E. Boyokokuroglu, F. Birdane, M. Cemek, and H. Yavus, "Anti-inflammatory and antinociceptive effects of *Melissa officinalis* L. in rodents," *Revista de Medicina Veterinaria*, vol. 158, no. 2, pp. 75–81, 2007.
- [12] A. M. Ahmed, A. F. El Fouhil, R. A. Mohamed et al., "Curcumin ameliorates experimental autoimmune acute myocarditis in rats as evidenced by decrease in thioredoxin immunoreactivity," *Folia Morphologica*, vol. 74, no. 3, pp. 318–324, 2015.
- [13] S. Zhang, X. Liu, C. Sun et al., "Apigenin attenuates experimental autoimmune myocarditis by modulating Th1/Th2 cytokine balance in mice," *Inflammation*, vol. 39, no. 2, pp. 678–686, 2016.
- [14] M. Milenković, N. Arsenović-Ranin, Z. Stojić-Vukanić, B. Bufan, D. Vučićević, and I. Jančić, "Quercetin ameliorates experimental autoimmune myocarditis in rats," *Journal of Pharmaceutical Sciences*, vol. 13, no. 3, pp. 311–319, 2010.
- [15] S. Ersoy, I. Orhan, N. N. Turan, G. Sahan, M. Ark, and F. Tosun, "Endothelium-dependent induction of vasorelaxation by *Melissa officinalis* L. ssp. *officinalis* in rat isolated thoracic aorta," *Phytomedicine*, vol. 15, no. 12, pp. 1087–1092, 2008.
- [16] A. Shakeri, A. Sahebkar, and B. Javadi, "*Melissa officinalis* L. - A review of its traditional uses, phytochemistry and pharmacology," *Journal of Ethnopharmacology*, vol. 188, pp. 204–228, 2016.
- [17] N. Dragicin, V. Jakovljevic, M. Andjic et al., "*Melissa officinalis* L. as a nutritional strategy for cardioprotection," *Frontiers in Physiology*, vol. 12, no. 12, 2021.
- [18] A. Hijazi, D. S. Al Masri, H. Farhan, M. Nasser, H. Rammal, and H. Annan, "Effect of different ethanol concentrations, using different extraction techniques, on the antioxidant capacity of Lebanese *Eryngium creticum*," *Journal of Pharmaceutical, Chemical and Biological Sciences*, vol. 3, no. 2, pp. 262–271, 2015.
- [19] P. Schmerler, S. Jeuthe, D. O h-Ici et al., "Mortality and morbidity in different immunization protocols for experimental autoimmune myocarditis in rats," *Acta Physiologica*, vol. 210, no. 4, pp. 889–898, 2014.
- [20] V. Jakovljevic, P. Milic, J. Bradic et al., "Standardized *Aronia melanocarpa* extract as novel supplement against metabolic syndrome: a rat model," *International Journal of Molecular Sciences*, vol. 20, no. 1, p. 6, 2019.
- [21] J. Stypmann, M. A. Engelen, C. Troatz, M. Rothenburger, L. Eckardt, and K. Tiemann, "Echocardiographic assessment of global left ventricular function in mice," *Laboratory Animals*, vol. 43, no. 2, pp. 127–137, 2009.
- [22] J. Bradic, V. Zivkovic, I. Srejovic et al., "Protective effects of *Galium verum* L. extract against cardiac ischemia/reperfusion injury in spontaneously hypertensive rats," *Oxidative Medicine and Cellular Longevity*, vol. 2019, Article ID 4235405, 11 pages, 2019.
- [23] V. Sukumaran, K. Watanabe, P. T. Veeraveedu et al., "Olmestartan, an AT1 antagonist, attenuates oxidative stress, endoplasmic reticulum stress and cardiac inflammatory mediators in rats with heart failure induced by experimental autoimmune myocarditis," *International Journal of Biological Sciences*, vol. 7, no. 2, pp. 154–167, 2011.
- [24] R. C. Devi, S. M. Sim, and R. Ismail, "Effect of *Cymbopogon citratus* and citral on vascular smooth muscle of the isolated thoracic rat aorta," *Evidence-Based Complementary and Alternative Medicine*, vol. 2012, Article ID 539475, 8 pages, 2012.
- [25] J. Sretenovic, V. Zivkovic, I. Srejovic, and Z. Milosavljevic, "The effects of high doses of nandrolone decanoate on cardiac

- muscle tissue,” *Serbian Journal of Experimental and Clinical Research*, vol. 17, no. 4, pp. 303–308, 2016.
- [26] I. Kindermann, C. Barth, F. Mahfoud et al., “Update on myocarditis,” *Journal of the American College of Cardiology*, vol. 59, no. 9, pp. 779–792, 2012.
- [27] J. Suzuki, M. Ogawa, H. Futamatsu, H. Kosuge, Y. M. Sagesaka, and M. Isobe, “Tea catechins improve left ventricular dysfunction, suppress myocardial inflammation and fibrosis, and alter cytokine expression in rat autoimmune myocarditis,” *European Journal of Heart Failure*, vol. 9, no. 2, pp. 152–159, 2007.
- [28] X. Cheng, Y. H. Liao, J. Zhang et al., “Effects of atorvastatin on Th polarization in patients with acute myocardial infarction,” *European Journal of Heart Failure*, vol. 7, no. 7, pp. 1099–1104, 2005.
- [29] M. Mirna, V. Paar, T. Kraus et al., “Autoimmune myocarditis is not associated with left ventricular systolic dysfunction,” *European Journal of Clinical Investigation*, vol. 49, no. 8, 2019.
- [30] R. Gazola, D. Machado, C. Ruggiero, G. Singi, and M. Macedo Alexandre, “Lippia alba, Melissa officinalis and Cymbopogon citratus: effects of the aqueous extracts on the isolated hearts of rats,” *Pharmacological Research*, vol. 50, no. 5, pp. 477–480, 2004.
- [31] S. Joukar, Z. Zarisfi, G. Sepehri, and A. Bashiri, “Efficacy of Melissa officinalis in suppressing ventricular arrhythmias following ischemia-reperfusion of the heart: a comparison with amiodarone,” *Medical Principles and Practice*, vol. 23, no. 4, pp. 340–345, 2014.
- [32] Y. Yoshida, T. Shioi, and T. Izumi, “Resveratrol ameliorates experimental autoimmune myocarditis,” *Circulation Journal*, vol. 71, no. 3, pp. 397–404, 2007.
- [33] M. Sedighi, M. Faghihi, M. Rafeian-Kopaei, B. Rasoulian, and A. Nazari, “Cardioprotective effect of ethanolic leaf extract of Melissa officinalis L against regional ischemia-induced arrhythmia and heart injury after five days of reperfusion in rats,” *Iranian Journal of Pharmaceutical Research: IJPR*, vol. 18, no. 3, pp. 1530–1542, 2019.
- [34] C. Luo, L. Zou, H. Sun et al., “A review of the anti-inflammatory effects of rosmarinic acid on inflammatory diseases,” *Frontiers in Pharmacology*, vol. 11, 2020.
- [35] J. Han, D. Wang, L. Ye et al., “Rosmarinic acid protects against inflammation and cardiomyocyte apoptosis during myocardial ischemia/reperfusion injury by activating peroxisome proliferator-activated receptor gamma,” *Frontiers in Pharmacology*, vol. 8, 2017.
- [36] S. Arumugam, R. A. Thandavarayan, W. Arozal et al., “Quercetin offers cardioprotection against progression of experimental autoimmune myocarditis by suppression of oxidative and endoplasmic reticulum stress via endothelin-1/MAPK signalling,” *Free Radical Research*, vol. 46, no. 2, pp. 154–163, 2012.
- [37] S. Arumugam, S. Mito, R. A. Thandavarayan et al., “Mulberry leaf diet protects against progression of experimental autoimmune myocarditis to dilated cardiomyopathy via modulation of oxidative stress and MAPK-mediated apoptosis,” *Cardiovascular Therapeutics*, vol. 31, no. 6, 2013.
- [38] P. Shen, W. Lin, X. Deng et al., “Potential implications of quercetin in autoimmune diseases,” *Frontiers in Immunology*, vol. 12, no. 12, 2021.
- [39] B. Wu, J. Li, H. Ni et al., “TLR4 activation promotes the progression of experimental autoimmune myocarditis to dilated cardiomyopathy by inducing mitochondrial dynamic imbalance,” *Oxidative Medicine and Cellular Longevity*, vol. 2018, Article ID 3181278, 15 pages, 2018.
- [40] Z. Yuan, K. Shioji, Y. Kihara, H. Takenaka, Y. Onozawa, and C. Kishimoto, “Cardioprotective effects of carvedilol on acute autoimmune myocarditis: anti-inflammatory effects associated with antioxidant property,” *American Journal of Physiology. Heart and Circulatory Physiology*, vol. 286, no. 1, pp. H83–H90, 2004.
- [41] A. Hamza, M. M. Ahmed, H. M. Elwey, and A. Amin, “Melissa officinalis protects against doxorubicin-induced cardiotoxicity in rats and potentiates its anticancer activity on MCF-7 cells,” *PLoS One*, vol. 11, no. 11, 2016.
- [42] K. Dastmalchi, H. D. Dorman, P. P. Oinonen, Y. Darwis, I. Laakso, and R. Hitunen, “Chemical composition and *in vitro* antioxidative activity of a lemon balm (*Melissa officinalis* L.) extract,” *LWT*, vol. 41, no. 3, pp. 391–400, 2008.
- [43] A. Khojasteh, M. H. Mirjalili, M. A. Alcalde, R. M. Cusido, R. Eibl, and J. Palazon, “Powerful plant antioxidants: a new biosustainable approach to the production of rosmarinic acid,” *Antioxidants*, vol. 9, no. 12, 2020.
- [44] L. Pérez-Fons, M. T. Garzón, and V. Micol, “Relationship between the antioxidant capacity and effect of rosemary (*Rosmarinus officinalis* L.) polyphenols on membrane phospholipid order,” *Journal of Agricultural and Food Chemistry*, vol. 58, no. 1, pp. 161–171, 2010.

Research Article

The Attenuation of Chronic Ulcerative Colitis by (R)-salbutamol in Repeated DSS-Induced Mice

Liangjun Deng ¹, Haihua Guo,¹ Shanping Wang ¹, Xiaoming Liu,² Yue Lin,¹ Rui Zhang,¹ and Wen Tan ^{3,4}

¹Institute of Biomedical and Pharmaceutical Sciences, Guangdong University of Technology, Guangzhou, 510006 Guangdong, China

²Institute of Gastroenterology of Guangdong Province, Department of Gastroenterology, Nanfang Hospital, Southern Medical University, 510515 Guangzhou, China

³Jeffrey Cheah School of Medicine and Health Sciences, Monash University Malaysia, Bandar Sunway 47500, Malaysia

⁴Post-Doctoral Innovation Base, Jinan University Affiliation, Yuanzhi Health Technology Co., Ltd., Hengqin New District, Zhuhai, Guangdong 519000, China

Correspondence should be addressed to Wen Tan; uscnwt@163.com

Received 21 October 2021; Revised 31 December 2021; Accepted 10 January 2022; Published 7 February 2022

Academic Editor: Ivan Srejavic

Copyright © 2022 Liangjun Deng et al. This is an open access article distributed under the Creative Commons Attribution License, which permits unrestricted use, distribution, and reproduction in any medium, provided the original work is properly cited.

Racemic salbutamol ((RS)-sal), which consist of the same amount of (R)-sal and (S)-sal, has been used for asthma and COPD due to its bronchodilation effect. However, the effect of (R)-sal on repeated dextran sulfate sodium (DSS)-induced chronic colitis has not yet been investigated. In this study evaluated the potential effect of (R)-, (S)-, and (RS)-sal in mice with repeated DSS-induced chronic colitis and investigated the underlying mechanisms. Here, we verified that chronic colitis was significantly attenuated by (R)-sal, which was evidenced by notably mitigated body weight loss, disease activity index (DAI), splenomegaly, colonic lengths shortening, and histopathological scores. (R)-sal treatment noticeably diminished the levels of inflammatory cytokines (such as TNF- α , IL-6, IL-1 β , and IFN- γ). Notably, the efficacy of (R)-sal was better than that of (RS)-sal. Further research revealed that (R)-sal mitigated colonic CD4 leukocyte infiltration, decreased NF- κ B signaling pathway activation, improved the Nrf-2/HO-1 signaling pathway, and increased the expression of ZO-1 and occludin. In addition, (R)-sal suppressed the levels of TGF- β 1, α -SMA, and collagen in mice with chronic colitis. Furthermore, the 16S rDNA sequences analyzed of the intestinal microbiome revealed that (R)-sal could mitigate the intestinal microbiome structure and made it more similar to the control group, which mainly by relieving the relative abundance of pathogens (such as Bacteroides) and increasing the relative abundance of probiotics (such as Akkermansia). Therefore, (R)-sal ameliorates repeated DSS-induced chronic colitis in mice by improving inflammation, suppressing oxidative stress, mitigating intestinal barrier function, relieving intestinal fibrosis, and regulating the intestinal microbiome community. These results indicate that (R)-sal maybe a novel treatment alternative for chronic colitis.

1. Introduction

Ulcerative colitis (UC) is one of the inflammatory bowel diseases (IBD) that is chronic and recurrent. The clinical characteristics of UC mainly include abdominal pain, weight loss, and bloody diarrhea [1–3], which seriously decrease the quality of life for patients [4]. The histopathological and inflammatory changes in UC are generally observed in the colon and rectum. UC is mainly prevalent in western countries in the past; however, in recent years, the incidences of UC have

rapidly increased in Asia, such as China, India, and South Korea [5–8]. Although the exact pathogenesis of UC remains poorly understood, the accumulating data have suggested that UC is closely related to inflammation and oxidative stress imbalance, impairment of the intestinal barrier, and abnormalities in the intestinal microbiota [9–12].

Nuclear factor-kappa B (NF- κ B) is an important transcriptional regulation factor in the process of inflammation, usually in an inactive state due to its combination with its inhibitor kappa B (IKB) [13]. NF- κ B can be activated by

stimulating factors, then induce the expression of a variety of genes, produce multiple cytokines to participate in the inflammatory response, and play an important role in maintaining normal physiological functions. However, when NF- κ B is overactivated, it will induce autoimmune diseases such as UC [13].

Nuclear factor erythroid 2-related factor 2 (Nrf-2) is an important transcription factor for antioxidative stress. Under normal conditions, Nrf-2 is linked to Kelch-Like ECH-Associated Protein 1 (Keap1) through E3 ubiquitin ligase and is degraded through ubiquitination. However, under oxidative stress, which can activate Nrf-2, then made it dissociates from Keap1, enters the nucleus, and upregulates the transcription of downstream antioxidant enzymes [14]. Thus, Nrf-2 can play a core role in antioxidative stress. It has been demonstrated that the expression of Nrf-2 was decreased in the DSS-induced UC model [15], which suggests that drugs can activate Nrf-2 which was expected to be applied in the treatment of UC.

The treatment medicines for UC depend on mesalamine, glucocorticoids, and immunomodulatory agents. However, the long-term use of these drugs is limited due to potential side effects, safety, and costs. Therefore, the development of alternative drugs for the treatment of UC is urgently needed.

Racemic salbutamol ((RS)-sal) is a short-acting β 2-adrenergic receptor agonist consisting of an equal mixture of (R)-sal and (S)-sal. (RS)-sal can effectively inhibit the release of allergenic substances such as histamine and prevent bronchospasm, which commonly can be used for the treatment of bronchial asthma and asthmatic bronchitis [16]. Besides, there are some evidences demonstrating that β 2-adrenergic receptor agonists exhibit anti-inflammatory effects by regulating the immune system [17, 18], which may contribute to the therapeutic effects in some inflammatory diseases, such as UC. A previous study in our group demonstrated that (RS)-sal exerted anti-inflammatory activity properties. However, the effect of sal in dextran sulfate sodium (DSS)-induced chronic colitis has not been investigated.

In view of this, the aim of our research was to evaluate the potential amelioration effect of (R)-sal in mice with repeated DSS-induced chronic ulcerative colitis and to elucidate the mechanisms underlying its therapeutic effect. In addition, we explored the differences in the mitigated effects of (R)-, (S)-, and (RS)-sal on chronic ulcerative colitis.

2. Materials and Methods

2.1. Materials. (R)-sal, (S)-sal, and (RS)-sal were supplied by Dongguan Key-Pharma Biomedical Company (Guangdong, China). DSS (MW 36-50 kDa) was obtained from MP Bio-medicals Co., Ltd. (California, USA). The positive drug 5-ASA was obtained from Shanghai Yuanye Bio-Technology Co., Ltd. (Shanghai, China). The reagent for detecting fecal occult blood was supplied by Baso Diagnostics, Inc. (Zhuhai, China). The enzyme-linked immunosorbent assay (ELISA) kits for detecting the inflammatory cytokines interferon- γ (IFN- γ), interleukin- (IL-) 1 β , IL-6, and tumor necrosis fac-

tor- α (TNF- α) were offered by Neobioscience Technology Company (Shenzhen, China). The antibodies of β -actin (ab227387), occludin (ab216327), and CD4 (ab183685) were obtained from Abcam Inc. (Burlingame, USA). The antibodies of zonula occludens-1 (ZO-1) (bs-1329R) and Nrf-2 (bs-1074R) were obtained from Bioss (Beijing, China). The antibodies of NF- κ B p65 (10745-1-AP) and heme oxygenase-1 (HO-1) (10701-1-AP) were purchased from Proteintech (Rosemont, USA). The antibody of phospho-NF- κ B p65 (p-NF- κ B p65) was purchased from Cell Signaling Technology (Danvers, USA). The antibodies of transforming growth factor- β 1 (TGF- β 1) (BA0290) and alpha smooth muscle actin (α -SMA) (BM0002) were offered by Boster Biological Technology Co., Ltd. (Wuhan, China). All chemical reagents employed were of analytical grade.

2.2. Animals. Male C57BL/6 mice (18-20 g, 6 weeks) were procured from the Medical Experimental Animal Centre of Southern Medical University (Guangzhou, China) and then housed under a pathogen-free experimental facility. These mice were acclimatized for seven days before being randomly divided into different experimental groups. All animal experimental protocols and care in this study were performed in compliance with the guidelines of the Institutional Animal Care and Use Committee and were approved by the Animal Experimentation Committee of Southern Medical University (L2017010).

2.3. Repeated DSS-Induced Chronic Colitis in Mice and Treated with (R)-, (S)-, and (RS)-sal. The mice were adapted to their environment for seven days, then randomly divided into 5 groups: the control group, DSS group, DSS+(S)-sal group (1.0 mg/kg), DSS+(RS)-sal group (2.0 mg/kg), and DSS +(R)-sal group (1.0 mg/kg) ($n = 8$). Experimental chronic colitis was induced by giving three cycles of 2.5% DSS according to the previous description [19, 20] with a slight modification. The first day of the experiment was defined as day 0. The timelines of this animal experiment are described in Figure 1(a). In brief, the control group only received water during the experiment. The other groups were induced by drinking 2.5% DSS treatment (three cycles for 7 days) and recovery by drinking water without DSS (two cycles for 7 days). The DSS+(S)-sal group, DSS+(RS)-sal group, and DSS+(R)-sal group were orally administered the corresponding drugs from day 14. The control group and DSS group were treated with the same dose of water. The body weight change in each group was detected once a day, and the disease activity index (DAI) was assessed at a specific time during the treatment period. DAI scores were blindly evaluated as described previously [21]. At day 35, mice were euthanized, and their blood samples were collected from the orbit. The colon samples were quickly removed, and their lengths were recorded. Subsequently, the colons were analyzed by histology examination. Spleen samples were quickly removed, and their weight was recorded.

2.4. Pharmaceutical Effect of (R)-sal on Repeated DSS-Stimulated Chronic Colitis. The mice were adapted for seven days and then randomly divided into 5 groups: the control

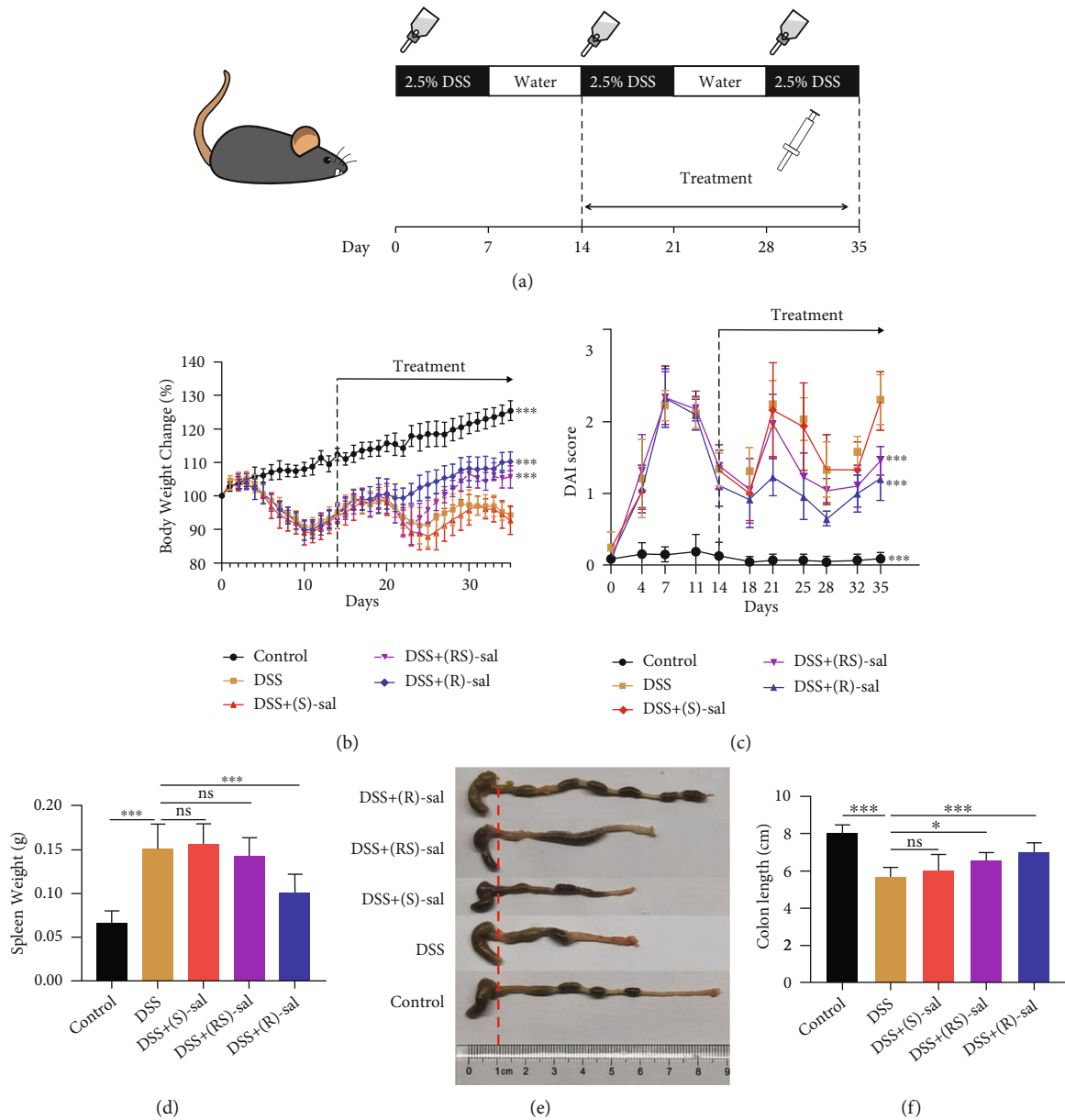


FIGURE 1: Effects of (R)-, (S)-, and (RS)-sal on repeated DSS-induced chronic colitis. (a) Schematic diagram of DSS-induced chronic colitis experiments. (b) Body weight change was recorded during the experiment (treatment from day 14 to day 35). (c) DAI scores were recorded at certain time points (treatment from day 14 to day 35). (d) Spleen weight in different groups. (e) Representative colons from different groups. (f) Colon length in different groups. * $P < 0.05$, ** $P < 0.01$, *** $P < 0.001$ versus the DSS group.

group, DSS group, DSS+5-ASA group (50 mg/kg), DSS+(R)-sal-L group (0.5 mg/kg), and DSS+(R)-sal-H group (1.0 mg/kg) ($n = 8$). The experimental chronic colitis was induced by giving three cycles of 2.5% DSS according to the previous description [19, 20] with slight modification. The first day of the experiment was defined as day 0. The timelines of this animal experiment are described in Figure 2(a). In brief, the control group only received water during the experiment. The other groups were induced by drinking 2.5% DSS treatment (three cycles for 7 days), and recovery was induced by drinking water without DSS (two cycles for 7 days). The DSS+5-ASA group, DSS+(R)-sal-L group, and DSS+(R)-sal-H group were orally administered the corre-

sponding drugs from day 14. The control group and DSS group were treated with the same dose of water. The body weight change of each group was detected once a day, and the DAI was assessed at a specific time during the treatment period. DAI scores were blindly evaluated as described previously [21]. At day 35, the mice were euthanized, and their blood samples were collected from the orbit. The colon samples were quickly removed, and their lengths were recorded. Subsequently, the colons were divided into two sections: one section was analyzed via histology examination and the other was analyzed in biochemical assays. Spleen samples were quickly removed, and their weight was recorded.

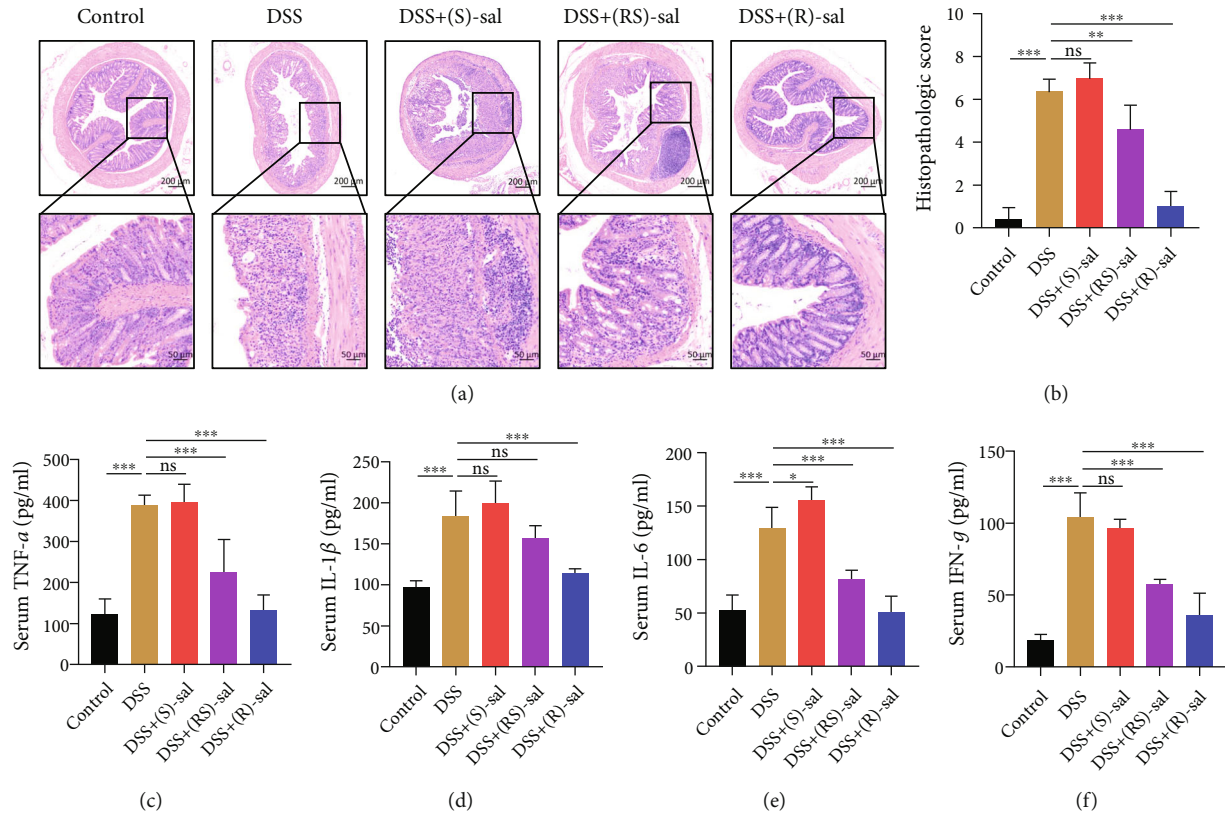


FIGURE 2: The mitigating effect of (R)-, (S)-, and (RS)-sal in the histological evaluation and the secretion of inflammatory cytokines. (a) Representative image of HE staining in different groups. (b) Histological scores of different groups. (c) TNF- α , (d) IL-1 β , (e) IL-6, and (f) IFN- γ levels were measured by ELISA kits. * $P < 0.05$, ** $P < 0.01$, *** $P < 0.001$ compared with the DSS group.

2.5. Histopathological Examinations. After the mice were euthanized, distal colon samples were detached and immediately fixed in 10% formalin for 48 h. Next, the distal colon samples were embedded in paraffin, cut into 4 mm sections, then stained with hematoxylin and eosin (HE), periodic acid-Schiff (PAS), and picosirius red staining. The images of samples were acquired by microscope. The colon histopathological scores were determined according to previously described methods [21] with slight modification, which was performed in a blind fashion and evaluated as follows: inflammation (scores varied from 0 to 4) and epithelium (scores varied from 0 to 4).

2.6. Detection of Inflammatory Cytokines by ELISA. The serum was obtained from whole blood samples by centrifugation (3000 rpm, 15 minutes). The concentrations of IFN- γ , IL-1 β , TNF- α , and IL-6 in the serum were measured by respective ELISA kits based on the manufacturer's protocol.

2.7. Quantitative Real-Time PCR. Total RNA was isolated from colon samples using RNAprep pure Tissue Kit (TIANGE, Beijing, China) in RNase-free environment according to the manufacturer's protocol. RNA was reverse transcribed into cDNA by RevertAid First Strand cDNA Synthesis Kit (Thermo, MA, USA). The relative concentration of IFN- γ , IL-1 β , TNF- α , and IL-6 was detected by

FastStart Universal SYBR Green Master (Rox) (Roche, Basel, Switzerland). The primer sequences to detect IFN- γ , IL-1 β , TNF- α , and IL-6 are revealed in Table 1. The expression of these mRNA was normalized with the reference gene GAPDH. Data were analyzed by $2^{-\Delta\Delta CT}$ method to evaluate the relative expression.

2.8. Western Blotting. The colon tissue protein was extracted by homogenization in radio immunoprecipitation assay (Biosharp, Anhui, China) and protease inhibitors (Biosharp, Anhui, China). The protein sample concentrations were measured by bicinchoninic acid assay kit (DINGGUO, Beijing, China) according to the manufacturer's instructions. After denaturation, the 10% sodium dodecyl sulfate-polyacrylamide gel electrophoresis was used to separate proteins. Then, the proteins were transferred onto polyvinylidene difluoride (PVDF) membranes. Each membrane was blocked by 5% skim milk for 1 h at room temperature. The membranes were exposed to the following primary antibodies overnight at 4°C with shaking: anti- β -actin (1:6000), anti-ZO-1 (1:1000), antioccludin (1:1000), anti-NF- κ B p65 (1:1000), anti-p-NF- κ B p65 (1:1000), anti-Nrf-2 (1:1000), and anti-HO-1 (1:3000). After that, each membrane was incubated with secondary antibody at 37°C for 1 h. Finally, the enhanced chemiluminescence

TABLE 1: The primers used in qPCR assay.

Gene	Primers	Sequences (5'-3')
TNF- α	Forward	AAGTTCCCAAATGGCCTCCC
	Reverse	CCACTTGGTGGTTTGTGAGTG
IL-1 β	Forward	GCAGTGGTTCGAGGCCTAAT
	Reverse	GCTGCTTCAGACACTTGCAC
IL-6	Forward	GACAAAGCCAGAGTCCTTCAGA
	Reverse	TGTGACTCCAGCTTATCTCTTGG
IFN- γ	Forward	AGACAATCAGGCCATCAGCAA
	Reverse	GTGGGTTGTTGACCTCAAACCT
GAPDH	Forward	CCTCGTCCCGTAGACAAAATG
	Reverse	TGAGGTCAATGAAGGGGTCGT

reagent (BOSTER, Wuhan, China) was used to visualize each protein band. The protein bands were evaluated by ImageJ software, and β -actin was used to normalize the protein relative expression.

2.9. Immunofluorescence Measurement. Immunofluorescence was performed as described previously [22]. In brief, the paraffin-embedded colon tissues were sectioned, dewaxed, and rehydrated. Then, the slices blocked endogenous peroxidase activity with 3% H₂O₂, and antigens were repaired by citrate buffer solution. The slices were incubated with 3% bovine serum albumin to diminish nonspecific staining. The slices were incubated with the following primary antibodies at 4°C overnight: anti-CD4 (1:1000), anti-ZO-1 (1:500), antioccludin (1:200), anti-TGF- β 1 (1:200), anti- α -SMA (1:200), and anti-Nrf-2 (1:400). After that, each slice was incubated with the respective secondary antibody for 30 min. Slices were counterstained with 4,6-diamidino-2-phenylindole (DAPI). The representative images were obtained under microscope, and the positive area of immunoreactivity was analyzed with Image-Pro Plus 6.0.

2.10. Gut Microbiota 16S rDNA Analysis. Gut contents ($n = 8$) were collected from the mice and stored at -80°C. DNA from the microbial community was extracted from the gut contents using the HiPure Soil DNA Kit. The quality and concentration of extracted DNA samples were evaluated by NanoDrop spectrophotometry (Thermo Scientific, Wilmington, USA). The V3-V4 variable region of the 16S rDNA gene was amplified by PCR. Subsequently, the PCR amplicons were purified by AMPure XP Beads (Beckman Agen-court, USA). Amplicons were extracted from 2% agarose gels and purified with AMPure XP Beads (Beckman Agen-court, USA), followed by quantification on the ABI StepOnePlus Real-Time PCR System (Life Technologies, Foster City, USA). The purified samples were sequenced and analyzed based on the Illumina platform. Sequencing service was provided by Genedenovo Inc. (Guangzhou, China).

2.11. Statistical Analysis. All data in these experiments were presented as the arithmetic mean \pm standard deviation (SD). Statistical differences were analyzed by GraphPad Prism

8.0 (La Jolla, CA, USA). These results were analyzed by one-way or two-way ANOVA multiple comparison tests. $P < 0.05$, $P < 0.01$, and $P < 0.001$ were set as statistically significant.

3. Results

3.1. Differential Effects of (R)-, (S)-, and (RS)-sal on DSS-Induced Chronic Colitis. The colitis caused by DSS is similar to the pathological features of human colitis [20]. In order to assess the mitigation capacity of (R)-, (S)-, and (RS)-sal in chronic colitis, a chronic colitis mouse model was induced by DSS. The chronic colitis was induced by adding 2.5% DSS treatment in the drinking water (three cycles for 7 days), and recovery was by drinking water without DSS (two cycles for 7 days). (R)-, (S)-, and (RS)-sal were orally administered to mice from day 14 (Figure 1(a)). As exhibited in Figures 1(b) and 1(c), body weight loss and DAI scores were noticeably increased in repeated DSS-induced chronic colitis mice compared with the control group. (R)-sal and (RS)-sal dramatically relieved these changes compared with the DSS group. However, treatment with (S)-sal could not diminish the body weight loss or DAI scores. The colon length reduced, and splenomegaly was used to represent the severity of DSS-induced chronic colitis. As shown in Figure 1(d), oral administration of (R)-sal, instead of (S)-sal or (RS)-sal, notably suppressed spleen swelling compared with the DSS group. Furthermore, treatment with (R)-sal and (RS)-sal dramatically improved the colon length shortening compared with the DSS group (Figures 1(e) and 1(f)). However, (S)-sal treatment could not suppress this change in DSS-induced chronic colitis mice.

Besides, the HE staining of colonic tissue was used to evaluate the histological effects of (R)-, (S)-, and (RS)-sal in repeated DSS-induced chronic colitis mice. As shown in Figures 3(a) and 3(b), compared with the control, the mice in repeated DSS-induced chronic colitis exhibited the intestinal barrier damage, reduced crypts, exacerbated inflammatory infiltration in the colon, and increased the histological score, whereas (R)-, (S)-, and (RS)-sal showed different effects on chronic colitis. (R)-sal and (RS)-sal dramatically suppressed inflammatory cell infiltration, intestinal barrier damage, and crypt destruction. Conversely, treatment with (S)-sal could improve nothing on chronic colitis.

It is well known that inflammatory cytokines play an important role in the pathogenesis of colitis. Therefore, in order to probe the anti-inflammatory effects of (R)-, (S)-, and (RS)-sal, the expressions of IFN- γ , IL-1 β , TNF- α , and IL-6 were measured by ELISA. As shown in Figures 3(c)–3(f), these proinflammatory cytokines notably increased in repeated DSS-induced chronic colitis compared with the control group. Treatment with (R)-sal or (RS)-sal diminished the expression of these proinflammatory cytokines. Nevertheless, in comparison with the DSS group, administration of (S)-sal could not attenuate the production of proinflammatory cytokines. Collectively, these results demonstrated that (R)-sal should be further investigated for its attenuated effects on repeated DSS-induced chronic colitis.

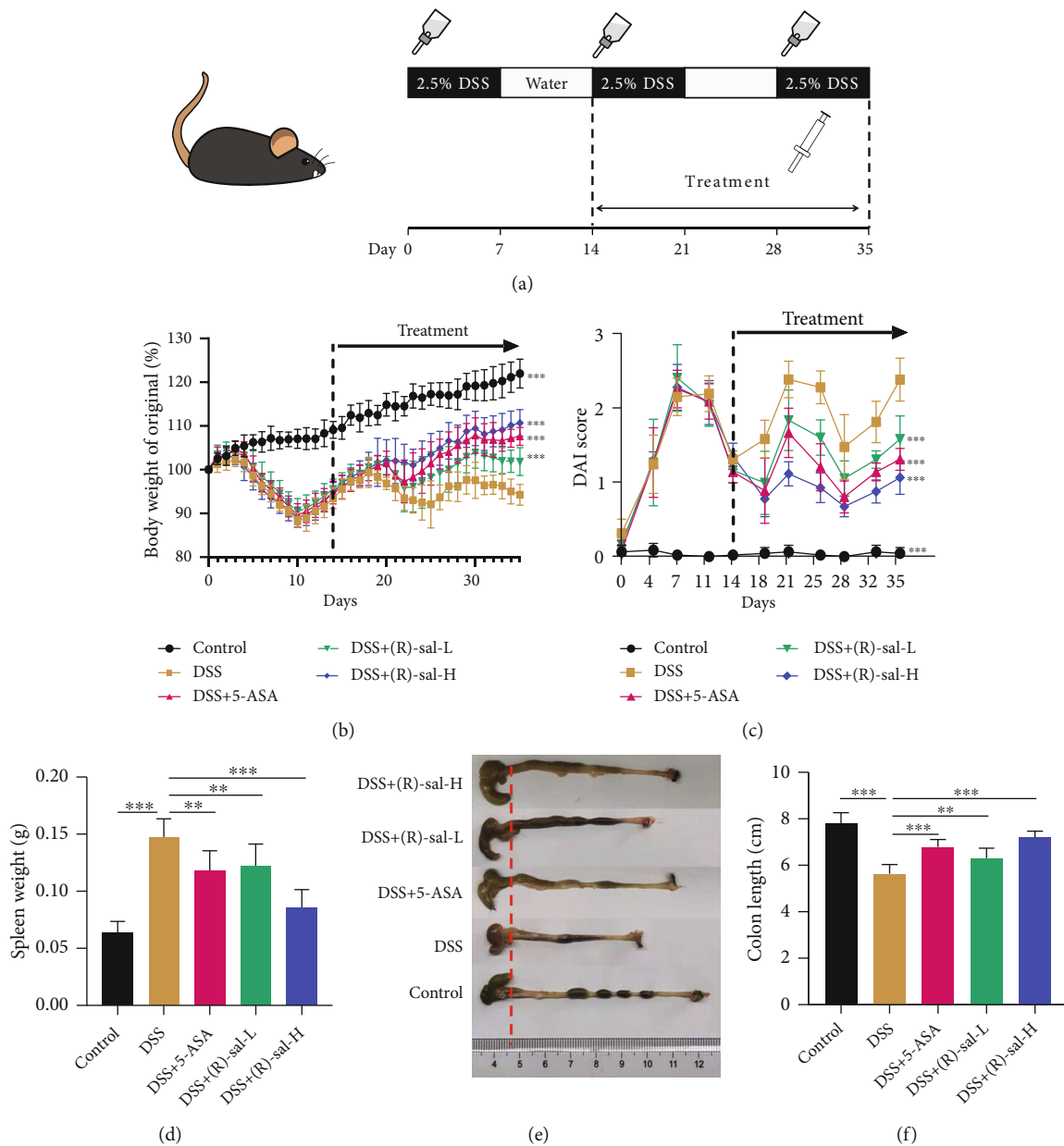


FIGURE 3: (R)-sal improved the symptoms on repeated DSS-induced chronic colitis. (a) Schematic diagram of repeated DSS-induced chronic colitis experiments. (b) Body weight change was measured daily during the experiment (treatment from day 14 to day 35). (c) DAI scores were recorded at certain time points (treatment from day 14 to day 35). (d) Spleen weight in different groups. (e) Representative colons from different groups. (f) Colon length in different groups. * $P < 0.05$, ** $P < 0.01$, *** $P < 0.001$ versus the DSS group.

3.2. (R)-sal Ameliorated the Symptoms on DSS-Induced Chronic Colitis. To evaluate the effect of (R)-sal on repeated DSS-induced chronic colitis, the mice with chronic colitis were treated with different doses of (R)-sal. 5-ASA was chosen as a positive control drug. This experiment scheme is illustrated in Figure 2(a). The body weight changes, DAI, spleen weight, and colon length, which are representative symptoms in chronic colitis, were recorded in this research. As exhibited in Figures 2(b)–2(f), (R)-sal notably mitigated these symptoms in a dose-dependent manner compared with the DSS group. Interestingly, the (R)-sal-H group even

showed more improvement than the 5-ASA group in the aforementioned indices.

The histopathological examination of colon implied that DSS induced colon structure damage, the loss of crypt and goblet cells, and considerable inflammatory cell infiltration in the colon. As shown in Figures 4(a) and 4(b), the histological score of the DSS group was remarkably elevated compared with that of the control group, whereas the mice with repeated DSS-induced chronic colitis treated with different doses of (R)-sal had notably diminished damage. Compared with the DSS group, different doses of (R)-sal oral administration

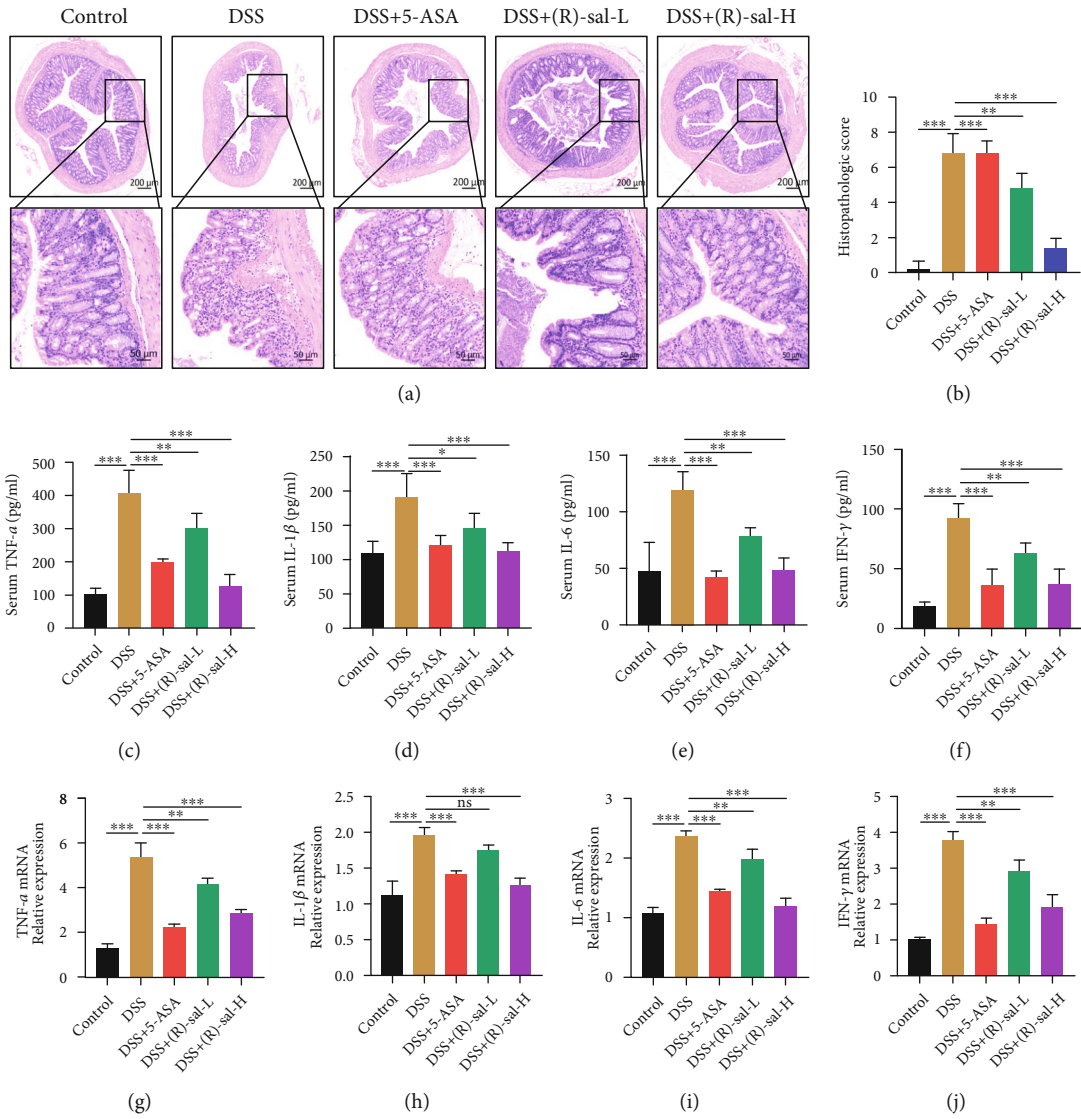


FIGURE 4: Continued.

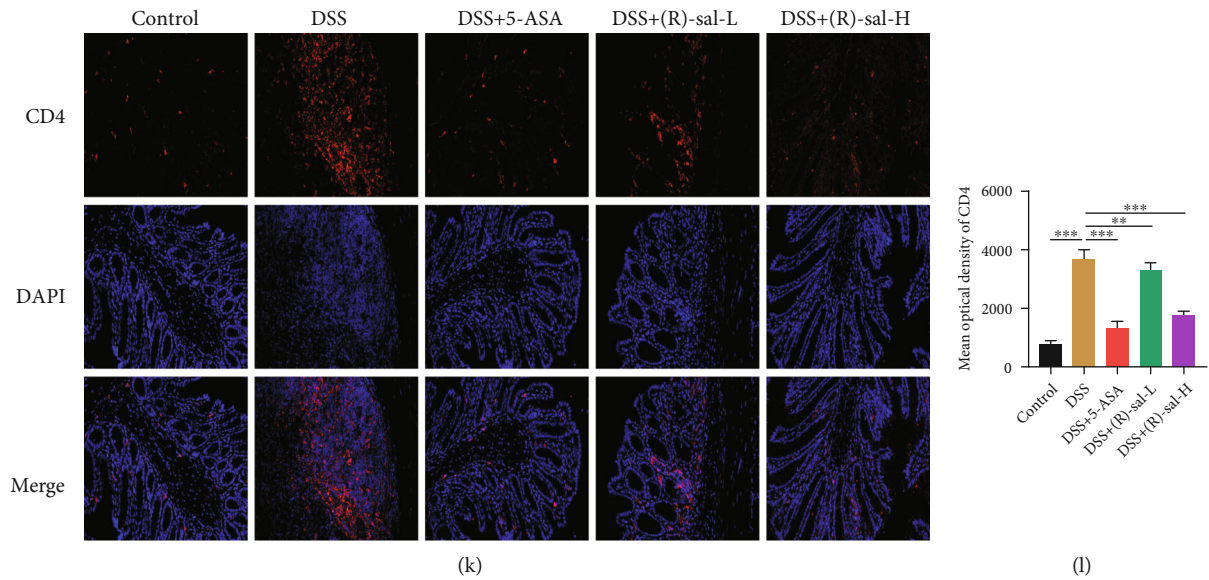


FIGURE 4: (R)-sal relieved the histological evaluation and inflammation on DSS-induced chronic colitis. (a) Representative image of HE in different groups. (b) Histological scores in different groups. (c) TNF- α , (d) IL-1 β , (e) IL-6, and (f) IFN- γ levels were examined by ELISA kits. (g) TNF- α , (h) IL-1 β , (i) IL-6, and (j) IFN- γ levels were examined by qPCR. (k) Representative image of CD4 staining in different groups. (l) The mean optical density of CD4 in different groups. * $P < 0.05$, ** $P < 0.01$, and *** $P < 0.001$ compared with the DSS group.

noticeably relieved the histological score in colon tissue. The result demonstrated that (R)-sal could outstandingly mitigate the colon injury in DSS-induced chronic colitis.

Moreover, inflammatory cytokines in the serum were investigated by ELISA. The results are shown in Figures 4(c)–4(f). The inflammatory cytokines, such as IFN- γ , IL-1 β , TNF- α , and IL-6, were remarkably exacerbated in the DSS group compared with the control group, which indicated that inflammatory reactions were exacerbated in the DSS group. However, different doses of (R)-sal suppressed the expression of these inflammatory cytokines than the DSS group. Besides, the mRNA expression of these inflammatory cytokines in colon tissue was measured by qRT-PCR. As shown in Figures 4(g)–4(j), the mRNA expression of these inflammatory cytokines was noticeably exacerbated in the DSS group compared with the control group. In contrast, treatment with different doses of (R)-sal ameliorated the mRNA expression of inflammatory cytokines. These data indicate that (R)-sal exhibited an anti-inflammatory effect, which could inhibit the secretion of inflammatory cytokines on DSS-induced chronic colitis.

Sustained and chronic inflammation is one of the symptoms of chronic colitis and is closely related to its pathogenesis. CD4 leukocytes can induce inflammatory response from the immune system by diverse microbial pathogen activation. Therefore, to further analyze the improvement effects of (R)-sal in inflammation, we measured the expression of immune cell CD4 leukocytes in chronic colitis colon tissue by immunofluorescence. As shown in Figures 4(k) and 4(l), compared with the control group, CD4 leukocytes that infiltrated in colon structures were dramatically exacerbated, which means that the inflammatory response was activated in mice with chronic colitis. After (R)-sal oral treatment, the positive signal of CD4 was notably suppressed than the DSS group, which means that the inflammation was remarkably relieved.

3.3. (R)-sal Suppressed NF- κ B Signaling Pathway Activation in Mice with Chronic Colitis. The NF- κ B signaling pathway induces the production of inflammatory factors in the pathological process of chronic colitis and plays core role in the inflammatory response. Consequently, the NF- κ B signaling pathway correlative proteins NF- κ B p65 and p-NF- κ B p65 were evaluated by western blot. As illustrated in Figure 5, the level of p-NF- κ B p65 in the DSS group was significantly increased than that in the control group, which means the NF- κ B signaling pathway was activated by induced DSS. Nevertheless, different doses of (R)-sal dramatically diminished the p-NF- κ B p65 expression in colon tissue compared with the DSS group. These results verified that (R)-sal suppressed NF- κ B pathway activation. Interestingly, different doses of (R)-sal exhibited little effect on NF- κ B p65 when compared with the DSS group.

3.4. (R)-sal Activated Nrf-2/HO-1 Expression in Mice with Chronic Colitis. The Nrf-2 signaling pathway exhibits anti-oxidative regulatory features. It has been reported that there was negative correlation between the Nrf-2 and the NF- κ B signaling pathway [23]. The oxidative environment leads to enlarging the level of ROS, which causes tissue damage and triggers inflammatory response [24, 25]. In order to evaluate the antioxidative role, the expression of Nrf-2 in the colon was detected by immunofluorescence. Compared with the control group, the dramatically attenuated Nrf-2 was detected in mice with chronic colitis, and this phenomenon was reversed by oral administration of (R)-sal in a dose-dependent manner (Figures 6(a) and 6(b)). Surprisingly, there was no noticeable variation in the (R)-sal-H group compared with the 5-ASA group.

To further assess the mechanism of (R)-sal, Nrf-2 and its downstream protein HO-1 were evaluated by western blot. As shown in Figures 6(c)–6(e), the expression of Nrf-2 and

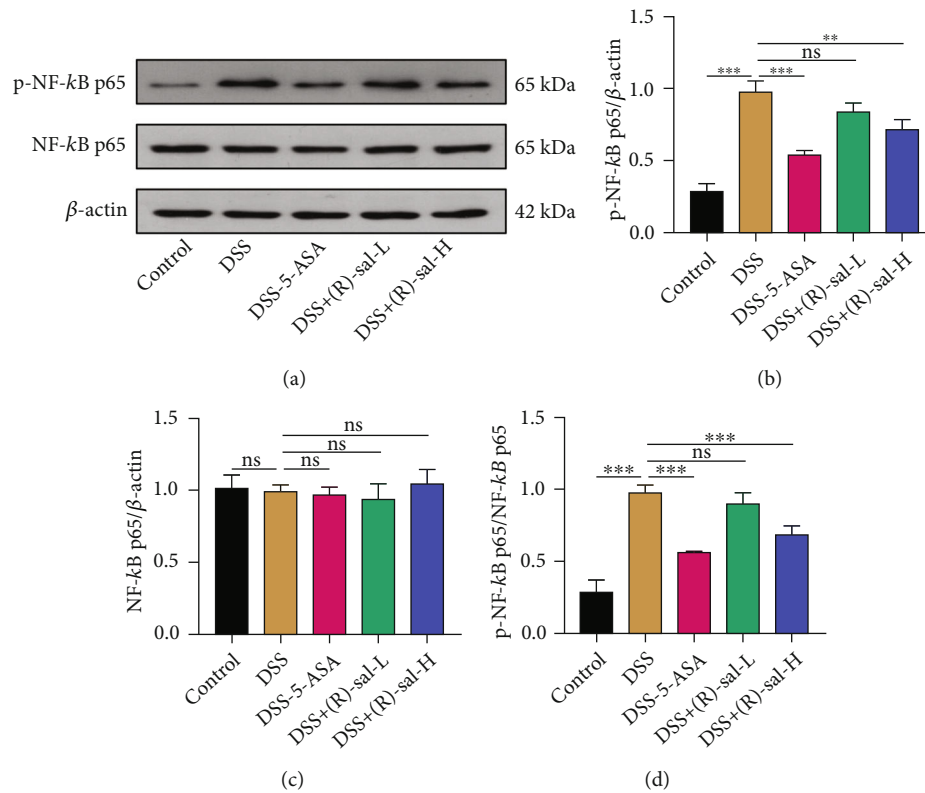


FIGURE 5: The effect of (R)-sal on NF-κB pathway. (a) Western blot analysis of the expression of NF-κB p65 and p-NF-κB p65 in colon tissue. (b–d) The relative expression of p-NF-κB p65, NF-κB p65, and p-NF-κB p65/NF-κB p65, respectively. * $P < 0.05$, ** $P < 0.01$, and *** $P < 0.001$ versus the DSS group.

HO-1 were remarkably diminished in mice with chronic colitis, while treatment with different doses of (R)-sal dramatically elevated the levels of Nrf-2 and HO-1. Interestingly, the (R)-sal-H group exhibited upregulating the expression of Nrf-2 and HO-1 compared with the 5-ASA group. This is consistent with the above antioxidant results assessed by immunofluorescence, demonstrating that (R)-sal could notably activate the Nrf-2 signaling pathway.

3.5. (R)-sal Improved the Intestinal Barrier in Mice with Chronic Colitis. The intestinal barrier is a protection mechanism against damage from intestinal pernicious bacteria, which could prevent the exacerbation of colitis [26]. Glycogen protein, ZO-1, and occludin are crucial components of the intestinal barrier. Therefore, to observe the ameliorated effects of (R)-sal on intestinal barrier integrity, PAS staining and the expression of ZO-1 and occludin were analyzed by western blotting and immunofluorescence in the colon tissue samples.

As shown in Figures 7(a) and 7(b), compared with the control group, goblet cells were dramatically damaged in the DSS group. Oral administration of different doses of (R)-sal could notably elevate the number of goblet cells in the colon. Besides, in contrast to the control group, the expressions of ZO-1 and occludin were dramatically diminished in mice with chronic colitis, whereas (R)-sal reversed these changes in a dose-dependent fashion (Figures 7(c)–7(e)).

Interestingly, the expressions of ZO-1 and occludin in the DSS+(R)-sal-H group were more elevated than those in the DSS+5-ASA group. Additionally, the expressions of ZO-1 and occludin were also investigated by immunofluorescence (Figure 8), and the results verified that (R)-sal could also upregulate the expression of ZO-1 and occludin in colon tissue, which was consistent with the western blot results. These results revealed that (R)-sal could improve the intestinal barrier in mice with chronic colitis.

3.6. (R)-sal Attenuated Intestinal Fibrosis in Mice with Chronic Colitis. During the progression of chronic colitis, irregular myofibroblast activation results in extracellular matrix accumulation, eventually causing intestinal fibrosis [27]. TGF-β1 and α-SMA are the key biomarkers for intestinal fibrosis formation. Therefore, the effect of (R)-sal on intestinal fibrosis was assessed by TGF-β1 and α-SMA immunofluorescence. As shown in Figure 9, the results verified that there were lots of positive signals for TGF-β1 and α-SMA in colon tissue in the DSS group compared with the control group. These results demonstrated that intestinal fibrosis was detected in DSS-induced chronic colitis mice. Interestingly, compared with the DSS group, treatment with different doses of (R)-sal exhibited noticeable attenuation of the expression of TGF-β1 and α-SMA.

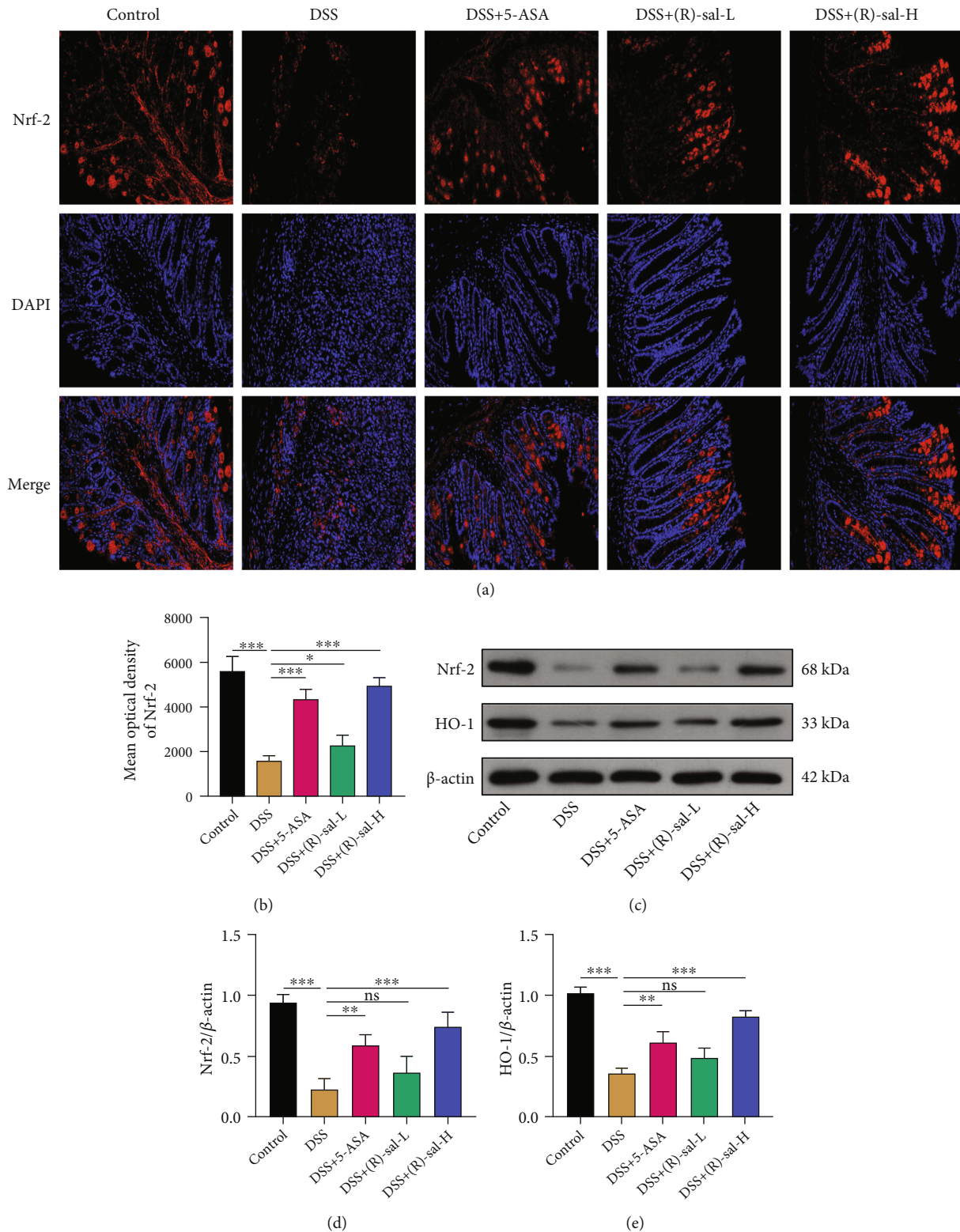


FIGURE 6: The effect of (R)-sal on Nrf-2/HO-1 pathway. (a) Representative image of Nrf-2 staining in different groups. (b) The mean optical density of Nrf-2 in different groups. (c) Western blot analysis of the expression of Nrf-2 and HO-1 in colon tissue. The relative expression of (d) Nrf-2 and (e) HO-1. * $P < 0.05$, ** $P < 0.01$, and *** $P < 0.001$ versus the DSS group.

Besides, the fibrosis-related collagen depositions in colon tissue were examined by picosirius red stain. As shown in Figure 10, there were lots of collagen depositions on repeated

DSS-induced chronic colitis mice compared with those on the control group. Importantly, oral administration with (R)-sal could appear to have improvement effects against

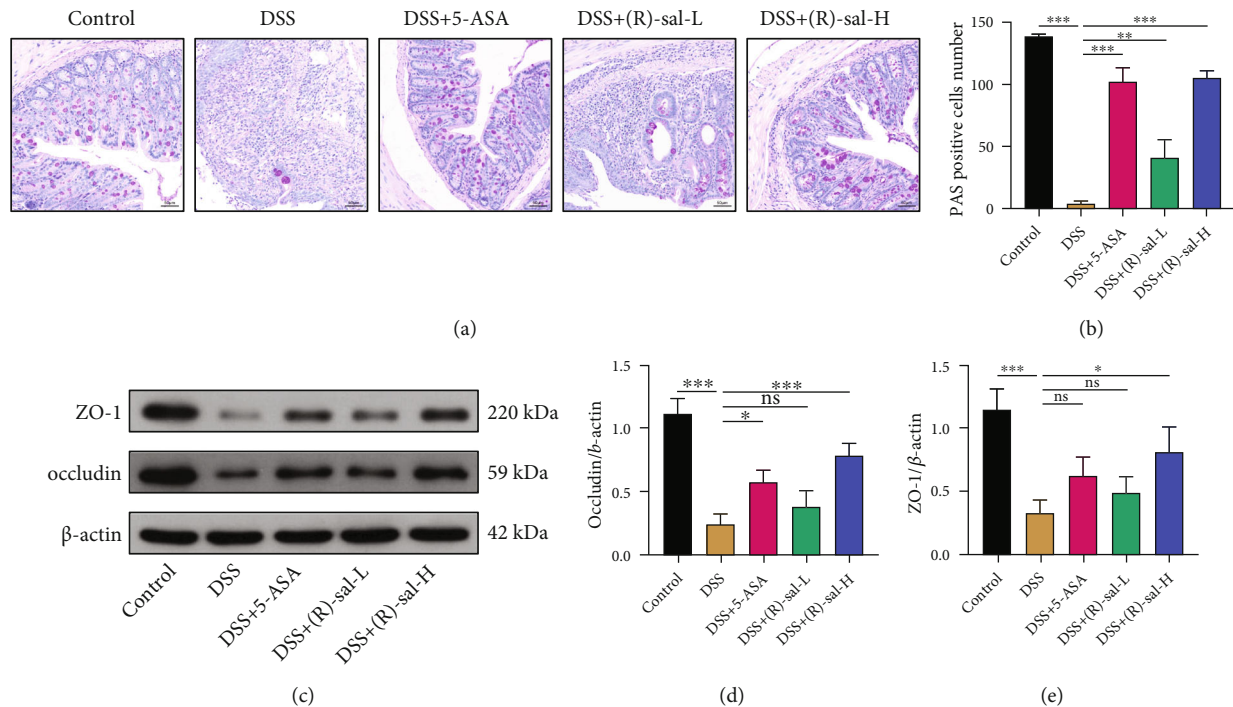


FIGURE 7: The effect of (R)-sal on intestinal barrier function. (a) Representative image of PAS staining from different groups. (b) The PAS positive cell number in different groups. (c) Western blot analysis of the expression of ZO-1 and occludin in colon tissue. The relative expression of (d) occludin and (e) ZO-1, respectively. * $P < 0.05$, ** $P < 0.01$, *** $P < 0.001$ versus the DSS group.

collagen depositions, which contributed to suppressed intestinal fibrosis on DSS-induced chronic colitis mice. Clearly, the efficacy of the (R)-sal-H group was better than that of the 5-ASA group.

3.7. (R)-sal Regulated the Intestinal Microbiome in Mice with Chronic Colitis. Many researches have confirmed that the intestinal microbiome plays core role in UC pathogenesis [28, 29]. The modulation of the intestinal microbiome serves as a potential therapeutic strategy for chronic colitis. To further evaluate the effects of (R)-sal on the chronic colitis intestinal microbiome, the 16S rDNA sequencing of intestinal contents was performed.

Principal coordinate analysis (PCoA) based on the weight UniFrac distance matrices was used to observe the effect of (R)-sal on intestinal microbiome structural alterations. As shown in Figure 11(a), the intestinal microbiome was changed in the DSS group, which was notably different with the control group. However, oral treatment with (R)-sal changed the abnormal intestinal microbiome structure compared with the DSS group, making it more similar to the control group.

Besides, the heat map of OTU levels in the intestinal microbiome was used to further investigate the intestinal microbiome structure change in each group. The heat map exhibited the top 20 relative abundance OTU levels in each group. As shown by the heat map (Figure 11(b)), the intestinal microbiome structures among the control and DSS+(R)-sal-H groups were different than those among the DSS group, and the intestinal microbiome structure in the control group was similar to that

in the DSS+(R)-sal-H group. The results of this analysis revealed that treatment with (R)-sal could diminish chronic colitis-induced changes in the intestinal microbiome structure at the OTU level.

In order to evaluate the effect of (R)-sal on adjusting the intestinal microbiome structure, the intestinal microbiome distribution at the phylum and genus levels was further investigated among these groups. As shown in Figure 11(c), the histograms exhibited species changes in the three groups at the phylum level and their relative abundance. Bacteroidetes, Firmicutes, and Proteobacteria were the preponderant species among these groups. The indicator value analysis (IndVal) was used to find the species with statistical significance. Verrucomicrobia and Proteobacteria were notably different species in each group (Figures 11(e) and 11(f)). Compared with the control group, the relative abundance of Verrucomicrobia was suppressed, and the relative abundance of Proteobacteria was elevated in the DSS group. Conversely, treatment with (R)-sal could change this trend.

Figure 11(d) illustrates alterations in the relative abundance of each group at the genus level. Compared with the control group, the relative abundances of Bacteroides, Parasutterella, Ruminococcaceae_UCG-005, and Romboutsia were raised to different degrees, and the relative abundance of Akkermansia was attenuated by DSS induction (Figures 11(g)–11(k)). However, these changes in bacteria could be ameliorated by the oral administration of (R)-sal. These results demonstrate that oral administration of (R)-sal could improve intestinal microbiome structure changes in mice with chronic colitis.

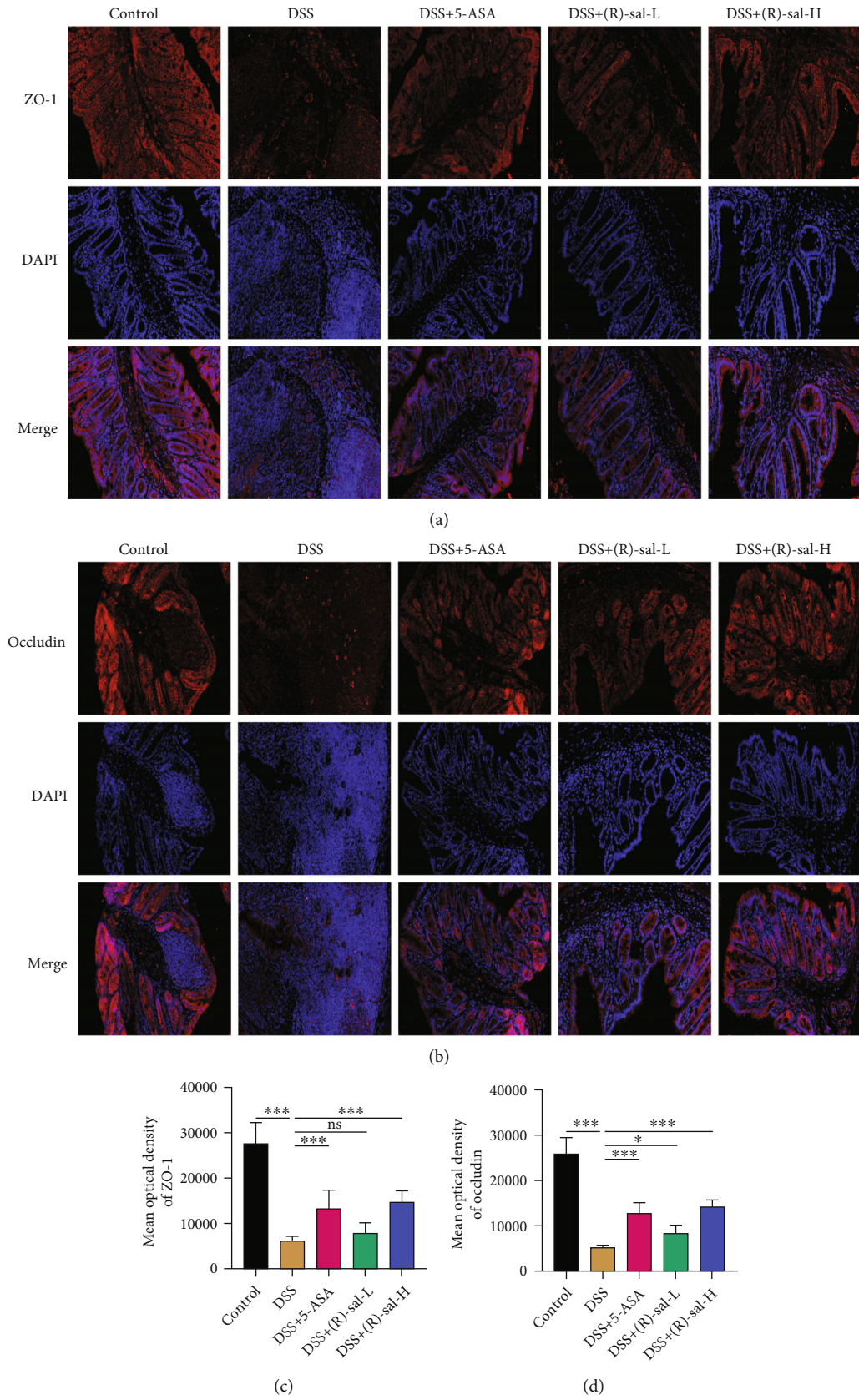
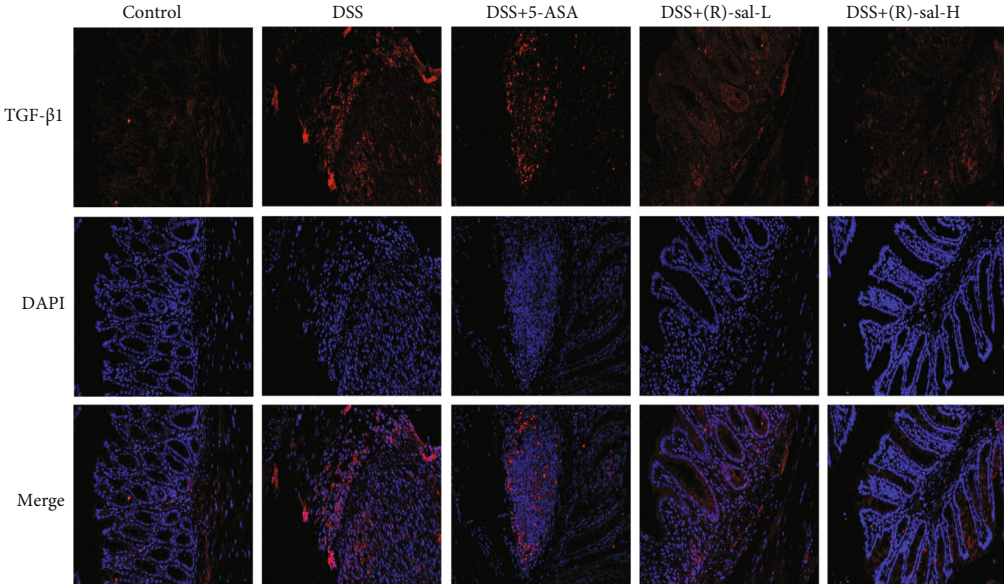
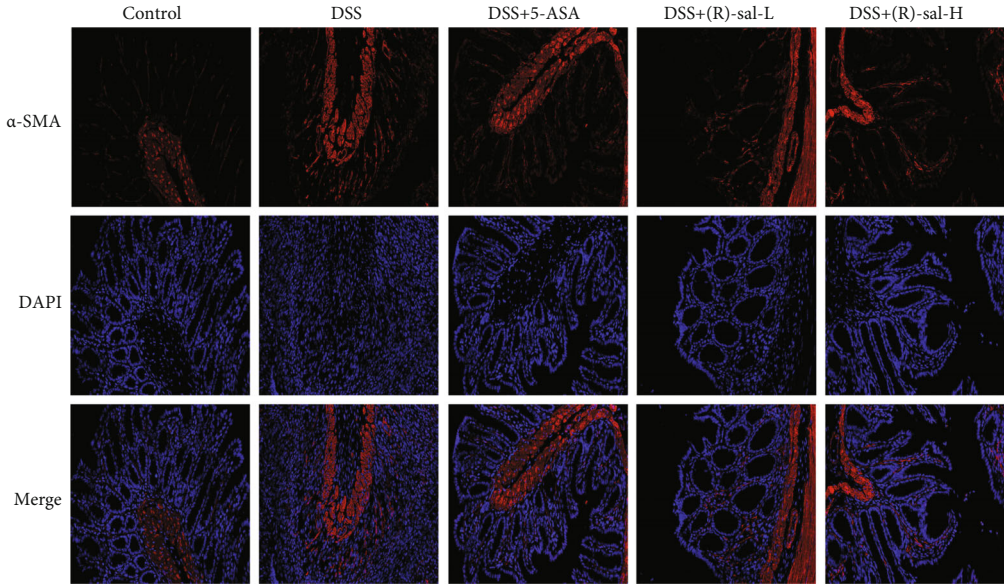


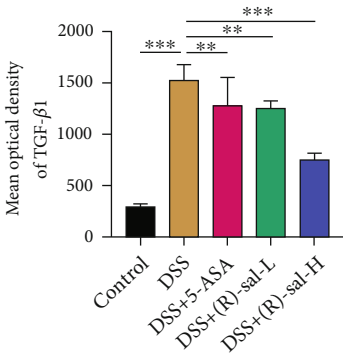
FIGURE 8: (R)-sal improved intestinal integrity by regulating the levels of ZO-1 and occludin. (a) Representative image of ZO-1 staining in different groups. (b) Representative image of occludin staining in different groups. (c) The mean optical density of ZO-1 in different groups. (d) The mean optical density of occludin in different groups. * $P < 0.05$, ** $P < 0.01$, and *** $P < 0.001$ versus the DSS group.



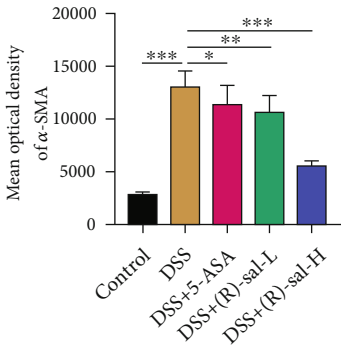
(a)



(b)



(c)



(d)

FIGURE 9: The effect of (R)-sal on intestinal tissue fibrosis. (a) Representative image of TGF-β1 staining in different groups. (b) Representative image of α-SMA staining in different groups. (c) The mean optical density of TGF-β1 in different groups. (d) The mean optical density of α-SMA in different groups. * $P < 0.05$, ** $P < 0.01$, and *** $P < 0.001$ versus the DSS group.

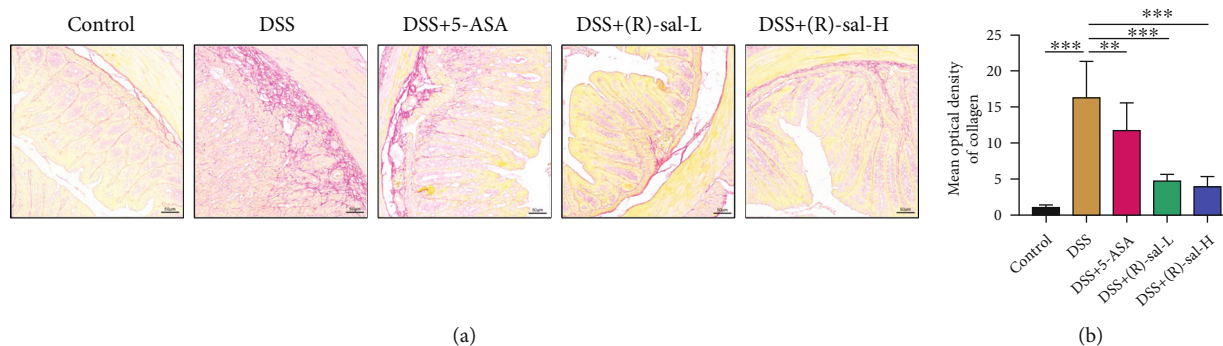


FIGURE 10: The effect of (R)-sal on the depositions of collagen. (a) Representative image of picosirius red staining in different groups. (b) The mean optical density of collagen in different groups. * $P < 0.05$, ** $P < 0.01$, and *** $P < 0.001$ versus the DSS group.

3.8. Safety Evaluation of (R)-sal. The safety of (R)-sal after long-term treatment in mice with chronic colitis was further investigated. There were no effects on the survival status of mice treated with (R)-sal during the study. The heart, liver, spleen, lung, and kidney tissues from the DSS+(R)-sal-H group were subjected to histopathological examination (Figure 12). The result verified that there was little notable damage in these tissues by oral administration of (R)-sal.

4. Discussion

UC is an inflammatory disorder that is characterized by recurrence and complicated etiology. Several factors play a core role in the pathogenesis of UC, including the environment, genetics, immune system, intestinal barrier, and intestinal microbiome [30, 31]. The potential adverse effects have limited current therapeutic drug applications [32, 33]. Therefore, it is necessary to develop safer and effective medicine for UC. In this study, we verified that (R)-sal, instead of (S)-sal or (RS)-sal, mitigated chronic colitis, with underlying mechanisms including the reduction in inflammatory reaction activation, activation of Nrf-2/HO-1 expression, improvement in the intestinal barrier, attenuation of intestinal fibrosis, and regulation of the intestinal microbiome in mice with chronic colitis.

It has been reported that there were different effects with regard to (R)-enantiomers and (S)-enantiomers in trials [34]. Therefore, different enantiomers were used to investigate the amelioration in chronic colitis. The results verified that (R)-sal, instead of (S)-sal, could noticeably improve chronic colitis in mice. In addition, although (RS)-sal contains the same amount of (R)-sal, the relieving effect of (RS)-sal on chronic colitis is less than that of single (R)-sal, which may be due to the existence of toxicity (S)-sal in (RS)-sal, weakening its amelioration effect. Therefore, there was significance beneficial effect to use (R)-sal in mice with chronic colitis.

Among the immune-regulatory factors, the inflammatory reaction has been thought to be a core mechanism in the pathophysiology of chronic colitis [35]. Proinflammatory cytokines play an active role in inflammatory reactions, which could induce macrophage migration and inflammatory mediator release [36], thereby further amplifying the inflammatory reaction. Previous studies have shown that

proinflammatory cytokines were the typical features on repeated DSS-induced chronic colitis [37]. In this research, oral administration of (R)-sal dramatically suppressed the oversecretion of proinflammatory cytokines in mice with chronic colitis, which demonstrated that (R)-sal diminished abnormal inflammatory reactions. These results indicated that the colon exhibited an inflammatory state on repeated DSS-induced chronic colitis and that (R)-sal could improve this state. In addition, use of (S)-sal leads to further deterioration of this disease. Therefore, in chronic colitis, long-term use of (RS)-sal could weaken the effect of (R)-sal. In this model, colitis was repeatedly induced, and (R)-sal was given after the colitis appeared in order to investigate the therapeutic effect. In addition, this study showed significant therapeutic effect of (R)-sal; furthermore, (R)-sal was more effective in either active or recovery states when colitis was induced by DSS or withdraw, in comparison of (RS)-sal and 5-ASA.

To further investigate the anti-inflammatory mechanism of (R)-sal, the NF- κ B related proteins NF- κ B p65 and p-NF- κ B p65 were detected in colon tissue. NF- κ B plays a core role in regulating the process of inflammation [38]. It has been reported that activation of NF- κ B could elevate proinflammatory cytokine expression [39]. These cytokines trigger positive feedback regulation in inflammation activation, which ultimately damages colon tissue [40, 41]. The results of this study revealed that the levels of p-NF- κ B p65 were dramatically increased in the DSS group compared with the control group, which illustrated that the NF- κ B signaling pathway was activated in mice with chronic colitis. Treatment with (R)-sal dramatically suppressed p-NF- κ B p65 expression, which was consistent with previous proinflammatory cytokine expression changes. These results demonstrated that (R)-sal could relieve inflammation by mitigating the activation of the NF- κ B pathway.

The Nrf-2 signaling pathway is a significant pathway which involved in regulating the level of antioxidant medium [42, 43]. The Nrf-2 downstream antioxidant protein HO-1 could increase expression after Nrf-2 pathway activation [44]. HO-1 is an antioxidant protein that constitutes a defense network against oxidative stress damage and prevents colon tissue oxidative damage [45, 46]. Besides, there is an interaction between Nrf-2 and NF- κ B pathway [47]. Suppression of the expression of Nrf-2 would exacerbate oxidative stress generation, which further induces NF- κ B activation.

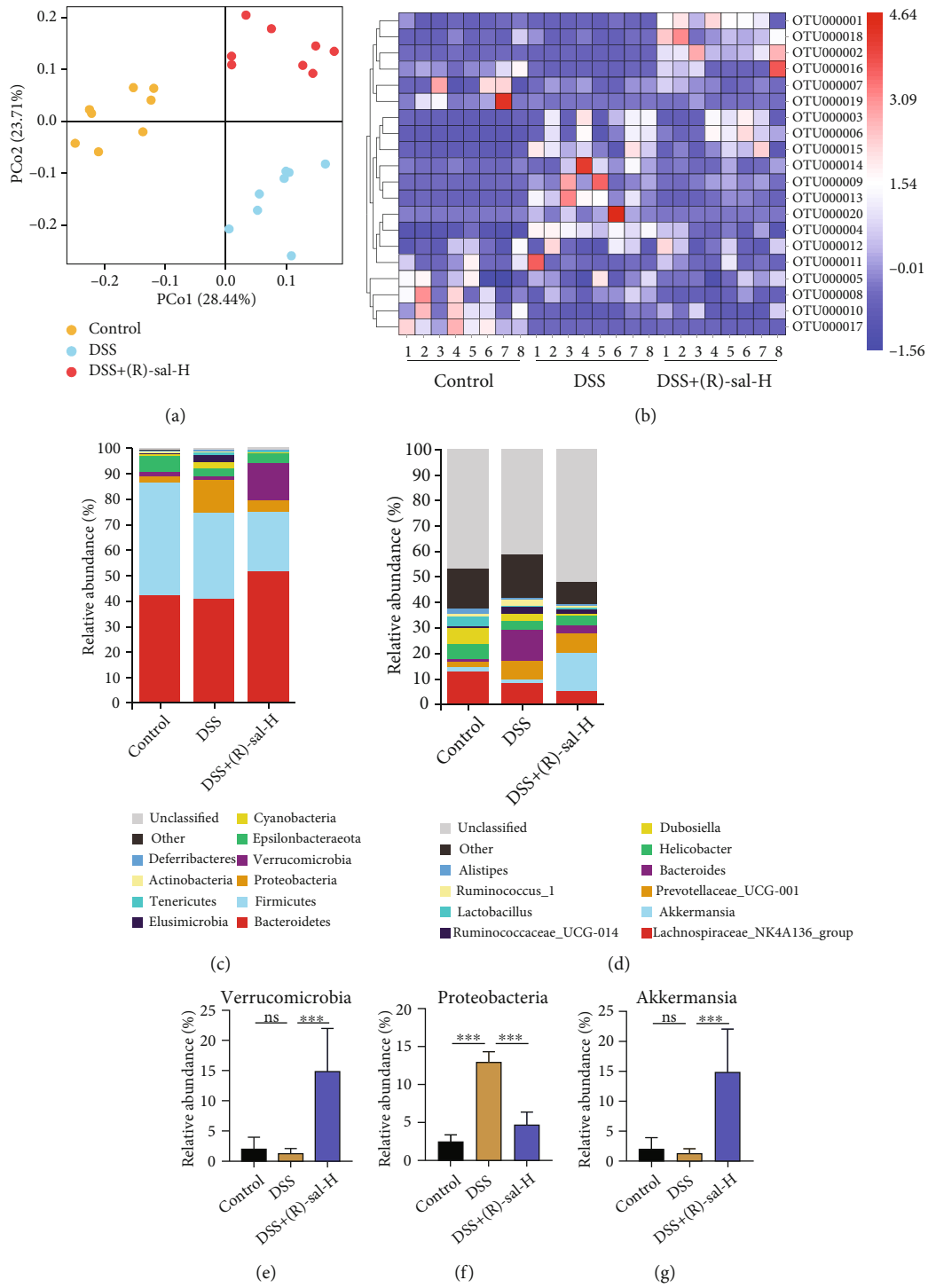


FIGURE 11: Continued.

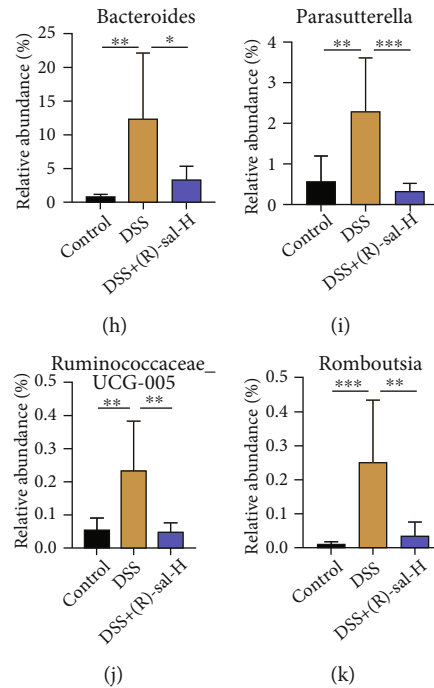


FIGURE 11: The effect of (R)-sal on the intestinal microbiome. (a) PCoA plot based on the weighted UniFrac index at the OTU level. (b) Heat map revealing the top 20 abundance microbial at the OTU level. (c) The intestinal microbiome structure at the phylum level. (d) The intestinal microbiome structure at the genus level. (R)-sal regulated (e) Verrucomicrobia and (f) Proteobacteria at the phylum level. (R)-sal modulated (g) Akkermansia, (h) Bacteroides, (i) Parasutterella, (j) Ruminococcaceae_UCG-005, and (k) Romboutsia at the genus level. * $P < 0.05$, ** $P < 0.01$, and *** $P < 0.001$ versus the DSS group.

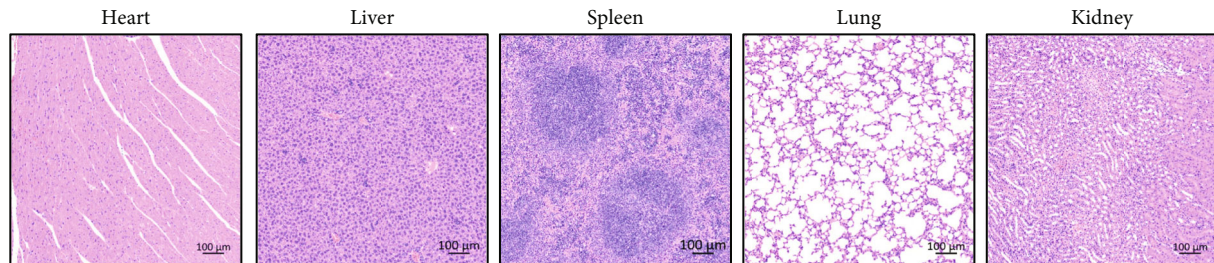


FIGURE 12: No toxicity was observed with the treatment of (R)-sal in mice with chronic colitis. Representative image of HE staining in the heart, liver, spleen, lung, and kidney tissue.

Furthermore, CREB binding protein (CBP) is a transcription factor between Nrf-2 and NF- κ B, which means that there is competition between Nrf-2 and NF- κ B, namely, negative feedback regulation [48]. Saber et al. [49] found that olmesartan could notably improve colitis due to olmesartan being able to suppress NF- κ B and activate Nrf-2. In this research, the expression of Nrf-2 and HO-1 in colon tissue was remarkably relieved in mice with chronic colitis compared with control mice, and this abnormality could be noticeably reversed by oral administration of (R)-sal. These results demonstrated that (R)-sal could relieve chronic colitis by activating the Nrf-2 pathway.

The intestinal barrier protects against the invasion of pathogenic microorganisms and diminishes colon tissue damage [50, 51]. Tight junction proteins (such as the cytoplasmic scaffolding protein ZO-1 and the transmembrane barrier protein occludin) and glycogen proteins are core elements in the intestinal barrier, which play crucial roles in

maintaining the integrity of the intestine [52]. Damage to the intestinal barrier is considered one of the core factors for colitis formation [53]. Therefore, the protective effects of (R)-sal in PAS, ZO-1, and occludin were further investigated in mice with chronic colitis. Similar to previous researches, the expressions of ZO-1, occludin, and glycogen proteins were noticeably suppressed compared with the control group, which reflected that the intestinal barrier was damaged in mice with chronic colitis. Surprisingly, treatment with (R)-sal remarkably elevated the levels of ZO-1, occludin, and glycogen proteins, which improved the integrity in colon tissue. These results demonstrated the improved effect of (R)-sal on intestinal barrier integrity, which may offer potential therapy for chronic colitis.

Intestinal fibrosis is considered a crucial element in the evolution of chronic colitis [54]. Chronic inflammation continuously stimulates related cell proliferation and persistent depositions of collagen, which caused extracellular matrix

(ECM) abnormally exacerbates and sedimentary, eventually leading to intestinal fibrosis [55]. Mesenchymal cells, epithelial cells, endothelial cells, stellate cells, and fibrocytes contribute to ECM accumulation [56, 57]. Previous research has demonstrated that lots of ECM accumulated in the colon tissue, which leads to the formation of colon fibrosis in IBD patients [58]. TGF- β 1 is a key profibrotic cytokines which secreted by a variety of cells such as intestinal fibroblasts and intestinal epithelial cells in colon tissue [56]. During chronic colitis, the secretion of TGF- β 1 is exacerbated, which acts on intestinal interstitial cells to elevate ECM secretion [59, 60]. Therefore, the expression of TGF- β 1 could reflect the degree of intestinal fibrosis. These results demonstrated that the expression of TGF- β 1 was dramatically elevated in the colon of mice with chronic colitis, and this abnormal performance was attenuated by oral administration of (R)-sal. In addition, the biomarker of fibrosis α -SMA and the deposits of collagen were further assessed in colon tissue. The upregulated level of α -SMA and collagen was proven in mice with chronic colitis, and treatment with (R)-sal reversed this status. Use of 5-ASA has less role in fibrosis development, while by surprise, (R)-sal showed a remarked protective effect in antifibrosis.

Recently, intestinal microbiome dysbiosis was thought to play the crucial role in activating the immune defense system [61–63]. Many researches have reported that intestinal microbiome dysbiosis was closely related to the progression of UC [40, 64]. Besides, according to many researches, treatment with DSS in mice could remarkably alter the intestinal microbiome composition [65, 66]. To further assess the effect of (R)-sal on the intestinal microbiome structure on DSS-induced chronic colitis mice, 16S rDNA gene sequencing was executed in different groups. The PCoA parameters were used to evaluate similarities in these groups. As expected, some changes in the microbiome structure were found in the DSS and (R)-sal-H groups. In this research, based on PCoA parameter analysis, the microbiome structure was more similar between the control and (R)-sal-H groups at the OTU level than the DSS group. Moreover, the heat map of microbial composition at the OTU level also further confirmed this phenomenon. These findings demonstrated that treatment with (R)-sal could ameliorate the intestinal microbiome structure, which was different from the DSS group.

To further investigate the improvement in microbial composition by (R)-sal, the gut microbiota structure composition at the taxonomic hierarchy level was examined. At the phylum level, Bacteroidetes, Firmicutes, and Proteobacteria were found to compose the main part of the microbiota structure, which is similar to previous research [67, 68]. The intestinal microbiome in mice with chronic colitis showed that the ratio of Proteobacteria was dramatically exacerbated, which was consistent with a previous study [40]. Oral administration of (R)-sal reversed the ratio of Proteobacteria in mice with chronic colitis. It has been reported that Proteobacteria was thought to be harmful [66]. Verrucomicrobia was thought to be closely related to regulation of the mucosal inflammation [69]. Emerging studies have shown the ratio of Verrucomicrobia was suppressed in UC patients [70]. Treatment with (R)-sal notably elevated the

ratio of Verrucomicrobia, which helped to improve the mucosal inflammation in chronic colitis.

At the genus level, (R)-sal could also reverse some special microbial ratio changes in mice with chronic colitis. Treatment with DSS dramatically elevated the relative abundances of Bacteroides, Parasutterella, Romboutsia, and Ruminococcaceae_UCG-005; nevertheless, treatment with (R)-sal could regulate these changes in varying degrees. Bacteroides has been found to be noticeably elevated in UC patients, which could stimulate and aggravate colon inflammation [71, 72]. Parasutterella could induce enteritis and septicemia, and it has been reported that the relative abundances were positively correlated with intestinal chronic inflammation and irritable bowel syndrome severity [73–75]. Therefore, suppression of the level of proinflammatory microbiota could help to regulate inflammation, thus mitigating chronic colitis.

Akkermansia is a probiotic that can maintain intestinal barrier function and regulate the immune response by producing various metabolites [76]. It has been reported that the relative abundance of Akkermansia was notably attenuated in UC patients [77]. Surprisingly, (R)-sal remarkably elevated the relative abundance of Akkermansia compared with the mice with chronic colitis, which could contribute to improve the intestinal barrier function and regulate the immune response. In this research, treatment with (R)-sal was found to regulate the relative abundances of some special intestinal microbiomes, which helped to promote the amelioration of chronic colitis.

5. Conclusion

In conclusion, the results of our study demonstrate (R)-sal significantly effective in treatment chronic colitis. Furthermore, that (R)-sal, instead of (S)-sal or (RS)-sal, markedly attenuate chronic colitis in mice through several mechanisms, including suppressing gut inflammation, regulating oxidative stress, ameliorating intestinal barrier integrity, suppressing colon fibrosis, and diminishing intestinal microbiome dysbiosis. These results reveal a therapeutical potential of long-term usage of (R)-sal in chronic colitis with reduced side effect in comparison of other traditional therapeutical options.

Data Availability

The data underlying this article are available in the article.

Conflicts of Interest

The authors declare that they have no known competing financial interests or personal relationships that could have appeared to influence the work reported in this paper.

Authors' Contributions

Liangjun Deng, Shanping Wang, and Wen Tan designed research. Wen Tan supervised the research. Liangjun Deng, Haihua Guo, and Yue Lin performed the experiments.

Liangjun Deng, Haihua Guo, Xiaoming Liu, and Rui Zhang analyzed the data. Liangjun Deng and Shanping Wang wrote the manuscript.

Acknowledgments

This work was supported by the National Science and Technology Major Project (grant number 2019ZX09301120) and Guangdong Basic and Applied Basic Research Foundation (grant number 2021A1515110714).

References

- [1] A. J. Walsh, R. V. Bryant, and S. P. L. Travis, "Current best practice for disease activity assessment in IBD," *Nature Reviews Gastroenterology & Hepatology*, vol. 13, no. 10, pp. 567–579, 2016.
- [2] S. Vermeire, G. Van Assche, and P. Rutgeerts, "Classification of inflammatory bowel disease," *Current Opinion in Gastroenterology*, vol. 28, no. 4, pp. 321–326, 2012.
- [3] J. E. Lennard-Jones, "Classification of inflammatory bowel disease," *Scandinavian Journal of Gastroenterology. Supplement*, vol. 170, pp. 2–6, 1989, discussion 16–9.
- [4] M. Duijvestein, R. Battat, N. Vande Casteele et al., "Novel therapies and treatment strategies for patients with inflammatory bowel disease," *Current Treatment Options in Gastroenterology*, vol. 16, no. 1, pp. 129–146, 2018.
- [5] S. C. Ng, H. Y. Shi, N. Hamidi et al., "Worldwide incidence and prevalence of inflammatory bowel disease in the 21st century: a systematic review of population-based studies," *Lancet*, vol. 390, no. 10114, pp. 2769–2778, 2017.
- [6] S. Bopanna, A. N. Ananthakrishnan, S. Kedia, V. Yajnik, and V. Ahuja, "Risk of colorectal cancer in Asian patients with ulcerative colitis: a systematic review and meta-analysis," *The Lancet Gastroenterology & Hepatology*, vol. 2, no. 4, pp. 269–276, 2017.
- [7] B. D. Ye, H. Choi, M. Hong et al., "Identification of ten additional susceptibility loci for ulcerative colitis through Immunochip analysis in Koreans," *Inflammatory Bowel Diseases*, vol. 22, no. 1, pp. 13–19, 2016.
- [8] H. J. Kim, H. J. Hann, S. N. Hong et al., "Incidence and natural course of inflammatory bowel disease in Korea, 2006–2012: a nationwide population-based study," *Inflammatory Bowel Diseases*, vol. 21, no. 3, pp. 623–630, 2015.
- [9] T. Oshima and H. Miwa, "Gastrointestinal mucosal barrier function and diseases," *Journal of Gastroenterology*, vol. 51, no. 8, pp. 768–778, 2016.
- [10] S. van der Post, K. S. Jabbar, G. Birchenough et al., "Structural weakening of the colonic mucus barrier is an early event in ulcerative colitis pathogenesis," *Gut*, vol. 68, no. 12, pp. 2142–2151, 2019.
- [11] E. A. Franzosa, A. Sirota-Madi, J. Avila-Pacheco et al., "Gut microbiome structure and metabolic activity in inflammatory bowel disease," *Nature Microbiology*, vol. 4, no. 2, pp. 293–305, 2019.
- [12] X. Bai, X. Gou, P. Cai et al., "Sesamin enhances Nrf2-mediated protective defense against oxidative stress and inflammation in colitis via AKT and ERK activation," *Oxidative Medicine and Cellular Longevity*, vol. 2019, Article ID 2432416, 20 pages, 2019.
- [13] T. Karrasch and C. Jobin, "NF- κ B and the intestine: friend or foe?," *Inflammatory Bowel Diseases*, vol. 14, no. 1, pp. 114–124, 2008.
- [14] K. Taguchi, H. Motohashi, and M. Yamamoto, "Molecular mechanisms of the Keap1-Nrf2 pathway in stress response and cancer evolution," *Genes to Cells*, vol. 16, no. 2, pp. 123–140, 2011.
- [15] Y. Tan and C. Zheng, "Effects of Alpinetin on intestinal barrier function, inflammation and oxidative stress in dextran sulfate sodium-induced ulcerative colitis mice," *American Journal of the Medical Sciences*, vol. 355, no. 4, pp. 377–386, 2018.
- [16] B. N. Chorley, Y. H. Li, S. J. Fang, J. A. Park, and K. B. Adler, "(R)-albuterol elicits antiinflammatory effects in human airway epithelial cells via iNOS," *American Journal of Respiratory Cell and Molecular Biology*, vol. 34, no. 1, pp. 119–127, 2006.
- [17] S. Wang, F. Liu, K. S. Tan et al., "Effect of (R)-salbutamol on the switch of phenotype and metabolic pattern in LPS-induced macrophage cells," *Journal of Cellular and Molecular Medicine*, vol. 24, no. 1, pp. 722–736, 2020.
- [18] F. Liu, S. Wang, B. Liu, Y. Wang, and W. Tan, "(R)-salbutamol improves imiquimod-induced psoriasis-like skin dermatitis by regulating the Th17/Tregs balance and glycerophospholipid metabolism," *Cell*, vol. 9, no. 2, 2020.
- [19] S. Wirtz, V. Popp, M. Kindermann et al., "Chemically induced mouse models of acute and chronic intestinal inflammation," *Nature Protocols*, vol. 12, no. 7, pp. 1295–1309, 2017.
- [20] B. Chassaing, J. D. Aitken, M. Malleshappa, and M. Vijay-Kumar, "Dextran sulfate sodium (DSS)-induced colitis in mice," *Current Protocols in Immunology*, vol. 104, no. 1, 2014.
- [21] H. S. Cooper, S. N. Murthy, R. S. Shah, and D. J. Sedergran, "Clinicopathologic study of dextran sulfate sodium experimental murine colitis," *Laboratory Investigation*, vol. 69, no. 2, pp. 238–249, 1993.
- [22] H. Li, C. Fan, H. Lu et al., "Protective role of berberine on ulcerative colitis through modulating enteric glial cells-intestinal epithelial cells-immune cells interactions," *Acta Pharmaceutica Sinica B*, vol. 10, no. 3, pp. 447–461, 2020.
- [23] S. Saber, M. Basuony, and A. S. Eldin, "Telmisartan ameliorates dextran sodium sulfate-induced colitis in rats by modulating NF- κ B signalling in the context of PPAR γ agonistic activity," *Archives of Biochemistry and Biophysics*, vol. 671, pp. 185–195, 2019.
- [24] A. Bhattacharyya, R. Chattopadhyay, S. Mitra, and S. E. Crowe, "Oxidative stress: an essential factor in the pathogenesis of gastrointestinal mucosal diseases," *Physiological Reviews*, vol. 94, no. 2, pp. 329–354, 2014.
- [25] X. Li, J. Zhan, Y. Hou et al., "Coenzyme Q10 regulation of apoptosis and oxidative stress in H₂O₂ induced BMSC death by modulating the Nrf2/NQO-1 signaling pathway and its application in a model of spinal cord injury," *Oxidative Medicine and Cellular Longevity*, vol. 2019, Article ID 6493081, 2019.
- [26] Y. Lee, K. Sugihara, M. G. Gilliland III, S. Jon, N. Kamada, and J. J. Moon, "Hyaluronic acid-bilirubin nanomedicine for targeted modulation of dysregulated intestinal barrier, microbiome and immune responses in colitis," *Nature Materials*, vol. 19, no. 1, pp. 118–126, 2020.
- [27] K. Suzuki, X. Sun, M. Nagata et al., "Analysis of intestinal fibrosis in chronic colitis in mice induced by dextran sulfate sodium," *Pathology International*, vol. 61, no. 4, pp. 228–238, 2011.

- [28] A. Larabi, N. Barnich, and H. T. T. Nguyen, "New insights into the interplay between autophagy, gut microbiota and inflammatory responses in IBD," *Autophagy*, vol. 16, no. 1, pp. 38–51, 2020.
- [29] D. Parada Venegas, M. K. de la Fuente, G. Landskron et al., "Corrigendum: Short chain fatty acids (SCFAs)-mediated gut epithelial and immune regulation and its relevance for inflammatory bowel diseases," *Frontiers in Immunology*, vol. 10, 2019.
- [30] D. H. Kim and J. H. Cheon, "Pathogenesis of inflammatory bowel disease and recent advances in biologic therapies," *Immune Network*, vol. 17, no. 1, pp. 25–40, 2017.
- [31] K. L. Glassner, B. P. Abraham, and E. M. M. Quigley, "The microbiome and inflammatory bowel disease," *Journal of Allergy and Clinical Immunology*, vol. 145, no. 1, pp. 16–27, 2020.
- [32] A. Stallmach, S. Hagel, and T. Bruns, "Adverse effects of biologics used for treating IBD," *Best Practice & Research Clinical Gastroenterology*, vol. 24, no. 2, pp. 167–182, 2010.
- [33] Y. Wang, C. E. Parker, T. Bhanji, B. G. Feagan, J. K. MacDonald, and Cochrane IBD Group, "Oral 5-aminosalicylic acid for induction of remission in ulcerative colitis," *Cochrane Database of Systematic Reviews*, vol. 4, 2016.
- [34] D. Handley, "The asthma-like pharmacology and toxicology of (S)-isomers of beta agonists," *Journal of Allergy and Clinical Immunology*, vol. 104, no. 2, pp. S69–S76, 1999.
- [35] K. Wang, X. Jin, Q. Li et al., "Propolis from different geographic origins decreases intestinal inflammation and Bacteroides spp. populations in a model of DSS-induced colitis," *Molecular Nutrition and Food Research*, vol. 62, no. 17, 2018.
- [36] Z. Zhang, S. Li, H. Cao et al., "The protective role of phloretin against dextran sulfate sodium-induced ulcerative colitis in mice," *Food & Function*, vol. 10, no. 1, pp. 422–431, 2019.
- [37] S. Kanwal, T. P. Joseph, S. Aliya et al., "Attenuation of DSS induced colitis by *Dictyophora indusiata* polysaccharide (DIP) via modulation of gut microbiota and inflammatory related signaling pathways," *Journal of Functional Foods*, vol. 64, 2020.
- [38] I. Papaconstantinou, C. Zeglinas, M. Gazouli et al., "The impact of peri-operative anti-TNF treatment on anastomosis-related complications in Crohn's disease Patients. A Critical Review. A Critical Review," *Journal of Gastrointestinal Surgery*, vol. 18, no. 6, pp. 1216–1224, 2014.
- [39] T. Lawrence, "The nuclear factor NF-kappaB pathway in inflammation," *Cold Spring Harbor Perspectives in Biology*, vol. 1, no. 6, p. a001651, 2009.
- [40] L. Peng, X. Gao, L. Nie et al., "Astragalol attenuates dextran sulfate sodium (DSS)-induced acute experimental colitis by alleviating gut microbiota dysbiosis and inhibiting NF-kB activation in mice," *Frontiers in Immunology*, vol. 11, 2020.
- [41] I. Siddique and I. Khan, "Mechanism of regulation of Na-H exchanger in inflammatory bowel disease: role of TLR-4 signaling mechanism," *Digestive Diseases and Sciences*, vol. 56, no. 6, pp. 1656–1662, 2011.
- [42] K. J. Maloy and F. Powrie, "Intestinal homeostasis and its breakdown in inflammatory bowel disease," *Nature*, vol. 474, no. 7351, pp. 298–306, 2011.
- [43] A. K. Jaiswal, "Nrf2 signaling in coordinated activation of antioxidant gene expression," *Free Radical Biology & Medicine*, vol. 36, no. 10, pp. 1199–1207, 2004.
- [44] B. Xu, Y. Qin, D. Li et al., "Inhibition of PDE4 protects neurons against oxygen-glucose deprivation-induced endoplasmic reticulum stress through activation of the Nrf-2/HO-1 pathway," *Redox Biology*, vol. 28, 2020.
- [45] Y. Mei, Z. Wang, Y. Zhang et al., "FA-97, a new synthetic caffeic acid phenethyl ester derivative, ameliorates DSS-induced colitis against oxidative stress by activating Nrf2/HO-1 pathway," *Frontiers in Immunology*, vol. 10, 2020.
- [46] M. Zhang, C. Xu, D. Liu, M. K. Han, L. Wang, and D. Merlin, "Oral delivery of nanoparticles loaded with ginger active compound, 6-shogaol, attenuates ulcerative colitis and promotes wound healing in a murine model of ulcerative colitis," *Journal of Crohn's and Colitis*, vol. 12, no. 2, pp. 217–229, 2018.
- [47] R. K. Thimmulappa, H. Lee, T. Rangasamy et al., "Nrf2 is a critical regulator of the innate immune response and survival during experimental sepsis," *Journal of Clinical Investigation*, vol. 116, no. 4, pp. 984–995, 2006.
- [48] G.-H. Liu, J. Qu, and X. Shen, "NF-kB/p65 antagonizes Nrf2-ARE pathway by depriving CBP from Nrf2 and facilitating recruitment of HDAC3 to MafK," *Biochimica et Biophysica Acta-Molecular Cell Research*, vol. 1783, no. 5, pp. 713–727, 2008.
- [49] S. Saber, R. M. Khalil, W. S. Abdo, D. Nassif, and E. El-Ahwany, "Olmesartan ameliorates chemically-induced ulcerative colitis in rats via modulating NF-kB and Nrf-2/HO-1 signaling crosstalk," *Toxicology and Applied Pharmacology*, vol. 364, pp. 120–132, 2019.
- [50] E. C. Martens, M. Neumann, and M. S. Desai, "Interactions of commensal and pathogenic microorganisms with the intestinal mucosal barrier," *Nature Reviews Microbiology*, vol. 16, no. 8, pp. 457–470, 2018.
- [51] J. Yi, K. Bergstrom, J. Fu et al., "Dcl1 in tuft cells promotes inflammation-driven epithelial restitution and mitigates chronic colitis," *Cell Death and Differentiation*, vol. 26, no. 9, pp. 1656–1669, 2019.
- [52] C. Chelakkot, J. Ghim, and S. H. Ryu, "Mechanisms regulating intestinal barrier integrity and its pathological implications," *Experimental and Molecular Medicine*, vol. 50, pp. 1–9, 2018.
- [53] T. Eom, Y. S. Kim, C. H. Choi, M. J. Sadowsky, and T. Unno, "Current understanding of microbiota- and dietary-therapies for treating inflammatory bowel disease," *Journal of Microbiology*, vol. 56, no. 3, pp. 189–198, 2018.
- [54] K. Scheibe, C. Kersten, A. Schmied et al., "Inhibiting interleukin 36 receptor signaling reduces fibrosis in mice with chronic intestinal inflammation," *Gastroenterology*, vol. 156, no. 4, pp. 1082–1097.e11, 2019.
- [55] M. V. Lenti and A. Di Sabatino, "Intestinal fibrosis," *Molecular Aspects of Medicine*, vol. 65, pp. 100–109, 2019.
- [56] S. Specia, I. Giusti, F. Rieder, and G. Latella, "Cellular and molecular mechanisms of intestinal fibrosis," *World Journal of Gastroenterology*, vol. 18, no. 28, pp. 3635–3661, 2012.
- [57] F. Rieder, T. Karrasch, S. Ben-Horin et al., "Results of the 2nd scientific workshop of the ECCO (III): basic mechanisms of intestinal healing," *Journal of Crohn's & Colitis*, vol. 6, no. 3, pp. 373–385, 2012.
- [58] D. Q. Shih and S. R. Targan, "Insights into IBD pathogenesis," *Current Gastroenterology Reports*, vol. 11, no. 6, pp. 473–480, 2009.

- [59] H. W. Koon, D. Shih, I. Karagiannides et al., "Substance P modulates colitis-associated fibrosis," *American Journal of Pathology*, vol. 177, no. 5, pp. 2300–2309, 2010.
- [60] S. N. Flier, H. Tanjore, E. G. Kokkotou, H. Sugimoto, M. Zeisberg, and R. Kalluri, "Identification of epithelial to mesenchymal transition as a novel source of fibroblasts in intestinal fibrosis," *Journal of Biological Chemistry*, vol. 285, no. 26, pp. 20202–20212, 2010.
- [61] X. Gao, Q. Cao, Y. Cheng et al., "Chronic stress promotes colitis by disturbing the gut microbiota and triggering immune system response," *Proceedings of the National Academy of Sciences of the United States of America*, vol. 115, no. 13, pp. E2960–E2969, 2018.
- [62] N. E. Iliot, J. Bollrath, C. Danne et al., "Defining the microbial transcriptional response to colitis through integrated host and microbiome profiling," *ISME Journal*, vol. 10, no. 10, pp. 2389–2404, 2016.
- [63] J. D. Forbes, G. Van Domselaar, and C. N. Bernstein, "The gut microbiota in immune-mediated inflammatory diseases," *Frontiers in Microbiology*, vol. 7, p. 1081, 2016.
- [64] X. Ma, Y. Hu, X. Li et al., "Periplaneta americana ameliorates dextran sulfate sodium-induced ulcerative colitis in rats by Keap1/Nrf-2 activation, intestinal barrier function, and gut microbiota regulation," *Frontiers in Pharmacology*, vol. 9, no. 944, 2018.
- [65] J. J. Limon, J. Tang, D. Li et al., "_Malassezia_ Is Associated with Crohn 's Disease and Exacerbates Colitis in Mouse Models," *Cell Host & Microbe*, vol. 25, no. 3, pp. 377–388.e6, 2019.
- [66] T. Ohkusa and S. Koido, "Intestinal microbiota and ulcerative colitis," *Journal of Infection and Chemotherapy*, vol. 21, no. 11, pp. 761–768, 2015.
- [67] G. P. Donaldson, S. M. Lee, and S. K. Mazmanian, "Gut biogeography of the bacterial microbiota," *Nature Reviews Microbiology*, vol. 14, no. 1, pp. 20–32, 2016.
- [68] M. Rajilic-Stojanovic, H. Smidt, and W. M. de Vos, "Diversity of the human gastrointestinal tract microbiota revisited," *Environmental Microbiology*, vol. 9, no. 9, pp. 2125–2136, 2007.
- [69] X. Bian, W. Wu, L. Yang et al., "Administration of Akkermansia muciniphila ameliorates dextran sulfate sodium-induced ulcerative colitis in mice," *Frontiers in Microbiology*, vol. 10, p. 2259, 2019.
- [70] M. Derrien, C. Belzer, and W. M. de Vos, "Akkermansia muciniphila and its role in regulating host functions," *Microbial Pathogenesis*, vol. 106, pp. 171–181, 2017.
- [71] S. Rabizadeh, K.-J. Rhee, S. Wu et al., "Enterotoxigenic Bacteroides fragilis: a potential instigator of colitis," *Inflammatory Bowel Diseases*, vol. 13, no. 12, pp. 1475–1483, 2007.
- [72] K. Lucke, S. Miehke, E. Jacobs, and M. Schuppler, "Prevalence of Bacteroides and Prevotella spp. in ulcerative colitis," *Journal of Medical Microbiology*, vol. 55, no. 5, pp. 617–624, 2006.
- [73] Y.-J. Chen, H. Wu, S.-D. Wu et al., "Parasutterella, in association with irritable bowel syndrome and intestinal chronic inflammation," *Journal of Gastroenterology and Hepatology*, vol. 33, no. 11, pp. 1844–1852, 2018.
- [74] O. Franzen, J. Hu, X. Bao, S. H. Itzkowitz, I. Peter, and A. Bashir, "Improved OTU-picking using long-read 16S rRNA gene amplicon sequencing and generic hierarchical clustering," *Microbiome*, vol. 3, p. 43, 2015.
- [75] R. J. Chiodini, S. E. Dowd, W. M. Chamberlin, S. Galandiuk, B. Davis, and A. Glassing, "Microbial population differentials between mucosal and submucosal intestinal tissues in advanced Crohn's disease of the ileum," *PLoS One*, vol. 10, no. 7, article e0134382, 2015.
- [76] R. Zhai, X. Xue, L. Zhang, X. Yang, L. Zhao, and C. Zhang, "Strain-specific anti-inflammatory properties of two Akkermansia muciniphila strains on chronic colitis in mice," *Frontiers in Cellular and Infection Microbiology*, vol. 9, p. 239, 2019.
- [77] H. Earley, G. Lennon, A. Balfe, J. C. Coffey, D. C. Winter, and P. R. O'Connell, "The abundance of _Akkermansia muciniphila_ and its relationship with sulphated colonic mucins in health and ulcerative colitis," *Scientific Reports*, vol. 9, no. 1, 2019.

Research Article

GPX4-Regulated Ferroptosis Mediates S100-Induced Experimental Autoimmune Hepatitis Associated with the Nrf2/HO-1 Signaling Pathway

Lujian Zhu,¹ Dazhi Chen,² Yin Zhu,¹ Tongtong Pan,¹ Dingchao Xia,¹ Tingchen Cai,¹ Hongwei Lin,¹ Jing Lin,¹ Xiaozhi Jin,¹ Faling Wu,¹ Sijie Yu,¹ Kailu Zhu,¹ Lanman Xu ^{1,3} and Yongping Chen ¹

¹Department of Infectious Diseases, The First Affiliated Hospital of Wenzhou Medical University, Zhejiang Provincial Key Laboratory for Accurate Diagnosis and Treatment of Chronic Liver Diseases, Wenzhou Key Laboratory of Hepatology, Hepatology Institute of Wenzhou Medical University, Wenzhou, China

²Department of Gastroenterology, Peking University First Hospital, Beijing, China

³Department of Infectious Diseases and Liver Diseases, Ningbo Medical Centre Lihuili Hospital, Affiliated Lihuili Hospital of Ningbo University, Ningbo Institute of Innovation for Combined Medicine and Engineering, Ningbo, China

Correspondence should be addressed to Lanman Xu; 13587646315@163.com and Yongping Chen; cyp@wmu.edu.cn

Lujian Zhu and Dazhi Chen contributed equally to this work.

Received 25 July 2021; Revised 5 October 2021; Accepted 3 November 2021; Published 20 December 2021

Academic Editor: Miodrag Lukic

Copyright © 2021 Lujian Zhu et al. This is an open access article distributed under the Creative Commons Attribution License, which permits unrestricted use, distribution, and reproduction in any medium, provided the original work is properly cited.

Autoimmune hepatitis (AIH) is an inflammatory autoimmune disease of the liver. Oxidative stress triggered by reactive oxygen radicals is a common pathophysiological basis for the pathogenesis of many liver diseases, and ferroptosis is associated with the toxic accumulation of reactive oxygen species. The signaling transduction pathways responsible for iron processing and lipid-peroxidation mechanisms are believed to drive ferroptosis. However, the specific mechanisms regulating ferroptosis remain unclear. The aims of this investigation were to identify the possible effector functions of ferroptosis, based on glutathione peroxidase 4 (GPX4) regulation in an S100-induced autoimmune hepatitis mouse model and hepatocyte injury models. The S100 liver antigen-induced AIH mouse model was used to detect ferroptotic biomarkers using western blotting. Upregulated levels of cyclooxygenase2 (COX2) and Acyl-Coenzyme A synthase long-chain family member 4 (ACSL4) were observed in the S100-induced AIH model group, while levels of GPX4 and ferritin heavy chain 1 (FTH1) were downregulated ($P < 0.05$). The expression profiles of COX2, ACSL4, GPX4, and FTH1 were restored following the administration of ferrostatin-1. In addition, Nrf2 and HO-1 levels in the S100-induced AIH model mice after treatment with ferrostatin-1 were downregulated compared to the nonferrostatin-1-treated S100-induced AIH model mice ($P < 0.05$). Moreover, COX2 and ACSL4 levels were significantly upregulated, with significant FTH1 downregulation, in the AIH model mice when liver-specific GPX4 was silenced using AAV8 constructs. These data indicate that inhibition of ferroptosis significantly ameliorated the influence of AIH on the Nuclear factor E2-related factor 2 (Nrf2)/Heme oxygenase-1 (HO-1) signaling pathway, and that ferroptosis may act as an initiator or intermediate mediator leading to AIH.

1. Introduction

Autoimmune hepatitis (AIH) is characterized by inflammation, the presence of autoantibodies, hypergammaglobulinemia, and interface hepatitis [1]. It is more common in

women and appears to be increasing in increasing prevalence. Chronic liver disease is a serious threat to health and thus has economic consequences [2]. Although the pathogenetic mechanism of AIH is not clear, the mouse AIH model induced by the liver-specific antigen S100 is widely used to study AIH [3].

Typically, mice which are injected intraperitoneally with equal amounts of liver S100 antigen emulsified and mixed with complete Freund's adjuvant on day-0 and day-7 show significant liver inflammation and elevated autoimmune IgG. Although previous studies have implicated genetic susceptibility, molecular mimicry, as well as external factors in AIH pathogenesis [4], the precise pathogenetic mechanism remains unclear. Therefore, an in-depth study of the underlying mechanisms responsible for AIH can assist the development of novel therapies for AIH.

Ferroptosis is defined as iron-dependent cell death mediated by phospholipid peroxidation. Ferroptosis results from dysregulated iron metabolism involving the iron-storage protein ferritin, composed of a ferritin light chain (FTL) and a ferritin heavy chain 1 (FTH1) [5]. Since FTH possesses iron oxidase activity, it converts ferrous iron (Fe^{2+}) to the oxidized ferric (Fe^{3+}) form, allowing iron binding to the ferritin outer layer and thus lowering the concentration of free iron in the cell [6]. High levels of free iron are associated with lipid peroxidation. There are several mechanisms involved in the prevention of lipid peroxidation including the action of glutathione peroxidase 4 (GPX4) that scavenges phospholipid peroxides as a protective measure against ferroptosis [7]. Abnormal iron metabolism and lipid peroxidation are believed to play pivotal parts in ferroptosis. In addition, lipid peroxidation is influenced by a spectrum of different lipids and enzymes [8]. Even though lipid peroxidation acts as a key process driving ferroptosis, the regulators of lipid metabolism in ferroptosis remain unclear [9]. Acyl-Coenzyme A synthetase long-chain family member 4 (ACSL4) is essential for apoptosis in iron chain cancer cells. ACSL4 expression has been shown to be significantly reduced in ferroptosis-resistant cells [10]. Thus, ACSL4 participates in the catalysis of polyunsaturated fatty acid oxidation. The enzyme lysophosphatidylcholine acyltransferase 3 (LPCAT3) mediates lipotoxicity in ferroptosis [10–12]. Furthermore, several intracellular signaling pathways play pivotal parts in ferroptosis. For example, investigations have implicated ferroptosis in pathological conditions in a variety of organs, including the brain, kidney, liver, and heart [13]. Ferroptosis is seen in the accumulation of iron and reactive oxygen species (ROS) and inhibits the activities of the XC- and GPX4 systems by reducing cysteine uptake and consuming glutathione [14]. The harmful actions of lipid peroxidation during the actual ferroptotic process can be inhibited through lipophilic-free radical traps (such as vitamin E, ferrostatin-1, and liproxstatin-1). However, the influence of ferroptosis on AIH remains unclear. Nuclear factor erythroid-related factor 2 (Nrf2) is a transcription factor that maintains stability and homeostasis in stressed intracellular environments, and, although it appears to be involved, its underlying mechanism of action is unknown [15]. Increasing evidence has implicated Nrf2 in ferroptosis pathogenesis [16]. In our present study, heme oxygenase-1 expression was found to be significantly increased in the livers of S100-induced AIH mice, while other studies have suggested that excessive Nrf2/HO-1 stimulation can lead to ferroptosis by disrupting the balance of ferric ions [17, 18]. Here, we hypothesized that ferroptosis plays a pivotal role in Nrf2/

HO-1 signaling in S100-induced AIH. Therefore, in the current investigation, ferroptosis and its mechanism were evaluated in the AIH mouse model to determine its possible pathogenic role in AIH and to generate novel therapies for patients with AIH.

2. Materials and Methods

2.1. Animal Models. Male C57BL/6 WT mice weighing 23–25 g were purchased from Hangzhou Ziyuan Experimental Animal Technology Co, Ltd. (China). The study and animal handling were approved by the Animal Policy and Welfare Committee of Wenzhou Medical University (approval document no. wyd2020-0861). The care of the mice was in accordance with NIH guidelines (Guide for the Care and Use of Laboratory Animals). The mice were housed in a pathogen-free environment with a 12:12 h light-dark cycle and fed on standard rodent chow. All mice were allowed to acclimatize to their new environment for a minimum of 14 days prior to the commencement of the AIH modeling. Ten experimental mice were randomly selected to be given an intraperitoneal injection of S100 injection, thus, comprising the mouse AIH model group.

2.2. Preparation of Mouse Liver Tissue. To prepare the liver-specific antigen S100, three mice were randomly selected and sacrificed under pentobarbital sodium anesthesia. The livers were perfused with phosphate-buffered saline (PBS) and removed as previously described and used to prepare fresh S100 antigen [3]. In brief, the liver was homogenized in pre-cooled PBS, followed by a 60-minute centrifugation at 150 g. The supernatant was further centrifuged for 60 minutes in an ultracentrifuge (100 000 g) [3]. The S100-containing supernatant was concentrated to 5 mL through an Amicon® Ultra-15 ultrafiltration system (Millipore, USA), followed by separation on an AKTA Pure (GE Healthcare, USA) 90 cm CL-6B Sepharose® column (Pharmacia, USA). Three protein peaks were eluted from the column, with peak 2 being the harmful component and peaks 1 and 3 the required and nontoxic components, respectively, of the hepatic antigen. The protein fraction from the first peak was used at a concentration of 0.5–2.0 g/L. For the establishment of the AIH model, the hepatic S100 antigen was emulsified with an equal volume of Freund's complete adjuvant (Solarbio, China) and was used to immunize 10 mice from the same batch intraperitoneally on day-0 and day-7 (Figure 1(a)). During the modeling, two of the mice in the AIH model group died. Four weeks after the injection, the mice were sacrificed under pentobarbital sodium anesthesia. Blood samples were collected and centrifuged at 3000 rpm at 4°C for 15 min to obtain the serum. Liver samples were either fixed in 4% paraformaldehyde for immunohistochemical and histological examination or frozen at -80°C.

2.3. Ferrostatin-1 Treatment of Mice. Ten control mice were fed with conventional rodent chow and water throughout the modeling period. Experiments were conducted to further demonstrate whether ferroptosis occurs in S100-induced AIH and whether intervention with ferrostatin-1

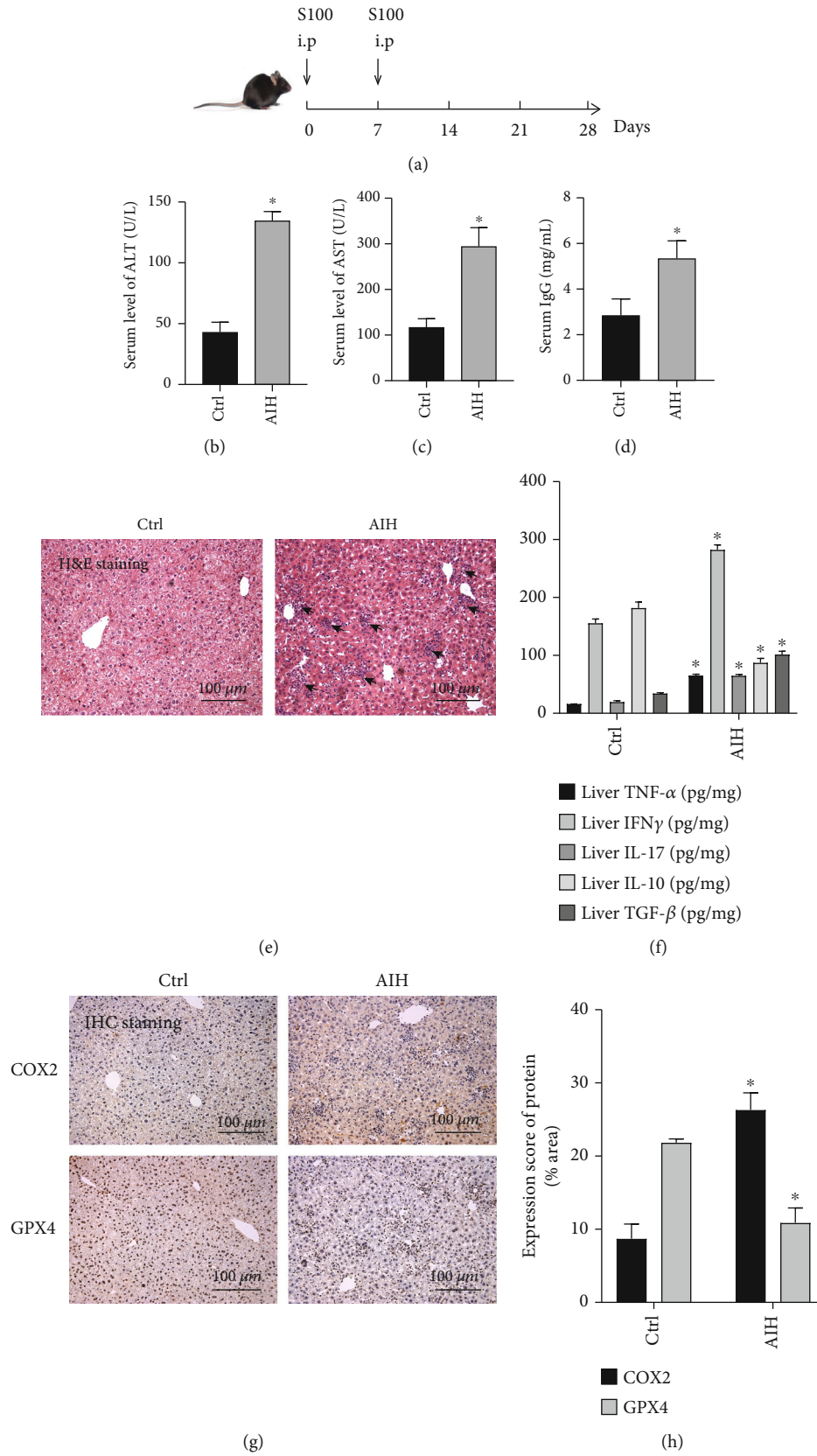


FIGURE 1: Continued.

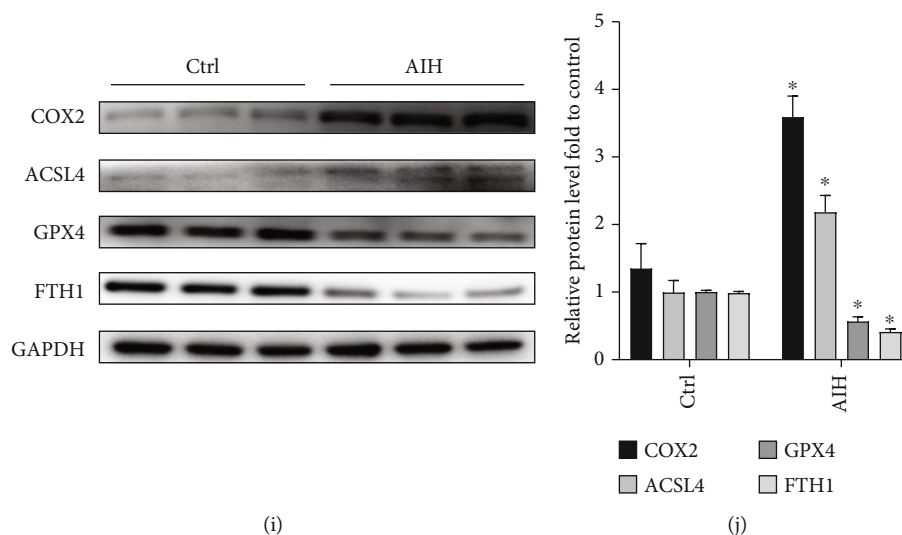


FIGURE 1: Ferroptosis plays an important role in S100-induced autoimmune hepatitis. (a) Experimental protocol for the modeling of S100-induced AIH model mice. (b)–(d) The serum ALT, AST, and IgG expression levels in the control and AIH groups. (e) Representative H&E staining of liver tissue sections. The black arrow indicates lymphocytic infiltration (original magnification 20 \times). (f) TNF- α , IFN γ , IL-17, IL-10, and TGF- β levels in liver. (g) IHC staining of COX2 and GPX4 in liver sections (original magnification 20 \times). (h) Semiquantitative IHC results. (i)–(j) Western blotting showing protein expression of COX2, ACSL4, GPX4, and FTH1 in the pre-experimental control and AIH groups. GAPDH was used as a loading control; * $P < 0.05$, compared with the control group.

intervention is able to ameliorate it. The mice in the experimental group received intraperitoneally injected ferrostatin-1 (1 mg/kg body weight in 5% DMSO) [19].

The following experimental groups were used: (i) normal control group, (ii) S100-induced AIH model group, (iii) normal mice + Ferrostatin-1 intervention group, and (iv) S100-induced AIH + Ferrostatin-1 treatment group. A total of 40 experimental mice were used with 10 mice in each group. The AIH model was established as described above. Ferrostatin-1 was injected intraperitoneally as shown in Figure 2(a), using the same dose and procedure for both normal and AIH mice. After completion of the Ferrostatin-1 intervention, the four groups of mice were sacrificed under pentobarbital anesthesia at the same time, and blood samples and liver tissues were collected for further experimental analysis.

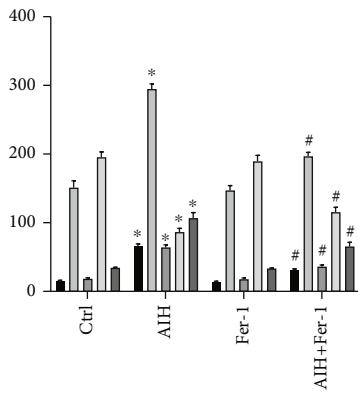
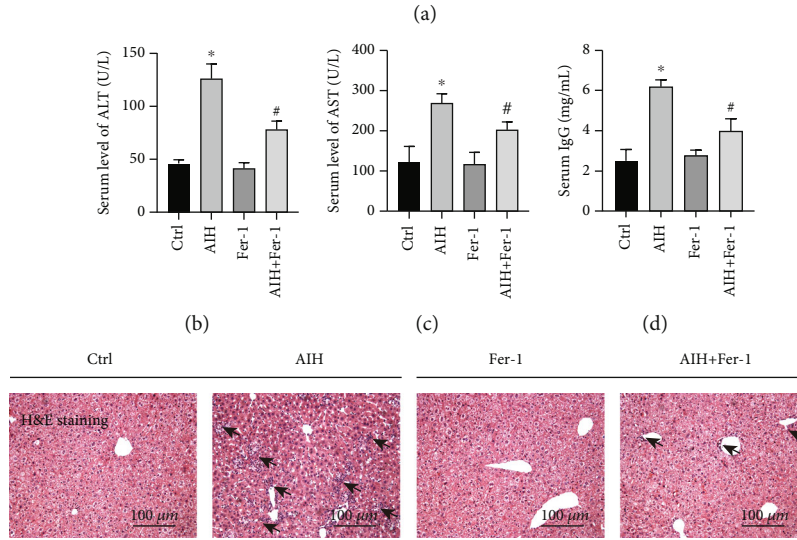
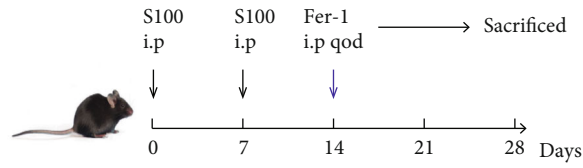
2.4. AAV8-m-GPX4 Treatment of Mice. AAV8-m-GPX4 was used to silence GPX4 gene expression to investigate whether S100-induced ferroptosis in AIH is associated with GPX4 expression. The experimental groups were as follows: (i) normal mice + AAV8-m-GPX4 group, (ii) AIH + AAV8-m-GPX4 group, (iii) normal mice + AAV8-negative control group, and (iv) AIH + AAV8-negative control group. A total of 40 mice were used with 10 mice in each group. The timing of the AAV injection is shown in Figure 3(a). Four weeks after the first intraperitoneal injection of S100, the four groups of mice were sacrificed, and blood and hepatic tissue samples were extracted for further experimental analysis.

2.5. H&E Staining. The liver tissue was fixed with 4% paraformaldehyde, embedded in paraffin, and 5 μ m sections cut. The sections were stained with hematoxylin and eosin (H&E). The lymphocytic infiltration level, inflammatory

necrosis, and destruction of liver structures were observed under light microscopy (Olympus, Japan).

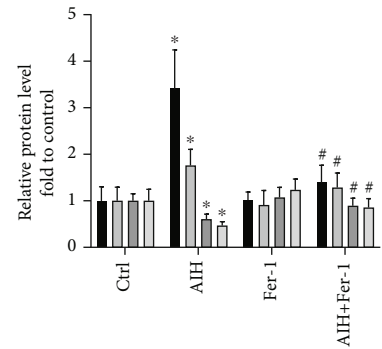
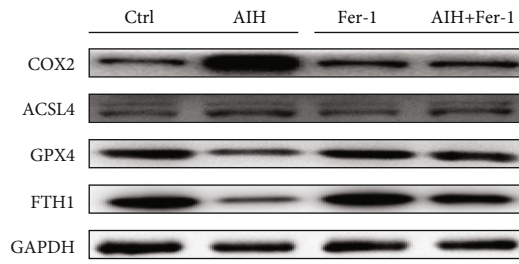
2.6. Enzyme-Linked Immunosorbent Assay (ELISA). The concentrations of the inflammatory cytokines (TNF- α , IFN γ , and IL-17), the fibrotic cytokine TGF- β , and the anti-inflammatory cytokine IL-10 that play important roles in AIH progression were measured in liver tissue lysates. The following mouse ELISA kits were used, all from Multisciences (Lianke) Biotech (Hangzhou, China): TNF- α (EK282/3-48), IFN γ (EK280/3-48), IL-17 (EK217/2-48), IL-10 (EK210/4-48), and TGF- β (EK981-48), according to the manufacturer's instructions. Although different kits have different methodologies for the assay, the main experimental steps are similar. Hereby, we use the measurement of TNF- α concentration as an example of ELISA method. In brief, TNF- α standard, blank control, and sample under test (100 μ l/well) were added to a 96-well plate. Then, add 50 μ l dilution of antibody to each well (1 : 100 dilution). Seal the plates with a plate sealing membrane and incubate at room temperature for 90 minutes. After washing off the unbound biotinylated antibody, add 100 μ l labeled Streptavidin-HRP to each well (1 : 100 dilution) and incubate at room temperature for 30 minutes. After washing, add 100 μ l substrate TMB to each well and incubate at room temperature for 15 minutes, avoiding light. The reaction was terminated by the termination reagent and the optical density (OD) value was measured by an enzyme marker at the wavelength of a 450 nm. The concentration of cellular inflammatory factors was computed using the standard curve regression equation of standard absorbance values.

2.7. Western Blot Analysis. The liver tissue was homogenized in lysis buffer. After centrifugation, the protein



- Liver TNF-α (pg/mg)
- Liver IFNγ (pg/mg)
- Liver IL-17 (pg/mg)
- Liver IL-10 (pg/mg)
- Liver TGF-β (pg/mg)

(f)



- COX2
- ACSL4
- GPX4
- FTH1

(h)

FIGURE 2: Continued.

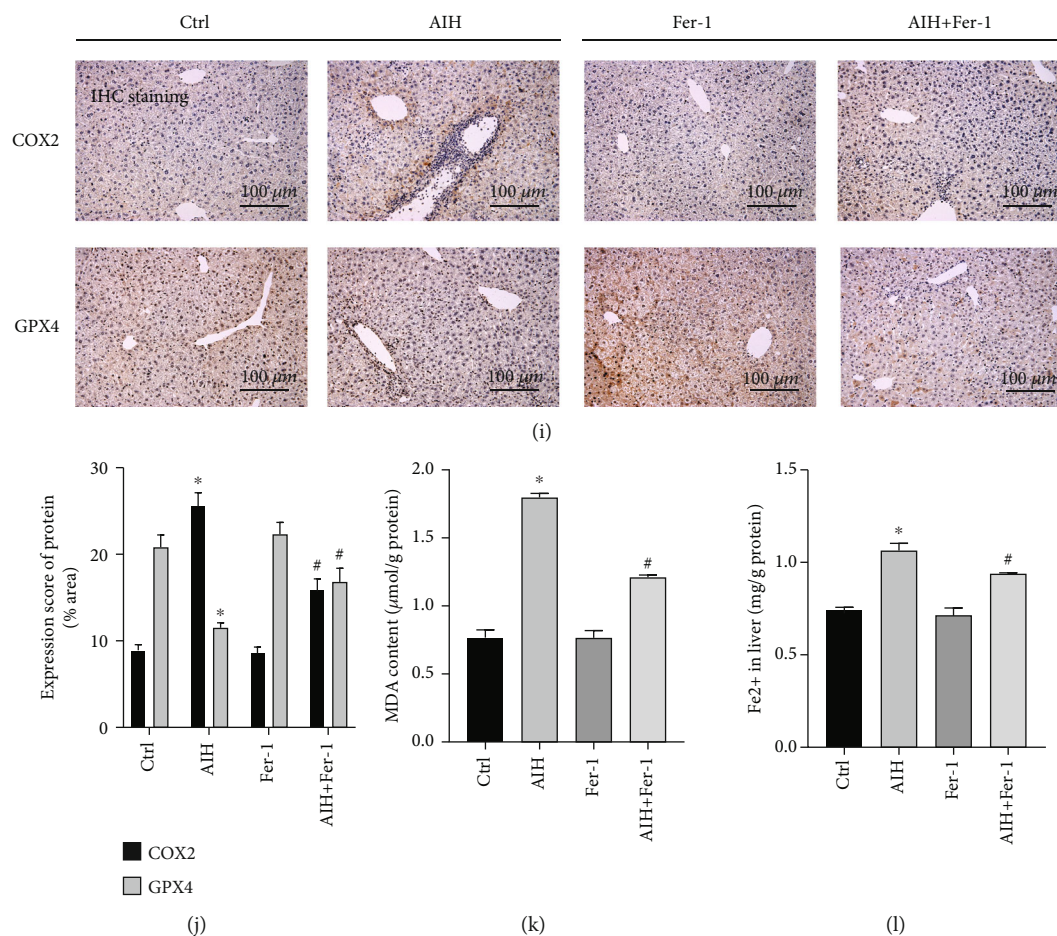


FIGURE 2: Ferrostatin-1, a ferroptosis inhibitor, significantly improves S100-induced autoimmune hepatitis. (a) Experimental protocol for Ferrostatin-1 treatment of S100-induced AIH model mice. (b)–(d) ALT, AST, and IgG levels in the control group, AIH group, Ferrostatin-1-treated group, and AIH + Ferrostatin-1 group are shown. (e) Representative H&E staining of liver tissue sections. The black arrow indicates the lymphocytic infiltration (original magnification 20×). (f) TNF- α , IFN γ , IL-17, IL-10, and TGF- β levels in liver; (g) and (h) Western blot showing protein expression of COX2, ACSL4, GPX4, and FTH1 in the control, AIH, Ferrostatin-1, and AIH + Ferrostatin-1 groups; GAPDH was used as a loading control. (i) IHC images of COX2 and GPX4 in liver sections (original magnification 20×). (j) Semiquantitative IHC results. (k) Detection of lipid peroxidation by measuring malondialdehyde (MDA) levels. (l) Fe²⁺ levels in liver; * $P < 0.05$, compared with control group; # $P < 0.05$, compared with AIH group.

concentration of the lysate was measured using BCA Protein Assay Kit (Beyotime, P0012, China), in line with the manufacturer's protocols. Equivalent amounts (50 μ g) of protein were separated on SDS-PAGE and transferred to PVDF membranes (Millipore). The membranes were blocked with 5% skimmed milk in Tris-buffered saline with 0.1% Tween 20 (TBST) and incubated with antibodies against COX2 (1:1000, 12375-1-AP, Proteintech), ACSL4 (1:1000, A16848, ABclonal), GPX4 (1:1000, BM5231, Boster), FTH1 (1:1000, A19544, ABclonal), Nrf2 (1:1000, 16396-1-AP, Proteintech), HO-1 (1:1000, 10701-1-AP, Proteintech), or GAPDH (1:10 000, 60004-1-AP, Proteintech) overnight at 4°C. After washing, the membranes were incubated with horseradish peroxidase- (HRP-) conjugated secondary antibodies against rabbit or mouse IgG (1:5000, LF101 and LF102, respectively, Epizyme) for 1 hour at room temperature. A Bio-Rad immunoblot analysis detection system (Bio-Rad, Hercules, CA, USA) was used for visualization. Protein band densities were assessed by ImageJ analysis

software, and the relative densities against the loading control (GAPDH) were calculated.

2.8. Real-Time Quantitative Polymerase Chain Reaction (RT-qPCR). Total RNA was collected from homogenized liver tissue with TRIzol® reagent, and 1g total RNA was reverse-transcribed into cDNA using the PrimeScript RT Master Mix® (Perfect Real Time) kit (RR036A, Takara, Japan). The quantitative polymerase chain reaction was performed in a 10 μ L reaction mixture containing specific primers and TBGreen Premix Ex Taq II. Amplification was performed in a real-time fluorescent quantitative PCR system (AB 7500). The primers employed consisted of the following:

ACTB (5'-CCTCACTGTCCACCTTCC-3', 5'-GGGTGTAAACGCAGCTC-3'),

Nrf2 (5'-TCTTCACTGCCCTCATC-3', 5'-CTCCTGCCAACTTGCTC-3'),

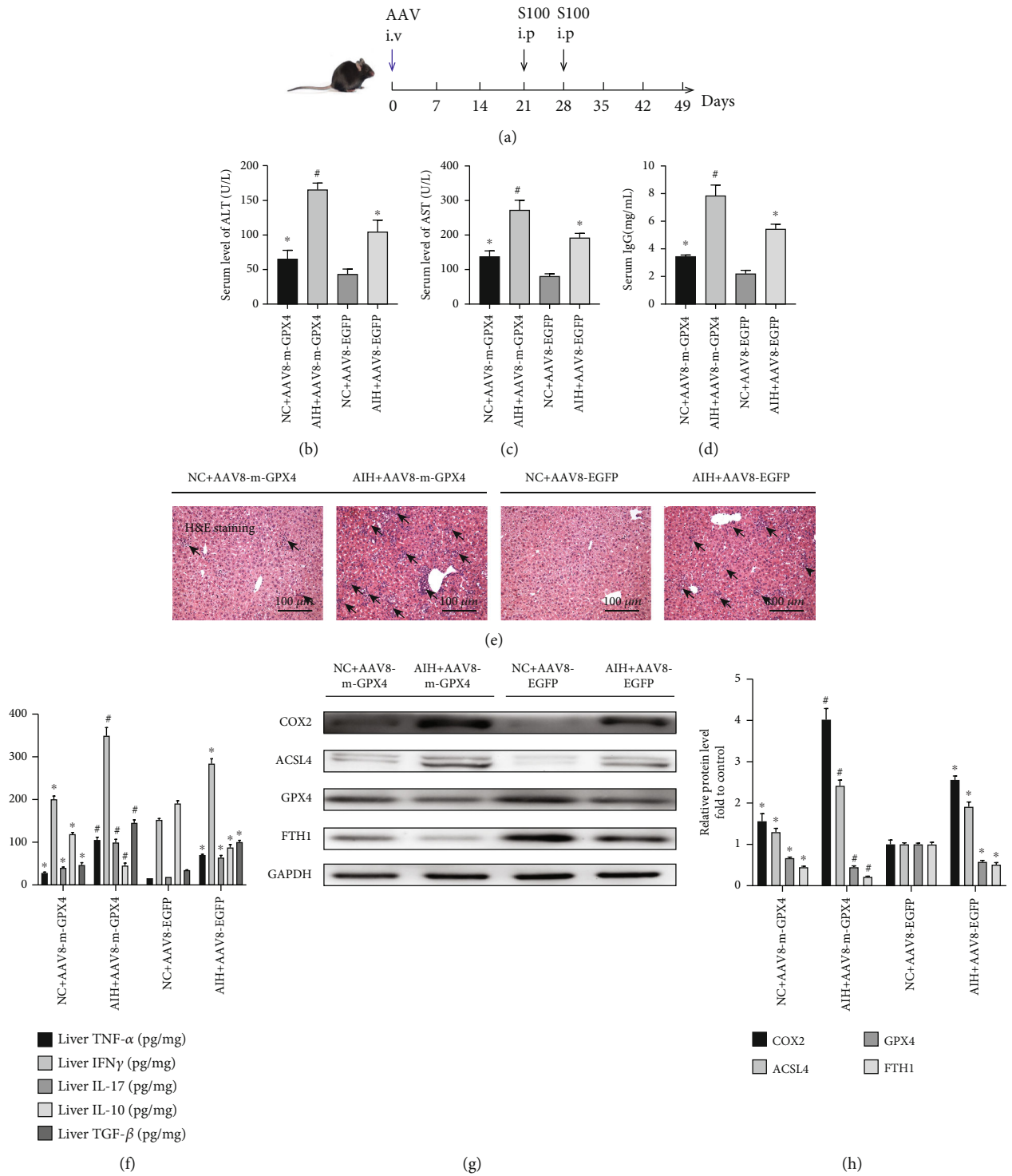


FIGURE 3: Continued.

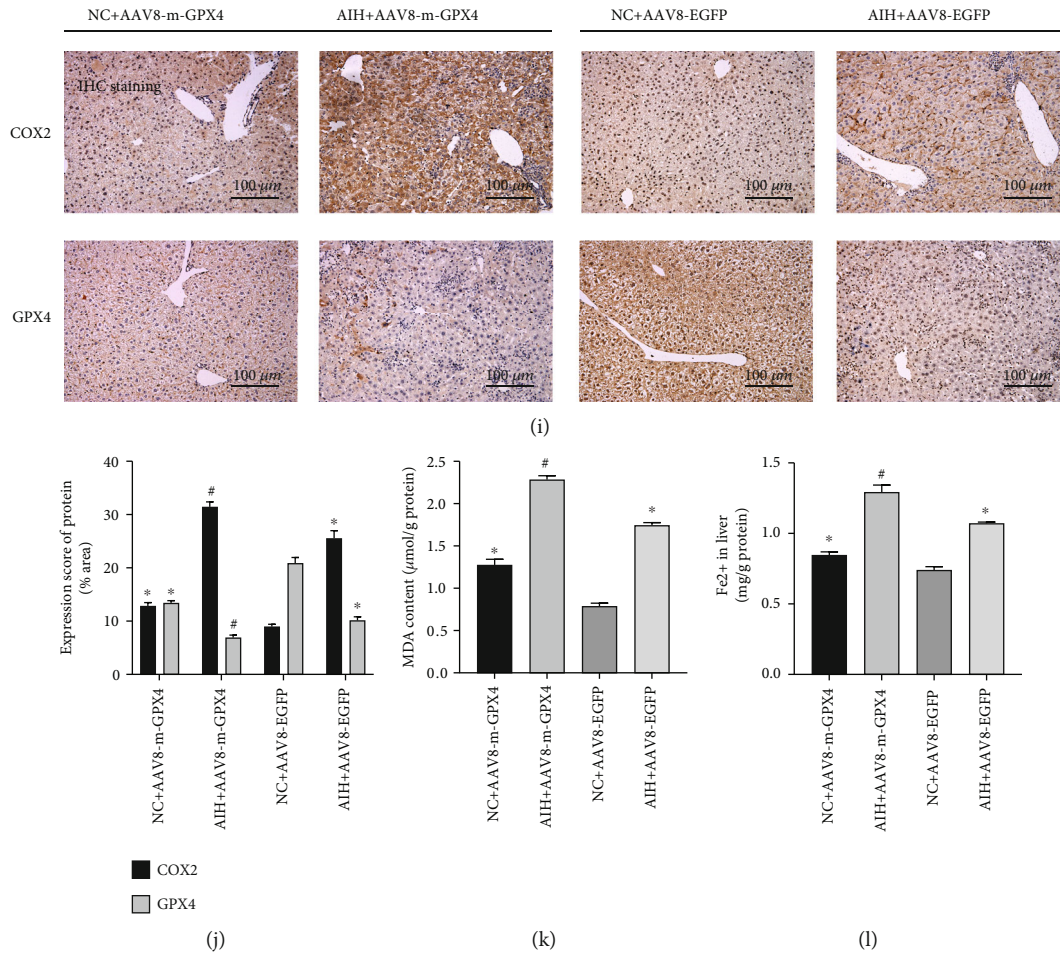


FIGURE 3: Exacerbation of S100-induced autoimmune hepatitis after GPX4 knockdown. (a) Experimental protocol for the transfection of AAV8-m-GPX4 and the establishment of the mouse AIH model; (b)–(d) ALT, AST, and IgG levels in the NC+AAV8-m-GPX4, AIH+AAV8-m-GPX4, NC+AAV8-EGFP, and AIH+AAV8-EGFP groups. (e) Representative H&E staining of liver tissue sections. The black arrow indicates lymphocytic infiltration (original magnification 20×); (f) TNF- α , IFN γ , IL-17, IL-10, and TGF- β levels in liver; (g) and (h) Western blot showing protein expression of COX2, ACSL4, GPX4, and FTH1 in the NC+AAV8-m-GPX4, AIH+AAV8-m-GPX4, NC+AAV8-EGFP, and AIH+AAV8-EGFP groups; GAPDH was used as a loading control. (i) IHC images of COX2 and GPX4 in liver sections (original magnification 20×). (j) Semiquantitative IHC results. (k) Detection of lipid peroxidation by measuring malondialdehyde (MDA) levels. (l) Fe²⁺ levels in liver; * $P < 0.05$, compared with the NC+AAV8-EGFP group; # $P < 0.05$, compared with the AIH+AAV8-EGFP group.

HO-1 (5'-ACAGCCCCCCCACCAAGTTC-3', 5'-GGCG GTCTTAGCCTCTTC-3').

Datasets were assessed using the 7500 real-time PCR system software. Actin levels were used for normalization. Three technical replicates of each RT-qPCR analysis were performed.

2.9. Immunohistochemistry (IHC). Immunohistochemistry was performed on paraffin-embedded mouse liver sections. The semiquantitative IHC datasets were based on the mean of three mice per group. Three sections from each mouse were assessed, with imaging collected by optical microscopy (Olympus, Japan). The staining intensity was analyzed using ImageJ software, and three microscopy fields were chosen at random to calculate the integrated optical density (IOD) for the target protein.

2.10. Serum Transaminases and IgG Analyses. Serum was collected from blood samples by centrifugation at 250 g for

10 minutes. Serum alanine aminotransferase (ALT) and aspartate aminotransferase (AST) concentrations were analyzed using a fully automated biochemical analyzer, following the manufacturer's protocols (Abbott Laboratories, Chicago, IL, USA). Serum IgG levels were determined with the Mouse ELISA Kit (EK271-48, Multisciences). All experiments were performed in accordance with the manufacturer's instructions.

2.11. Lipid Peroxidation Malondialdehyde (MDA) Assay. Histones were isolated using the Lipid Peroxidation Malondialdehyde Assay Kit (Beyotime, S0131, China). The malondialdehyde (MDA) concentration of each sample was measured at 532 nm using an enzyme marker (Thermo Multiskan MK3, Thermo Fisher, Waltham, MA, USA), and 490 nm was used as a control.

2.12. Iron Load Assay. Histones were isolated using the Iron Assay Kit protocol (ab83366, Abcam, Cambridge, UK). Liver

tissue (10 mg) was washed with prechilled PBS and homogenized with 4-10 parts iron analysis buffer using a chilled Dawes homogenizer (10-15 passes). The sample was centrifuged at 16 000 g for 10 minutes. The supernatant was collected and transferred to a clean centrifuge tube. Test wells were treated with 100 μ L of standard dilution and sample. Iron-reducing agent (5 μ L) was added to each well. The kit protein standards and tissue stock solution were mixed and added to the mixtures for 30 minutes at 37°C in a constant temperature incubator. One hundred microliters of the iron probe were then added to all wells containing iron standards and test samples. The samples were mixed and incubated at 37°C for 60 minutes, away from light. The absorbance was measured on a colorimetric enzyme standard immediately afterward (OD 593 nm).

2.13. Cell Culture. Alpha mouse liver 12 (AML12) cells were cultured in DMEM/F-12 (1 : 1) medium containing 10% fetal bovine serum with 40 ng/mL of dexamethasone and 1% insulin-transferrin-selenium-ethanolamine (ITS-X) at 37°C in a 5% CO₂ humidified thermostatic incubator. When the cells reached 70%-80% confluence, GPX4-specific knockdown siRNA and nonspecific control siRNA, as well as a GPX4-specific overexpression plasmid and a nonspecific control plasmid, were transfected with Lipofectamine 2000 Reagent (Thermo Fisher) strictly according to the manufacturer's instructions. After transfection, the supernatant was discarded, and incubation was continued with OPTI medium (Gibco, Thermo Fisher) for 6 hours followed by incubation for 48 hours in DMEM/F12 complete medium containing lipopolysaccharide (5 μ g/ml). GPX4-specific knockdown siRNA (5'-CUGACGAAAACUACACUCATT-3', 5'-UGAGUGUAGUUUACGUCAGTT-3') and nonspecific control siRNA (5'-UUCUCCGAACGUGUCACGUTT-3', 5'-ACGUGACACGUUCGGAGAATT-3'), and GPX4-specific overexpression plasmid and nonspecific control plasmid were purchased from GenePharma (Shanghai, China).

2.14. Immunofluorescence. AML12 cells were cultured for 48 hours in 12-well plates. After reaching approximately 80% confluence, the cells were washed with prechilled PBS and were fixed with 4% paraformaldehyde for 15 min, followed by permeabilization with 0.5% Triton X-100 in PBS for 20 min. The cells were then blocked with 5% BSA at 37°C for 1 h and incubated with the corresponding primary antibodies at 4°C overnight. The following day, the samples were incubated with Alexa Fluor 488-labeled goat anti-rabbit IgG secondary antibody (1 : 1000, 33106ES60, Teasen Biotechnology, Shanghai, China) for 1 h at room temperature in the dark, followed by incubation with DAPI for 5 minutes. Three regional fields of view were randomly selected from each fluorescent section under an ortho-fluorescent microscope (Leica, Germany), with the observer blinded to the experimental group.

2.15. Statistical Analysis. Statistical analyses employed GraphPad® 8.6.3 software. All studies were carried out on three separate occasions and were randomized. The *t*-test for unpaired outcomes was employed for comparative anal-

ysis. Datasets were represented as mean \pm SD, with $P < 0.05$ deemed to confer statistical significance.

3. Results

3.1. Ferroptosis Plays a Pivotal Role in S100-Induced AIH. The experimental design for the establishment of the S100-induced AIH model is illustrated in Figure 1(a). The levels of ALT and AST were significantly raised in the AIH group, together with increased levels of IgG (Figures 1(b)–1(d)). Histopathological H&E staining showed that the S100-induced AIH resulted in many areas of inflammatory necrosis, increased lymphocyte infiltration, and destruction of liver structures (Figure 1(e)). ELISA analysis showed that concentrations of the inflammatory cytokines TNF- α , IFN γ , and IL-17 and the fibrotic cytokine TGF- β levels were significantly increased in the livers of AIH mice compared to the control group, while the anti-inflammatory cytokine IL-10 levels were significantly decreased (Figure 1(f); $P < 0.05$). Western blot and immunohistochemical assays were also used to detect the occurrence of ferroptosis in autoimmune hepatitis. The western blot results indicated upregulated expression of COX2 and ACSL4 in the AIH experimental group, while the expression of GPX4 and FTH1 was severely downregulated (Figures 1(i) and 1(j); $P < 0.05$). The immunohistochemical results showed that COX2 staining was weaker in the control mouse hepatocytes, while COX2 was significantly increased in hepatocytes in S100-induced AIH. GPX4 staining was stronger in the control mouse hepatocytes, and in the S100-induced autoimmune hepatitis model group, GPX4 expression was significantly reduced (Figures 1(g) and 1(h); $P < 0.05$). Thus, our results suggest the occurrence of ferroptosis in S100-induced autoimmune hepatitis.

3.2. Ferrostatin-1, a Ferroptosis Inhibitor, Significantly Improves S100-Induced Autoimmune Hepatitis. Ferrostatin-1, a ferroptosis inhibitor, was used to investigate whether ferroptosis plays a part in S100-induced AIH. The experimental protocol is illustrated in Figure 2(a). The levels of ALT, AST, and IgG were significantly raised in the AIH group compared to the blank control group (Figures 2(b)–2(d); $P < 0.05$). After Ferrostatin-1 treatment, the S100-induced autoimmune hepatitis group had significantly lower ALT, AST, and IgG levels compared with the S100-induced autoimmune hepatitis model group ($P < 0.05$). Histological H&E staining suggested that Ferrostatin-1 effectively attenuated liver damage, protected liver structures, and limited liver inflammatory lymphocyte infiltration. Ferrostatin-1 treatment attenuated inflammation in the S100-induced autoimmune hepatitis group compared to the S100-induced autoimmune hepatitis model group (Figure 2(e)). ELISA analysis showed that Ferrostatin-1 reversed the upregulated expression of the inflammatory cytokines TNF- α , IFN γ , IL-17, the fibrotic cytokine TGF- β , and the anti-inflammatory cytokine IL-10 in the liver of S100-induced AIH mice to some extent (Figure 2(f); $P < 0.05$). Western blotting showed that Ferrostatin-1 significantly upregulated both GPX4 and FTH1 and significantly downregulated COX2 and ACSL4 (Figures 2(g) and 2(h);

$P < 0.05$). Meanwhile, the immunohistochemical results demonstrated that COX2 expression was significantly increased in hepatocytes in S100-induced AIH compared to the controls. However, COX2 expression was significantly inhibited in the S100-induced AIH group after Ferrostatin-1 treatment. In addition, Ferrostatin-1 treatment significantly increased GPX4 expression in hepatocytes (Figures 2(i) and 2(j); $P < 0.05$). In the lipid peroxidation malondialdehyde assay, Ferrostatin-1 reduced MDA levels in the S100-induced AIH group (Figure 2(k); $P < 0.05$) and also reversed to some extent the elevated levels of hepatic ferrous ions in mice after AIH induction (Figure 2(l); $P < 0.05$). Our findings further suggest that ferroptosis is associated with S100-induced AIH and that Ferrostatin-1 has a role in ameliorating S100-induced autoimmune hepatitis.

3.3. Ferrostatin-1 Ameliorates S100-Induced AIH via the Nrf2/HO-1 Signaling Pathway. Nrf2 plays a major part in the protection of cells from oxidative stress. Western blotting and RT-qPCR analysis revealed that both protein and mRNA expression levels of Nrf2 and HO-1 in the S100-induced AIH group were increased. However, more notably, S100-induced AIH significantly inhibited both Nrf2 and HO-1 protein and mRNA levels after Ferrostatin-1 treatment compared to the S100-induced AIH model group (Figures 4(a)–4(e); $P < 0.05$).

3.4. Aggravation of S100-Induced Autoimmune Hepatitis after GPX4 Knockdown. Two viruses, AAV8-m-GPX4 and AAV8-EGFP, were purchased from HANBIO [20]. The HANBIO constructs comprised a GPX4 knockdown sequence in an adeno-associated virus (AAV). Forty male C57BL/6 mice were randomly divided into four groups, (i) NC + AAV8-m-GPX4, (ii) AIH + AAV8-m-GPX4, (iii) NC + AAV8-EGFP, and (iv) AIH + AAV8-EGFP, with 10 mice in each group. Each mouse was injected with 1×10^{12} copies of the virus. The experimental protocol for transfection of AAVs and establishment of S100-induced autoimmune hepatitis model in mice is shown in Figure 3(a).

AAV8-m-GPX4 was used to interfere with the expression of GPX4 in knockdown normal controls and in the S100-induced autoimmune hepatitis model to verify the role of the GPX4 protein in S100-induced AIH and ferroptosis development. The expression of ALT, AST, and IgG in the AIH + AAV8-m-GPX4 group was significantly increased in comparison to the NC + AAV8-m-GPX4 group (Figures 3(b)–3(d); $P < 0.05$). However, notably, the NC + AAV8-m-GPX4 group showed slightly higher expression of ALT, AST, and IgG than the NC + AAV8-EGFP group ($P < 0.05$). In addition, the results of the H&E pathological staining suggested that liver damage, liver structural destruction, and liver lymphocyte infiltration were more severe in the AIH + AAV8-m-GPX4 group compared to the AIH + AAV8-EGFP group. Compared to the NC + AAV8-EGFP group, the NC + AAV8-m-GPX4 group showed slight liver damage as well as hepatic lymphocyte infiltration in H&E-stained sections (Figure 3(e)). Also, ELISA analysis showed that the levels of the inflammatory cytokines TNF- α , IFN γ , and IL-17, and the fibrotic cytokine

TGF- β were increased to some extent in the livers of the AIH + AAV8-EGFP group mice compared with the NC + AAV8-EGFP group, while the level of the anti-inflammatory cytokine IL-10 was decreased. After GPX4 knockdown, the expression of the inflammatory cytokines TNF- α , IFN γ , and IL-17 and the fibrotic cytokine TGF- β were upregulated to a greater extent in the livers of the AIH + AAV8-m-GPX4 group than those of the AIH + AAV8-EGFP group, while the anti-inflammatory cytokine IL-10 level was significantly downregulated (Figure 3(f); $P < 0.05$). In addition, Western blotting revealed that, in comparison to the NC + AAV8-EGFP group, the protein expression of COX2 and ACSL4 were strongly increased in the AIH + AAV8-EGFP group, while the protein expression of GPX4 and FTH1 were downregulated. The increase in COX2 and ACSL4 levels was greater in the AIH + AAV8-m-GPX4 group compared with the AIH + AAV8-EGFP group after GPX4 knockdown, while the relative protein expression of FTH1 was also significantly reduced (Figures 3(g) and 3(h); $P < 0.05$). The immunohistochemical results showed that COX2 staining in hepatocytes was significantly enhanced in the AIH + AAV8-m-GPX4 group compared to the AIH + AAV8-EGFP group, while GPX4 staining in hepatocytes was strongly reduced in the former in comparison to the AIH + AAV8-EGFP group. In addition, COX2 staining in hepatocytes was slightly enhanced in the NC + AAV8-m-GPX4 group compared to the NC + AAV8-EGFP group, while GPX4 staining in hepatocytes was reduced compared to the NC + AAV8-EGFP group in the former (Figures 3(i) and 3(j); $P < 0.05$). In terms of the lipid peroxidation malondialdehyde assays, MDA expression was increased to some extent after GPX4 knockdown in both AIH model groups with and without S100 induction (Figure 3(k); $P < 0.05$). Also, GPX4 knockdown increased the levels of ferrous ions to some extent (Figure 3(l); $P < 0.05$). This suggests that ferroptosis in S100-induced autoimmune hepatitis may be regulated through GPX4.

3.5. LPS-Induced Ferroptosis in AML12 Cells Occurs through GPX4 Regulation. To further investigate the mechanism of hepatic ferroptosis, LPS induction in AML12 hepatocyte cells was analyzed.

The experimental groups investigated were as follows: (i) control group, (ii) LPS-induced hepatocyte ferroptosis model group, (iii) LPS-induced hepatocyte ferroptosis group after GPX4-specific knockdown, (iv) LPS-induced hepatocyte ferroptosis group after nonspecific control siRNA transfection, (v) LPS-induced hepatocyte ferroptosis group after GPX4-specific plasmid overexpression, and (vi) LPS-induced hepatocyte ferroptosis group after nonspecific control plasmid transfection. Western blot analysis showed that the protein levels of COX2 and ACSL4 in the LPS-induced hepatocyte ferroptosis group were significantly raised, in contrast to those of GPX4 and FTH1 (Figures 5(a) and 5(b); $P < 0.05$). Furthermore, it is noteworthy that the protein levels of COX2 and ACSL4 increased after GPX4-specific knockdown siRNA transfection followed by LPS-induced hepatocyte ferroptosis compared

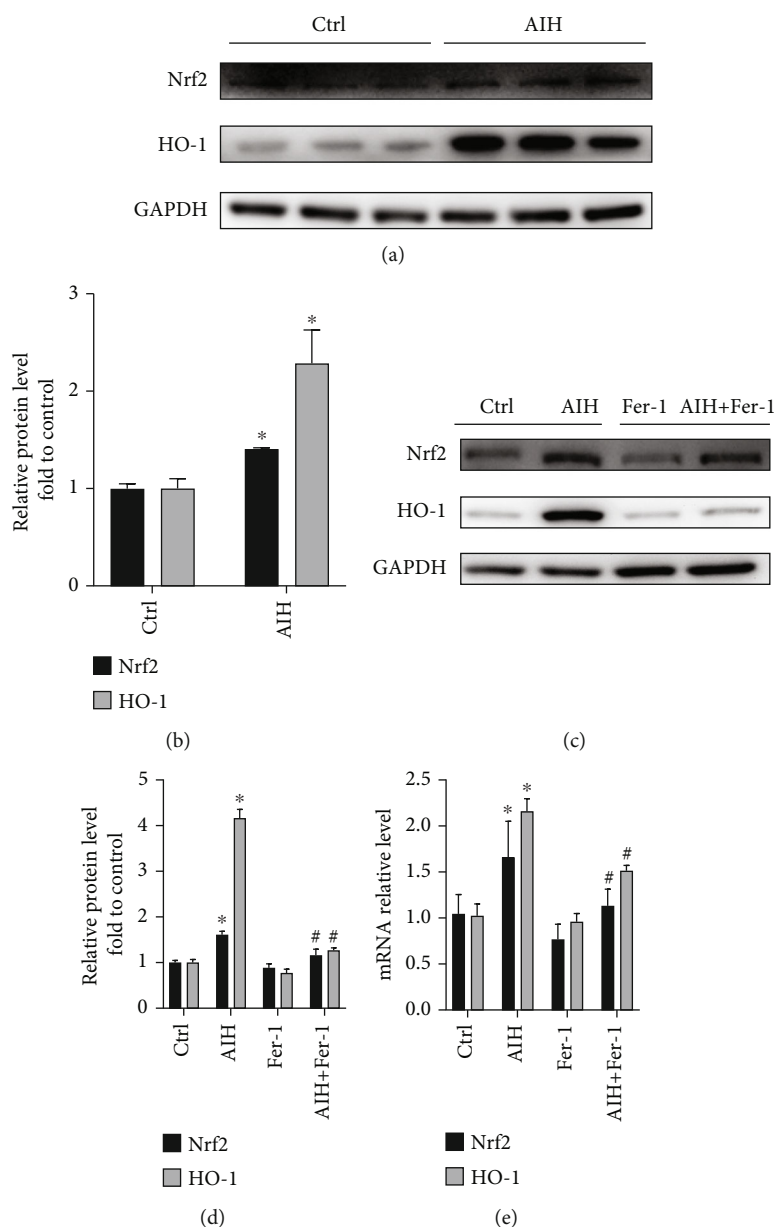


FIGURE 4: Ferrostatin-1 ameliorates S100-induced AIH via the Nrf2/HO-1 signaling pathway. (a) and (b) Western blot showing protein expression of Nrf2 and HO-1 in the pre-experimental control and AIH groups. (c) and (d) Western blot showing protein expression of Nrf2 and HO-1 in the control, AIH, Ferrostatin-1, and AIH + Ferrostatin-1 groups; GAPDH was used as a loading control. (e) RT-qPCR assay for Nrf2 and HO-1 mRNA expression in the control, AIH, Ferrostatin-1, and AIH + Ferrostatin-1 groups; ACTB was used as a loading control; * $P < 0.05$, compared with control group; # $P < 0.05$, compared with AIH group.

to the LPS-induced hepatocyte ferroptosis model group alone, with a greater increase in comparison to the controls. Levels of FTH1 were also downregulated to a greater extent after GPX4 knockdown. Notably, after transfection with GPX4-specific overexpression plasmids followed by the same concentration of LPS to induce hepatocyte ferroptosis, COX2 and ACSL4 expressions were downregulated in comparison to the LPS-induced hepatocyte ferroptosis model group alone, and more so when compared to the control, while the levels of FTH1 also increased with GPX4 overexpression.

Cellular immunofluorescence staining showed that COX2 staining (green) was abundant in the LPS-induced hepatocyte ferroptosis model group, mainly localized in the cytoplasm. In addition, after GPX4 knockdown followed by LPS-induced hepatocyte ferroptosis, there was more intense COX2 staining compared to the LPS-induced hepatocyte ferroptosis model group alone, while COX2 staining after GPX4 overexpression followed by the same concentration of LPS-induced hepatocyte ferroptosis was significantly diminished compared to the LPS-induced hepatocyte ferroptosis model group alone (Figures 5(c) and 5(d)). These

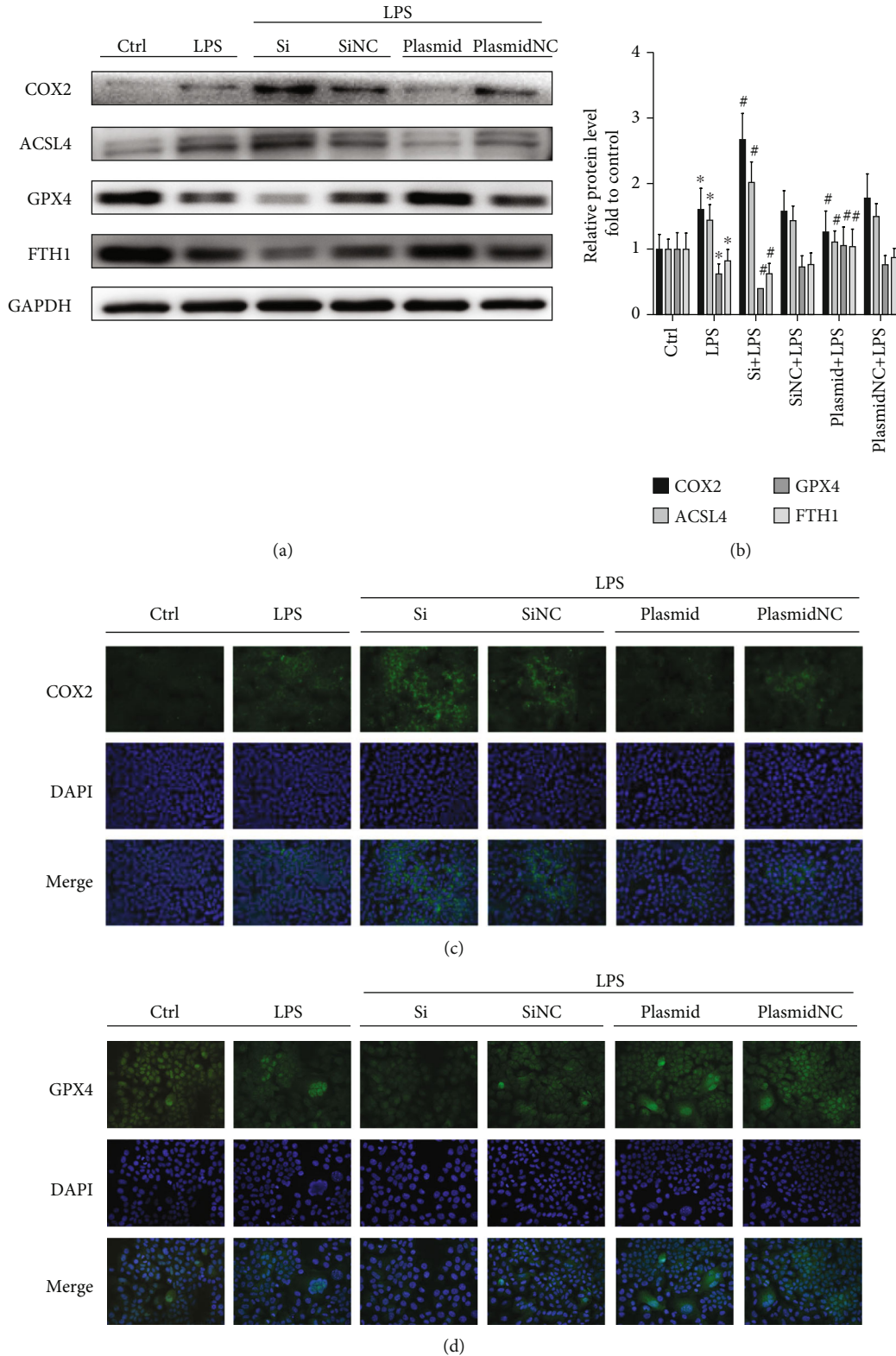


FIGURE 5: LPS-induced ferroptosis in AML12 cells occurs through the regulation of GPX4. (a) and (b) Western blot showing protein expression of COX2, ACSL4, GPX4, and FTH1 in the control, LPS, Si+LPS, SiNC+LPS, Plasmid+LPS, and PlasmidNC+LPS groups; GAPDH was used as a loading control; (c) and (d) COX2 and GPX4 immunofluorescence detection combined with DAPI staining for nuclei (scale bar: 75 μ m). * $P < 0.05$, compared with the control group; # $P < 0.05$, compared with the LPS group.

results suggest that GPX4 regulates the induction of LPS-induced ferroptosis in AML12 cells.

4. Discussion

The liver is the main iron storage site in the body, with iron in the form of ferritin and iron-containing hemoglobin. In the healthy liver, ferritin forms the main form of storage, with minimal availability of iron-containing heme. However, in the iron-overloaded liver, there are large accumulations of both ferritin and heme, especially in the case of hereditary or secondary diseases [21]. The evidence suggests that ferritin's role is to capture "free" iron within its spacious storage core, thus, protecting the cell against potential damage caused by reactive oxygen radicals generated by the Fenton reaction [22]. Several recent studies have shown that oxidative stress induced by ROS is the underlying pathophysiological mechanism in several liver diseases [23]. High levels of ROS lead to DNA damage, protein denaturation, and lipid peroxidation of and cyclooxygenase (COX) and lipoxygenase (LOX), together with affecting other enzyme functions [24]. Ferroptosis, a newly discovered type of iron-dependent nonapoptotic cell death, is biologically and morphologically distinct from apoptosis, necroptosis, and autophagy [25]. It is also characterized by free ferrous iron overload and the accumulation of lipid peroxides. However, lipid peroxide accumulation is mainly caused by the absence, or insufficient activity, of the selenium peroxidase glutathione peroxidase 4 (GPX4). GPX4 is a unique intracellular antioxidant enzyme that inhibits the production of lipid peroxidation in the cell membrane [26]. Given that the dynamic balance of iron is intimately linked to the maintenance of human health, disturbances in iron homeostasis can easily lead to a variety of medical conditions [27]. This investigation focused on the influence of ferroptosis in AIH and its possible regulatory mechanisms in the disease.

An *in vivo* mouse AIH model was established using S100, with the treated mice showing elevated serum ALT and AST levels, suggesting hepatic impairment. Elevation of serum IgG after 28 days indicated the presence of AIH. Meanwhile, the levels of the inflammatory cytokines TNF- α , IFN γ , and IL-17, and the fibrotic cytokine TGF- β , which play important roles in the pathology and progression of AIH, were increased, while the anti-inflammatory cytokine IL-10 level was decreased, further suggesting the presence of liver inflammation and fibrosis in the S100-induced AIH experimental mice. Specific inflammatory cytokines induce the activity of specific transcription factors that direct the differentiation of the relevant immune cell subtypes (Th1 and Treg cells secrete IFN γ and TGF- β , respectively, while Th17 cells secrete IL-17) [28]. There is growing evidence that both IL-17 and Th17 cells play key roles in the development and progression of AIH inflammation and that Th17 cells are important for the body's defense response [29]. Whereas the cellular source of TNF- α has not been specifically elucidated, several studies have also been reported suggesting that TNF- α may be released by activated monocytes, T cells, NK cells, mast cells, B cells, and Kupffer cells in the liver [30, 31]. In addition, histological analysis demonstrated

inflammatory infiltration in the liver after S100 intervention that was consistent with a significant increase in COX2 expression. Genome-wide CRISPR-based genetic screening and microarray analysis of ferroptosis-resistant cell lines has previously asserted that ACSL4 is a key molecular player in the ferroptotic process [12]. Furthermore, stabilized glutathione levels in normal cells provide protection against oxidative stress and ferroptosis-driven cellular damage. Lipid peroxidation may increase as a consequence of either a reduced GPX4 expression or a reduction in the level of its cofactor glutathione [32]. At the onset of ferroptosis, increased iron-dependent lipid ROS production overwhelm GPX4's ability to control polyunsaturated fatty acid peroxidation, resulting in aberrant control of lipid peroxides and hence peroxidation, which are hallmarks of ferroptosis and lead to cell death [33]. It has been demonstrated in several studies that GPX4 is a major target of ferroptosis. There is direct genetic evidence that GPX4 knockouts lead to cell death in a pathologically relevant form of ferroptosis [34]. Recently, it was shown that cell death by ferroptosis is triggered by the knockout of GPX4 in either kidney or T cells [35]. Coincidentally, previous studies have shown that GPX4 overexpression and knockdown modulated the lethality of multiple ferroptosis inducers, but not of compounds associated with other cell death mechanisms [36]. Knockdown of FTH1 in hepatocellular carcinoma cells increased the incidence of ferroptosis, suggesting that FTH1 may play an important protective role in cellular ferroptosis and that reduced homeostasis in iron stores during the onset of ferroptosis may lead to iron overload [37]. Thus, aberrant expression of FTH1 may lead to issues associated with iron storage and cell death through the disruption of antioxidant defense systems [38]. The S100-induced AIH model group, in this investigation, showed upregulation of both COX2 and ACSL4, together with downregulation of GPX4 and FTH1. Ferroptosis is known to be activated through iron-dependent lipid peroxidation [39]. Therefore, we quantified the level of lipid peroxidation in the liver using malondialdehyde (MDA). The dysregulation of COX2, ACSL4, GPX4, and FTH1 expression, as well as MDA and iron overload levels, suggest an important role for ferroptosis in S100-induced autoimmune hepatitis.

To verify the role of ferroptosis, we used the ferroptosis inhibitor Ferrostatin-1 for therapeutic intervention in the S100-induced AIH mice. It was found that Ferrostatin-1 significantly attenuated the ALT, AST, and IgG serum levels, as well as the level of microscopic inflammatory infiltrates in H&E-stained sections in the S100-induced AIH mice. In addition, the expression of ferroptosis biomarkers (including ACSL4, GPX4, and FTH1) was significantly reduced by Ferrostatin-1 treatment. Furthermore, iron-dependent oxidative stress and lipid peroxidation are common features of ferroptosis and inflammatory diseases [40]. Ferrostatin-1 reduced MDA levels in the AIH mouse livers. Thus, our data clearly illustrate that ferroptosis may be the main underlying mechanism that mediates S100-induced autoimmune hepatitis.

Nrf2, a master controller of the antioxidant response, is a transcription factor that is often aberrantly regulated in oxidative stress [41]. The stability of inactivated Kelch-like

ECH-associated protein 1 (Keap1)/Nrf2 heterodimers is maintained by thiol antioxidants in the cytosol under non-stress conditions [42]. However, during oxidative stress, Nrf2 is dissociated from the Keap1 heterodimer in the cytosol, allowing Nrf2 to translocate to the nucleus where Nrf2 interacts with antioxidant response elements (ARE) to trigger the transcription of target genes (including HO-1) to mitigate oxidative stress [43]. In the present study, S100 induced an increase in hepatic Nrf2/HO-1 expression in the mouse AIH models. Furthermore, treatment with ferrostatin-1 reversed these effects, indicating that ferrostatin-1 may attenuate S100-induced AIH through inhibition of Nrf2/HO-1 pathway-mediated ferroptosis. These data suggest that the Nrf2/HO-1 pathway plays a pivotal role in thwarting ferroptosis. This highlights the role of ferroptosis in S100-induced AIH, with ferrostatin-1 ameliorating the AIH condition, mediated by the Nrf2/HO-1 signaling pathway.

Our investigation delved deeper into possible mechanisms of ferroptosis in AIH. The regulation of GPX4 in *in vitro* cellular experiments and *in vivo* animal experiments was assessed. AAV8-m-GPX4 was administered to S100-induced AIH mice to suppress GPX4 expression by liver-specific knockdown of the GPX4 gene. Tail-vein injection of AAV8-m-GPX4 to silence GPX4 expression resulted in increased levels of serum ALT, AST, and IgG, as well as increased infiltration of inflammatory cells. In addition, the expression of ferroptosis biomarkers (including COX2, ACSL4, and FTH1) was significantly increased in mice with S100-induced autoimmune hepatitis after specific knockdown of GPX4. Previous studies have shown that localized GPX4 deficiency can lead to increased levels of lipid peroxidation [44]. In the current study, liver-specific GPX4 knockdown also increased the MDA and iron-overload levels in the livers of S100-induced AIH mice. It has recently been shown that cell death due to ferroptosis is caused by a deletion of the GPX4 gene in the kidney [35]. The data presented in our study clearly demonstrate that GPX4 is vital for preventing the deleterious effects of lipid peroxidation and ferroptosis in autoimmune hepatitis. The *in vitro* cell experiments used GPX4-specific knockdown siRNA and a GPX4-specific overexpression plasmid to regulate LPS-induced ferroptosis model in AML12 cells. It was found that the expression of other ferroptosis biomarkers (including COX2, ACSL4, and FTH1) were significantly enhanced after GPX4 knockdown. Consequently, these results of this investigation implicate ferroptosis as an initiator or mediator of AIH pathogenesis, and that the occurrence of ferroptosis in AIH is regulated by GPX4.

5. Conclusions

In conclusion, our results demonstrate an essential role for ferroptosis in S100-induced AIH pathogenesis. It was also demonstrated that the Nrf2/HO-1 signaling pathway play a key part in inhibiting ferroptosis. Notably, S100-induced ferroptosis in AIH was found to be closely linked to GPX4 regulatory control. These results increase our knowledge of the molecular interactions underlying AIH and suggest

directions for the development of novel therapeutic strategies to treat the disease.

Data Availability

The data will be available upon reasonable request.

Conflicts of Interest

The authors declare that they have no competing interests.

Authors' Contributions

Lujian Zhu, Dazhi Chen, Lanman Xu, and Yongping Chen contributed to conception, designed experiments, and were responsible for the whole work; Yin Zhu, Tongtong Pan, Dingchao Xia, Tingchen Cai, Hongwei Lin, Jing Lin, Xiaozhi Jin, Faling Wu, Sijie Yu, and Kailu Zhu performed experiments; Lujian Zhu and Dazhi Chen analyzed experimental results and wrote the manuscript. All authors contributed to data analysis, drafting, or revising the article, have agreed on the journal to which the article will be submitted, gave final approval for the version to be published, and agree to be accountable for all aspects of the work. All authors approved the final version of the article, including the authorship list. Lujian Zhu and Dazhi Chen contributed equally to this work.

Acknowledgments

This research was supported by Wenzhou Science and Technology Bureau major scientific and technological innovation to attack health care projects (no. ZY2019008), Wenzhou Science and Technology Bureau basic medical and health science and technology projects (no. Y20210147), Zhejiang Provincial Natural Science Foundation of China (no. LD21H030002), and the National Natural Science Foundation of China (no. 81770585 and no. 82070593).

References

- [1] P. Muratori, A. Granito, M. Lenzi, and L. Muratori, "Limitation of the simplified scoring system for the diagnosis of autoimmune hepatitis with acute onset," *Liver international: official journal of the International Association for the Study of the Liver*, vol. 41, no. 3, pp. 529–534, 2021.
- [2] S. Xi, L. Yue, M. Shi et al., "The effects of Taoren-Honghua herb pair on pathological microvessel and angiogenesis-associated signaling pathway in mice model of CCl4-induced chronic liver disease," *Evidence-based Complementary and Alternative Medicine: Ecam*, vol. 2016, article 2974256, 11 pages, 2016.
- [3] A. Lohse, M. Manns, H. Dienes, K. H. M. Zum Büschenfelde, and I. R. Cohen, "Experimental autoimmune hepatitis: disease induction, time course and T-cell reactivity," *Hepatology*, vol. 11, no. 1, pp. 24–30, 1990.
- [4] S. Berardi, F. Lodato, A. Gramenzi et al., "High incidence of allograft dysfunction in liver transplanted patients treated with pegylated-interferon alpha-2b and ribavirin for hepatitis C recurrence: possible de novo autoimmune hepatitis?," *Gut*, vol. 56, no. 2, pp. 237–242, 2007.

- [5] Y. Xie, W. Hou, X. Song et al., "Ferroptosis: process and function," *Cell Death and Differentiation*, vol. 23, no. 3, pp. 369–379, 2016.
- [6] R. Berg, K. Møller, and D. Bailey, "Neuro-oxidative-nitrosative stress in sepsis," *Journal of Cerebral Blood Flow and Metabolism: Official Journal of the International Society of Cerebral Blood Flow and Metabolism*, vol. 31, no. 7, pp. 1532–1544, 2011.
- [7] B. Stockwell, X. Jiang, and W. Gu, "Emerging mechanisms and disease relevance of ferroptosis," *Trends in Cell Biology*, vol. 30, no. 6, pp. 478–490, 2020.
- [8] A. Bogdan, M. Miyazawa, K. Hashimoto, and Y. Tsuji, "Regulators of iron homeostasis: new players in metabolism, cell death, and disease," *Trends in Biochemical Sciences*, vol. 41, no. 3, pp. 274–286, 2016.
- [9] Y. Yang, W. Tai, N. Lu et al., "lncRNA ZFAS1 promotes lung fibroblast-to-myofibroblast transition and ferroptosis via functioning as a ceRNA through miR-150-5p/SLC38A1 axis," *Aging*, vol. 12, no. 10, pp. 9085–9102, 2020.
- [10] H. Yuan, X. Li, X. Zhang, R. Kang, and D. Tang, "Identification of ACSL4 as a biomarker and contributor of ferroptosis," *Biochemical and Biophysical Research Communications*, vol. 478, no. 3, pp. 1338–1343, 2016.
- [11] W. Yang, K. Kim, M. Gaschler, M. Patel, M. S. Shchepinov, and B. R. Stockwell, "Peroxidation of polyunsaturated fatty acids by lipoxygenases drives ferroptosis," *Proceedings of the National Academy of Sciences of the United States of America*, vol. 113, no. 34, pp. E4966–E4975, 2016.
- [12] S. Doll, B. Proneth, Y. Tyurina et al., "ACSL4 dictates ferroptosis sensitivity by shaping cellular lipid composition," *Nature Chemical Biology*, vol. 13, no. 1, pp. 91–98, 2017.
- [13] X. Sheng, C. Shan, J. Liu, J. Yang, B. Sun, and D. Chen, "Theoretical insights into the mechanism of ferroptosis suppression via inactivation of a lipid peroxide radical by liproxstatin-1," *Physical chemistry chemical physics : PCCP*, vol. 19, no. 20, pp. 13153–13159, 2017.
- [14] L. Wang, H. Cai, Y. Hu et al., "A pharmacological probe identifies cystathionine β -synthase as a new negative regulator for ferroptosis," *Cell Death & Disease*, vol. 9, no. 10, p. 1005, 2018.
- [15] M. Benhar, I. Shytaj, J. Stamler, and A. Savarino, "Dual targeting of the thioredoxin and glutathione systems in cancer and HIV," *The Journal of Clinical Investigation*, vol. 126, no. 5, pp. 1630–1639, 2016.
- [16] M. Ito, T. Tanaka, and M. Nangaku, "Nuclear factor erythroid 2-related factor 2 as a treatment target of kidney diseases," *Current Opinion in Nephrology and Hypertension*, vol. 29, no. 1, pp. 128–135, 2020.
- [17] L. Chang, S. Chiang, S. Chen, Y. L. Yu, R. H. Chou, and W. C. Chang, "Heme oxygenase-1 mediates BAY 11-7085 induced ferroptosis," *Cancer Letters*, vol. 416, pp. 124–137, 2018.
- [18] O. Adedoyin, R. Boddu, A. Traylor et al., "Heme oxygenase-1 mitigates ferroptosis in renal proximal tubule cells," *American Journal of Physiology. Renal Physiology*, vol. 314, no. 5, pp. F702–F714, 2018.
- [19] Y. Chen, P. Zhang, W. Chen, and G. Chen, "Ferroptosis mediated DSS-induced ulcerative colitis associated with Nrf2/HO-1 signaling pathway," *Immunology Letters*, vol. 225, pp. 9–15, 2020.
- [20] J. Shi, D. Zheng, Y. Liu et al., "Overexpression of soluble TRAIL induces apoptosis in human lung adenocarcinoma and inhibits growth of tumor xenografts in nude mice," *Cancer Research*, vol. 65, no. 5, pp. 1687–1692, 2005.
- [21] E. Miyazaki, J. Kato, M. Kobune et al., "Denatured H-ferritin subunit is a major constituent of haemosiderin in the liver of patients with iron overload," *Gut*, vol. 50, no. 3, pp. 413–419, 2002.
- [22] H. Bonkovsky, "Iron and the liver," *The American Journal of the Medical Sciences*, vol. 301, no. 1, pp. 32–43, 1991.
- [23] A. Hegazy, A. Mohamed, S. Ali, N. M. Alghamdi, A. M. Abdel-Rahman, and S. al-Sobeai, "Chemical ingredients and antioxidant activities of underutilized wild fruits," *Heliyon*, vol. 5, no. 6, article e01874, 2019.
- [24] C. Ross, S. Brennan-Laun, and G. Wilson, "Tristetraprolin: roles in cancer and senescence," *Ageing Research Reviews*, vol. 11, no. 4, pp. 473–484, 2012.
- [25] W. Wang, M. Green, J. Choi et al., "CD8⁺ T cells regulate tumour ferroptosis during cancer immunotherapy," *Nature*, vol. 569, no. 7755, pp. 270–274, 2019.
- [26] H. Mei, L. Zhao, W. Li et al., "Inhibition of ferroptosis protects house ear institute-organ of Corti 1 cells and cochlear hair cells from cisplatin-induced ototoxicity," *Journal of Cellular and Molecular Medicine*, vol. 24, no. 20, pp. 12065–12081, 2020.
- [27] T. Ganz, "Systemic iron homeostasis," *Physiological Reviews*, vol. 93, no. 4, pp. 1721–1741, 2013.
- [28] D. Martínez-Méndez, C. Villarreal, L. Mendoza, and L. Huerta, "An integrative network modeling approach to T CD4 cell activation," *Frontiers in Physiology*, vol. 11, p. 380, 2020.
- [29] Y. Tang, Z. Bian, L. Zhao et al., "Interleukin-17 exacerbates hepatic steatosis and inflammation in non-alcoholic fatty liver disease," *Clinical and Experimental Immunology*, vol. 166, no. 2, pp. 281–290, 2011.
- [30] R. Locksley, N. Killeen, and M. Lenardo, "The TNF and TNF receptor superfamilies: integrating mammalian biology," *Cell*, vol. 104, no. 4, pp. 487–501, 2001.
- [31] G. Kalliolias and L. Ivashkiv, "TNF biology, pathogenic mechanisms and emerging therapeutic strategies," *Nature reviews Rheumatology*, vol. 12, no. 1, pp. 49–62, 2016.
- [32] B. Dash, P. Belmonte, S. Fine et al., "Murine T cell maturation entails protection from MBL2, but complement proteins do not drive clearance of cells that fail maturation in the absence of NKAP," *Journal of Immunology*, vol. 203, no. 2, pp. 408–417, 2019.
- [33] H. Tang and H. Tang, "Cell recovery by reversal of ferroptosis," *Biology Open*, vol. 8, no. 6, 2019.
- [34] J. Friedmann Angeli, M. Schneider, B. Proneth et al., "Inactivation of the ferroptosis regulator Gpx4 triggers acute renal failure in mice," *Nature Cell Biology*, vol. 16, no. 12, pp. 1180–1191, 2014.
- [35] X. Lei, J. Zhu, W. Cheng et al., "Paradoxical roles of antioxidant enzymes: basic mechanisms and health implications," *Physiological Reviews*, vol. 96, no. 1, pp. 307–364, 2016.
- [36] W. Yang, R. SriRamaratnam, M. Welsch et al., "Regulation of ferroptotic cancer cell death by GPX4," *Cell*, vol. 156, no. 1–2, pp. 317–331, 2014.
- [37] X. Sun, Z. Ou, R. Chen et al., "Activation of the p62-Keap1-NRF2 pathway protects against ferroptosis in hepatocellular carcinoma cells," *Hepatology (Baltimore, Md.)*, vol. 63, no. 1, pp. 173–184, 2016.
- [38] N. Meguid, S. Ghozlan, M. Mohamed et al., "Expression of reactive oxygen species-related transcripts in Egyptian

- children with autism,” *Biomarker Insights*, vol. 12, article 117727191769103, 2017.
- [39] L. Zhang, W. Liu, F. Liu et al., “Corrigendum to “IMCA induces ferroptosis mediated by SLC7A11 through the AMPK/mTOR pathway in colorectal cancer”,” *Oxidative Medicine and Cellular Longevity*, vol. 2020, Article ID 6901472, 2 pages, 2020.
- [40] H. Mao, Y. Zhao, H. Li, and L. Lei, “Ferroptosis as an emerging target in inflammatory diseases,” *Progress in Biophysics and Molecular Biology*, vol. 155, pp. 20–28, 2020.
- [41] X. Jin, D. Chen, F. Wu et al., “Hydrogen sulfide protects against ammonia-induced neurotoxicity through activation of Nrf2/ARE signaling in astrocytic model of hepatic encephalopathy,” *Frontiers in Cellular Neuroscience*, vol. 14, article 573422, 2020.
- [42] N. Brandes, S. Schmitt, and U. Jakob, “Thiol-based redox switches in eukaryotic proteins,” *Antioxidants & Redox Signaling*, vol. 11, no. 5, pp. 997–1014, 2009.
- [43] B. Shen, W. Wang, L. Ding et al., “Nuclear factor erythroid 2-related factor 2 rescues the oxidative stress induced by di-N-butylphthalate in testicular Leydig cells,” *Human & Experimental Toxicology*, vol. 34, no. 2, pp. 145–152, 2015.
- [44] M. Wortmann, M. Schneider, J. Pircher et al., “Combined deficiency in glutathione peroxidase 4 and vitamin E causes multiorgan thrombus formation and early death in mice,” *Circulation Research*, vol. 113, no. 4, pp. 408–417, 2013.

Research Article

Hydrogen-Rich Water Ameliorates Murine Chronic Graft-versus-Host Disease through Antioxidation

Liren Qian , Jiaxin Liu, Weina Ma, Yu Liu, Xiaona Wang, and Daihong Liu 

Senior Department of Hematology, The Fifth Medical Center, Chinese PLA General Hospital, Chinese PLA Medical School, Beijing, China

Correspondence should be addressed to Daihong Liu; daihongrm@163.com

Received 7 August 2021; Accepted 25 September 2021; Published 14 October 2021

Academic Editor: Ivan Srejavic

Copyright © 2021 Liren Qian et al. This is an open access article distributed under the Creative Commons Attribution License, which permits unrestricted use, distribution, and reproduction in any medium, provided the original work is properly cited.

Background. Allogeneic hematopoietic stem cell transplantation (allo-HSCT) is an important treatment option for various hematopoietic diseases and certain hereditary diseases. Chronic graft-versus-host disease (cGVHD) has become the main life-threatening complication and cause of death in later stage postallo-HSCT. Current treatment options for cGVHD are limited. Hydrogen gas (H_2) has been demonstrated that has antioxidative, anti-inflammatory, and antifibrosis effects. The aim of this study was to confirm whether oral administration hydrogen-rich water exerted therapeutic effects on a scleroderma cGVHD mouse model and tried to explain the mechanism underlying it. **Methods.** A mouse cGVHD model was established by haploidentical bone marrow transplantation. To evaluate therapeutic effects of H_2 on cGVHD, survival rate, changes in clinical scores, and skin pathologic characteristics of cGVHD mice were observed. To evaluate its therapeutic mechanism, we detected the expression levels of antioxidative enzymes heme oxygenase-1 (HO-1) and NAD (P)H: quinone acceptor oxidoreductase 1 (NQO1) in skin homogenates. We also detected the expression level of the apoptotic protein caspase-3 in skin homogenates. **Results.** 1-month survival rate of cGVHD mice in the hydrogen group reached 93.3%, significantly higher than 66.7% in the nonhydrogen group ($p < 0.05$). Clinical score of cGVHD mice was improved by hydrogen-rich water at 96 days posttransplantation (2.2 versus 4.5, $p < 0.05$). The skin pathological condition of cGVHD mice was significantly improved by hydrogen-rich water. At 96 days posttransplantation, average skin pathological hematoxylin and eosin (HE) staining score in the hydrogen group was 1.05, which was significantly lower than 3.2 in the nonhydrogen group ($p < 0.01$). Average Masson staining score was 0.6 point in the hydrogen group, lower than 0.9 point in the nonhydrogen group ($p < 0.05$). Both the relative expression levels of HO-1 and NQO1 proteins in skin specimens of cGVHD mice in the hydrogen group were lower than that in the nonhydrogen group (2.47 versus 6.21 and 1.83 versus 3.59, $p < 0.05$). The relative expression level of caspase-3 protein in skin specimens of cGVHD mice increased to 7.17 on the 96th day after transplantation, significantly higher than 4.36 in the hydrogen group. **Conclusion.** In this study, we found that oral hydrogen-rich water improved the survival rate and clinical symptoms of cGVHD mice by antioxidant and antiapoptosis. This study would pave the way for further clinical study, which may provide a new treatment option for cGVHD.

1. Introduction

Allogeneic hematopoietic stem cell transplantation (allo-HSCT) is an important treatment option for various hematopoietic diseases and certain hereditary diseases. Chronic graft-versus-host disease (cGVHD) has become the main life-threatening complication and cause of death in later stage postallo-HSCT [1, 2]. With the decrease in early mortality posttransplantation, the increasing upper age limit of recipients, and the widespread application of unrelated

donors and peripheral blood hematopoietic stem cells, the incidence of cGVHD has gradually increased [3, 4]. 2-year cumulative incidence of cGVHD posttransplantation that needs treatment was 30%-40% [2]. Glucocorticoids with or without calcineurin inhibitors (CNI) were always used as the initial treatment of cGVHD in the past few decades [2]. However, glucocorticoids may cause serious adverse effects after long-term application, including severe infections, peptic ulcers, femoral head necrosis, osteoporosis, diabetes, and hypertension [5]. Besides, during the tapering of

glucocorticoids, cGVHD symptoms often relapse or even aggravate [5]. If the disease relapses or progresses, second-line treatment is often required. 50%-60% cGVHD patients need second-line therapy [6, 7]. However, there is currently no standard preferred second-line treatment [8]. Although some new drugs such as ruxolitinib have brought unprecedented curative effects in this field in recent years [9–11], clinical trials are still encouraged, and a better therapy method is in urgent need for cGVHD [12].

In 2007, Ohsawa et al. systematically confirmed the free radicals scavenging ability of hydrogen [13]. They found that H_2 had similar therapeutic effects in a cerebral ischemia-reperfusion injury rat model by scavenging hydroxyl radicals ($\cdot OH$) comparing with tacrolimus. Besides to its free radical scavenging ability, researchers also found that hydrogen has anti-inflammatory effects in autoimmune hepatitis [14], systemic inflammatory response syndrome [15], inflammatory bowel disease [16], allergic dermatitis [17], lipopolysaccharide- (LPS-) induced paw edema [18], and other animal inflammatory disease models, which is also similar to tacrolimus. Moreover, H_2 has antifibrosis effects. It was found that breathing 4% H_2 significantly delayed the progression of pulmonary fibrosis in a radiation induced pulmonary fibrosis model [19]. They confirmed that H_2 significantly reduced the fibrotic lesions in the lungs of mice. The main pathophysiological process of cGVHD is immunoinflammatory responses, and the characteristic pathological change is fibrosis [12, 20, 21]. Oxidative stress, inflammation imbalance, and fibrosis play important roles in the progression of cGVHD [12, 20, 21]. Therefore, we speculated that H_2 may exert potential therapeutic effects on cGVHD after allo-HSCT. In this study, an attempt was made to confirm whether oral administration hydrogen-rich water exerted therapeutic effects on a scleroderma cGVHD mouse model and tried to explain the mechanism underly it.

2. Materials and Methods

2.1. Hydrogen-Rich Water Production. Hydrogen-rich water was produced by dissolving hydrogen in sterile drinking water for 6 hours under high pressure (0.4 MPa) to a supersaturated level as we previously reported [22–24]. Hydrogen-rich water was freshly prepared every 12 hours, which ensured that a concentration of more than 0.6 mmol/L was maintained. Gas chromatography (Biogas Analyzer Systems-1000, Mitleben, Japan) was used to confirm the content of hydrogen in saline by the method described by Ohsawa et al. [13].

2.2. Mice. All the protocols were approved by the Chinese PLA General Hospital in accordance with the Guide for Care and Use of Laboratory Animals published by the US NIH (publication No. 96-01). Female C57BL/6N mice and male B6D2F1 mice were obtained from Beijing Vital River Laboratory Animal, Inc. (Beijing, China, <http://www.vitalriver.com.cn>). All mice were studied at between 10 and 12 weeks of age. Mice were housed in autoclaved cages with sterile food and water.

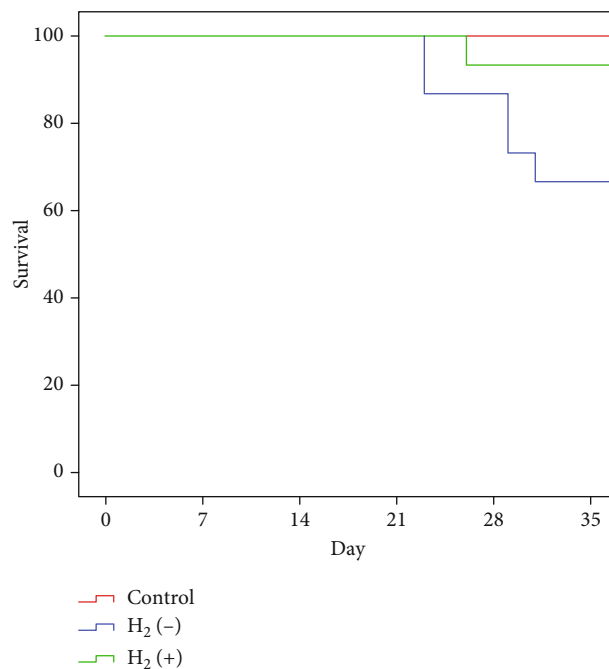


FIGURE 1: The survival rate of chronic GVHD mice in the hydrogen group was significantly higher than that in the nonhydrogen group ($p < 0.05$).

2.3. Chronic Graft-versus-Host Disease (cGVHD) Model. A cGVHD model was established as previously described [25]. B6D2F1 mice received total body irradiation (TBI) on day 1 (5.5 Gy, two doses on the same day, with an interval of 3–4 hours). On day 0, the control group was injected with 5×10^6 T cell-depleted bone marrow cells (TCD-BM) of C57BL/6 mice through the tail vein. In the cGVHD model group, 5×10^6 TCD-BM plus purified 1×10^6 splenic T cells of C57BL/6 mice were injected to irradiated B6D2F1 mice. In the hydrogen group, mice were given hydrogen-rich water from the 8th day posttransplantation when the mice have cGVHD symptoms until they were sacrificed. In the control group and nonhydrogen group, mice were routinely fed with sterile water.

2.4. Survival Assays. After transplantation, the mice were returned to individually ventilated cages and routinely cared. Their survival status was observed daily, and the survival was checked and recorded for 30 days.

2.5. Evaluation of cGVHD. Chronic GVHD symptoms of mice are clinically scored every five days after transplantation, mainly from the following 5 aspects [26]: weight loss (scored 0: <10%; scored 1: 10%–25%; scored 2: >25%), activity (scored 0: normal; scored 1: mild to moderately decreased; scored 2: stationary unless stimulated), posture (scored 0: normal; scored 1: hunching only at rest; scored 2: severe hunching impairs movement), fur texture (scored 0: normal; scored 1: mild to moderate ruffling; scored 2: severe ruffling/poor grooming), and skin integrity (scored 0: normal; scored 1: incomplete paw/tail scales; scored 2: obvious areas of denuded skin). The scores of these five

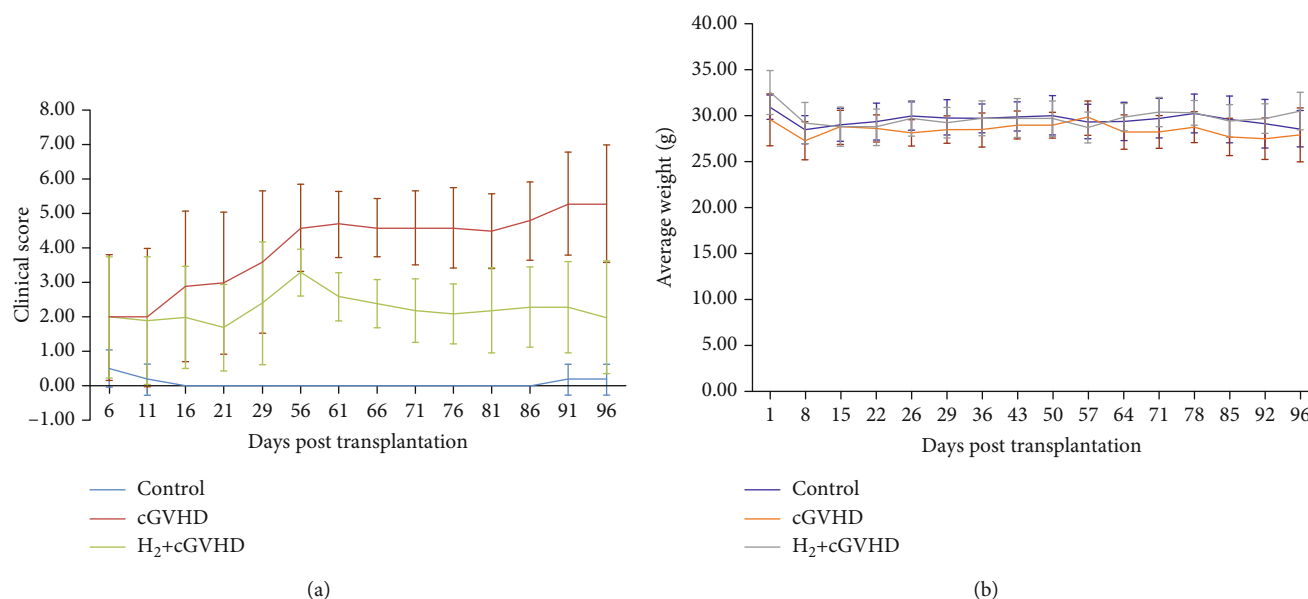


FIGURE 2: With the time of drinking H₂-rich water increased, the clinical improvement of chronic GVHD mice becomes more obvious. At 96 days after transplantation, the clinical score of chronic GVHD mice in the hydrogen group was significantly lower than that in the nonhydrogen group (Figure 2(a), $p < 0.05$). The weight of chronic GVHD mice in the hydrogen group was not statistically different from that in the nonhydrogen group (Figure 2(b), $p > 0.05$).

aspects were added together to evaluate the severity of cGVHD.

2.6. Tissue Histopathology. About 2 cm² shaved skin from interscapular region was selected. The hematoxylin and eosin (HE) staining was performed as we previously described [27]. A dermatologist, blinded to the groups of animals, scored from five aspects: epidermal structural changes, inflammatory cell infiltration, reduction or loss of hair follicles, dermal fibrosis, and reduction or loss of fat. Each index is rated as 0-2 points according to the severity of the lesion. The total score is between 0 and 10 points [28]. Masson staining was also performed according to the previous literature [23], and scores were given according to the thickness and looseness of collagen fibers: 0 (normal), 0.5 (minor), 1 (mild), 2 (moderate), and 3 (severity). The skin of each group was scored for pathology 96 days after transplantation.

2.7. Western Blot. The specimens of skin tissue were collected and lysed as previously described [29]. The skin samples were collected and frozen in dry ice and stored at -70°C until assayed by WB analysis. We homogenized the skin specimens on ice by sonication and dissolved in lysis buffer, which contains phosphate-buffered saline (PBS, pH 7.4), 1% Tergitol NP-40 (Sigma-Aldrich, St. Louis, MO), 0.5% sodium deoxycholate (Sigma), 1% sodium dodecyl sulfate (SDS) (Sigma), 1 mM EDTA (Sigma), 1 mM EGTA (Sigma), 1% protease inhibitor cocktail (Sigma), and 0.6 mM phenylmethanesulfonyl fluoride (PMSF). Then, the homogenate was centrifuged at 14,000 rpm for 30 minutes at 4°C [30]. Protein concentrations were detected by NanoDrop 1000 spectrophotometer (Thermo Fisher Scientific) [31]. The expression levels of HO-1, NQO1, and caspase-3 proteins

in the skin tissues of different groups were detected by western blot analysis as previously described [32]. In the western blot analysis, we obtained the following antibodies from Cell Signaling Technology: anti-HO-1, anti-NQO1, anti-caspase-3, and anti- β -actin.

3. Results

3.1. Therapeutic Effects of Hydrogen on cGVHD Mice

3.1.1. Hydrogen Increased the Survival Rate of cGVHD Mice. Oral giving more than 2 weeks of hydrogen-rich water improved the survival rate of cGVHD mice (Figure 1). The 30-day survival rate of cGVHD mice in the hydrogen water group was 93.3%, significantly higher than that in the nonhydrogen cGVHD group (66.7%, $p < 0.05$).

3.1.2. Hydrogen Improved cGVHD Mice Clinical Symptoms. Compared with the nonhydrogen group, the clinical symptoms of the mice in the hydrogen group began to improve after drinking hydrogen-rich water for one week (Figure 2(a)). With the time of drinking hydrogen-rich water increased, the improvement of clinical symptoms becomes more obvious. At 96 days posttransplantation, average clinical score of the cGVHD mice in the hydrogen group was 2.0 points, which was less than that in the nonhydrogen water group (5.3 points, $p < 0.05$). The average body weight of cGVHD mice in the hydrogen group was higher compared with that of the nonhydrogen water group without statistical difference (30.50 g vs. 27.92 g, $p > 0.05$, Figure 2(b)).

3.1.3. Hydrogen Improved cGVHD Mice Skin Pathology. The skin pathological condition of cGVHD mice has been significantly improved after given hydrogen-rich water. At 96 days posttransplantation, the average skin pathological HE

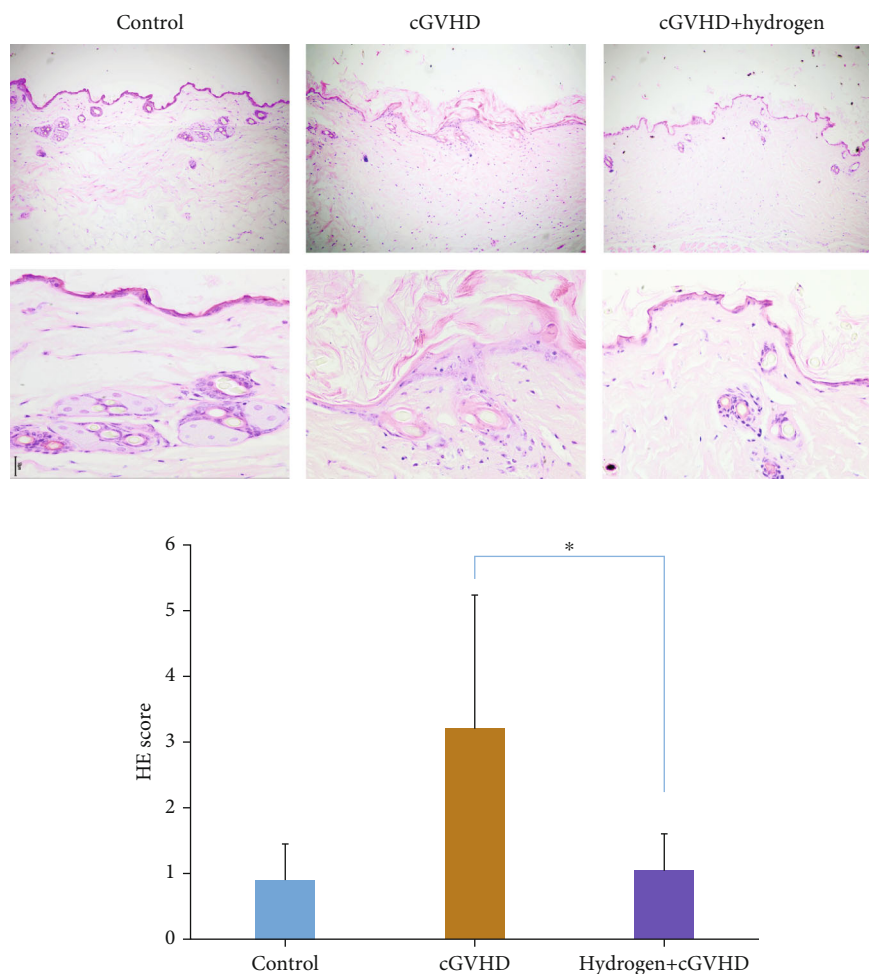


FIGURE 3: The skin pathological HE staining score of chronic GVHD mice in the hydrogen group was significantly lower than that in the nonhydrogen group ($p < 0.01$).

staining score in the hydrogen group was 1.05, significantly lower than 3.2 in the nonhydrogen group ($p < 0.01$, Figure 3). The average Masson staining score was 0.6 point in the hydrogen group, also lower than 0.9 point in the nonhydrogen group ($p < 0.05$, Figure 4).

3.2. The Mechanism of Hydrogen on cGVHD Mice

3.2.1. Hydrogen Reduced the Expression Level of HO-1 and NQO1. The relative expression level of HO-1 protein (β -actin) in the skin tissue of cGVHD mice in the hydrogen group was 2.47, which was significantly lower than 6.21 in the skin tissue of the nonhydrogen group cGVHD mice (Figure 5(a)). We found that the relative expression of NQO1 protein (β -actin) in the skin tissue of cGVHD mice in the hydrogen group was 1.83, which was significantly lower than 3.59 in the nonhydrogen group (Figure 5(b)).

3.2.2. Hydrogen Reduced the Expression Level of Caspase-3. The relative expression of caspase-3 protein (β -actin) in the skin tissue of cGVHD mice significantly increased to 7.17 on the 96th day after transplantation, which was much higher than 4.36 in the hydrogen group, suggesting that

molecular hydrogen significantly reduced the relative expression of apoptotic protein, which indicated that hydrogen has antiapoptotic ability by reducing the expression of caspase-3 protein (Figure 6).

4. Discussion

To our knowledge, this is the first study that proved oral saturated hydrogen-rich water has therapeutic effects on cGVHD in mice with scleroderma. It was confirmed that it exerted therapeutic effects by antioxidation and antiapoptosis. We demonstrated that hydrogen reduced the expression levels of HO-1 and NQO1 proteins in the cGVHD mice. We consider that hydrogen may neutralize oxygen free radicals and reduce the increased levels of HO-1 and NQO1 proteins caused by reactive oxygen species.

In our study, oral saturated hydrogen-rich water increased the 30-day survival rate of cGVHD mice by nearly 30%. The increase in the survival rate illustrated that hydrogen-rich water has therapeutic effects on mouse cGVHD as a whole. In addition, in this cGVHD animal model, we observed that oral hydrogen-rich water significantly improved the clinical symptoms of cGVHD in mice

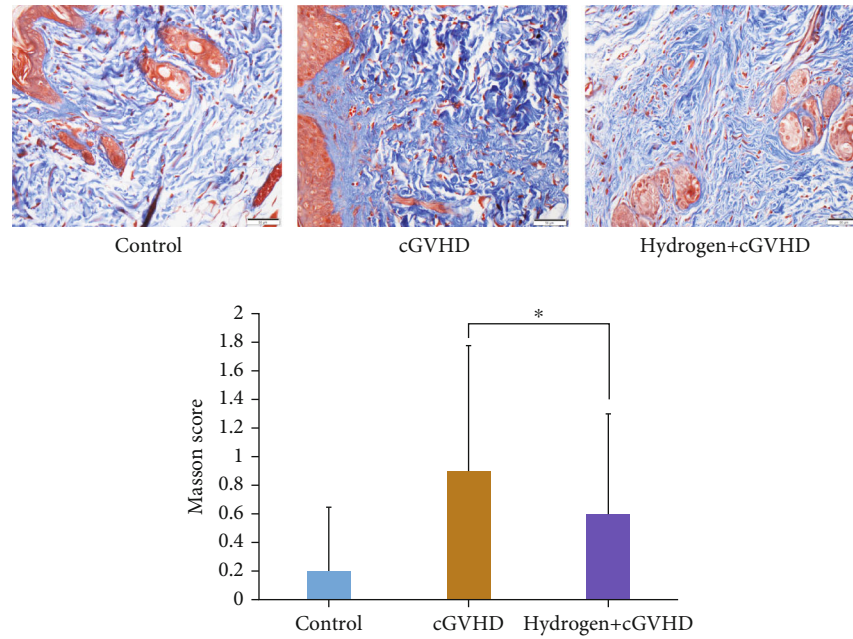


FIGURE 4: The skin pathological Masson staining fibrosis score of chronic GVHD mice in the hydrogen group was significantly lower than that in the nonhydrogen group ($p < 0.05$).

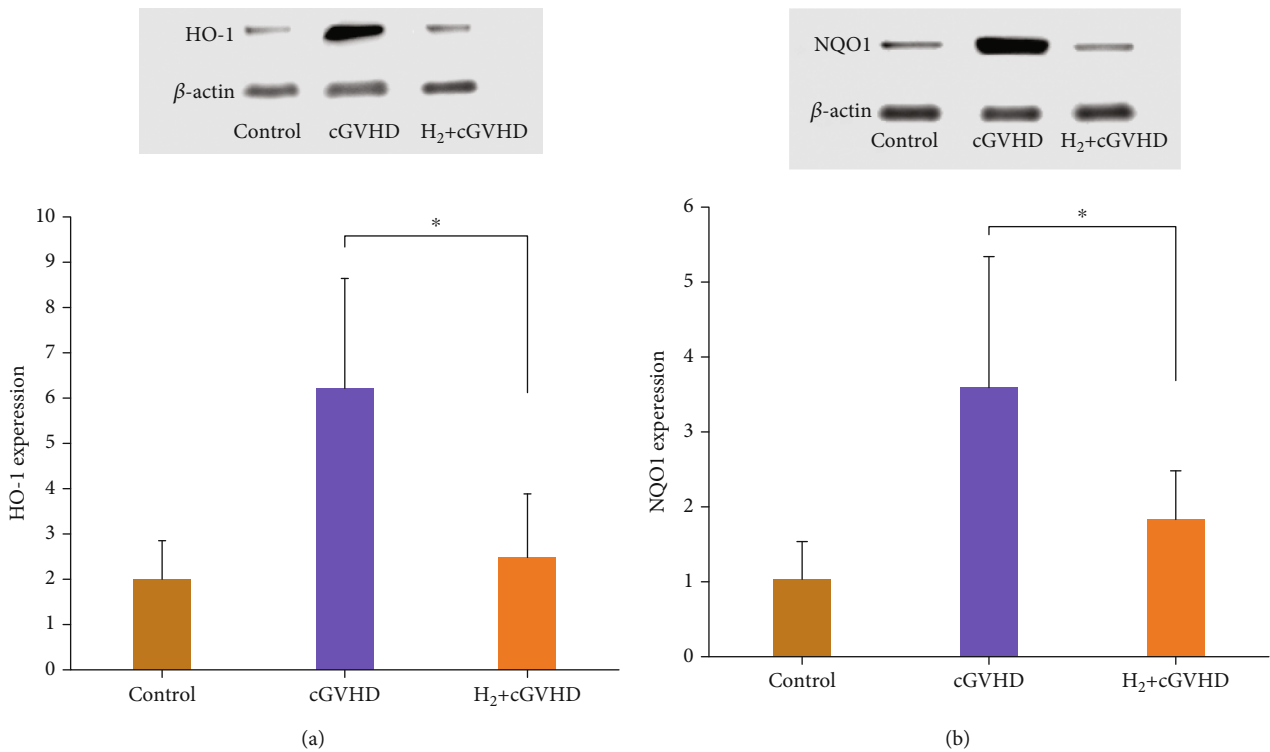


FIGURE 5: The relative expression level of HO-1 protein in the skin tissue of chronic GVHD mice in the hydrogen group was significantly lower than that in the nonhydrogen group (Figure 5(a), $p < 0.05$). The relative expression level of NQO1 protein in the skin tissue of chronic GVHD mice in the hydrogen group was significantly lower than that in the nonhydrogen group (Figure 5(b), $p < 0.05$).

and improved the skin pathology of mice. Fibrosis has been proven playing an important role in the development of cGVHD disease [19]. Fibrosis leads to organ failure in patients with cGVHD, including scleroderma, bronchitis

obliterans, and liver cirrhosis. Our research found that hydrogen-rich water mitigated the degree of skin fibrosis in cGVHD mice and improved the clinical symptoms of scleroderma in cGVHD mice. Formation of fibrosis often requires

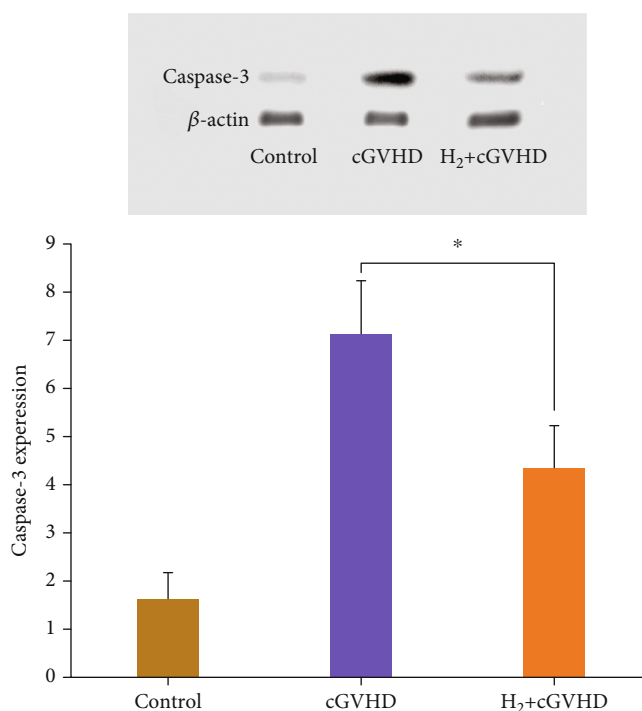


FIGURE 6: The relative expression level of caspase-3 protein in the skin tissue of chronic GVHD mice in the hydrogen group was significantly lower than that in the nonhydrogen group ($p < 0.05$).

a relatively long-term process. Long-term oral hydrogen-rich water has no obvious toxic and side effects, making it can be used in a long-term. This feature is adapted to the long-term, repeated, and prolonged disease characteristics of cGVHD, which makes hydrogen-rich water very suitable for cGVHD. Previously, we have demonstrated that the survival rate of another cGVHD mice model was increased by intraperitoneally injecting hydrogen-rich saline, and the pathological changes in skin was also improved [27]. In this study, we used oral hydrogen-rich water, which is more convenient than hydrogen-rich saline for injection and inhalation of hydrogen gas.

HO-1 and NQO1 are two important antioxidant enzymes. HO-1 mainly catalyzes and decomposes heme into ferrous iron, carbon monoxide, and biliverdin and prevents the prooxidation effect of heme. Its byproduct bilirubin and reduced bilirubin exert effective antioxidative ability by scavenging free radicals [33, 34]. The expression level of HO-1 is significantly positively correlated with the levels of ROS. When the ROS levels in the body increased by various pathological conditions like hypoxia and acidosis, HO-1 would rise rapidly, playing a cytoprotective role in the body [34], which promoted heme catabolism and prevents induction of programmed cell death [35]. NQO1 is a cell-protecting antioxidant enzyme that exerts antioxidant effects from many aspects. NQO1 catalyzed quinone to hydroquinone, promoting the excretion of quinone. It also reduced quinones, quinoneimines, nitroaromatics, and azo dyes, thereby reducing the redox cycle to produce ROS, preventing oxidative damage [36]. Wefers et al. first confirmed that NQO1 has a direct antioxidant effect [37]. It was confirmed

that NQO1 relies on the two-electron reduction mechanism, preventing quinone from participating in the oxidation cycle and generating active oxygen. As oxidative stress events occur in the body, NQO1 will also increase and play a protective role. Previously, we have confirmed that hydrogen regulated the levels of antioxidant enzymes superoxide dismutase (SOD), glutathione (GSH), and lipid oxidation product malondialdehyde (MDA) in the peripheral blood of mice injured by irradiation [22], exerting its radioprotective effects. In the current study, we found that in the skin tissues of mice, the expression levels of HO-1 and NQO1 proteins in the hydrogen group were significantly lower than those in the nonhydrogen cGVHD group. Many studies have confirmed that molecular hydrogen can directly react with oxygen free radicals such as hydroxyl radicals, thereby reducing oxidative damage [13, 19]. We believed that molecular hydrogen may reduce the oxidative stress level in cGVHD mice, thereby reducing the expression levels of HO-1 and NQO1 proteins in cGVHD mice.

Caspase-3 is one of the executioner caspases in apoptosis. It plays a vital role in cell apoptosis. It is responsible for cleaving most of the currently known apoptosis-related substrates. At the terminal of apoptosis, it is responsible for decomposing structural and regulatory proteins that shut down cell functions [38]. Chronic GVHD leads to apoptosis of tissue cells, resulting in a series of clinical manifestations. Our research found that the level of apoptosis protein caspase-3 in the molecular hydrogen group was significantly reduced. At present, we still consider molecular hydrogen exerting its antiapoptotic effect through antioxidation.

This research supplied novel ideas that were for treating cGVHD and has potential clinical application prospects, mainly due to the following points: first, H₂ is nontoxic side effects and no residue in the body [39], which is adapted for the long-term, repeated, and prolonged disease characteristics of cGVHD. Second, hydrogen molecules have great penetrating ability because they are very small. They can quickly penetrate biological membranes and reach high concentration in cells to exert therapeutic effects [13]. Third, the price of H₂ is low and easy to get. Although the current study confirmed that oral hydrogen-rich water has therapeutic effects on cGVHD and attempted to explain its mechanism, this research was limited confirming its therapeutic effect in a scleroderma cGVHD model. Chronic GVHD often involves multiple organs, including lungs, eyes, joints, gastrointestinal tract, and liver. As for whether hydrogen has therapeutic effects on cGVHD with other organs, it still needs to be further explored. Current studies on H₂ have so far been mostly limited to animal or clinical observational researches. Current clear mechanism is its ability of scavenging free radicals. Its antiapoptotic and antifibrosis effects still mainly depended on its ability of scavenging free radicals. As for whether hydrogen gas is a signal molecule, the regulation of HO-1, NQO1, and caspase-3 protein expression levels through signal pathways still needs further research to confirm.

With the increasing incidence of cGVHD, it has become one of the most difficult complications of allo-HSCT [2]. In view of the major drawbacks of current treatments, a better therapy method is in urgent need for cGVHD. This study demonstrated therapeutic effects of oral administration of hydrogen-rich water on a scleroderma cGVHD mouse model. As to whether H₂ has therapeutic effects on cGVHD through other mechanisms, further research is still needed.

Data Availability

All data relevant to the study are included in the article.

Conflicts of Interest

The authors declare no competing interest.

Acknowledgments

This work was supported by a grant from the National Natural Science Foundation of China (Grant No. 81800180) and a grant from the National Defense Science and Technology Innovation Special Zone Project-Spark Project (Grant No.20-163-00-TS-009-006-01).

References

- [1] L. M. Curtis, A. Ostojic, D. J. Venzon et al., "A randomized phase 2 trial of pomalidomide in subjects failing prior therapy for chronic graft-versus-host disease," *Blood*, vol. 137, no. 7, pp. 896–907, 2021.
- [2] P. J. Martin, "How I treat steroid-refractory acute graft-versus-host disease," *Blood*, vol. 135, no. 19, pp. 1630–1638, 2020.
- [3] S. J. Lee, G. Vogelsang, and M. E. Flowers, "Chronic graft-versus-host disease," *Biology of Blood and Marrow Transplantation*, vol. 9, no. 4, pp. 215–233, 2003.
- [4] C. Anasetti, B. R. Logan, S. J. Lee et al., "Peripheral-blood stem cells versus bone marrow from unrelated donors," *The New England Journal of Medicine*, vol. 367, no. 16, pp. 1487–1496, 2012.
- [5] S. Sarantopoulos, A. R. Cardones, and K. M. Sullivan, "How I treat refractory chronic graft-versus-host disease," *Blood*, vol. 133, no. 11, pp. 1191–1200, 2019.
- [6] Y. Inamoto, M. E. Flowers, B. M. Sandmaier et al., "Failure-free survival after initial systemic treatment of chronic graft-versus-host disease," *Blood*, vol. 124, no. 8, pp. 1363–1371, 2014.
- [7] L. Qian, M. Liu, J. Shen, J. Cen, and D. Zhao, "Hydrogen in patients with corticosteroid-refractory/dependent chronic graft-versus-host-disease: a single-arm, multicenter, open-label, phase 2 trial," *Frontiers in Immunology*, vol. 11, article 598359, 2020.
- [8] G. Socie and J. Ritz, "Current issues in chronic graft-versus-host disease," *Blood*, vol. 124, no. 3, pp. 374–384, 2014.
- [9] S. Ghobrial, C. Gonzalez, N. Yazigi et al., "Efficacy and feasibility of ruxolitinib in chronic steroid-refractory GVHD in a pediatric intestine transplant," *Pediatric Transplantation*, vol. 25, no. 3, article e13836, 2021.
- [10] M. Schoettler, C. Duncan, L. Lehmann, E. Furutani, M. Subramaniam, and S. Margossian, "Ruxolitinib is an effective steroid sparing agent in children with steroid refractory/dependent bronchiolitis obliterans syndrome after allogeneic hematopoietic cell transplantation," *Bone Marrow Transplantation*, vol. 54, no. 7, pp. 1158–1160, 2019.
- [11] R. Zeiser, N. Polverelli, R. Ram et al., "Ruxolitinib for glucocorticoid-refractory chronic graft-versus-host disease," *The New England Journal of Medicine*, vol. 385, no. 3, pp. 228–238, 2021.
- [12] M. E. Flowers and P. J. Martin, "How we treat chronic graft-versus-host disease," *Blood*, vol. 125, no. 4, pp. 606–615, 2015.
- [13] I. Ohsawa, M. Ishikawa, K. Takahashi et al., "Hydrogen acts as a therapeutic antioxidant by selectively reducing cytotoxic oxygen radicals," *Nature Medicine*, vol. 13, no. 6, pp. 688–694, 2007.
- [14] M. Kajiya, K. Sato, M. J. Silva et al., "Hydrogen from intestinal bacteria is protective for Concanavalin A-induced hepatitis," *Biochemical and Biophysical Research Communications*, vol. 386, no. 2, pp. 316–321, 2009.
- [15] K. Xie, Y. Yu, Z. Zhang et al., "Hydrogen gas improves survival rate and organ damage in zymosan-induced generalized inflammation model," *Shock*, vol. 34, no. 5, pp. 495–501, 2010.
- [16] M. Kajiya, M. J. Silva, K. Sato, K. Ouhara, and T. Kawai, "Hydrogen mediates suppression of colon inflammation induced by dextran sodium sulfate," *Biochemical and Biophysical Research Communications*, vol. 386, no. 1, pp. 11–15, 2009.
- [17] Y. S. Yoon, M. E. Sajo, R. M. Ignacio, S. K. Kim, C. S. Kim, and K. J. Lee, "Positive effects of hydrogen water on 2, 4-dinitrochlorobenzene-induced atopic dermatitis in NC/Nga mice," *Biological & Pharmaceutical Bulletin*, vol. 37, no. 9, pp. 1480–1485, 2014.
- [18] Z. Xu, J. Zhou, J. Cai, Z. Zhu, X. Sun, and C. Jiang, "Anti-inflammation effects of hydrogen saline in LPS activated macrophages and carrageenan induced paw oedema," *Journal of Inflammation*, vol. 9, no. 1, p. 2, 2012.

- [19] Y. Terasaki, I. Ohsawa, M. Terasaki et al., "Hydrogen therapy attenuates irradiation-induced lung damage by reducing oxidative stress," *American Journal of Physiology-Lung Cellular and Molecular Physiology*, vol. 301, no. 4, pp. L415–L426, 2011.
- [20] C. K. Min, "The pathophysiology of chronic graft-versus-host disease: the unveiling of an enigma," *The Korean Journal of Hematology*, vol. 46, no. 2, pp. 80–87, 2011.
- [21] R. Zeiser and B. R. Blazar, "Pathophysiology of chronic graft-versus-host disease and therapeutic targets," *The New England Journal of Medicine*, vol. 377, no. 26, pp. 2565–2579, 2017.
- [22] L. Qian, F. Cao, J. Cui et al., "Radioprotective effect of hydrogen in cultured cells and mice," *Free Radical Research*, vol. 44, no. 3, pp. 275–282, 2010.
- [23] L. Qian, F. Cao, J. Cui et al., "The potential cardioprotective effects of hydrogen in irradiated mice," *Journal of Radiation Research*, vol. 51, no. 6, pp. 741–747, 2010.
- [24] Y. Chuai, J. Shen, L. Qian et al., "Hydrogen-rich saline protects spermatogenesis and hematopoiesis in irradiated BALB/c mice," *Medical Science Monitor*, vol. 18, no. 3, pp. BR89–BR94, 2012.
- [25] J. du, K. Paz, R. Flynn et al., "Pirfenidone ameliorates murine chronic GVHD through inhibition of macrophage infiltration and TGF- β production," *Blood*, vol. 129, no. 18, pp. 2570–2580, 2017.
- [26] K. R. Cooke, L. Kobzik, T. R. Martin et al., "An experimental model of idiopathic pneumonia syndrome after bone marrow transplantation: I. the roles of minor H antigens and endotoxin," *Blood*, vol. 88, no. 8, pp. 3230–3239, 1996.
- [27] L. Qian, X. Liu, J. Shen, D. Zhao, and W. Yin, "Therapeutic effects of hydrogen on chronic graft-versus-host disease," *Journal of Cellular and Molecular Medicine*, vol. 21, no. 10, pp. 2627–2630, 2017.
- [28] B. E. Anderson, J. M. McNiff, C. Matte, I. Athanasiadis, W. D. Shlomchik, and M. J. Shlomchik, "Recipient CD4+ T cells that survive irradiation regulate chronic graft-versus-host disease," *Blood*, vol. 104, no. 5, pp. 1565–1573, 2004.
- [29] A. Yamamoto, E. Ashihara, Y. Nakagawa et al., "Allograft inflammatory factor-1 is overexpressed and induces fibroblast chemotaxis in the skin of sclerodermatous GVHD in a murine model," *Immunology Letters*, vol. 135, no. 1–2, pp. 144–150, 2011.
- [30] C. J. Alves, L. P. de Santana, A. J. dos Santos et al., "Early motor and electrophysiological changes in transgenic mouse model of amyotrophic lateral sclerosis and gender differences on clinical outcome," *Brain Research*, vol. 1394, pp. 90–104, 2011.
- [31] P. Desjardins, J. B. Hansen, and M. Allen, "Microvolume spectrophotometric and fluorometric determination of protein concentration," *Current Protocols in Protein Science*, vol. 55, no. 1, pp. 3–10, 2009.
- [32] T. Kawamura, C. S. Huang, X. Peng et al., "The effect of donor treatment with hydrogen on lung allograft function in rats," *Surgery*, vol. 150, no. 2, pp. 240–249, 2011.
- [33] R. Tenhunen, H. S. Marver, and R. Schmid, "The enzymatic conversion of heme to bilirubin by microsomal heme oxygenase," *Proceedings of the National Academy of Sciences of the United States of America*, vol. 61, no. 2, pp. 748–755, 1968.
- [34] R. Gozzelino, V. Jeney, and M. P. Soares, "Mechanisms of cell protection by heme oxygenase-1," *Annual Review of Pharmacology and Toxicology*, vol. 50, no. 1, pp. 323–354, 2010.
- [35] E. Seixas, R. Gozzelino, A. Chora et al., "Heme oxygenase-1 affords protection against noncerebral forms of severe malaria," *Proceedings of the National Academy of Sciences of the United States of America*, vol. 106, no. 37, pp. 15837–15842, 2009.
- [36] A. T. Dinkova-Kostova and P. Talalay, "NAD(P)H:quinone acceptor oxidoreductase 1 (NQO1), a multifunctional antioxidant enzyme and exceptionally versatile cytoprotector," *Archives of Biochemistry and Biophysics*, vol. 501, no. 1, pp. 116–123, 2010.
- [37] H. Wefers, T. Komai, P. Talalay, and H. Sies, "Protection against reactive oxygen species by NAD (P)H: quinone reductase induced by the dietary antioxidant butylated hydroxyanisole (BHA). Decreased hepatic low-level chemiluminescence during quinone redox cycling," *FEBS Letters*, vol. 169, no. 1, pp. 63–66, 1984.
- [38] S. J. Martin and D. R. Green, "Protease activation during apoptosis: death by a thousand cuts?," *Cell*, vol. 82, no. 3, pp. 349–352, 1995.
- [39] J. H. Abraini, M. C. Gardette-Chauffour, E. Martinez, J. C. Rostain, and C. Lemaire, "Psychophysiological reactions in humans during an open sea dive to 500 m with a hydrogen-helium-oxygen mixture," *Journal of Applied Physiology*, vol. 76, no. 3, pp. 1113–1118, 1994.

Research Article

The Efficacy of Antioxidative Stress Therapy on Oxidative Stress Levels in Rheumatoid Arthritis: A Systematic Review and Meta-analysis of Randomized Controlled Trials

Liuting Zeng ¹, Ganpeng Yu ², Kailin Yang ³, Jun Li,² Wensa Hao,⁴ and Hua Chen ¹

¹Department of Rheumatology and Clinical Immunology, Peking Union Medical College Hospital, Chinese Academy of Medical Sciences & Peking Union Medical College, Beijing, China

²People's Hospital of Ningxiang City, Ningxiang City, Hunan Province, China

³Beijing Anzhen Hospital, Capital Medical University, Beijing, China

⁴Institute of Materia Medica, Chinese Academy of Medical Sciences and Peking Union Medical College, Beijing, China

Correspondence should be addressed to Liuting Zeng; 2057188405@qq.com, Ganpeng Yu; yuganpeng.guke@hotmail.com, Kailin Yang; yang.cardiology@ccmu.edu.cn, and Hua Chen; chhuaa332211@163.com

Received 19 July 2021; Accepted 4 September 2021; Published 7 October 2021

Academic Editor: Ivan Srejevic

Copyright © 2021 Liuting Zeng et al. This is an open access article distributed under the Creative Commons Attribution License, which permits unrestricted use, distribution, and reproduction in any medium, provided the original work is properly cited.

Objective. To explore the efficacy of antioxidative stress therapy on oxidative stress levels in rheumatoid arthritis (RA) by a systematic review and meta-analysis of randomized controlled trials. **Methods.** Chinese and English databases such as PubMed, Embase, China National Knowledge Infrastructure (CNKI), and China Biomedical Literature were searched, mainly searching for clinical randomized controlled trials of antioxidant therapy for rheumatoid arthritis. The search time is from the establishment of the database to July 2021. Two researchers independently carried out literature search, screening, and data extraction. The bias risk tool provided by the Cochrane Collaboration was used to evaluate the bias risk of all the included literature, and the RevMan 5.3 software was used for meta-analysis. **Results.** A total of 24 RCTs (28 records) and 1277 participants were included. The time span of randomized controlled trials (RCTs) is from 1986 to 2020. These RCTs involve 14 types of antioxidants or antioxidant therapies, and these therapies have varying degrees of improvement on oxidative stress in RA patients. The summary results showed that the MDA in the experiment group is lower (SMD -0.82, 95% CI -1.35 to -0.28, $P = 0.003$). The difference of TAC, SOD, NO, GPx, CAT, and GSH between two groups was of no statistical significance (TAC (SMD 0.27, 95% CI -0.21 to 0.75, $P = 0.27$), SOD (SMD 0.12, 95% CI -0.16 to 0.40, $P = 0.41$), NO (SMD -2.03, 95% CI -4.22 to 0.16, $P = 0.07$), GPx (SMD 0.24, 95% CI -0.07 to 0.54, $P = 0.13$), CAT (SMD 2.95, 95% CI -2.6 to 8.51, $P = 0.30$), and GSH (SMD 2.46, 95% CI -0.06 to 4.98, $P = 0.06$)). For adverse events, the summary results showed that the difference was of no statistical significance (RR 1.16, 95% CI 0.79 to 1.71, $P = 0.45$). In addition, antioxidant therapy has also shown improvement in clinical efficacy indexes (number of tender joints, number of swollen joints, DAS28, VAS, and HAQ) and inflammation indexes (ESR, CRP, TNF- α , and IL6) for RA patients. **Conclusion.** The existing evidence shows potential benefits, mainly in reducing MDA and increasing TAC and GSH in some subgroups. However, more large samples and higher quality RCTs are needed to provide high-quality evidence, so as to provide more clinical reference information for the antioxidant treatment of RA.

1. Introduction

Rheumatoid arthritis (RA) is a chronic systemic autoimmune disease of unknown etiology [1]. In the United States, RA affects more than 1.3 million adults, accounting for 0.6%–1% of the population [1, 2]. Epidemiological research shows

that the prevalence of rheumatoid arthritis in China is 0.2%~0.36%, which has increased from 5.8 million cases in 2015 to 5.9 million cases in 2019, and the 3-year disability rate has reached 70%; it has become a serious public health problem [3, 4]. The clinical manifestation of RA is mainly a chronic inflammatory (nonsuppurative inflammation)

disease of peripheral multiple joints. It may be accompanied by extra-articular systemic damage (causing subcutaneous nodules, pericarditis, myocarditis, pulmonary fibrosis, pleurisy, splenomegaly, renal amyloidosis, peripheral neuritis, arteritis, etc.) [5]. The pathological features of RA are mainly manifested as synovitis of the joints (which can later spread to articular cartilage, bone tissue, joint ligaments, and tendons), followed by extensive inflammation of connective tissues such as serosa, heart, lung, and eyes [5, 6]. When the disease involves cartilage and bone, joint deformities may occur, that is, synovial inflammation, exudation, cell proliferation, granuloma formation, cartilage and bone tissue destruction, and finally joint stiffness and dysfunction [6]. The cartilage destruction of joints is related to the abnormal expression of cytokines, and the imbalance between protective cytokines and destructive cytokines is the basis of RA pathology [7]. In addition, inflammatory chemokines and immune-inflammatory cells jointly promote the exacerbation of the pathological process of RA [8].

Current research shows that in addition to inflammation [9], oxidative stress products also play an important role in the pathogenesis and pathological progress of RA [10]. Oxidative stress can produce too many free radicals, which will cause the oxidation of many molecules in the body. Excessive free radicals in the body of RA patients increase the level of the oxidation marker malondialdehyde (MDA), and the antioxidant enzyme superoxide dismutase (SOD) system is disturbed, which leads to the weakening of the body's antioxidant capacity and aggravating bone destruction [11–14]. In addition, oxidative stress is closely related to the energy metabolism of synovial tissue in RA patients [15]. Therefore, research on oxidative stress, SOD antioxidation, and regulation relationship in patients with RA can reveal the pathological mechanism of RA and find new anti-RA drugs. At present, many randomized controlled trials (RCTs) of antioxidants [16–20] in the treatment of RA patients have been published. However, the results and interventions of these RCTs are diverse, and the quality of the evidence provided varies, which cannot provide clinical doctors with evidence to formulate treatment measures against oxidative stress. Therefore, it is urgent to conduct a comprehensive and in-depth systematic review and meta-analysis of these RCTs for the treatment of RA against oxidative stress. Therefore, this study will conduct a comprehensive systematic review and meta-analysis of RCTs for the treatment of RA against oxidative stress for the first time, in order to provide clinicians with high-quality evidence and promote the clinical practice of antioxidant treatment of RA in the future and to further improve the adjuvant therapy for RA patients.

2. Why Is This Systematic Review Important?

Oxidative stress plays a central role in the pathogenesis of RA. At present, evidence of clinical randomized controlled trials surrounding oxidative stress interventions has been reported one after another. However, the results and interventions of these RCTs are diverse, and the quality of the evidence provided is not uniform, and the levels are not uniform, which cannot provide clinical doctors and patients

with evidence and treatment measures for the pathological mechanism of oxidative stress. Therefore, it is urgent to conduct a comprehensive and in-depth systematic review and meta-analysis of these RCTs for antioxidative stress treatment, in order to provide clinicians with high-quality evidence in the future, promote the clinical practice of RA treatment, and further improve the adjuvant treatment measures of RA.

3. Materials and Methods

3.1. Protocol. This systematic review and meta-analysis was conducted strictly in accordance with the protocol registered in PROSPERO (CRD42021256587) and PRISMA guidelines (see Supplementary Materials (available here)) [21].

3.2. Literature Search Strategy. English databases and Chinese databases were searched with the retrieval time up to July 2021. English databases include PubMed, Embase, MEDLINE Complete, Web of Science, and Cochrane Library. Chinese databases include Wanfang Database on Academic Institutions in China, China National Knowledge Infrastructure (CNKI), VIP Database for Chinese Technical Periodicals, and China Biology Medicine (CBM). This study also searched the Cochrane Library and ClinicalTrials.gov. The search strategy of PubMed and Embase is shown in Table S1 as an example.

3.3. Inclusion and Exclusion Criteria

3.3.1. Participants. Participants are RA patients. The diagnosis of RA conforms to the RA diagnostic criteria in the 2010 Rheumatoid Arthritis Diagnostic and Treatment Guidelines of the Chinese Medical Association Rheumatology Branch or the standard RA diagnostic criteria proposed by the American Academy of Rheumatology in 1987/European Rheumatism League in 2017 or other recognized diagnostic criteria for RA.

3.3.2. Intervention. The treatment of the experimental group is antioxidative stress therapy with no limitations to forms, preparations, and so on; the therapy could be combined with conventional therapy or the therapy in the control group. The treatment of the control group was conventional therapy or placebo or other nonantioxidative stress therapies.

3.3.3. Outcomes. The outcomes were clinical efficacy indexes, inflammation indexes, adverse events, and oxidative stress-related indicators. Clinical efficacy indexes include the number of tender joints, number of swollen joints, 28-joint disease activity score (DAS28), Health Assessment Questionnaire (HAQ), and Visual Analog Scale (VAS); inflammation indexes include erythrocyte sedimentation rate (ESR), C-reactive protein (CRP), tumor necrosis factor-(TNF-) α , and Interleukin-(IL-) 6; oxidative stress-related indicators include malondialdehyde (MDA), glutathione (GSH), Catalase (CAT), glutathione peroxidase (GPx), nitric oxide (NO), superoxide dismutase (SOD), and total antioxidant capacity (TAC).

3.3.4. Study Design. The study design includes randomized controlled trials (RCTs), with no limitations to publication time, language, quality, and publication status.

3.3.5. Exclusion Criteria. Exclusion criteria include non-RCT, review, cohort study, and patients with other rheumatism (such as systemic lupus erythematosus and Sjogren's syndrome).

3.4. Literature Screening and Risk of Bias Assessment. The two researchers jointly formulate a literature search strategy, independently collect literature, read literature titles and abstracts, and conduct preliminary screening. Then, the two researchers read the full text of the selected literature and finally determined the literature that met the inclusion criteria. The Cochrane Risk Bias Assessment Form is used to systematically evaluate the quality of the included literature. If opinions are inconsistent, they are resolved through discussion. The content of the risk assessment of bias includes [22] (1) random allocation method, (2) allocation plan hiding, (3) blind method, (4) completeness of result data, (5) selective reporting of research results, and (6) other sources of bias.

3.5. Data Extraction. The two researchers independently extracted data from the included literature, filled in the data extraction form, and cross-checked. The extracted content includes general information of the literature (such as author, sample size, patient's age, intervention time, and frequency) and related efficacy evaluation indicators [23].

3.6. Statistical Analysis. The Review Manager 5.3 software was used for statistical analysis. Subgroup analysis was carried out according to the intervention measures of RCTs. A heterogeneity test was performed on the included literature. If $I^2 > 50\%$ and $P < 0.1$, it is considered that there is a large heterogeneity, and the source of the heterogeneity is analyzed. If $I^2 < 50\%$ and $P > 0.1$, the heterogeneity is considered low (i.e., RCTs are homogeneous). The random effect model was used for analysis. For continuous variables, if the indicator units or measurement methods were different, or the value differs by more than 10 times, standardized mean difference (SMD) and 95% confidence interval (CI) would be used as the effect size indicator; for indicators with the same unit, weighted mean difference (WMD) and 95% confidence interval (CI) were used as the effect size indicator. For dichotomous variables, the risk ratio (RR) and 95% CI were used as the effect size indicator [23]. The publication bias was detected by STATA 15 with the Egger method (continuous variable) for outcomes with more than 5 RCTs. $P > 0.1$ is considered to have no publication bias.

4. Results

4.1. Results of the Search. The total records identified through database searching and other sources were 1984. According to the search strategy, a total of 29 articles were obtained through preliminary search. By eliminating duplicate documents and carefully reading the title and abstract, a total of 1955 articles were excluded. After carefully reading

the full text and comparing the selection criteria, 28 records were screened out and finally included (Figure 1).

4.2. Description of Included Trials. Among the 28 records, 2 records [19, 20] belong to Abdollahzad et al. 2015, 2 records [24, 25] belong to Javadi et al. 2017 [24, 25], 2 records [26, 27] belong to Moosavian et al. 2020, and 2 records [28, 29] belong to Mirtaheri et al. 2015; therefore, a total of 24 RCTs and 1277 participants (most of them are female) were included. The time span of RCTs is from 1986 to 2020. Among those RCTs, 3 RCTs utilized N-acetylcysteine [16–18]; 2 RCTs utilized CoQ10 [19, 20, 30, 31]; 2 RCTs utilized probiotic [31, 32]; Ghavipour et al. 2016 utilized pomegranate extract [33]; 2 RCTs utilized quercetin [24, 25, 34]; Khojah et al. 2018 utilized resveratrol [35]; Moosavian et al. 2020 utilized garlic tablets [26, 27]; Aryaeian et al. 2009 [36] utilized conjugated linoleic acids, conjugated linoleic acids plus vitamin E, and vitamin E; 3 RCTs utilized vitamin E [36–38]; 4 RCTs utilized selenium [39–42]; Karagülle et al. 2017 utilized spa therapy [43]; Jaswal et al. 2003 utilized vitamins A, E, and C combination [44]; León Fernández et al. 2016 utilized ozone [45]; Ishibashi et al. 2014 utilized H₂-saline [46]; and 2 RCTs utilized alpha-lipoic acid [28, 29, 34]. Among those RCTs, 7 RCTs were registered clinical trials. Two RCTs were from Belgium; 2 RCTs were from China; 2 RCTs were from Germany; 8 RCTs were from Iran; Bae et al. 2009 was from Korea; Khojah et al. 2018 was from Egypt; Edmonds et al. 1997 was from the UK; Tarp et al. 1986 was from Denmark; Karagülle et al. 2017 was from Turkey; Jaswal et al. 2003 was from India; León Fernández et al. 2016 was from Cuba; and Ishibashi et al. 2014 was from Japan. Bae et al. 2009 [34] contains two intervention methods, so they were divided into Bae et al. 2009a and Bae et al. 2009b. Aryaeian et al. 2009 [36] has 3 intervention methods, so they were divided into Aryaeian et al. 2009a, Aryaeian et al. 2009b, and Aryaeian et al. 2009c. The details of study characteristics are presented in Table 1.

4.3. Risk of Bias Assessment. The RCTs were assessed by “risk of bias” assessment tools. The summary and graph of risk of bias are shown in Figures 2 and 3.

4.3.1. Random Sequence Generation and Allocation Concealment. Thirteen (13) RCTs describe random sequence generation methods [16, 17, 19, 20, 24–33, 36, 43, 45] and were rated as low risk of bias. The other RCTs do not describe random sequence generation methods and were rated as unclear risk of bias. Fourteen RCTs [18–20, 34–42, 44–46] did not describe allocation concealment methods and were assessed as unclear risk of bias.

4.3.2. Blinding, Incomplete Outcome Data, and Selective Reporting. Only 6 RCTs [16, 17, 26, 27, 31–33] describe the implementation process of the blind method and were rated as low risk of bias. Four RCTs [18, 24, 25, 44, 46] did not describe the implementation process of blinding, and the indicators of this study are biochemical indicators (such as MDA); they are assessed as low risk of bias. Twelve (12) RCTs [20, 28, 29, 34, 36–43, 45] claimed to use blinding but did not describe the implementation process of blinding

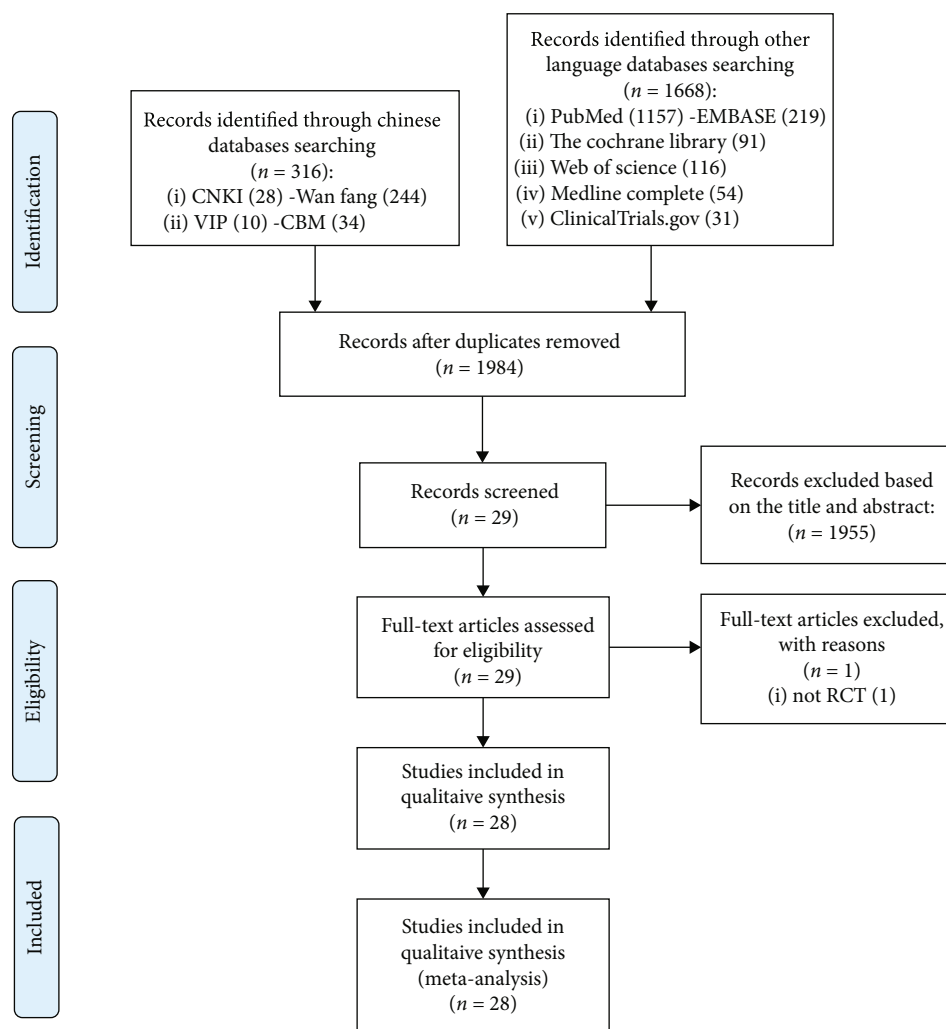


FIGURE 1: Flow diagram.

and included subjective indicators (such as DAS28 and VAS), so they were assessed as unclear risk of bias. Two RCTs [30, 35] did not utilize blinding, and the indicators of this study are subjective indicators (such as VAS and DAS28); they are assessed as high risk of bias. Six RCTs [16, 17, 28, 29, 31, 33, 34] have missing data, and the number of missing is unbalanced, but no appropriate statistical treatment method is specified, and the risk of bias is estimated to be unclear.

4.4. Other Potential Bias. Other sources of bias were not observed in 24 RCTs; therefore, the risks of other bias of the RCTs were low.

4.5. Outcomes

- (1) **Oxidative Stress Index and Adverse Events.** A total of 11 RCTs reported MDA; the summary results showed that the MDA in the experiment group is lower (SMD -0.82, 95% CI -1.35 to -0.27, $P = 0.003$; random effect model) (Figure 4). Eight RCTs reported TAC; the summary results showed that

the difference was of no statistical significance (SMD 0.27, 95% CI -0.21 to 0.75, $P = 0.27$; random effect model) (Figure 5). Four RCTs reported SOD; the summary results showed that the difference was of no statistical significance (SMD 0.12, 95% CI -0.16 to 0.40, $P = 0.41$; random effect model) (Figure 6). Three RCTs reported NO; the summary results showed that the difference was of no statistical significance (SMD -2.03, 95% CI -4.22 to 0.16, $P = 0.07$; random effect model) (Figure 7). Three RCTs reported GPx; the summary results showed that the difference was of no statistical significance (SMD 0.24, 95% CI -0.07 to 0.54, $P = 0.13$; random effect model) (Figure 8). Two RCTs reported CAT; the summary results showed that the difference was of no statistical significance (SMD 2.95, 95% CI -2.6 to 8.51, $P = 0.30$; random effect model) (Figure 9). Three RCTs reported GSH; the summary results showed that the difference was of no statistical significance (SMD 2.46, 95% CI -0.06 to 4.98, $P = 0.06$; random effect model) (Figure 10). Five RCTs reported adverse events; Abdollahzad et al. 2015

TABLE 1: The characteristics of the included studies.

Subgroup	Study	Trial registration number	Country	Sample size (female/male)		Intervention	Control group	Relevant outcomes	Mean age (years)		Disease duration (years)		Baseline CRP (mg/L)		Baseline ESR (mm/h)		Baseline DAS28		Duration
				Trial group	Control group				Trial group	Control group	Trial group	Control group	Trial group	Control group	Trial group	Control group	Trial group	Control group	
N-acetylcysteine	Husami et al. 2019 [16]	IRCT20190722965N2	Iran	23 (20/3)	19 (19/0)	N-acetylcysteine 600 mg Bid-conventional treatment (mainly methotrexate, sulfasalazine, hydroxychloroquine, prednisolone, calcium D, folic acid, nonsteroidal anti-inflammatory drugs)	Placebo-conventional treatment (mainly methotrexate, sulfasalazine, hydroxychloroquine, prednisolone, calcium D, folic acid, nonsteroidal anti-inflammatory drugs)	CRP, ESR, TNF- α , IL6, MDA, TAC, NO	53.91 \pm 13.90	50.68 \pm 11.15	10.52 \pm 7.19	10.05 \pm 7.56	8.57 \pm 0.99	7.89 \pm 1.11	26.91 \pm 4.29	26.26 \pm 6.77	—	—	12 weeks
N-acetylcysteine	Babaei et al. 2018 [17]	Cannot be found	Iran	27 (22/5)	24 (23/1)	N-acetylcysteine 600 mg Bid-conventional treatment (mainly methotrexate, sulfasalazine, hydroxychloroquine, calcium D, folic acid)	Placebo-conventional treatment (mainly methotrexate, sulfasalazine, hydroxychloroquine, calcium D, folic acid)	DAS28, ESR, number of tender joints, number of swollen joints, HAQ, VAS, adverse events	53.2 \pm 12.5	31.6 \pm 11.3	10 \pm 7.0	9.8 \pm 8.2	31.4 \pm 19.6	29.2 \pm 19.3	—	—	5.1 \pm 1.2	5.3 \pm 1.1	12 weeks
COQ10	Yin et al. 2017 [18]	—	China	48 (42/6)	—	N-acetylcysteine 600 mg-conventional treatment (mainly sulfasalazine, methotrexate)	Conventional treatment (mainly sulfasalazine, methotrexate)	None	36-75	—	—	—	—	—	—	—	—	—	12 weeks
COQ10	Abdolkhazad et al. 2015 [19, 20]	IRCT20131004105N1.6	Iran	21 (19/2)	22 (20/2)	CoQ10 100 mg-conventional treatment (mainly methotrexate, sulfasalazine, hydroxychloroquine, prednisolone)	Placebo (wheat starch)-conventional treatment (mainly methotrexate, sulfasalazine, hydroxychloroquine, prednisolone)	DAS28, number of tender joints, number of swollen joints, TNF- α , IL6, VAS, ESR, MDA, TAC, adverse events	48.77 \pm 11.58	50.41 \pm 11.28	6.91 \pm 5.87	6.94 \pm 6.50	—	—	39.64 \pm 25.53	40.27 \pm 25.75	5.01 \pm 1.21	4.88 \pm 0.96	8 weeks
Probiotic	Zhu et al. 2020 [30]	—	China	45 (35/10)	45 (37/8)	CoQ10 10 mg TID-conventional treatment (mainly methotrexate, low-dose prednisone)	Placebo (wheat starch)-conventional treatment (mainly methotrexate, low-dose prednisone)	CRP, ESR, TNF- α , IL6, MDA, TAC	48.15 \pm 11.68	47.36 \pm 12.11	5.2 (1.9, 8.6)*	5.1 (2.2, 8.1)*	56.15 \pm 20.13	57.42 \pm 18.46	4.221 \pm 16.11	41.26 \pm 15.26	—	—	12 weeks
Probiotic	Vagher-Mehrabany et al. 2016 [31]	IRCT201207024105N1.0	Iran	22 (22/0)	24 (24/0)	Probiotic (Lactobacillus casei 01)-conventional treatment (mainly methotrexate, hydroxychloroquine, prednisolone)	Placebo-conventional treatment (mainly methotrexate, hydroxychloroquine, prednisolone)	MDA, SOD, GfX, CAT, TAC	41.14 \pm 12.65	41.29 \pm 9.77	4.75 (3.0, 9.0)*	5.25 (3.75, 10.0)*	—	—	—	—	—	—	8 weeks
Pomegranate extract	Zamani et al. 2017 [32]	IRCT20161165023N94	Iran	27 (22/5)	27 (24/3)	Synbiotic capsule (Lactobacillus acidophilus, Lactobacillus casei, and Bifidobacterium bifidum (2 \times 10 ⁸ colony-forming units/g each)+400 mg inulin)	Placebo (starch only)	CRP, DAS28, VAS, NO, TAC, GSH, MDA	49.3 \pm 11.0	49.5 \pm 12.9	7.7 \pm 6.1	7.5 \pm 6.4	6.03 \pm 4.84*	5.64 \pm 5.14*	—	—	4.2 \pm 0.7	3.5 \pm 0.8	8 weeks
Pomegranate extract	Ghasipour et al. 2017 [33]	IRCT201202183236N2	Iran	30 (20/10)	30 (20/10)	Pomegranate extract (contained 40% ellagic acid) with no changes to current medication (mainly methotrexate, hydroxychloroquine, sulfasalazine, and prednisolone)	Placebo with no changes to current medication (mainly methotrexate, hydroxychloroquine, sulfasalazine, and prednisolone)	DAS28, HAQ, ESR, CRP, number of tender joints, number of swollen joints, MDA, GfX	48.4 \pm 11.4	49.1 \pm 12.2	10.9 \pm 5.8	12.3 \pm 5.8	29.0 \pm 15.6	30.6 \pm 19.6	8.0 \pm 4.2	6.6 \pm 4.5	4.9 \pm 0.8	4.7 \pm 1.1	8 weeks
Quercetin	Javadi et al. 2017 [24, 25]	IRCT13807252594N2	Iran	20 (20/0)	20 (20/0)	Quercetin 500 mg-conventional treatment (mainly methotrexate, hydroxychloroquine, sulfasalazine, cyclosporine, prednisolone, NSAIDs)	Placebo-conventional treatment (mainly methotrexate, hydroxychloroquine, sulfasalazine, cyclosporine, prednisolone, NSAIDs)	CRP, TNF- α , number of tender joints, number of swollen joints, VAS, MDA, TAC	46.55 \pm 9.94	48.00 \pm 6.39	5.17 \pm 3.83	4.87 \pm 3.03	2.89 \pm 2.95*	3.28 \pm 2.32*	19.00 \pm 8.62	21.10 \pm 12.38	3.22 \pm 0.93	3.13 \pm 1.1	8 weeks
Quercetin	Bae et al. 2009 [34]	—	Korea	20 (19/1)	—	Quercetin+vitamin C (166 mg 133 mg/capsule)-conventional treatment (mainly hydroxychloroquine, sulfasalazine, methotrexate with folic, lincillamine, NSAID, low-dose steroid)	Placebo-conventional treatment (mainly hydroxychloroquine, sulfasalazine, methotrexate with folic, lincillamine, NSAID, low-dose steroid)	CRP, TNF- α , IL6, 4.00*	52.1 \pm 10.3	10.2 \pm 5.9	Not known	0.85 (0.28, 4.00)*	1.05 (0.22, 6.44)*	—	—	—	—	—	4 weeks

TABLE 1: Continued.

Subgroup	Study	Trial registration number	Country	Sample size		Intervention	Control group	Relevant outcomes	Mean age (years)		Disease duration (years)		Disease severity		Baseline CRP (mg/L)		Baseline ESR (mm/h)		Baseline DAS28		Duration
				Trial group	Control group				Trial group	Control group	Trial group	Control group	Trial group	Control group	Trial group	Control group	Trial group	Control group	Trial group	Control group	
Resveratrol	Khojeh et al. 2018 [51]	—	Egypt	50 (36/14)	50 (32/18)	Resveratrol 1000 mg-conventional treatment	Placebo-conventional treatment	Number of tender joints, number of swollen joints, DAS28, CRP, ESR, TNF- α , IL6	46.53 \pm 12.3	44.2 \pm 16.4	9.4 \pm 5.8	9.8 \pm 5.5	Not known	2.7 \pm 0.7	2.9 \pm 0.8	39.44 \pm 11.5	43.8 \pm 14.8	4.62 \pm 0.99	4.91 \pm 0.92	12 weeks	
Garlic tablets	Mosavian et al. 2020 [26, 27]	IRCT200411080198586	Iran	31 (31/0)	31 (31/0)	Garlic tablets 500 mg (equivalent to 2500 mg of fresh garlic and containing 2.5 mg allicin) Bid with no changes to current medication (mainly prednisolone, methotrexate, sulfasalazine)	Placebo with no changes to current medication (mainly prednisolone, methotrexate, sulfasalazine)	number of tender joints, number of swollen joints, MDA, TAC	51.06 \pm 13.8	51.39 \pm 10.38	6.58 \pm 7.75	6.61 \pm 8.11	All patients are moderate and severe	15.44 \pm 13.76	13.57 \pm 14.04	23.63 \pm 13.82	20.10 \pm 11.71	4.61 \pm 0.92	4.52 \pm 0.78	8 weeks	
Conjugated linoleic acids	Arystein et al. 2009 [36]	—	Iran	22 (19/3)	22 (19/3)	Conjugated linoleic acid 2 g with no changes to current medication (mainly hydroxychloroquine, chloroquine and methotrexate, lower amounts of NSAIDs)	Conjugated linoleic acid 2 g with no changes to current medication (mainly hydroxychloroquine, chloroquine and methotrexate, lower amounts of NSAIDs)	VAS, ESR, CRP, DAS28, number of tender joints, number of swollen joints	46.23 \pm 13.07	47.95 \pm 11.14	9.59 \pm 8.41	8.88 \pm 8.65	Mile: 11; moderate: 13; severe: 3	7.19 \pm 10.13	6.44 \pm 7.90	26.81 \pm 15.50	28.36 \pm 21.55	4.63 \pm 1.26	4.35 \pm 0.95	12 weeks	
Conjugated linoleic acids + vitamin E	Arystein et al. 2009 [36]	—	Iran	22 (17/5)	22 (19/3)	Conjugated linoleic acids 2 g + vitamin E 400 mg with no changes to current medication (mainly hydroxychloroquine, chloroquine and methotrexate, lower amounts of NSAIDs)	Placebo with no changes to current medication (mainly hydroxychloroquine, chloroquine and methotrexate, lower amounts of NSAIDs)	VAS, ESR, CRP, DAS28, number of tender joints, number of swollen joints	43.77 \pm 12.75	47.95 \pm 11.14	7.04 \pm 6.19	8.88 \pm 8.65	Mile: 8; moderate: 10; severe: 4	5.24 \pm 6.44	6.44 \pm 7.90	28.65 \pm 17.26	28.36 \pm 21.55	4.59 \pm 1.11	4.35 \pm 0.95	12 weeks	
Vitamin E	Arystein et al. 2009 [36]	—	Iran	21 (17/4)	21 (17/4)	Vitamin E 400 mg with no changes to current medication (mainly hydroxychloroquine, chloroquine and methotrexate, lower amounts of NSAIDs)	Placebo with no changes to current medication (mainly hydroxychloroquine, chloroquine and methotrexate, lower amounts of NSAIDs)	VAS, ESR, CRP, DAS28, number of tender joints, number of swollen joints	49.33 \pm 11.89	47.95 \pm 11.14	7.24 \pm 5.82	8.88 \pm 8.65	Mile: 7; moderate: 12; severe: 2	9.06 \pm 14.33	6.44 \pm 7.90	40.43 \pm 26.22	28.36 \pm 21.55	4.52 \pm 1.08	4.35 \pm 0.95	12 weeks	
Vitamin E	Edmonds et al. 1997 [37]	—	The UK	20 (16/4)	20 (15/5)	Vitamin E 600 mg bid with no changes to current medication (mainly NSAID, methotrexate, Salazopyrin, azathioprine, D-penicillamine, Mycristin, sulfasalazine, corticosteroids)	Placebo with no changes to current medication (mainly NSAID, methotrexate, Salazopyrin, azathioprine, D-penicillamine, Mycristin, sulfasalazine, corticosteroids)	Adverse events	24.75	32.66	—	—	Not known	—	—	—	—	—	—	12 weeks	
Vitamin E	Wittenberg et al. 1998 [38]	—	Germany	42 (39/3)	43 (30/13)	Vitamin E 400 mg Tid with no changes to basic treatment and physical therapy; other NSAIDs are not allowed during treatment	Tid with no changes to basic treatment and physical therapy; other NSAIDs are not allowed during treatment	VAS, adverse events	61 \pm 9	58 \pm 9	10 \pm 9	11 \pm 11	Not known	—	—	—	—	—	—	3 weeks	
Selenium	Tarp et al. 1986 [39]	—	Denmark	20 (14/6)	20 (15/5)	Selenium 256 μ g with no changes to current medication (mainly gold, 2 D-penicillamine, antimalarials and NSAIDs)	Placebo with no changes to current medication (mainly gold, 2 D-penicillamine, antimalarials and NSAIDs)	Number of swollen joints, ESR	54.3 \pm 12.4	54.6 \pm 12.7	16.4 \pm 10.1	10.5 \pm 8.0	Not known	—	—	47 \pm 35	39 \pm 26	—	—	24 weeks	
Selenium	Perez et al. 1992 [40]	—	Belgium	8 (8/0)	7 (7/0)	Selenium 200 μ g	Placebo	VAS, ESR	61 \pm 11	—	—	—	Not known	—	—	23 \pm 15	30 \pm 17	—	—	24 weeks	
Selenium	Perez et al. 2001 [41]	—	Belgium	28 (21/7)	27 (20/7)	Selenium 200 μ g with stable dose of corticosteroids and of disease-modifying drugs (such as NSAIDs and low-dose glucocorticosteroids)	Placebo with stable dose of corticosteroids and of disease-modifying drugs (such as NSAIDs and low-dose glucocorticosteroids)	Number of swollen joints, CRP, ESR, VAS	61 \pm 13	60 \pm 13	—	—	All patients are moderate	28 \pm 17	28 \pm 17	34 \pm 16	29 \pm 12	—	—	12 weeks	
Selenium	Heintz et al. 1997 [42]	—	Germany	38 (37/1)	32 (30/2)	Selenium 200 μ g	Placebo with no changes to basic treatment and the corticosteroids were adjusted as needed	Number of tender joints, number of swollen joints, CRP	58.2 \pm 12.78	57.2 \pm 13.27	12.69 \pm 8.3	12.03 \pm 7.8	Not known	23.4 \pm 18	17.1 \pm 28	—	—	—	—	12 weeks	
Selenium	Karagöle et al. 2017 [43]	—	Turkey	15 (13/2)	22 (22/0)	Selenium 200 μ g	Standard drug treatment (mainly methotrexate, hydroxychloroquine, leflunomide or sulfasalazine, glucocorticoids and NSAIDs)	VAS, HAQ, DAS28, MDA, number of tender joints, number of swollen joints, SOD, adverse events	53.3 \pm 11.1	52.3 \pm 12.3	12.3 \pm 12.9	13.4 \pm 12.0	Not known	—	—	38.5 \pm 18.0	38.5 \pm 18.0	6.5 \pm 0.9	5.9 \pm 1.6	12 weeks	

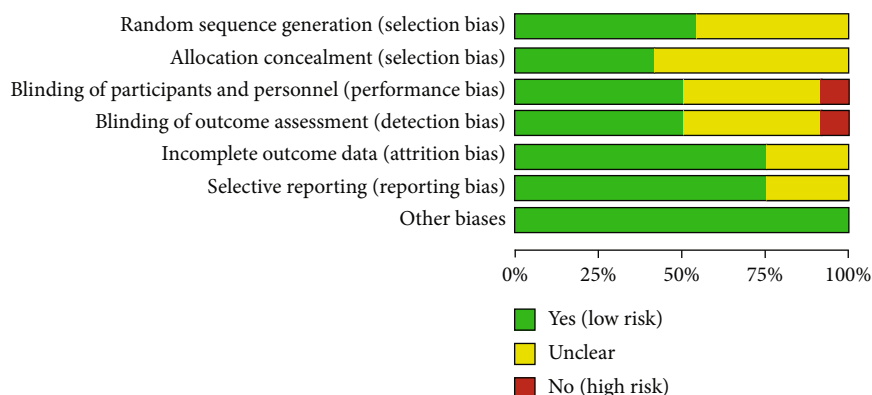


FIGURE 2: Risk of bias graph.

showed that no obvious adverse events were seen in the two groups. The summary results showed that the difference was of no statistical significance (RR 1.16, 95% CI 0.79 to 1.71, $P = 0.45$; random effect model).

- (2) *Clinical Efficacy Indexes*. Nine RCTs reported the number of swollen joints; the summary results showed that the number of swollen joints in the experiment group is lower (WMD -1.15, 95% CI -1.82 to -0.47, $P = 0.0008$; random effect model) (Figure 12). Seven RCTs reported the number of tender joints; the summary results showed that the number of tender joints in the experiments group is lower (WMD -2.50, 95% CI -3.12 to -1.89, $P < 0.00001$; random effect model) (Figure 13). Eleven RCTs reported the DAS28; the summary results showed that the DAS28 in the experiment group is lower (WMD -1.02, 95% CI -1.37 to -0.68, $P < 0.00001$; random effect model) (Figure 14). Nine RCTs reported the VAS; the summary results showed that the VAS in the experiment group is lower (SMD -0.66, 95% CI -1.02 to -0.31, $P = 0.0003$; random effect model) (Figure 15). Nine RCTs reported the HAQ; the summary results showed that the HAQ in the experiment group is lower (SMD -0.74, 95% CI -0.97 to -0.50, $P < 0.00001$; random effect model) (Figure 16).
- (3) *Inflammation Indexes*. Thirteen RCTs reported the ESR; the summary results showed that the ESR in the experiment group is lower (WMD -7.89, 95% CI -12.21 to -3.58, $P = 0.0003$; random effect model) (Figure 17). Eleven RCTs reported the CRP; the summary results showed that the CRP in the experiments group is lower (WMD -1.06, 95% CI -1.83 to -0.29, $P = 0.007$; random effect model) (Figure 18). Six RCTs reported the TNF- α ; the summary results showed that the TNF- α in the experiment group is lower (SMD -0.49, 95% CI -0.89 to -0.09, $P = 0.02$; random effect model) (Figure 19). Four RCTs reported IL6; the summary results showed that the difference was of no statistical significance (SMD -0.32, 95% CI -1.28 to 0.63, $P = 0.51$; random effect model) (Figure 20).

4.5.1. *N-acetylcysteine*. Three RCTs utilized to N-acetylcysteine treat RA. Hashemi et al. 2019 assessed the CRP, ESR, TNF- α , IL6, MDA, TAC, and NO. Batooei et al. 2018 assessed the DAS28, ESR, number of tender joints, number of swollen joints, HAQ, VAS, and adverse events. Yin et al. 2017 did not report any outcomes related to oxidative stress. The summary results of ESR showed that there was no statistically significant difference between the two groups after N-acetylcysteine intervention (WMD -0.87, 95% CI -2.85 to 1.12, $P = 0.39$) (Figure 17).

Hashemi et al. 2019 showed that the MDA and NO in the experiment group were lower (MDA (SMD -0.75, 95% CI -1.38 to -0.12, $P = 0.02$); NO (SMD -0.65, 95% CI -1.27 to -0.02, $P = 0.04$)) (Figures 4 and 7), while the IL6 in the experimental group was higher (SMD -0.05, 95% CI -0.66 to 0.56, $P = 0.01$) (Figure 20). The TAC, CRP, and TNF- α in Hashemi et al. 2019 between two groups were of no statistical significance (TAC (SMD -0.05, 95% CI -0.66 to 0.56, $P = 0.87$), CRP (WMD -0.20, 95% CI -0.91 to 0.51, $P = 0.58$), and TNF- α (SMD -0.28, 95% CI -0.89 to 0.33, $P = 0.37$)) (Figures 5, 18, and 19).

Batooei et al. showed that the adverse events, number of tender joints, number of swollen joints, and DAS28 between two groups were of no statistical significance (adverse events (RR 1.33, 95% CI 0.24 to 7.32, $P = 0.74$), number of swollen joints (WMD -0.80, 95% CI -3.67 to 2.07, $P = 0.59$), number of tender joints (WMD -0.70, 95% CI -4.35 to 2.95, $P = 0.71$), and DAS28 (WMD -0.35, 95% CI -1.10 to 0.40, $P = 0.36$)) (Figures 11–16). The HAQ and VAS in Batooei et al. were lower (VAS (SMD -1.15, 95% CI -1.75 to -0.55, $P = 0.0002$); HAQ (SMD -0.85, 95% CI -1.42 to -0.27, $P = 0.004$)) (Figures 18 and 19).

Abdollahzad et al. 2015 reported the effect of N-acetylcysteine combined with pulmonary rehabilitation exercise treatment on lung function in patients with RA-related interstitial lung disease; they found that N-acetylcysteine combined with pulmonary rehabilitation exercise therapy has a significant effect.

4.5.2. *Coenzyme Q10*. Three RCTs utilized coenzyme Q10 to treat RA. Abdollahzad et al. 2015 assessed the MDA, TAC, DAS28, number of tender joints, number of swollen joints, ESR, TNF- α , IL6, VAS, and adverse events. Zhu et al. 2020

	Random sequence generation (selection bias)	Allocation concealment (selection bias)	Blinding of participants and personnel (performance bias)	Blinding of outcome assessment (detection bias)	Incomplete outcome data (attrition bias)	Selective reporting (reporting bias)	Other biases
Abdollahzad et al. 2015	+	?	?	?	+	+	+
Aryaeian et al. 2009	+	?	?	?	+	+	+
Bae et al. 2009	?	?	?	?	?	+	+
Batooei et al. 2018	+	+	+	+	?	+	+
Edmonds et al. 1997	?	?	?	?	+	+	+
Ghavipor et al. 2016	+	+	+	+	?	+	+
Hashemi et al. 2019	+	+	+	+	?	+	+
Heinle et al. 1997	?	?	?	?	+	+	+
Ishibashi et al. 2014	?	?	+	+	+	+	+
Jaswal et al. 2003	?	?	+	+	+	+	+
Javadi et al. 2017	+	+	+	+	+	+	+
Karagülle et al. 2017	+	+	?	?	+	+	+
Khojah et al. 2018	?	?	+	+	+	+	+
León fernández et al. 2016	+	?	+	+	+	+	+
Mirtaheri et al. 2015	+	+	+	+	?	+	+
Moosavian et al. 2020	+	+	+	+	+	+	+
Peretz et al. 1992	?	?	?	?	+	+	+
Peretz et al. 2001	?	?	?	?	+	+	+
Tarp et al. 1986	?	?	?	?	+	+	+
Vaghef-mehrabany et al. 2016	+	+	+	+	?	+	+
Wittenbrog et al. 1998	?	?	?	?	+	+	+
Yin et al. 2017	?	?	+	+	+	+	+
Zamani et al. 2017	+	+	+	+	+	+	+
Zhu et al. 2020	+	+	+	+	+	+	+

FIGURE 3: Risk of bias summary.

assessed the MDA, TAC, CRP, ESR, TNF- α , and IL6. The summary results in the CoQ10 subgroup showed that the MDA and ESR in CoQ10 groups were lower (MDA (SMD -0.71, 95% CI -1.06 to -0.36, $P < 0.0001$); ESR (WMD -14.27, 95% CI -19.41 to -9.13, $P < 0.00001$)) (Figures 4

and 17), while the difference of TAC between two groups was of no statistical significance (SMD -0.19, 95% CI -0.53 to 0.15, $P = 0.43$) (Figure 5). For TNF- α and IL6, the data representation of Abdollahzad et al. 2015 is median (interquartile range); hence, it cannot be merged with Zhu et al. 2020. However, both groups showed that after CoQ10 intervention, compared with the control group, the TNF- α in the experimental group decreased ($P < 0.05$). Meanwhile, Zhu et al. 2020 showed that compared with the control group, the IL6 in the experimental group decreased ($P < 0.01$) (Figure 20), while Abdollahzad et al. 2015 showed that there was no statistical difference between the two groups ($P > 0.05$).

Abdollahzad et al. 2015 showed that the DAS28 and VAS in experiments group were lower (DAS28 (WMD -1.70, 95% CI -2.34 to -1.06, $P < 0.00001$); VAS (SMD -2.29, 95% CI -3.06 to -1.51, $P < 0.00001$)) (Figures 14 and 15). It also showed that no obvious adverse events were seen in the two groups. Zhu et al. 2020 showed that the CRP in the experiment group was lower (WMD -3.92, 95% CI -6.51 to 1.33, $P = 0.003$). The data representation of the number of swollen joints and number of tender joints in Abdollahzad et al. 2015 is median (interquartile range), and the results showed that compared with the control group, the number of swollen joints and number of tender joints in the experimental group decreased.

4.5.3. Probiotics. Two RCTs utilized probiotics to treat RA. Vaghef-Mehrabany et al. 2016 assessed the MDA, SOD, GPx, CAT, and TAC. Zamani et al. 2017 assessed the TAC, GSH, MDA, CRP, DAS28, and VAS. The summary results in the probiotic subgroup showed that the MDA in the probiotic groups was lower (SMD -0.71, 95% CI -1.06 to -0.36, $P < 0.001$) (Figure 4), while the difference of TAC between two groups was of no statistical significance (SMD -0.19, 95% CI -0.53 to 0.15, $P = 0.27$) (Figure 5).

Vaghef-Mehrabany et al. 2016 showed that the difference of SOD, GPx, and CAT between two groups was of no statistical significance (SOD (SMD -0.10, 95% CI -0.68 to 0.48, $P = 0.73$), GPx (SMD -0.00, 95% CI -0.58 to 0.57, $P = 0.99$), and CAT (SMD -0.14, 95% CI -0.43 to 0.72, $P = 0.62$)) (Figures 6, 8, and 9).

Zamani et al. 2017 showed that the difference of GSH and VAS between two groups was of no statistical significance (GSH (SMD 0.29, 95% CI -0.20 to 0.78, $P = 0.25$); VAS (SMD -0.40, 95% CI -0.94 to 0.14, $P = 0.15$)) (Figures 10 and 15). It also showed that after probiotic intervention, compared with the control group, the DAS28 and CRP in the experimental group decreased (DAS28 (WMD -0.60, 95% CI -1.09 to -0.11, $P = 0.02$); CRP (WMD -3.86, 95% CI -6.63 to -1.09, $P = 0.006$)) (Figures 14 and 18).

4.5.4. Pomegranate Extract. Only one RCT utilized pomegranate extract to treat RA. Ghavipour et al. 2016 assessed the DAS28, HAQ, ESR, CRP, number of tender joints, number of swollen joints, MDA, and GPx. The summary results in the pomegranate extract subgroup showed that the MDA in the pomegranate extract groups was higher (SMD 0.56, 95% CI 0.02 to 1.10, $P = 0.04$) (Figure 4), while the difference

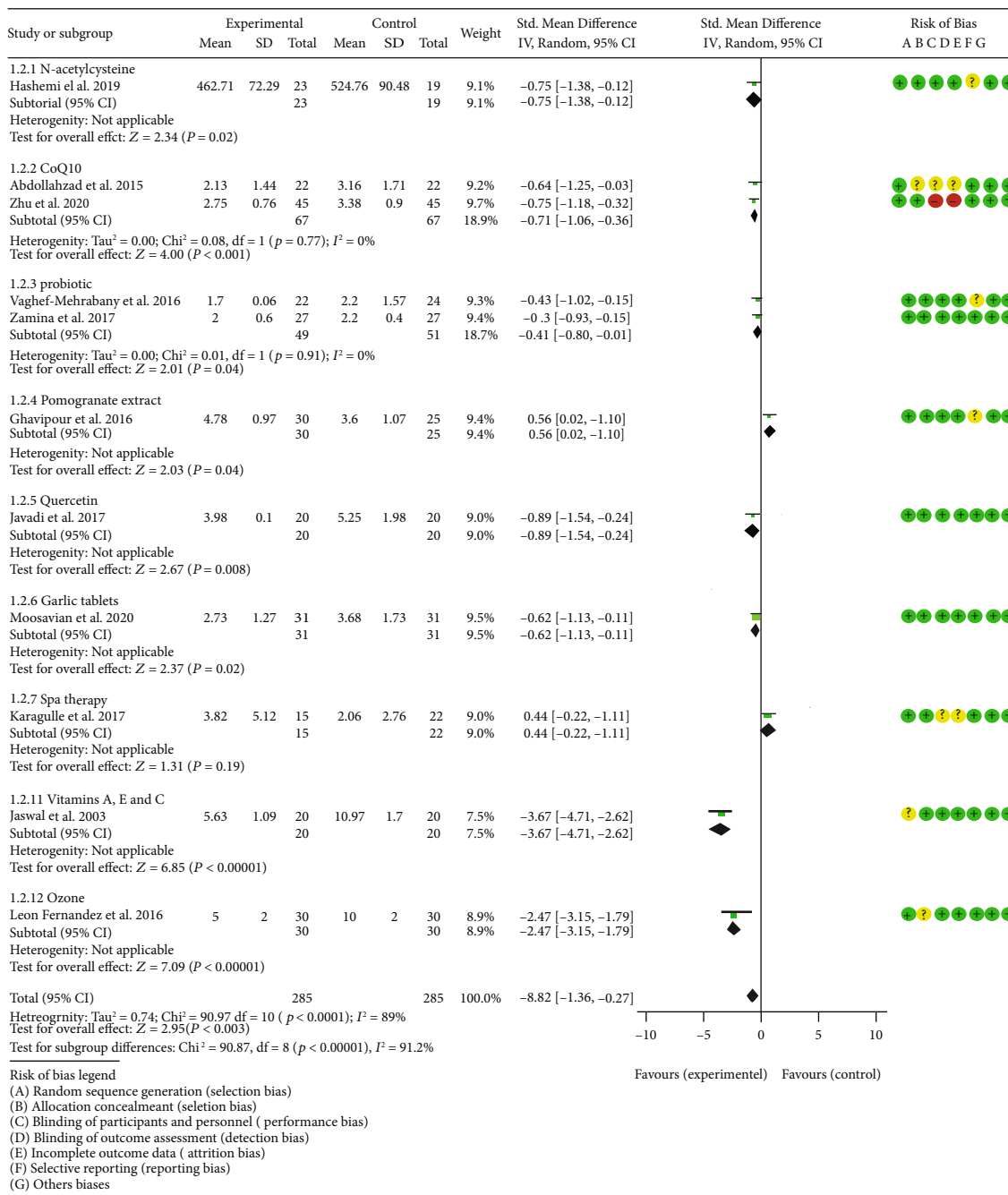


FIGURE 4: MDA.

of GPx, HAQ, and CRP between two groups was of no statistical significance (GPx (SMD 0.54, 95% CI 0.00 to 1.08, $P = 0.05$), HAQ (SMD -0.52, 95% CI -1.06 to 0.02, $P = 0.06$), and CRP (WMD 0.20, 95% CI -2.19 to 2.59, $P = 0.87$)) (Figures 8, 16, and 18). It also showed that the number of swollen joints, number of tender joints, DAS28, and ESR were lower (number of swollen joints (WMD -1.38, 95% CI -3.67 to -0.01, $P = 0.05$), number of tender joints (WMD -4.20, 95% CI -6.82 to -1.58, $P = 0.002$), DAS28 (WMD -0.80, 95% CI -1.41 to -0.19, $P = 0.010$), and ESR (WMD -9.40, 95% CI -17.73 to -1.07, $P = 0.003$)) (Figures 12–14 and 17).

4.5.5. *Quercetin*. Two RCTs utilized quercetin to treat RA. Javadi et al. 2017 assessed the DAS28, HAQ, ESR, CRP, TNF- α , number of tender joints, number of swollen joints, VAS, MDA, and TAC. Bae et al. 2009 reported CRP, TNF- α , and IL6.

Javadi et al. 2017 showed that MDA, VAS, and HAQ in the quercetin groups were lower (MDA (SMD -0.89, 95% CI -1.54 to -0.24, $P = 0.008$), VAS (SMD -0.83, 95% CI -1.48 to -0.18, $P = 0.01$), and HAQ (SMD -0.92, 95% CI -1.58 to -0.27, $P = 0.006$)) (Figures 4, 15, and 16), while the difference of TAC, DAS28, ESR, and CRP between two groups was of no statistical significance (TAC (SMD -0.25, 95% CI -0.87

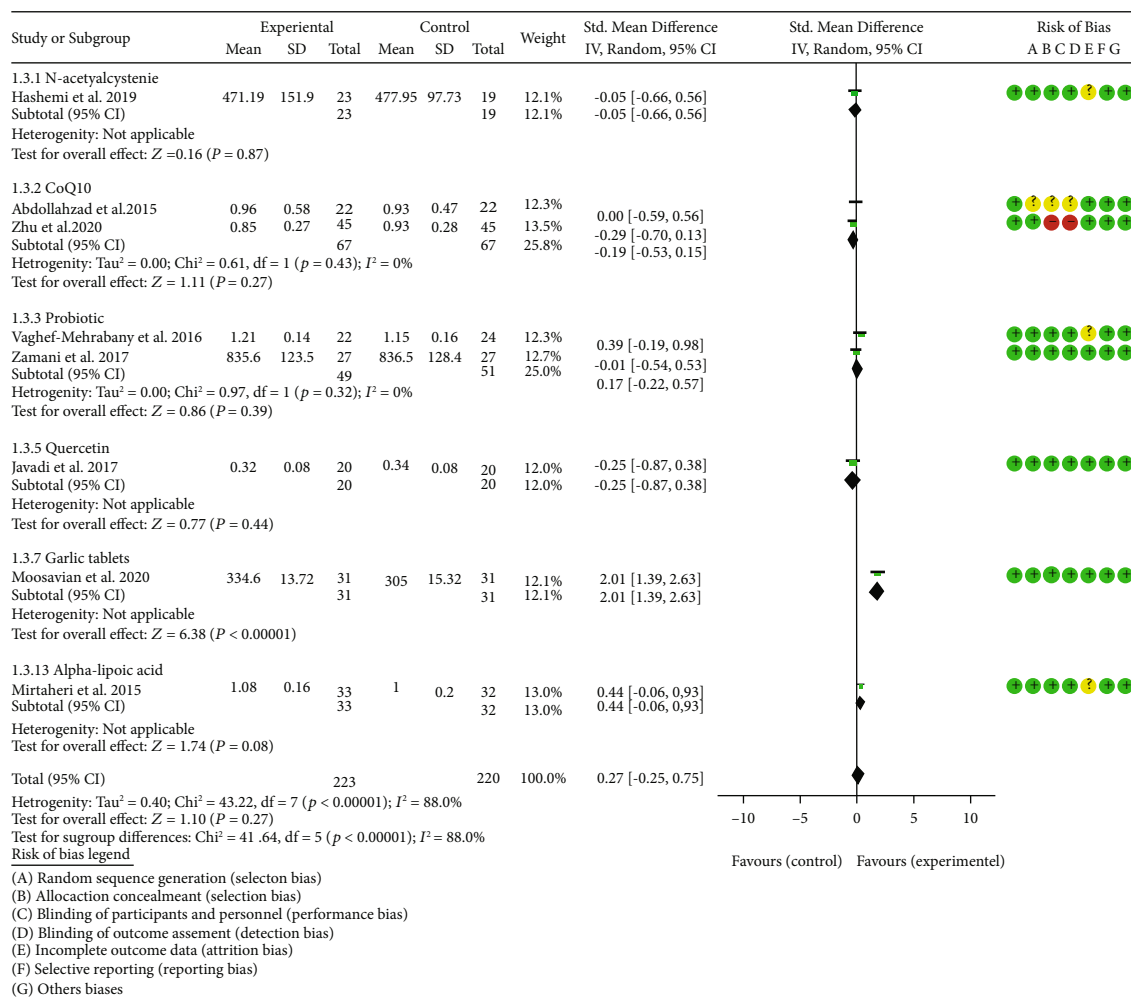


FIGURE 5: TAC.

to 0.38, $P = 0.44$), DAS28 (WMD -0.46, 95% CI -1.17 to 0.25, $P = 0.20$), ESR (WMD -5.10, 95% CI -13.86 to 3.66, $P = 0.25$), and CRP (WMD -0.51, 95% CI -1.98 to 0.96, $P = 0.50$) (Figures 5, 14, 17, and 18). The data representation of the TNF- α , number of tender joints, and number of swollen joints in Javadi et al. 2017 is median (interquartile range), and the results showed that compared with the control group, the TNF- α in the experimental group decreased ($P < 0.05$); meanwhile, the difference of the number of tender joints and number of swollen joints between the experimental group and the placebo group was of no statistical significance ($P > 0.05$).

Bae et al. 2009 showed that the difference of TNF- α and IL6 between two groups was of no statistical significance (TNF- α (SMD -0.07, 95% CI -1.26 to 1.12, $P = 0.91$); IL6 (SMD -0.09, 95% CI -1.27 to 1.10, $P = 0.89$)) (Figures 19 and 20). The data representation of the CRP is median (interquartile range), and the results showed that the difference of CRP between the experimental group and the placebo group was of no statistical significance ($P > 0.05$).

4.5.6. Resveratrol. Only one RCT utilized resveratrol to treat RA, and it reported number of tender joints, number of

swollen joints, DAS28, CRP, ESR, TNF- α , and IL6. The RCT evaluated 100 patients with RA. The control group used traditional RA therapy, while the test group was treated with 1 g resveratrol on the basis of traditional therapy. The treatment lasted 3 months. The study showed that the number of swollen and tender joints and the DAS28 in the resveratrol group were significantly reduced ($P < 0.05$) (Figures 12–14), and CRP, ESR, TNF- α , and IL6 were also reduced ($P < 0.05$) (Figures 17–20).

4.5.7. Garlic Tablets. Only one RCT utilized garlic tablets to treat RA. Moosavian et al. 2020 assessed the HAQ, VAS, CRP, ESR, TNF- α , number of tender joints, number of swollen joints, MDA, and TAC. The summary results showed that the MDA in the experiment groups was lower (SMD -0.62, 95% CI -1.13 to -0.11, $P = 0.008$) (Figure 4), while the TAC in the experiment groups was higher (SMD 2.01, 95% CI 1.39 to 2.63, $P < 0.00001$) (Figure 5). It also showed that the difference of number of tender and swollen joints, ESR, and CRP between two groups was of no statistical significance ($P > 0.05$) (Figures 12, 13, 17, and 18), while the HAQ, VAS, and TNF- α in the experimental group were lower ($P < 0.05$) (Figures 15, 16, and 19).

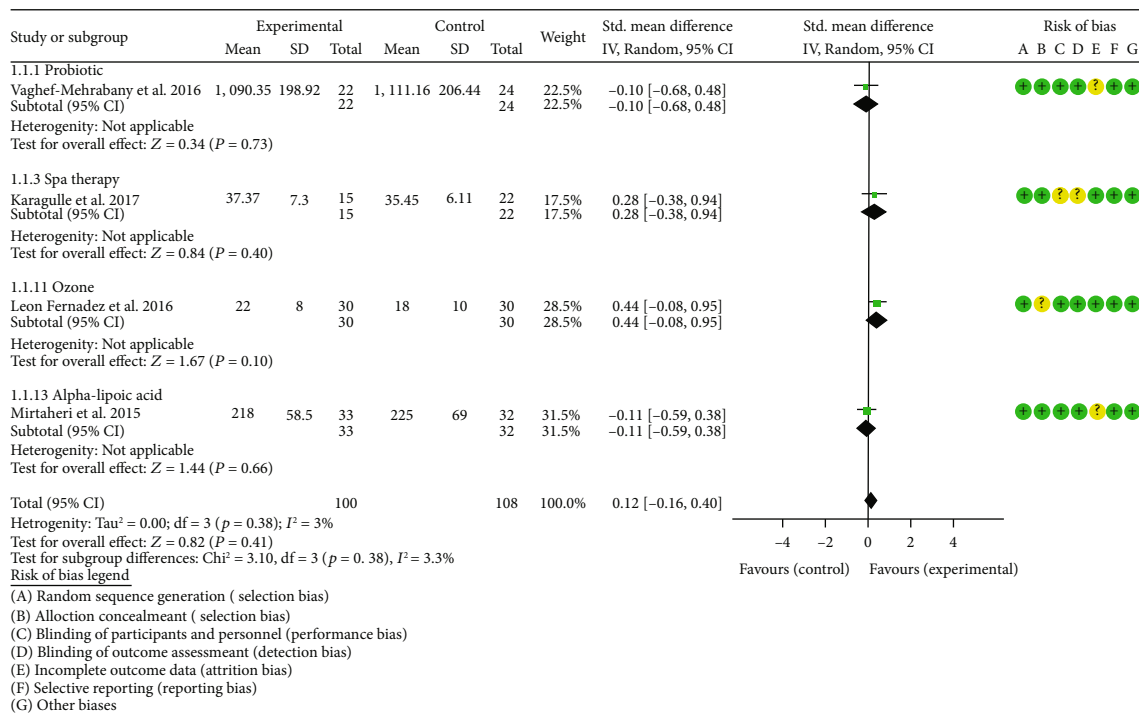


FIGURE 6: SOD.

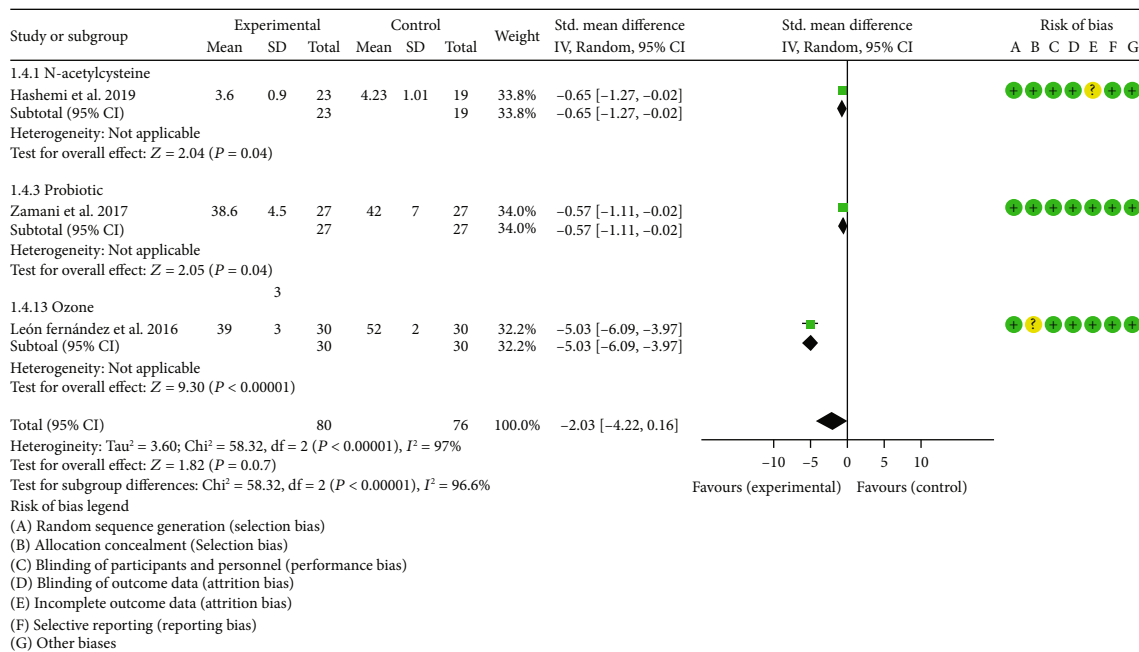


FIGURE 7: NO.

4.5.8. *Vitamin E and Conjugated Linoleic Acids*. Three RCTs utilized vitamin E to treat RA. Edmonds et al. 1997 reported adverse events; Wittenborg et al. 1998 reported VAS and adverse events; Aryaeian et al. 2009 reported VAS, ESR, CRP, DAS28, number of tender joints, and number of swollen joints. The summary results showed that the difference of adverse events and VAS between two groups was of no statistical significance (adverse events (RR 1.10, 95% CI 0.74 to

1.65, P = 0.64); VAS (SMD -0.02, 95% CI -0.04 to 0.36, P = 0.93)) (Figures 11 and 15).

Aryaeian et al. 2009 uses vitamin E alone and in combination with conjugated linoleic acids to intervene in RA patients. It showed that when conjugated linoleic acids were used alone, number of tender joints, number of swollen joints, and DAS28 were improved (P < 0.05) (Figures 12–14), but VAS, ESR, and CRP were not significantly improved

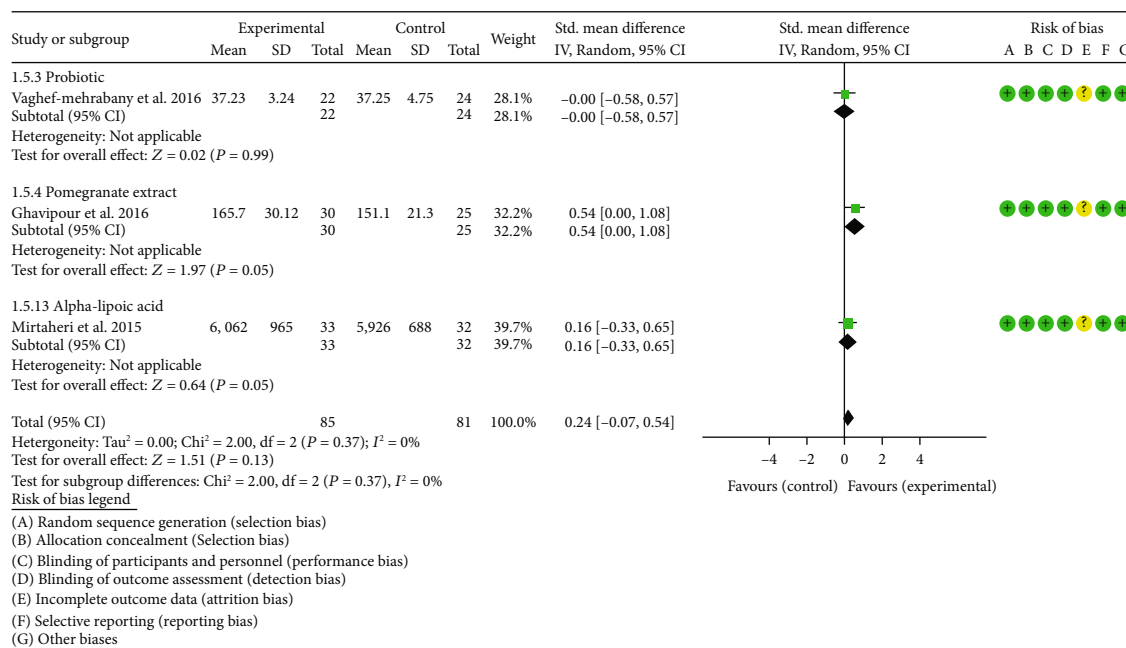


FIGURE 8: GPX.

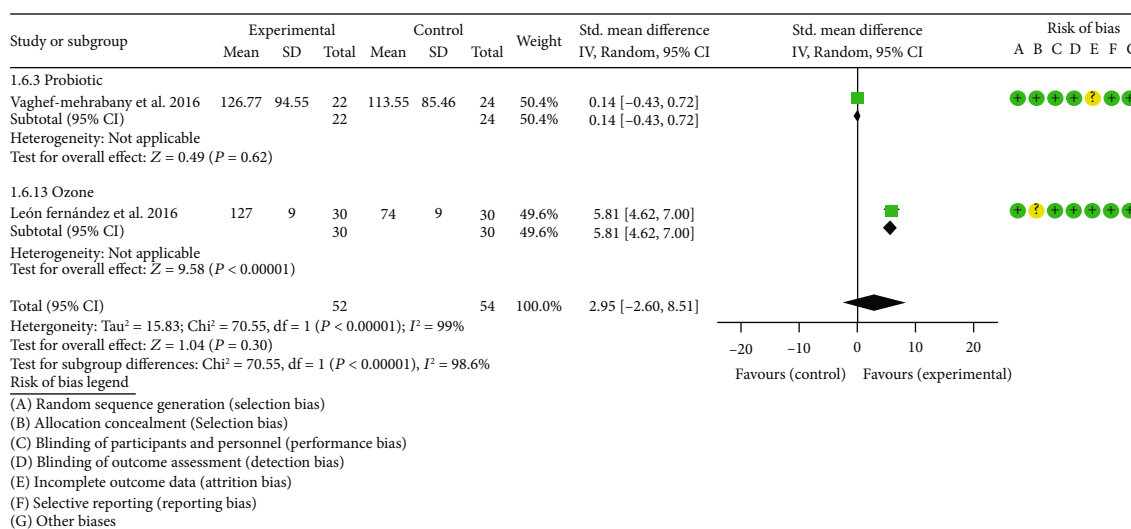


FIGURE 9: CAT.

($P > 0.05$) (Figures 15, 17, and 18). When conjugated linoleic acids were combined with vitamin E, number of swollen joints, VAS, and DAS28 were improved ($P < 0.05$) (Figures 13–15), but number of tender joints, ESR, and CRP were not significantly improved ($P > 0.05$) (Figures 13, 17, and 18).

4.5.9. Selenium. Four RCTs utilized selenium to treat RA. Tarp et al. 1986 reported the number of swollen joints and ESR; Peretz et al. 1992 reported VAS and ESR; Peretz et al. 2001 reported number of swollen joints, CRP, ESR, and VAS; Heinle et al. 1997 reported number of tender joints, number of swollen joints, and CRP. The summary results showed that the difference of number of swollen joints,

ESR, and CRP between the two groups was of no statistical significance (number of swollen joints (WMD 0.04, 95% CI -1.43 to 1.51, $P = 0.96$), ESR (WMD -6.69, 95% CI -14.50 to 1.11, $P = 0.09$), and CRP (WMD -8.84, 95% CI -17.84 to 0.16, $P = 0.05$)) (Figures 12, 17, and 18). The data representation of the VAS in Peretz et al. 1992 is median (interquartile range), and the results showed that compared with the control group, the VAS in the experimental group decreased ($P < 0.05$). However, the difference of VAS in Peretz et al. 2001 between two groups was of no statistical significance ($P > 0.05$) (Figure 15). Heinle et al. 1997 also showed that the difference of number of tender joints between two groups was of no statistical significance ($P > 0.05$) (Figure 13).

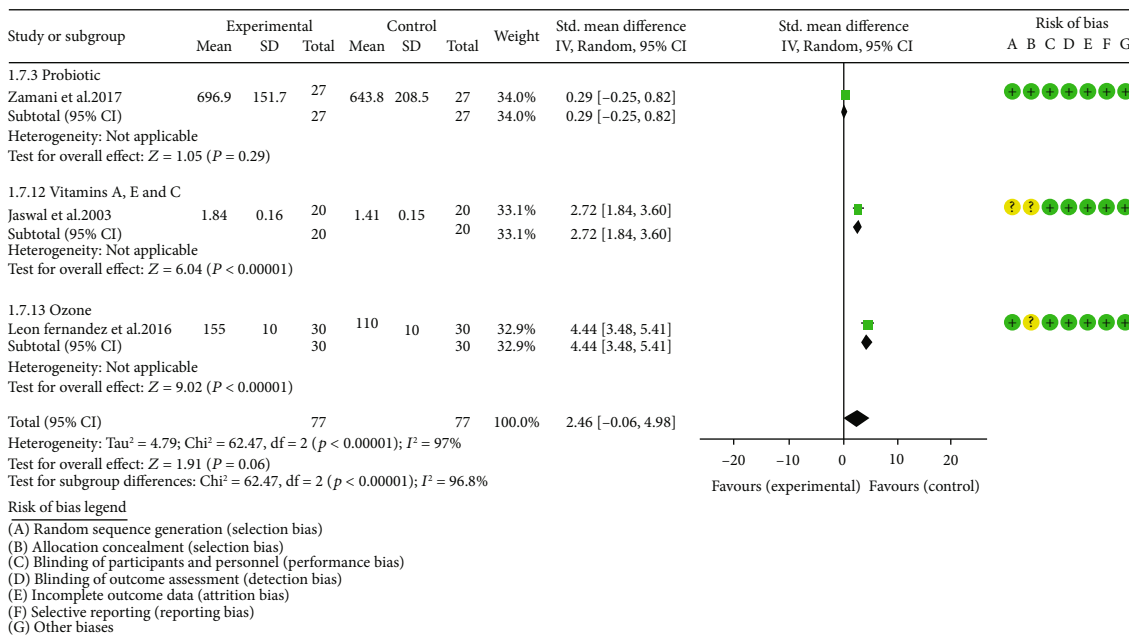


FIGURE 10: GSH.

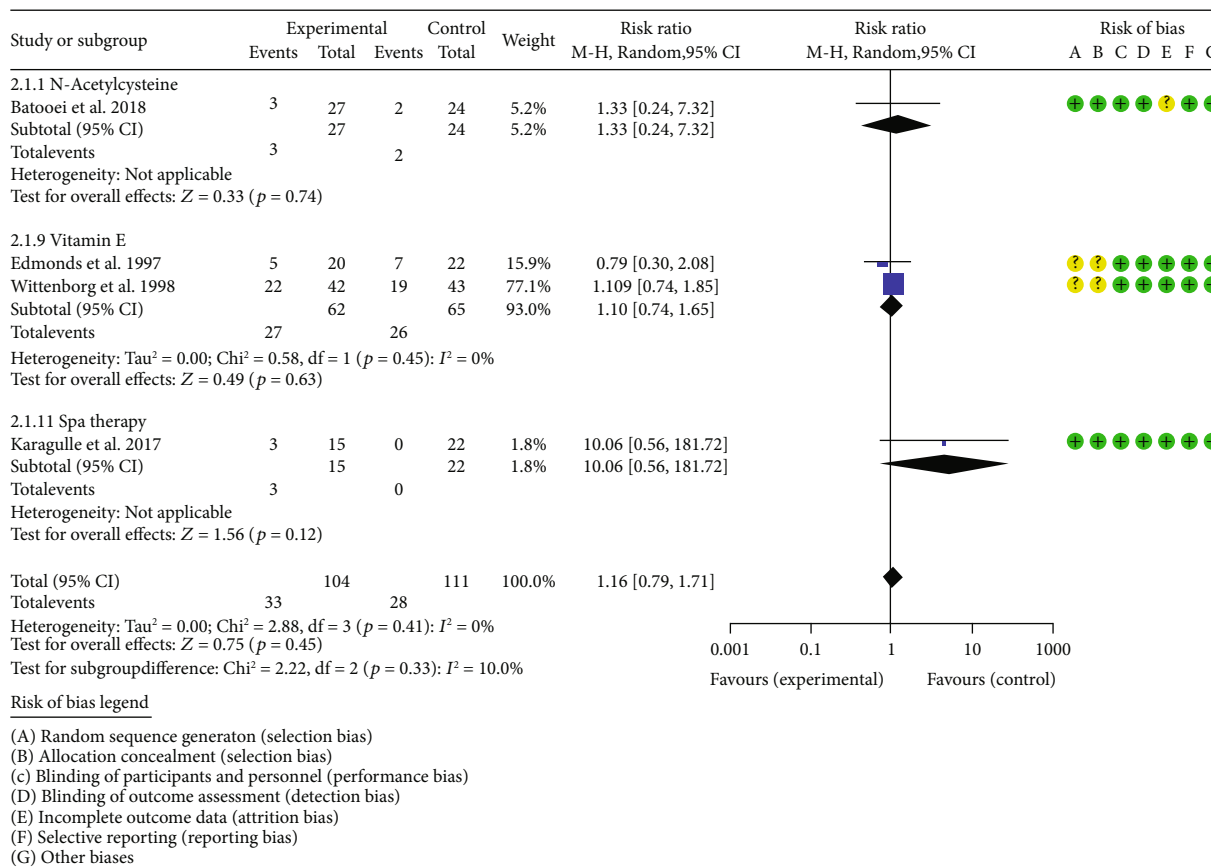


FIGURE 11: Adverse events.

4.5.10. Spa Therapy. Only one RCT utilized spa therapy to treat RA. Karagülle et al. 2017 assessed the VAS, HAQ, DAS28, number of tender joints, number of swollen joints, MDA, SOD, and adverse events. The summary results

showed that the difference of MDA, SOD, and adverse events between two groups was of no statistical significance (MDA (SMD 0.44, 95% CI -0.22 to 1.11, P = 0.19), SOD (SMD 0.28, 95% CI -0.08 to 0.95, P = 0.10), and adverse

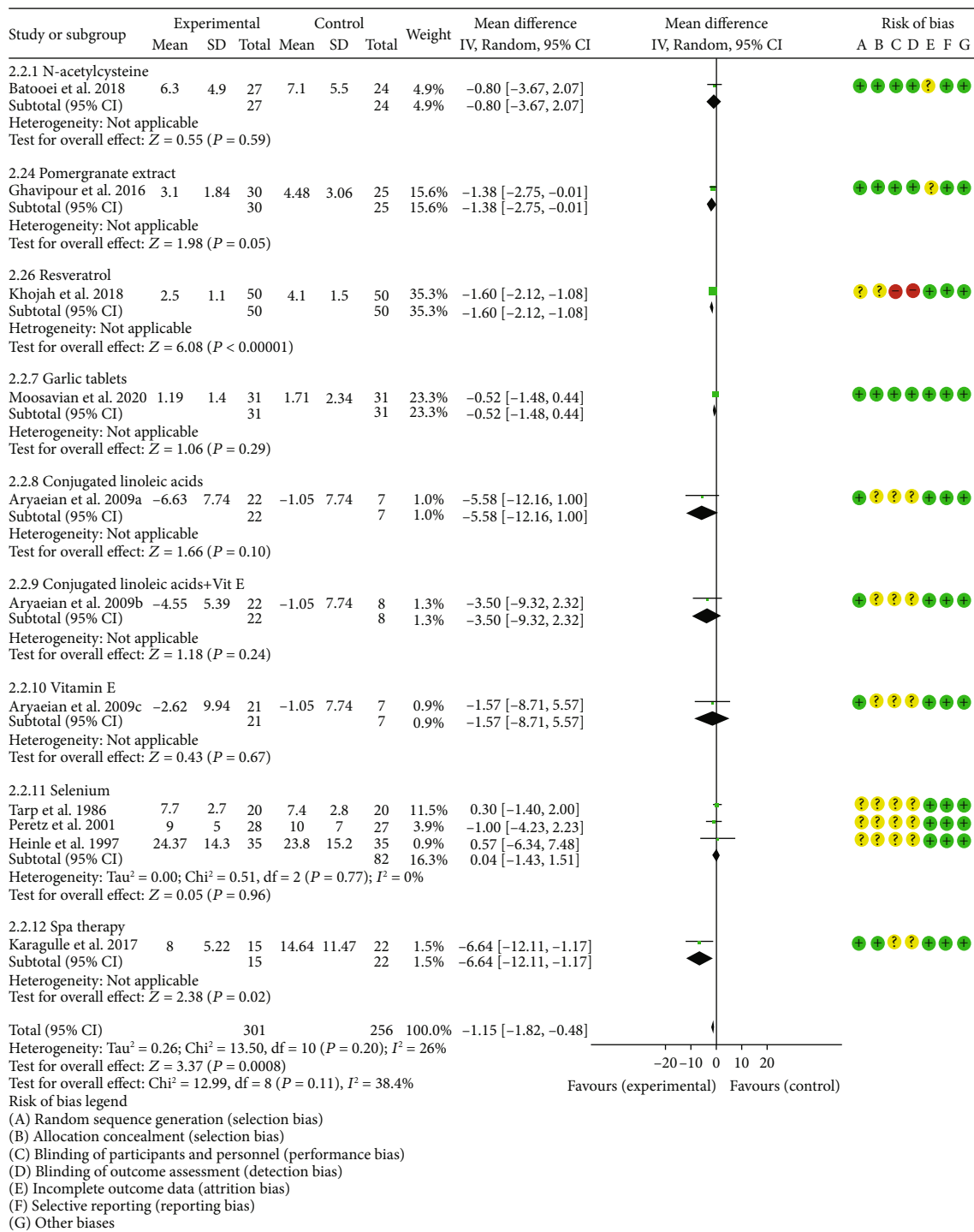


FIGURE 12: Number of swollen joints.

events (RR 1.16, 95% CI 0.79 to 1.71, $P = 0.45$) (Figures 4, 5, and 11). It also showed the number of swollen joints ($P < 0.05$) (Figure 12), while the difference of number of tender joints, DAS28, VAS, and HAQ between two groups was of no statistical significance ($P > 0.05$) (Figures 13–16).

4.5.11. Vitamins A, E, and C Combination. Only one RCT utilized vitamins A, E, and C combination to treat RA. Jaswal et al. 2003 assessed the MDA and GSH. The summary

results showed that the MDA in the experiment group was lower (SMD -3.67, 95% CI -4.71 to -2.62, $P < 0.00001$) (Figure 4), while the GSH in the experiment group was higher (SMD 2.72, 95% CI 1.84 to 3.60, $P < 0.00001$) (Figure 10).

4.5.12. Ozone. Only one RCT utilized ozone to treat RA. León Fernández et al. 2016 assessed the DAS28, HAQ, CRP, ESR, MDA, NO, GSH, SOD, and CAT. The summary

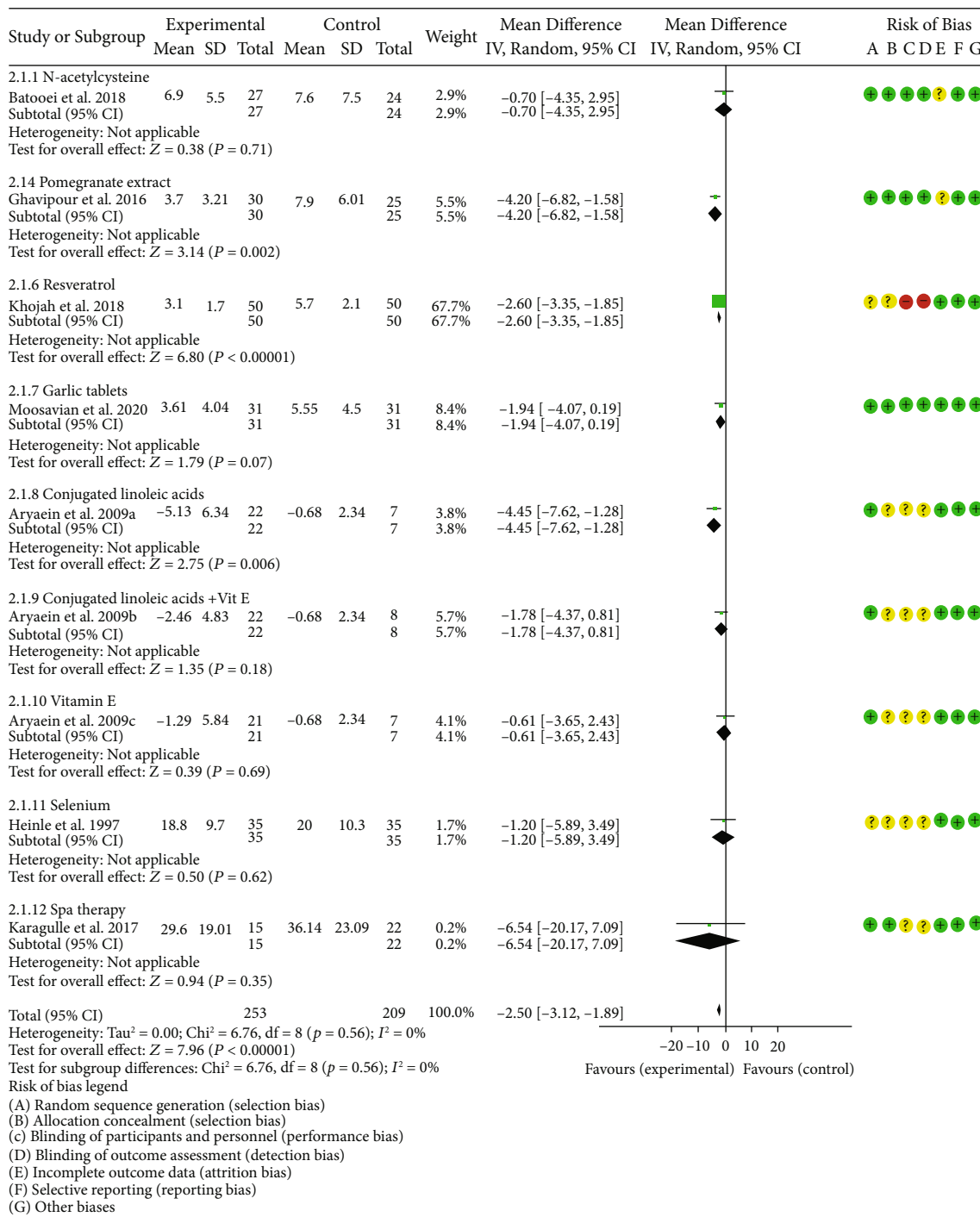


FIGURE 13: Number of tender joints.

results showed that the MDA, NO, DAS28, HAQ, and ESR in the experiment group were lower (SOD (SMD -2.47, 95% CI -4.71 to -2.62, $P < 0.00001$), NO (SMD -5.03, 95% CI -6.09 to -3.97, $P < 0.00001$), DAS28 (WMD -2.00, 95% CI -2.83 to -1.17, $P < 0.00001$), HAQ (SMD -1.01, 95% CI -1.55 to -0.47, $P = 0.0002$), and ESR (WMD -20.00, 95% CI -34.13 to -5.87, $P = 0.006$)) (Figures 4, 7, 14, 16, and 17), while the GSH and CAT in the experiment group were higher (GSH (SMD 4.44, 95% CI 3.48 to 5.41, $P < 0.00001$); CAT (SMD

5.81, 95% CI 4.62 to 7.00, $P < 0.00001$)) (Figures 9 and 10). The difference of SOD and CRP was of no statistical significance (SOD (SMD 0.44, 95% CI -0.08 to 0.95, $P = 0.10$); CRP (WMD -8.00, 95% CI -16.08 to 0.08, $P = 0.05$)) (Figures 6 and 18).

4.5.13. H_2 -Saline. Only one RCT utilized H_2 -saline to treat RA. Ishibashi et al. 2014 reported DAS28, CRP, TNF- α , and IL6. Their study found that H_2 -saline may improve

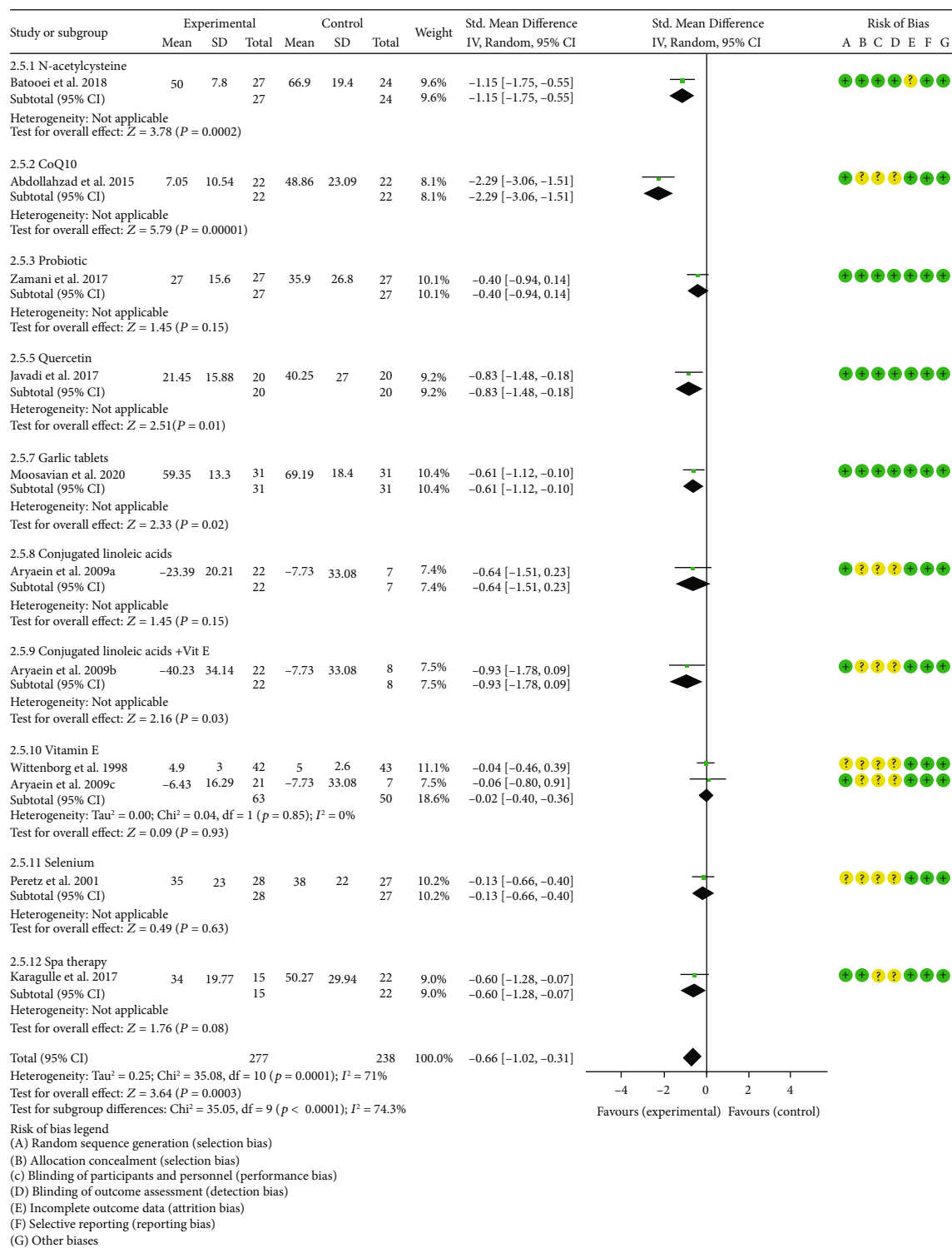


FIGURE 15: VAS.

The data representation of the CRP in Mirtaheri et al. 2015 and Bae et al. 2009 is median (interquartile range), and both two RCTs showed that the results showed that the difference of CRP between the experimental group and the control group was of no statistical significance ($P > 0.05$). The data representation of the IL6 in Mirtaheri et al. 2015 is also

median (interquartile range), but both two RCTs reported that the difference of IL6 between the experimental group and the control group was of no statistical significance ($P > 0.05$) (Figure 20). Mirtaheri et al. 2015 also showed that the difference of SOD, TAC, and GPx between two groups was of no statistical significance (TAC (SMD 0.44, 95% CI

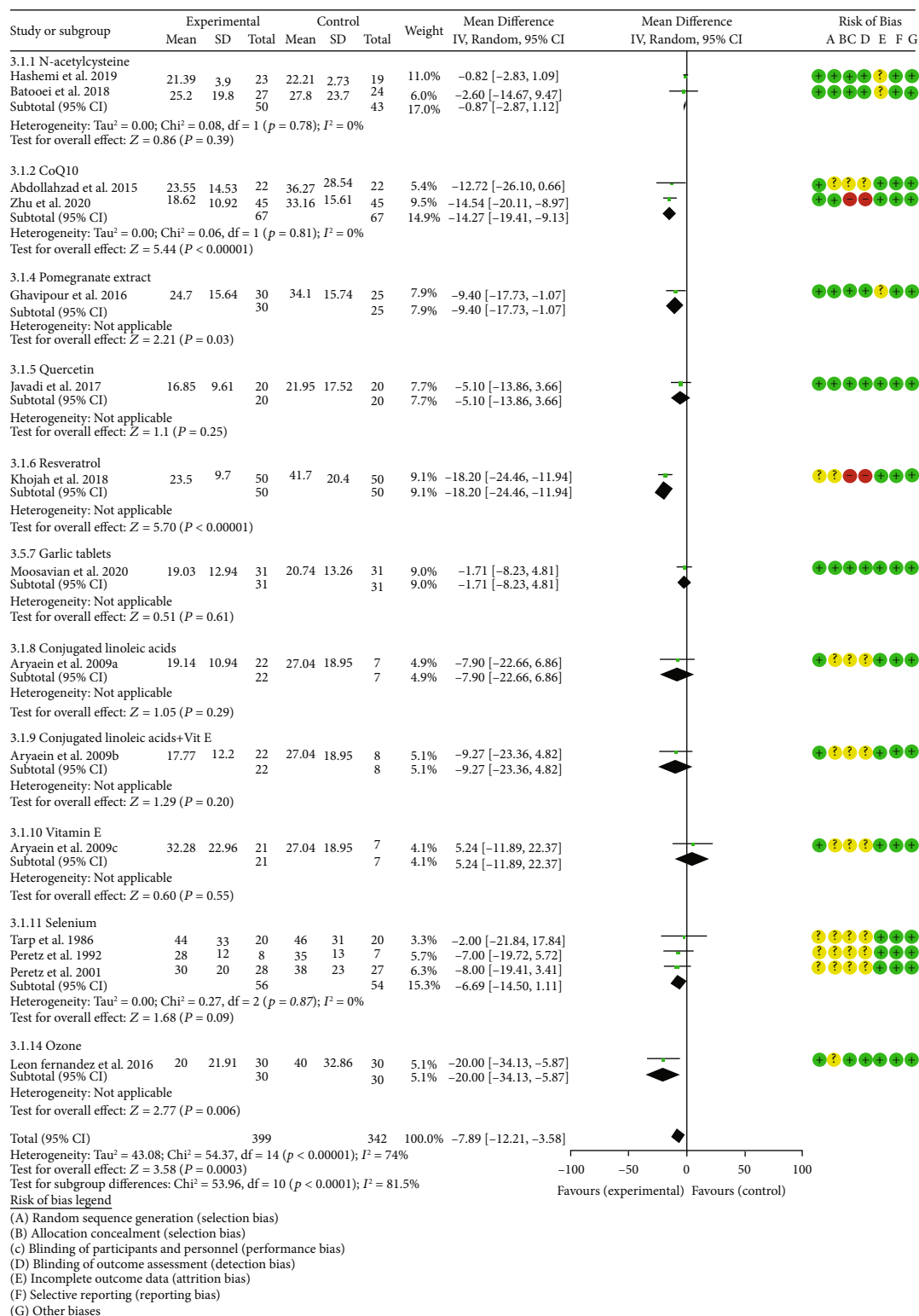


FIGURE 17: ESR.

pomegranate extract was higher, which is different from the results of other supplements. It has not been observed to improve GPx. Meanwhile, it may also reduce inflammation and relieve the condition (reduce number of swollen joints, number of tender joints, DAS28, and ESR). (5) Quercetin:

it may reduce the MDA level in RA patients. Meanwhile, it may relieve pain and improve the quality of life of patients (reduce VAS and HAQ). (6) Resveratrol: the results showed that it may alleviate the patient's condition (reduce number of swollen and tender joints and the DAS28) and improve

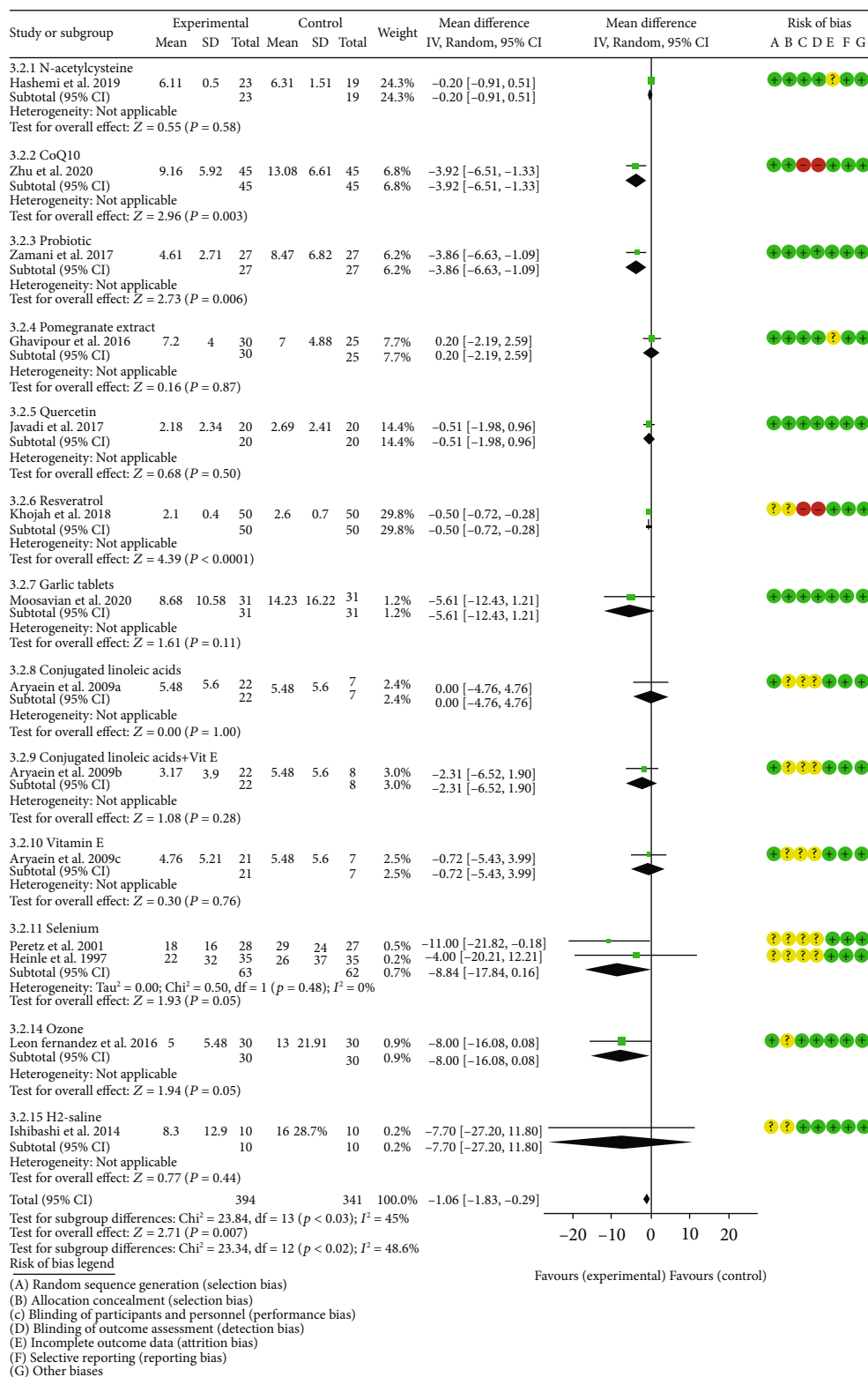
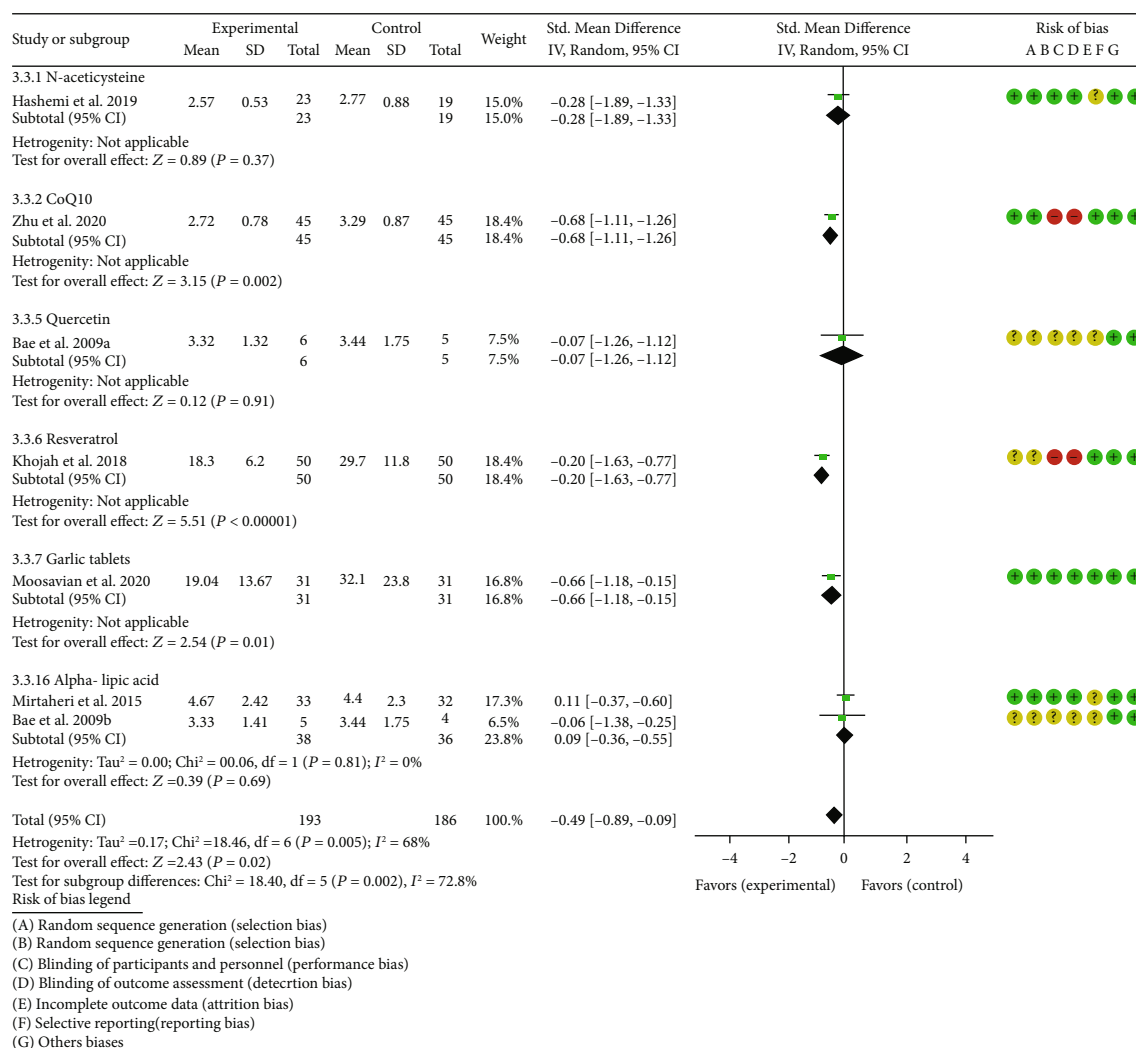


FIGURE 18: CRP.

inflammation (reduce CRP, ESR, TNF- α , and IL6). (7) Garlic tablets: it may reduce the MDA level in RA patients and increase the TAC of RA patients. It may also relieve pain and improve the quality of life of patients (reduce VAS and HAQ) and reduce inflammation (reduce TNF- α). (8)

Vitamin E and conjugated linoleic acids: whether conjugated linoleic acids were used alone (reduce the number of tender joints, number of swollen joints, and DAS28) or in combination with vitamin E (reduce number of swollen joints, VAS, and DAS28), it may improve the patient's condition.

FIGURE 19: TNF- α .

Meanwhile, the addition of vitamin E to conventional therapy will not increase the occurrence of adverse events. (9) Selenium: current research has not shown that selenium has a therapeutic effect on RA. What is interesting is that for VAS, RCT showed different results. Because the data is expressed in different ways, it cannot be combined, so it is impossible to draw a certain conclusion. (10) Spa therapy: it has no significant improvement on MDA and SOD, and it may reduce number of swollen joints. Meanwhile, spa therapy may not increase adverse events. (11) Vitamins A, E, and C combination: this combination may decrease MDA and increase GSH. (12) Ozone: it may reduce MDA and NO levels and increase CAT and GSH levels in RA patients. Meanwhile, it may also reduce inflammation and relieve the condition (reduce DAS28, HAQ, and ESR). (13) H₂-saline: The H₂-saline may improve the clinical symptoms of RA patients (decreased DAS28). (14) Alpha-lipoic acid: current research has not shown that alpha-lipoic acid has a therapeutic effect on RA.

In short, most antioxidants or antioxidant therapies can reduce MDA levels in RA patients, and a small number of therapies can increase GSH or TAC levels. And several anti-

oxidants or antioxidant therapies may relieve pain and improve the quality of life of patients and the patient's condition. However, pomegranate extract may cause an increase in MDA. However, since there is only one RCT in most subgroups, the interpretation of the results still requires caution.

5.2. Possible Mechanism of Antioxidant Treatment of RA. In 1986, Koster et al. found that compared with healthy controls, the serum sulfhydryl concentration of RA patients was lower [47]. Considering that the sulfhydryl group may act as a scavenger of peroxides, this discovery had already indicated that the oxidative stress in RA patients was excessive. Subsequently, the characteristics of oxidative stress in the pathogenesis of RA have been reported successively [14, 48–51]. Oxidative stress is a state where the body's oxidation and antioxidant effects are out of balance and tend to be oxidized. Oxidative stress can cause inflammatory infiltration of neutrophils and promote the massive production of reactive oxygen species (ROS) and reactive nitrogen species (RNS) free radicals [13, 52]. ROS mainly includes superoxide anion (O₂⁻) [53], hydrogen peroxide (H₂O₂)

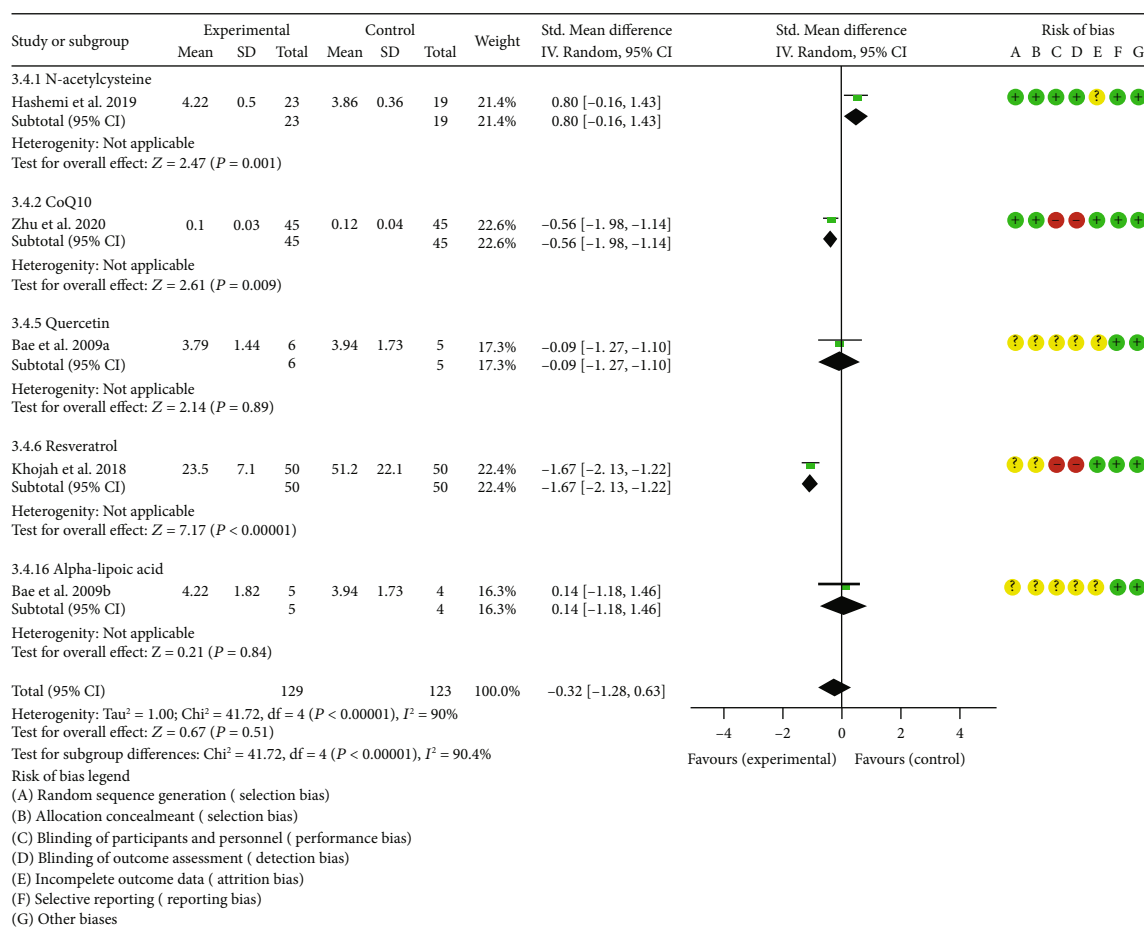


FIGURE 20: IL6.

[54, 55], hypochlorous acid (HClO) [56], and hydroxyl radical ($\cdot\text{OH}$) [57]. RNS mainly includes nitrogen monoxide (NO) [58–61] and peroxynitroso (ONOO $^-$) [62, 63]. In addition, a variety of highly active molecules including oxidative stress will be produced under pathological conditions [56, 63, 64]. In addition to increasing the number of ROS/RNS under oxidative stress, antioxidants will also remove ROS/RNS substances or compounds, thereby inhibiting the oxidative stress process in cells [65]. Current research shows that there are mainly two different types of antioxidants, namely, enzymatic system and nonenzymatic system. The first type is mainly composed of SOD [65–67], CAT [68], GPx [69], glutathione reductase (GR) [70], and thioredoxin reductase [71]. $\cdot\text{O}_2^-$ and H_2O_2 are the most ROS produced during oxidative stress [52, 69]. The former is cleared by SOD [65], and the latter is cleared by CAT [68], GPx [69], and perredoxin (PRX) [72]. The nonenzymatic antioxidant system is mainly composed of vitamins (A, C, and E), beta carotene, antioxidants, and minerals such as copper, ferritin, zinc, manganese, and selenium [52, 73].

Current basic research shows that oxidative stress plays a key role in the initiation and maintenance of systemic inflammation in RA [32, 45, 74, 75]. Under the pathological conditions of RA, ROS and RNS are produced by neutrophils, monocytes, and macrophages in joint tissues [76]. They can damage different types of cell structures in joints,

including DNA, carbohydrates, proteins, and lipids [14, 17, 43, 74], leading to an imbalance of oxidative stress in joint tissues. Among them, the most common oxidation promoting factor (ROS/RNS) in RA joints is composed of $\cdot\text{O}_2^-$, H_2O_2 , $\cdot\text{OH}$, NO $^\cdot$, ONOO $^-$, HOCl, and LOO $^\cdot$ [32, 45, 74, 75]. In addition, in the occurrence and progression of RA joint damage, the oxidative stress imbalance and the inflammatory biological network are interconnected in multiple directions, which eventually leads to RA (synovitis) and forms a vicious circle. For example, ROS increases in RA patients [10] (mainly H_2O_2), which in turn activates the NF- κB pathway [77]. NF- κB signal transduction immunity promotes more IL-1 and TNF- α . Activated macrophages and T cells in the synovium may induce the production of ROS through the release of TNF and IL-1. This way further amplifies the inflammation of synovitis, forming a positive feedback, and worsening the process of RA synovitis [78, 79]. It is specifically manifested in the disease progression of RA patients. Compared with inactive RA patients, RA patients with active disease show higher ROS levels, more severe inflammatory factor levels, and lower antioxidant potential. Moreover, compared with healthy controls, these active RA patients have worse antioxidant capacity [74]. It is manifested by a higher degree of lipid peroxidation found in the synovial fluid and blood samples of these patients with possible RA [80, 81].

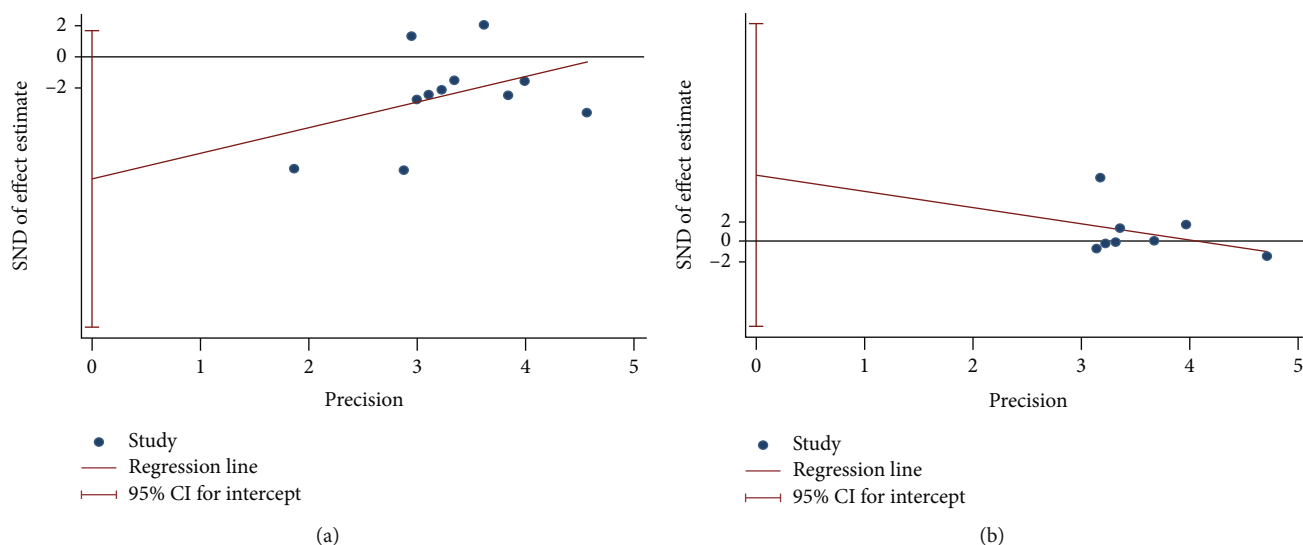


FIGURE 21: Publication bias of oxidative stress index: (a) MDA; (b) TAC.

In addition, the increase in intra-articular pressure caused by chronic long-term inflammation in the joints of RA patients may lead to chronic hypoxia, which in turn increases the production of ROS in the joints of RA individuals [82]. The oxidation of type II collagen in the joints of patients with RA [10] and the increased production of matrix metalloproteinases [33] will cause oxidative damage to the matrix (extracellular environment) of the joints [10]. These oxidative stress factors can also induce stromal cells and joint cells (chondrocytes) to undergo programmed cell death caused by endoplasmic reticulum oxidative stress, which in turn leads to early joint damage in RA [10]. Further studies have also shown that oxidative stress can also cause other complications in RA patients. For example, high levels of inflammation and oxidative stress in RA patients can cause endothelial dysfunction and cause vascular damage to the circulatory system [83, 84]. Controlling the oxidative stress imbalance and inflammation in the preclinical and chronic stages of RA can avoid complications in the circulatory system of RA patients [84]. Aiming at the mechanism of oxidative stress in the clinical diagnosis and treatment of RA patients, oxidative stress biomarkers have been used as relevant markers and protocols to assess the disease activity and prognosis of RA patients [50, 82]. For example, Quiñonez-Flores et al. [50] found that lipid peroxidation (through MDA level) can be used to detect disease activity in RA patients (disease activity score DAS28), which expands the potential applicability of oxidative biomarkers in the diagnosis and prognosis of RA patients.

5.3. Characteristic Analysis of Included Studies. A total of 24 RCTs were included in this study, with a time span from 1986 to 2020. These 24 RCTs used a total of 14 different therapies; they were N-acetylcysteine, CoQ10, probiotic, pomegranate extract, quercetin, resveratrol, garlic tablets, vitamin E and conjugated linoleic acids, selenium, spa therapy, vitamins A, E, and C, ozone, H₂-saline, and alpha-lipoic acid. Hashemi et al. 2019 [16], Batooei et al. 2018 [17],

Abdollahzad et al. 2015 [19, 20], Zhu et al. 2020 [30], Vaghef-Mehrabany et al. 2016 [31], Zamani et al. 2017 [32], Ghavipour et al. 2016 [33], Javadi et al. 2017 [24, 25], Moosavian et al. 2020 [26, 27], Aryaeian et al. 2009 [36], Karagülle et al. 2017 [43], and León Fernández et al. 2016 [45] described the random sequence generation methods. Hashemi et al. 2019 [16], Batooei et al. 2018 [17], Zhu et al. 2020 [30], Vaghef-Mehrabany et al. 2016 [31], Zamani et al. 2017 [32], Ghavipour et al. 2016 [33], Javadi et al. 2017 [24, 25], Moosavian et al. 2020 [26, 27], and Karagülle et al. 2017 [43] described allocation concealment methods. The other RCTs failed to describe the random sequence generation methods and/or allocation concealment methods. Since the main outcome of this meta-analysis is an objective indicator, it is less affected by whether or not blinding is used. Hence, although only Hashemi et al. 2019 [16], Batooei et al. 2018 [17], Zamani et al. 2017 [32], and Moosavian et al. 2020 [26, 27] uses blinding, all RCTs are assessed as low risk of bias regarding blinding. However, the implementation of blinding methods is still very important. Hashemi et al. 2019 [16], Batooei et al. 2018 [17], Vaghef-Mehrabany et al. 2016 [31], Ghavipour et al. 2016 [33], and Bae et al. 2009 [34] have incomplete outcome data. In addition, 2 RCTs were from Belgium; 2 RCTs were from China; 2 RCTs were from Germany; 8 RCTs were from Iran; Bae et al. 2009 was from Korea; Khojah et al. 2018 was from Egypt; Edmonds et al. 1997 was from the UK; Tarp et al. 1986 was from Denmark; Karagülle et al. 2017 was from Turkey; Jaswal et al. 2003 was from India; León Fernández et al. 2016 was from Cuba; and Ishibashi et al. 2014 was from Japan. The included RCTs in this study showed that the included patients were mainly women. This is consistent with the facts: the incidence of RA is higher in women than in men, and women are 2 to 3 times that of men, and it occurs more frequently in 30-50 years of age [85-87]. Therefore, the results of this study mainly show the effect of antioxidant therapy in women with RA. Although it also shows potential effects for men, more samples are needed to further

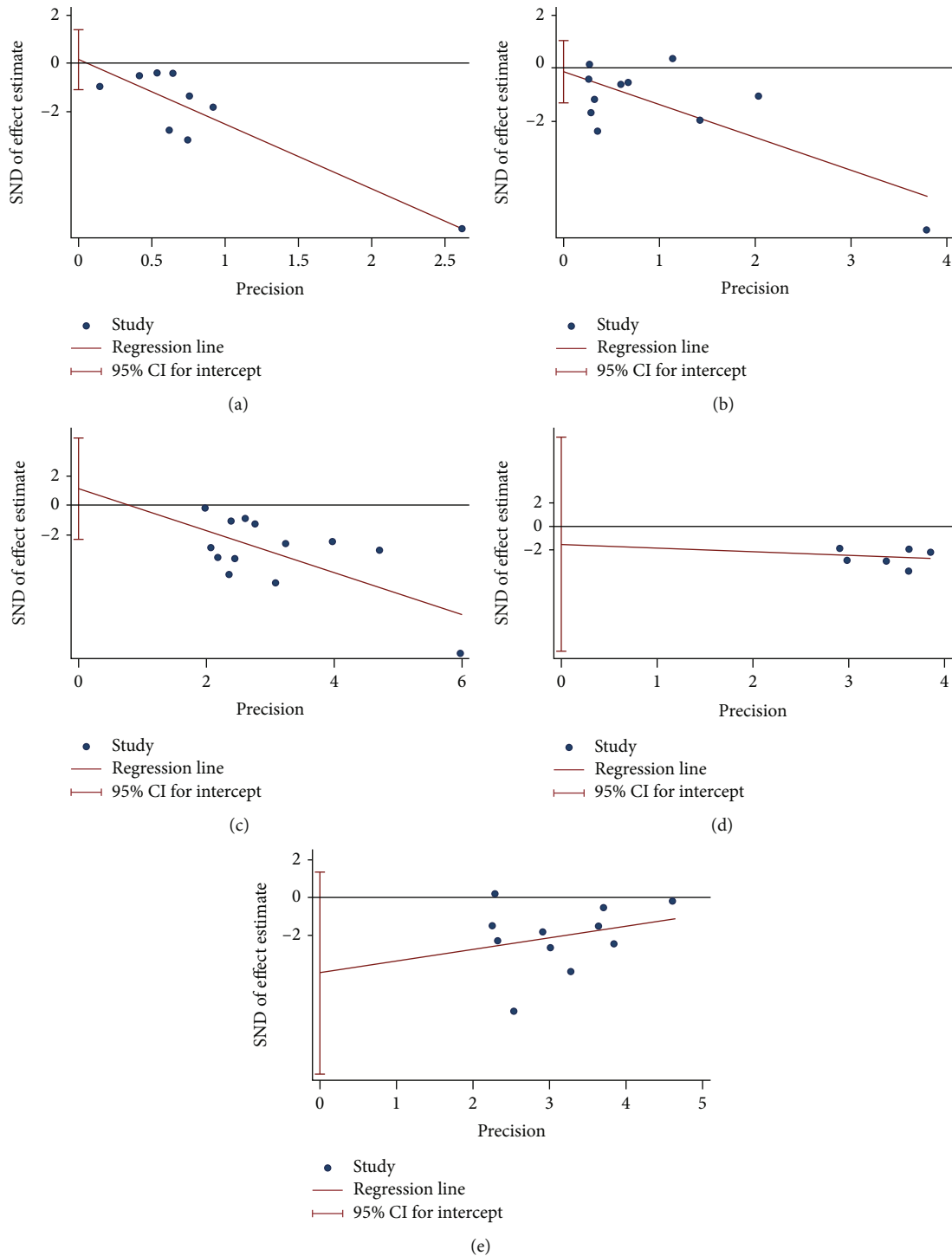


FIGURE 22: Publication bias of clinical efficacy indexes: (a) number of tender joints; (b) number of swollen joints; (c) DAS28; (d) HAQ; (e) VAS.

give better evidence. Most RCTs reported disease duration, baseline CRP, baseline ESR, and baseline DAS28, while a small number of RCTs did not report these baseline data. Baseline data suggest that the disease duration of most patients is more than 5 years, and most RCTs select moderate to severe patients in the active phase for the study.

In general, the quality of RCTs is medium to high. However, since most RCTs are not blinded, and a small number

of studies have not conducted allocation concealment and description of random sequence generation methods, the interpretation of the results still needs to be cautious.

5.4. Strengths and Limitations of This Research and Inspiration for Future Research. The strengths of this research is that it is the first meta-analysis involving the improvement of oxidative stress in RA patients with

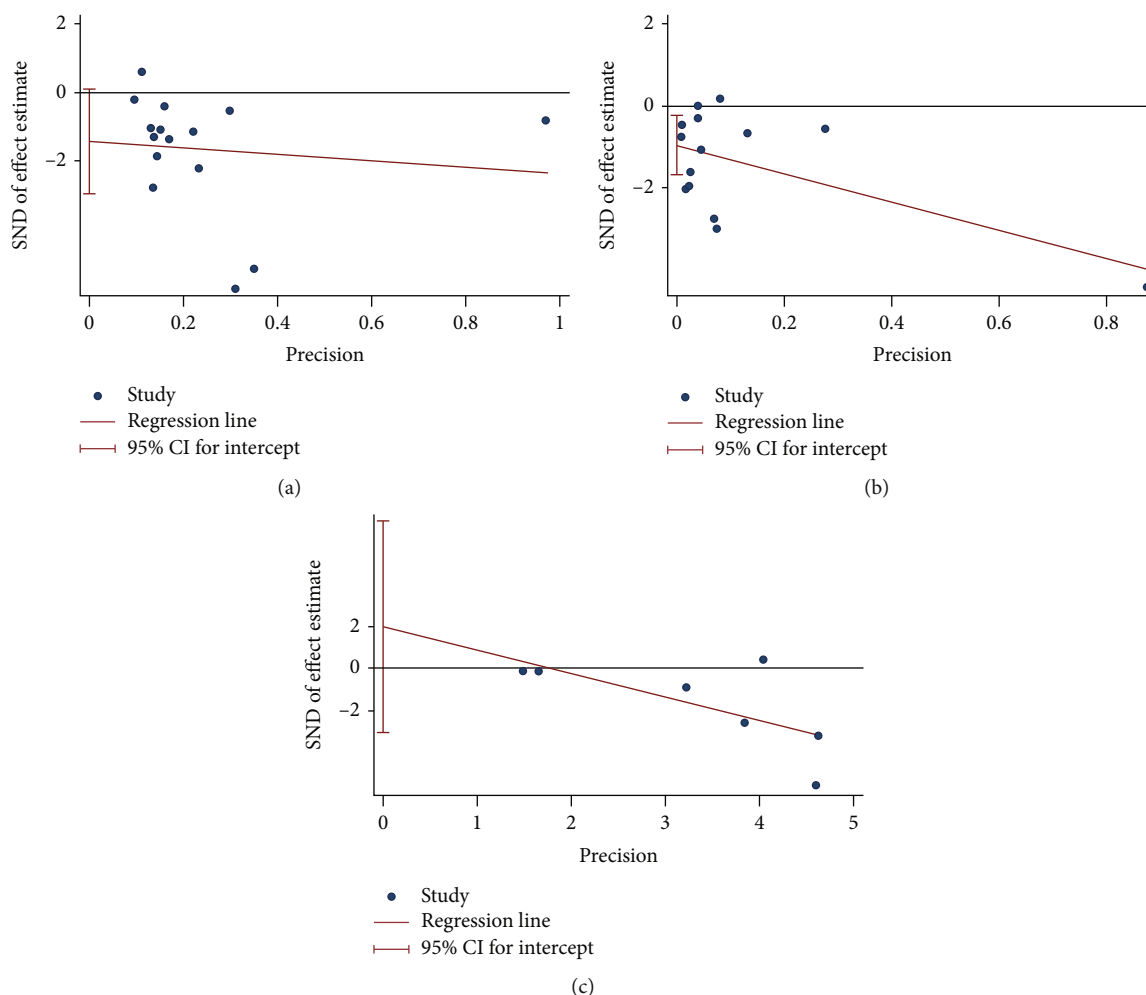


FIGURE 23: Publication bias of inflammation indexes: (a) ESR; (b) CRP; (c) TNF- α .

antioxidants and antioxidant therapies. The RCTs collected in this study span 34 years (1986-2020) involving 1277 participants, and a comprehensive systematic review and meta-analysis of previous related studies have been extensively conducted. The quality of RCT is generally high. In addition, the RCTs included this time involve multiple countries and ethnic groups, including Belgium, China, Cuba, Denmark, Egypt, the UK, Germany, India, Iran, Japan, Korea, and Turkey, which makes the results more applicable.

The limitations of this research is that most subgroups have only one RCT (such as the N-acetylcysteine, pomegranate extract, quercetin, garlic tablets, spa therapy, vitamins A, E, and C combination, and ozone subgroup in MDA; all subgroups of SOD, NO, GPx, CAT, and GSH). This affects the credibility of the results, because only one RCT cannot represent all the population. Meanwhile, there are many RCTs that do not involve indicators of oxidative stress, such as Yin et al. 2017 [18], Bae et al. 2009 [34], Khojah et al. 2018 [35], Aryaeian et al. 2009 [36], Tarp et al. 1986 [39], Peretz et al. 1992 [40], Peretz et al. 2001 [41], Heinle et al. 1997 [42], and Ishibashi et al. 2014 [46]. Therefore, more research on the effects of these therapies on oxidative stress indicators in RA patients is needed. Meanwhile, the intervention duration of these RCTs is different, which

may affect the effect of drug intervention in RA. In addition, although most RCTs are considered to be of high quality, blinding methods (such as Yin et al. 2017 [18], Abdollahzad et al. 2015 [19, 20], Zhu et al. 2020 [30], Vaghef-Mehrabany et al. 2016 [31], Ghavipour et al. 2016 [33], Javadi et al. 2017 [24, 25], Bae et al. 2009 [34], Khojah et al. 2018 [35], Aryaeian et al. 2009 [36], Edmonds et al. 1997 [37], Wittenborg et al. 1998 [38], Tarp et al. 1986 [39], Peretz et al. 1992 [40], Peretz et al. 2001 [41], Heinle et al. 1997 [42], Karagülle et al. 2017 [43], Jaswal et al. 2003 [44], León Fernández et al. 2016 [45], and Ishibashi et al. 2014 [46]) are not used. The main reason they were rated as low risk of bias was that the main outcome indicators were objective indicators (serum MDA, etc.). However, we still need to be vigilant, because the failure to implement blinding may affect other outcome indicators that are not focused on in this study. Therefore, in the future, more well-designed, randomized controlled double-blind clinical trials are needed to verify or modify the outcome indicators.

In MDA outcomes, there was a result contrary to most results: the MDA in the pomegranate extract group was higher than that of the control group. This is a very interesting result, because it suggests that pomegranate extract may

have a reverse effect. However, since there is only one RCT, the result is unstable. Therefore, we look forward to more pomegranate extract-related RCTs in the future. In addition, although current RCTs show that antioxidants or antioxidant therapies do not increase the incidence of adverse events, most RCTs do not report safety outcomes. Therefore, it is expected that future RCTs will report more on the incidence of corresponding adverse events to determine the safety of those therapy.

6. Conclusion

Oxidative stress plays an important role in the pathophysiology of RA. This study showed through systematic reviews and meta-analysis that although there are currently fewer RCTs for antioxidant therapy, the existing evidence shows potential benefits, mainly in reducing MDA and increasing TAC and GSH. Meanwhile, it was also found that the combination of antioxidant therapy and conventional therapy is the main choice for reducing RA disease and preventing cardiovascular complications in the future. However, considering the small number of patients recruited, the study design varies greatly between different RCT studies, and the characteristics of RA participants included in different RCT studies are not the same; it is difficult to immediately extrapolate these results to general RA patients. In the future, more large samples and higher quality RCTs are needed to provide high-quality evidence, so as to provide more clinical reference information for the antioxidant treatment of RA.

Data Availability

All data generated or analyzed during this study are included in this published article.

Conflicts of Interest

We declare no competing interests.

Authors' Contributions

Liuting Zeng and Ganpeng Yu contributed equally to this work. Liuting Zeng and Ganpeng Yu should be considered joint first authors. Hua Chen is the first corresponding author because he supervised the study.

Supplementary Materials

Supplementary 1. Table S1: search strategies for PubMed and Embase.

Supplementary 2. PRISMA 2020 checklist: checklist.

References

- [1] C. G. Helmick, D. T. Felson, R. C. Lawrence et al., "Estimates of the prevalence of arthritis and other rheumatic conditions in the United States: Part I," *Arthritis & Rheumatism*, vol. 58, no. 1, pp. 15–25, 2008.
- [2] E. Myasoedova, C. S. Crowson, H. M. Kremers, T. M. Therneau, and S. E. Gabriel, "Is the incidence of rheumatoid arthritis rising?: results from Olmsted County, Minnesota, 1955–2007," *Arthritis and Rheumatism*, vol. 62, no. 6, pp. 1576–1582, 2010.
- [3] C. Yu, M. Li, X. Duan et al., "Chinese registry of rheumatoid arthritis (CREDIT): I. Introduction and prevalence of remission in Chinese patients with rheumatoid arthritis," *Clinical and experimental rheumatology*, vol. 36, no. 5, pp. 836–840, 2018.
- [4] CREDIT Co-authors, S. Jin, M. Li et al., "Chinese Registry of rheumatoid arthritis (CREDIT): II. Prevalence and risk factors of major comorbidities in Chinese patients with rheumatoid arthritis," *Arthritis research & therapy*, vol. 19, no. 1, p. 251, 2017.
- [5] Y. Dai, W. Wang, Y. Yu, and S. Hu, "Rheumatoid arthritis-associated interstitial lung disease: an overview of epidemiology, pathogenesis and management," *Clinical Rheumatology*, vol. 40, no. 4, pp. 1211–1220, 2021.
- [6] D. L. Scott, F. Wolfe, and T. W. Huizinga, "Rheumatoid arthritis," *Lancet*, vol. 376, no. 9746, pp. 1094–1108, 2010.
- [7] I. B. McInnes and G. Schett, "The pathogenesis of rheumatoid arthritis," *The New England Journal of Medicine*, vol. 365, no. 23, pp. 2205–2219, 2011.
- [8] X. Song and Q. Lin, "Genomics, transcriptomics and proteomics to elucidate the pathogenesis of rheumatoid arthritis," *Rheumatology international*, vol. 37, no. 8, pp. 1257–1265, 2017.
- [9] G. R. Burmester and J. E. Pope, "Novel treatment strategies in rheumatoid arthritis," *Lancet*, vol. 389, no. 10086, pp. 2338–2348, 2017.
- [10] A. R. Phull, B. Nasir, I. U. Haq, and S. J. Kim, "Oxidative stress, consequences and ROS mediated cellular signaling in rheumatoid arthritis," *Chemico-biological interactions*, vol. 281, no. 7, pp. 121–136, 2018.
- [11] L. J. S. da Fonseca, V. Nunes-Souza, M. O. F. Goulart, and L. A. Rabelo, "Oxidative stress in rheumatoid arthritis: what the future might hold regarding novel biomarkers and add-on therapies," *Oxidative medicine and cellular longevity*, vol. 2019, no. 7, Article ID 7536805, p. 16, 2019.
- [12] A. Bala, C. Mondal, P. K. Haldar, and B. Khandelwal, "Oxidative stress in inflammatory cells of patient with rheumatoid arthritis: clinical efficacy of dietary antioxidants," *Inflammopharmacology*, vol. 25, no. 6, pp. 595–607, 2017.
- [13] M. J. Smallwood, A. Nissim, A. R. Knight, M. Whiteman, R. Haigh, and P. G. Winyard, "Oxidative stress in autoimmune rheumatic diseases," *Free Radical Biology and Medicine*, vol. 125, pp. 3–14, 2018.
- [14] S. Mateen, S. Moin, A. Q. Khan, A. Zafar, and N. Fatima, "Increased reactive oxygen species formation and oxidative stress in rheumatoid arthritis," *PLoS One*, vol. 11, no. 4, article e0152925, 2016.
- [15] E. Balogh, D. J. Veale, T. McGarry et al., "Oxidative stress impairs energy metabolism in primary cells and synovial tissue of patients with rheumatoid arthritis," *Arthritis Research & Therapy*, vol. 20, no. 1, p. 95, 2018.
- [16] G. Hashemi, M. Mirjalili, Z. Basiri et al., "A pilot study to evaluate the effects of oral N-acetyl cysteine on inflammatory and oxidative stress biomarkers in rheumatoid arthritis," *Current rheumatology reviews*, vol. 15, no. 3, pp. 246–253, 2019.
- [17] M. Batooei, A. Tahamoli-Roudsari, Z. Basiri et al., "Evaluating the effect of oral N-acetylcysteine as an adjuvant treatment on clinical outcomes of patients with rheumatoid arthritis: a

- randomized, double blind clinical trial,” *Reviews on Recent Clinical Trials*, vol. 13, no. 2, pp. 132–138, 2018.
- [18] T. T. Yin, X. Y. Gu, W. Z. Feng, Y. K. Hou, T. P. Yu, and M. Li, “Effects of N-acetylcysteine combined with pulmonary rehabilitation on exercise endurance and quality of life in patients with rheumatoid arthritis-related interstitial lung disease,” *Practical Medicines and Clinics*, vol. 20, no. 3, pp. 290–293, 2017.
- [19] H. Abdollahzad, M. A. Aghdashi, M. Asghari Jafarabadi, and B. Alipour, “Effects of coenzyme Q10 supplementation on inflammatory cytokines (TNF- α , IL-6) and oxidative stress in rheumatoid arthritis patients: a randomized controlled trial,” *Archives of Medical Research*, vol. 46, no. 7, pp. 527–533, 2015.
- [20] S. M. Nachvak, B. Alipour, A. M. Mahdavi et al., “Effects of coenzyme Q10 supplementation on matrix metalloproteinases and DAS-28 in patients with rheumatoid arthritis: a randomized, double-blind, placebo-controlled clinical trial,” *Clinical Rheumatology*, vol. 38, no. 12, pp. 3367–3374, 2019.
- [21] M. J. Page, J. E. McKenzie, P. M. Bossuyt et al., “The PRISMA 2020 statement: an updated guideline for reporting systematic reviews,” *BMJ*, vol. 372, p. n71, 2021.
- [22] J. J. Deeks, J. P. Higgins, and D. G. Altman, “Chapter 8: assessing risk of bias in included studies,” in *Cochrane Handbook or Systematic Reviews of Interventions Version 6.1.0*, J. P. Higgins and S. Green, Eds., UK, The Cochrane Collaboration, 2020.
- [23] J. J. Deeks, J. P. Higgins, and D. G. Altman, “Chapter 16: special topics in statistics,” in *Cochrane Handbook for Systematic Reviews of Interventions*, J. P. Higgins and S. Green, Eds., The Cochrane Collaboration, UK, 2020.
- [24] F. Javadi, A. Ahmadzadeh, S. Eghtesadi et al., “The effect of quercetin on inflammatory factors and clinical symptoms in women with rheumatoid arthritis: a double-blind, randomized controlled trial,” *Journal of the American College of Nutrition*, vol. 36, no. 1, pp. 9–15, 2017.
- [25] F. Javadi, S. Eghtesadi, A. Ahmadzadeh et al., “The effect of quercetin on plasma oxidative status, C-reactive protein and blood pressure in women with rheumatoid arthritis,” *International Journal of Preventive Medicine*, vol. 5, no. 3, pp. 293–301, 2014.
- [26] S. P. Moosavian, Z. Paknahad, and Z. Habibagahi, “A randomized, double-blind, placebo-controlled clinical trial, evaluating the garlic supplement effects on some serum biomarkers of oxidative stress, and quality of life in women with rheumatoid arthritis,” *International journal of clinical practice*, vol. 74, no. 7, article e13498, 2020.
- [27] S. P. Moosavian, Z. Paknahad, Z. Habibagahi, and M. Maracy, “The effects of garlic (*Allium sativum*) supplementation on inflammatory biomarkers, fatigue, and clinical symptoms in patients with active rheumatoid arthritis: a randomized, double-blind, placebo-controlled trial,” *Phytotherapy Research*, vol. 34, no. 11, pp. 2953–2962, 2020.
- [28] E. Mirtaheri, B. Pourghassem Gargari, S. Kolahi et al., “Effects of alpha-lipoic acid supplementation on inflammatory biomarkers and matrix metalloproteinase-3 in rheumatoid arthritis patients,” *Journal of the American College of Nutrition*, vol. 34, no. 4, pp. 310–317, 2015.
- [29] S. Kolahi, E. Mirtaheri, B. Pourghassem Gargari et al., “Oral administration of alpha-lipoic acid did not affect lipid peroxidation and antioxidant biomarkers in rheumatoid arthritis patients,” *International Journal for Vitamin and Nutrition Research*, vol. 89, no. 1-2, pp. 13–21, 2019.
- [30] K. D. Zhu, L. J. Wang, F. Y. Liu, and H. Y. Gu, “Effects of coenzyme Q₁₀ on the levels of pro-inflammatory cytokines and oxidative stress in patients with rheumatoid arthritis,” *Guangxi Medical Journal*, vol. 42, no. 4, pp. 417–420+460, 2020.
- [31] E. Vaghef-Mehrabany, A. Homayouni-Rad, B. Alipour, S. K. Sharif, L. Vaghef-Mehrabany, and S. Alipour-Ajiry, “Effects of probiotic supplementation on oxidative stress indices in women with rheumatoid arthritis: a randomized double-blind clinical trial,” *Journal of the American College of Nutrition*, vol. 35, no. 4, pp. 291–299, 2016.
- [32] B. Zamani, S. Farshbaf, H. R. Golkar, F. Bahmani, and Z. Asemi, “Synbiotic supplementation and the effects on clinical and metabolic responses in patients with rheumatoid arthritis: a randomised, double-blind, placebo-controlled trial,” *The British Journal of Nutrition*, vol. 117, no. 8, pp. 1095–1102, 2017.
- [33] M. Ghavipour, G. Sotoudeh, E. Tavakoli, K. Mowla, J. Hasanzadeh, and Z. Mazloom, “Pomegranate extract alleviates disease activity and some blood biomarkers of inflammation and oxidative stress in rheumatoid arthritis patients,” *European Journal of Clinical Nutrition*, vol. 71, no. 1, pp. 92–96, 2017.
- [34] S. C. Bae, W. J. Jung, E. J. Lee, R. Yu, and M. K. Sung, “Effects of antioxidant supplements intervention on the level of plasma inflammatory molecules and disease severity of rheumatoid arthritis patients,” *Journal of the American College of Nutrition*, vol. 28, no. 1, pp. 56–62, 2009.
- [35] H. M. Khojah, S. Ahmed, M. S. Abdel-Rahman, and E. H. Elhakeim, “Resveratrol as an effective adjuvant therapy in the management of rheumatoid arthritis: a clinical study,” *Clinical Rheumatology*, vol. 37, no. 8, pp. 2035–2042, 2018.
- [36] N. Aryaeian, F. Shahram, M. Djalali et al., “Effect of conjugated linoleic acids, vitamin E and their combination on the clinical outcome of Iranian adults with active rheumatoid arthritis,” *International Journal of Rheumatic Diseases*, vol. 12, no. 1, pp. 20–28, 2009.
- [37] S. E. Edmonds, P. G. Winyard, R. Guo et al., “Putative analgesic activity of repeated oral doses of vitamin E in the treatment of rheumatoid arthritis. Results of a prospective placebo controlled double blind trial,” *Annals of the rheumatic diseases*, vol. 56, no. 11, pp. 649–655, 1997.
- [38] A. Wittenborg, G. Petersen, G. Lorkowski, and T. Brabant, “Wirksamkeit von Vitamin E im Vergleich zu Diclofenac-Natrium in der Behandlung von Patienten mit chronischer Polyarthritits,” *Zeitschrift für Rheumatologie*, vol. 57, no. 4, pp. 215–221, 1998.
- [39] U. Tarp, K. Overvad, E. B. Thorling, H. Graudal, and J. C. Hansen, “Selenium treatment in rheumatoid arthritis,” *Acta Pharmacol Toxicol (Copenh)*, vol. 59, no. S7, pp. 382–385, 1986.
- [40] A. Peretz, J. Neve, J. Duchateau, and J. P. Famaey, “Adjuvant treatment of recent onset rheumatoid arthritis by selenium supplementation: preliminary observations,” *British Journal of Rheumatology*, vol. 31, no. 4, pp. 281–282, 1992.
- [41] A. Peretz, V. Siderova, and J. Nève, “Selenium supplementation in rheumatoid arthritis investigated in a double blind, placebo-controlled trial,” *Scandinavian Journal of Rheumatology*, vol. 30, no. 4, pp. 208–212, 2001.
- [42] K. Heinle, A. Adam, M. Gradl, M. Wiseman, and O. Adam, “Selenkonzentration in den Erythrozyten bei Patienten mit rheumatoider Arthritis,” *Medizinische Klinik (Munich)*, vol. 92, no. S3, pp. 29–31, 1997.

- [43] M. Karagülle, S. Kardeş, O. Karagülle et al., "Effect of spa therapy with saline balneotherapy on oxidant/antioxidant status in patients with rheumatoid arthritis: a single-blind randomized controlled trial," *International journal of biometeorology*, vol. 61, no. 1, pp. 169–180, 2017.
- [44] S. Jaswal, H. C. Mehta, A. K. Sood, and J. Kaur, "Antioxidant status in rheumatoid arthritis and role of antioxidant therapy," *Clinica Chimica Acta*, vol. 338, no. 1-2, pp. 123–129, 2003.
- [45] O. S. León Fernández, R. Viebahn-Haensler, G. L. Cabreja et al., "Medical ozone increases methotrexate clinical response and improves cellular redox balance in patients with rheumatoid arthritis," *European journal of pharmacology*, vol. 789, pp. 313–318, 2016.
- [46] T. Ishibashi, B. Sato, S. Shibata et al., "Therapeutic efficacy of infused molecular hydrogen in saline on rheumatoid arthritis: a randomized, double-blind, placebo-controlled pilot study," *International Immunopharmacology*, vol. 21, no. 2, pp. 468–473, 2014.
- [47] J. F. Koster, P. Biemond, and A. J. Swaak, "Intracellular and extracellular sulphhydryl levels in rheumatoid arthritis," *Annals of the Rheumatic Diseases*, vol. 45, no. 1, pp. 44–46, 1986.
- [48] M. Veselinovic, N. Barudzic, M. Vuletic et al., "Oxidative stress in rheumatoid arthritis patients: relationship to diseases activity," *Molecular and Cellular Biochemistry*, vol. 391, no. 1-2, pp. 225–232, 2014.
- [49] A. Garcia-Gonzalez, R. Gaxiola-Robles, and T. Zenteno-Savin, "Oxidative stress in patients with rheumatoid arthritis," *Revista de investigacion clinica; organo del Hospital de Enfermedades de la Nutricion*, vol. 67, no. 1, pp. 46–53, 2015.
- [50] C. Quiñonez-Flores, S. A. González-Chávez, D. del Río Nájera, and C. Pacheco-Tena, "Oxidative stress relevance in the pathogenesis of the rheumatoid arthritis: a systematic review," *BioMed Research International*, vol. 2016, Article ID 6097417, 14 pages, 2016.
- [51] I. Túnez, M. Feijóo, G. Huerta et al., "The effect of infliximab on oxidative stress in chronic inflammatory joint disease," *Current Medical Research and Opinion*, vol. 23, no. 6, pp. 1259–1267, 2007.
- [52] W. Droge, "Free radicals in the physiological control of cell function," *Physiological Reviews*, vol. 82, no. 1, pp. 47–95, 2002.
- [53] J. Vásquez-Vivar, B. Kalyanaraman, P. Martíásek et al., "Superoxide generation by endothelial nitric oxide synthase: the influence of cofactors," *Proceedings of the National Academy of Sciences of the United States of America*, vol. 95, no. 16, pp. 9220–9225, 1998.
- [54] J. R. Stone and S. Yang, "Hydrogen peroxide: a signaling messenger," *Antioxidants & Redox Signaling*, vol. 8, no. 3-4, pp. 243–270, 2006.
- [55] S. G. Rhee, "Redox signaling: hydrogen peroxide as intracellular messenger," *Experimental & Molecular Medicine*, vol. 31, no. 2, pp. 53–59, 1999.
- [56] J. L. Beal, S. B. Foster, and M. T. Ashby, "Hypochlorous acid reacts with the N-terminal methionines of proteins to give dehydromethionine, a potential biomarker for neutrophil-induced oxidative stress," *Biochemistry*, vol. 48, no. 46, pp. 11142–11148, 2009.
- [57] P. Pacher, J. S. Beckman, and L. Liaudet, "Nitric oxide and peroxynitrite in health and disease," *Physiological Reviews*, vol. 87, no. 1, pp. 315–424, 2007.
- [58] S. Moncada, "Nitric oxide in the vasculature: physiology and pathophysiology," *Annals of the New York Academy of Science*, vol. 811, no. 1 Atherosclerosis, pp. 60–69, 1997.
- [59] L. J. Ignarro, R. E. Byrns, G. M. Buga, and K. S. Wood, "Endothelium-derived relaxing factor from pulmonary artery and vein possesses pharmacologic and chemical properties identical to those of nitric oxide radical," *Circulation Research*, vol. 61, no. 6, pp. 866–879, 1987.
- [60] L. J. Ignarro, G. M. Buga, K. S. Wood, R. E. Byrns, and G. Chaudhuri, "Endothelium-derived relaxing factor produced and released from artery and vein is nitric oxide," *Proceedings of the National Academy of Sciences of the United States of America*, vol. 84, no. 24, pp. 9265–9269, 1987.
- [61] R. M. Palmer, A. G. Ferrige, and S. Moncada, "Nitric oxide release accounts for the biological activity of endothelium-derived relaxing factor," *Nature*, vol. 327, no. 6122, pp. 524–526, 1987.
- [62] G. Ferrer-Sueta and R. Radi, "Chemical biology of peroxynitrite: kinetics, diffusion, and radicals," *ACS Chemical Biology*, vol. 4, no. 3, pp. 161–177, 2009.
- [63] M. Trujillo, G. Ferrer-Sueta, and R. Radi, "Peroxynitrite detoxification and its biologic implications," *Antioxidants & Redox Signaling*, vol. 10, no. 9, pp. 1607–1620, 2008.
- [64] L. A. Ridgley, A. E. Anderson, and A. G. Pratt, "What are the dominant cytokines in early rheumatoid arthritis?," *Current Opinion in Rheumatology*, vol. 30, no. 2, pp. 207–214, 2018.
- [65] T. Fukai and M. Ushio-Fukai, "Superoxide dismutases: role in redox signaling, vascular function, and diseases," *Antioxidants & Redox Signaling*, vol. 15, no. 6, pp. 1583–1606, 2011.
- [66] J. McCord and I. Fridovich, "Superoxide Dismutase: AN ENZYMIC FUNCTION FOR ERYTHROCUPREIN (HEMO-CUPREIN)," *The Journal of Biological Chemistry*, vol. 244, no. 22, pp. 6049–6055, 1969.
- [67] J. McCord and I. Fridovich, "The Utility of Superoxide Dismutase in Studying Free Radical Reactions: I. RADICALS GENERATED BY THE INTERACTION OF SULFITE, DIMETHYL SULFOXIDE, AND OXYGEN," *The Journal of Biological Chemistry*, vol. 244, no. 22, pp. 6056–6063, 1969.
- [68] A. Deisseroth and A. L. Dounce, "Catalase: physical and chemical properties, mechanism of catalysis, and physiological role," *Physiological Reviews*, vol. 50, no. 3, pp. 319–375, 1970.
- [69] R. Margis, C. Dunand, F. K. Teixeira, and M. Margis-Pinheiro, "Glutathione peroxidase family - an evolutionary overview," *The FEBS Journal*, vol. 275, no. 15, pp. 3959–3970, 2008.
- [70] N. Couto, J. Wood, and J. Barber, "The role of glutathione reductase and related enzymes on cellular redox homeostasis network," *Free Radical Biology & Medicine*, vol. 95, pp. 27–42, 2016.
- [71] M. Balsera and B. B. Buchanan, "Evolution of the thioredoxin system as a step enabling adaptation to oxidative stress," *Free Radical Biology & Medicine*, vol. 140, pp. 28–35, 2019.
- [72] X. G. Lei, J. H. Zhu, W. H. Cheng et al., "Paradoxical roles of antioxidant enzymes: basic mechanisms and health implications," *Physiological Reviews*, vol. 96, no. 1, pp. 307–364, 2016.
- [73] S. G. Sukkar and E. Rossi, "Oxidative stress and nutritional prevention in autoimmune rheumatic diseases," *Autoimmunity Reviews*, vol. 3, no. 3, pp. 199–206, 2004.
- [74] A. Nakajima, Y. Aoki, Y. Shibata et al., "Identification of clinical parameters associated with serum oxidative stress in patients with rheumatoid arthritis," *Modern Rheumatology*, vol. 24, no. 6, pp. 926–930, 2014.

- [75] S. Türk, D. Ü. Cansu, H. Ü. Teke et al., “Can we predict thrombotic tendency in rheumatoid arthritis? A thromboelastographic analysis (with ROTEM),” *Clinical Rheumatology*, vol. 37, no. 9, pp. 2341–2349, 2018.
- [76] A. Balbir-Gurman, B. Fuhrman, Y. Braun-Moscovici, D. Markovits, and M. Aviram, “Consumption of pomegranate decreases serum oxidative stress and reduces disease activity in patients with active rheumatoid arthritis: a pilot study,” *The Israel Medical Association Journal: IMAJ*, vol. 13, no. 8, pp. 474–479, 2011.
- [77] M. Feijóo, I. Túnez, I. Tasset et al., “Infliximab reduces myeloperoxidase concentration in chronic inflammatory joint diseases,” *Pharmacology*, vol. 83, no. 4, pp. 211–216, 2009.
- [78] H. Hirvonen, H. Kautiainen, E. Moilanen, M. Mikkelsen, and M. Leirisalo-Repo, “The effect of cryotherapy on total antioxidative capacity in patients with active seropositive rheumatoid arthritis,” *Rheumatology International*, vol. 37, no. 9, pp. 1481–1487, 2017.
- [79] A. Wadley, J. J. C. S. V. van Zanten, A. Stavropoulos-Kalinooglou et al., “Three months of moderate-intensity exercise reduced plasma 3-nitrotyrosine in rheumatoid arthritis patients,” *European Journal of Applied Physiology*, vol. 114, no. 7, pp. 1483–1492, 2014.
- [80] B. Helli, K. Mowla, M. Mohammadshahi, and M. T. Jalali, “Effect of sesamin supplementation on cardiovascular risk factors in women with rheumatoid arthritis,” *Journal of the American College of Nutrition*, vol. 35, no. 4, pp. 300–307, 2016.
- [81] A. M. M. Attia, F. A. A. Ibrahim, N. A. Abd el-Latif et al., “Therapeutic antioxidant and anti-inflammatory effects of laser acupuncture on patients with rheumatoid arthritis,” *Lasers in Surgery and Medicine*, vol. 48, no. 5, pp. 490–497, 2016.
- [82] R. Bordy, P. Totoson, C. Prati, C. Marie, D. Wendling, and C. Demougeot, “Microvascular endothelial dysfunction in rheumatoid arthritis,” *Nature Reviews Rheumatology*, vol. 14, no. 7, pp. 404–420, 2018.
- [83] V. Pasceri and E. T. H. Yeh, “A tale of two diseases,” *Circulation*, vol. 100, no. 21, pp. 2124–2126, 1999.
- [84] A. J. Flammer, I. Sudano, F. Hermann et al., “Angiotensin-converting enzyme inhibition improves vascular function in rheumatoid arthritis,” *Circulation*, vol. 117, no. 17, pp. 2262–2269, 2008.
- [85] S. Safiri, A. A. Kolahi, D. Hoy et al., “Global, regional and national burden of rheumatoid arthritis 1990–2017: a systematic analysis of the global burden of disease study 2017,” *Annals of the rheumatic diseases*, vol. 78, no. 11, pp. 1463–1471, 2019.
- [86] T. Otón and L. Carmona, “The epidemiology of established rheumatoid arthritis,” *Best Practice & Research. Clinical Rheumatology*, vol. 33, no. 5, article 101477, 2019.
- [87] E. Myasoedova, J. Davis, E. L. Matteson, and C. S. Crowson, “Is the epidemiology of rheumatoid arthritis changing? Results from a population-based incidence study, 1985–2014,” *Annals of the rheumatic diseases*, vol. 79, no. 4, pp. 440–444, 2020.

Research Article

YAP-Dependent Induction of CD47-Enriched Extracellular Vesicles Inhibits Dendritic Cell Activation and Ameliorates Hepatic Ischemia-Reperfusion Injury

Zenan Yuan,^{1,2} Linsen Ye,^{1,2} Xiao Feng,^{1,2} Tian Zhou,³ Yi Zhou,⁴ Shuguang Zhu,^{1,2} Changchang Jia,⁵ Haibo Li,^{1,2} Dongbo Qiu,⁵ Kun Li,^{1,2} Wei Liu,^{1,2} Yang Li,^{1,2} Hui Tang,^{1,2} Guoying Wang,^{1,2} Qi Zhang,⁵ Yang Yang^{id},^{1,2} Guihua Chen^{id},^{1,2} and Hua Li^{id}^{1,2}

¹Department of Hepatic Surgery and Liver Transplantation Center, The Third Affiliated Hospital of Sun Yat-sen University, Guangzhou, China

²Guangdong Provincial Key Laboratory of Liver Disease Research, Guangzhou, China

³State Key Laboratory of Ophthalmology, Zhongshan Ophthalmic Center, Sun Yat-sen University, Guangzhou, China

⁴Department of General Surgery, Guangdong No.2 Provincial People's Hospital, Guangdong Province, China

⁵Cell-Gene Therapy Translational Medicine Research Center, The Third Affiliated Hospital of Sun Yat-sen University, Guangzhou, China

Correspondence should be addressed to Yang Yang; yyang1971@126.com, Guihua Chen; chgh1955@126.com, and Hua Li; lihua3@mail.sysu.edu.cn

Received 17 December 2020; Revised 10 May 2021; Accepted 30 May 2021; Published 22 June 2021

Academic Editor: Olga Pechanova

Copyright © 2021 Zenan Yuan et al. This is an open access article distributed under the Creative Commons Attribution License, which permits unrestricted use, distribution, and reproduction in any medium, provided the original work is properly cited.

Hepatic ischemia-reperfusion injury (IRI) is the most common cause of liver damage leading to surgical failures in hepatectomy and liver transplantation. Extensive inflammatory reactions and oxidative responses are reported to be the major processes exacerbating IRI. The involvement of Yes-associated protein (YAP) in either process has been suggested, but the role and mechanism of YAP in IRI remain unclear. In this study, we constructed hepatocyte-specific YAP knockout (YAP-HKO) mice and induced a hepatic IRI model. Surprisingly, the amount of serum EVs decreased in YAP-HKO compared to WT mice during hepatic IRI. Then, we found that the activation of YAP increased EV secretion through F-actin by increasing membrane formation, while inhibiting the fusion of multivesicular body (MVB) and lysosomes in hepatocytes. Further, to explore the essential elements of YAP-induced EVs, we applied mass spectrometry and noticed CD47 was among the top targets highly expressed on hepatocyte-derived EVs. Thus, we enriched CD47⁺ EVs by microbeads and applied the isolated CD47⁺ EVs on IRI mice. We found ameliorated IRI symptoms after CD47⁺ EV treatment in these mice, and CD47⁺ EVs bound to CD172 α on the surface of dendritic cells (DCs), which inhibited DC activation and the cascade of inflammatory responses. Our data showed that CD47-enriched EVs were released in a YAP-dependent manner by hepatocytes, which could inhibit DC activation and contribute to the amelioration of hepatic IRI. CD47⁺ EVs could be a potential strategy for treating hepatic IRI.

1. Introduction

Hepatic IRI occurs when blood flow is restored after a period of hepatic ischemia [1, 2]. Since the donated grafts are often highly susceptible to IRI, while the available organs are in severe shortage, IRI has become one of the main obstacles in liver transplantation [3]. There is an urgent need for devel-

oping protective strategies against IRI to promote the survival of patients after liver transplantation.

The mechanisms governing IRI are highly complex and have been the focus of investigation for decades with numerous factors been identified with specific function. Among the principle factors in hepatic IRI, Yes-associated protein (YAP), the key effector of the Hippo pathway, has been

reported to be a hinge joint in inflammation and oxidative stress, but its role and mechanism remain unclear. Some reports suggested that YAP played a protective role in the hepatic IRI model [4], while others found that YAP-expressing hepatocytes activated inflammation and aggregated liver fibrosis through the YAP/TAZ/CYR61 axis [5]. These conflicting findings suggested that the mechanisms in YAP's function have not been fully unveiled, since YAP has been found to regulate the binding of actin and angiominin (AMOT) family members [6], which play an irreplaceable role in endosomal transport and the secretion of extracellular vesicles (EVs) [7]. Here, we investigated the paracrine effect of YAP through the secretion of EVs.

EVs are phospholipid bilayer vesicles widely distributed in body fluids as a form of intercellular communication and modulation of cellular activities in recipient cells. Multiple immunomodulatory effects of EVs have been reported [8, 9], but the mechanism linking hepatic injury to associated immune responses through EVs has not been found. Initiated by hypoxic stress, IRI displayed extensive inflammatory responses that are driven by innate immunity and supported by adaptive immunity [4, 10]. Hepatic DCs act as one of the major mediators in local immune responses [11]. Activated DCs could [12] trigger both innate and adaptive immunity and aggregate local injury. However, reports also showed that hepatic DCs could limit certain inflammation and promote immune tolerance [13]. The immune-modulatory activity of DCs is regulated by the expression level of CD47, the well-known "don't eat me" signal [14]. By binding to the counter-receptor signal-regulated protein alpha (SIRP alpha/CD172a), which is mainly expressed on the surface of myeloid cells, CD47 could initiate the inhibitory signaling to restrain inflammation [15, 16].

In this study, we found CD47 on hepatic EVs targeted CD172⁺ DCs and potentially inhibited their activation, therefore alleviated hepatic IRI, whereas YAP expression is required for EV secretion of hepatocytes. Mechanistically, YAP induced EV secretion through F-actin by increasing membrane formation, with the inhibition of MVB and lysosome fusion. Our results revealed a novel mechanism for maintaining immune balance in hepatic IRI, via the regulation of YAP-EV-CD47 axis in hepatocyte-DC crosstalk, which suggested a novel therapeutic strategy utilizing CD47⁺ EVs in treating hepatic IRI.

2. Methods

2.1. Human Subjects. The selected samples were from 69 patients who underwent liver transplantation from donors after cardiac death (DCD) since April 2010 to April 2015 at the liver transplantation center of the third affiliated hospital, Sun Yat-sen University. Cases of 64 males and 5 females were included, with an average age of 47.43 years (21-72 years), and were all treated by modified piggyback orthotopic liver transplantation surgery. The details of the patient demographics are listed in Supplementary Table 1. The selection criteria were as published [17].

2.2. Animals. Six to eight weeks of C57BL/6J, BALB/c male mice were obtained from Guangzhou University of Chinese Medicine, China. YAP-HKO mice were constructed by crossing Albumin-Cre (*Alb-Cre*) mice and *Yap*^{fllox/fllox} mice from the Model Animal Research Center of Nanjing University (Nanjing, China). CD11c-DTR mice were purchased from Jackson Laboratory (Farmington, CT, USA). All the animal experiments conducted in this study were approved by the animal ethics committee of the third affiliated hospital of Sun Yat-sen University.

2.3. Mouse Hepatic IRI Model. The 70% liver ischemia-reperfusion (I/R) injury model was constructed after 0.6% pentobarbital sodium (100 μ L/10 g) was injected intraperitoneally [17]. In brief, the artery/portal vessel was clamped to the cephalad lobes for 90 minutes during ischemia, and reperfusion was performed by loosening the atraumatic vascular clamp. The sham operation group underwent the same operation except that blood vessels were not clamped. Animals received injections of EVs (100 μ g/kg b.w. in PBS) or PBS immediately before reperfusion.

2.4. Cells and Reagents. Human hepatic L02 cells from the Cell Bank of the Chinese Academy of Sciences in Shanghai were used in the *in vitro* experiments [18]. Antibodies against YAP1 (ab56701, Abcam), Alix (ab186429, Abcam), CD81 (D5O2Q, CST), TSG101 (ab125011, Abcam), β -actin (8H10D10, CST), calnexin (ab22595, Abcam), and CD47 (ab175388, Abcam) were used for western blot. When CD47 was blocked, two doses of 100 μ g (BE0270, BioXcell) were given intraperitoneally two days before IRI and the same day at IRI. The control group used the same dose of rat immunoglobulin G2a (IgG2a) isotype (BioXcell) [19].

2.5. EV Isolation and Analysis. EVs in mouse serum were isolated with an EV isolation kit (SmartSEC Mini EV Isolation System) and detected with an ELISA kit detecting CD81 exosome (EXOEL-CD81A-1) from System Biosciences.

L02 and primary hepatocytes (PMH) were cultured 48 hours at 37°C in serum-free DMEM. The supernatant was collected and centrifuged at 2,000 *g* for 10 min at 4°C to remove the cell debris [20]. Then, after filtering through 0.22 μ m filters, the filtrate was ultracentrifuged at 100,000 *g* for 120 minutes in a Beckman SW28Ti rotor. After the resuspension by PBS, the pellets were ultracentrifuged again at 100,000 *g* for 120 min. The final EV pellets were dissolved in PBS for further experiments [20].

To isolate CD47⁺ EVs, a total of 200 μ g PMH-EVs were mixed with nonblocking anti-CD47 antibody (REA170)-FITC for 30 min at 4°C. Then, incubated with anti-FITC magnetic beads (Miltenyi Biotec; 1 μ L/ μ g EVs) overnight at 4°C. CD47⁻ EVs and CD47⁺ EVs were separated by magnetic beads, and both supernatants were washed with PBS and pelleted by ultracentrifugation.

EVs were further analyzed by a Micro BCA Protein Assay Kit to determine protein concentrations (Thermo, #23235). Particle diameters and amounts were observed by the NanoSight system (NS300, Malvern, Ranch Cucamonga, CA,

USA). Further details of methods were described in supplementary materials (available here).

2.6. Real Time-PCR Analysis. Real-time PCR was performed using the following primer sequences [21]: YAP-forward: CCCAGACTACCTTGAAGCCA and YAP-reverse: CTTCCTGCAGACTTGGCATC; CYR61-forward: CTGCAGCAA AACTCAGCCCT and CACAGGGTCTGCCTTCTFAC and CYR61-reverse: CTTCTGCAGACTTGGCATC; TRX1-forward: ATGGTGAAGCTGATCGAGAGC and TRX1-reverse: GGCATATTCAGTAATAGAGGC; HO-1-forward: GCAGAGAATGCTGAGTTCATG and HO-1-reverse: CACATCTATGTGGCCCTGGAGGAGG; GAPDH-forward: GCGGGAAATCGTGCGTGAC and GAPDH-reverse: CGTCATACTCCTGCTTGCTG.

2.7. Histopathology and Immunostaining. Tissues were fixed by 4% paraformaldehyde and embedded in paraffin, followed by slicing with a microtome and staining with hematoxylin-eosin. For the graft biopsy, the immunohistochemical staining results were assigned the mean score considering the product of the intensity of the stain and the percentage of positive cells. 0 is negative, 1 to 4 are mildly positive, 5 to 8 are moderately positive, and 9 to 12 are strong positive [22, 23]. Negatives are included in the low group, while weakly positive, moderately positive, and strong positives are included in the high group. Each section was independently assessed by two pathologists. Frozen liver tissue sections or cells were fixed, blocked according to standard procedures [19]. For immunofluorescence analysis, we used antibody YAP (2F12, Novus), RAB7 (ab137029, Abcam), EEA1 (610456, BD Biosciences) [24], LysoTracker™ Red DND-99 (ThermoFisher), Rhodamine Phalloidin (PHDR1, Cytoskeleton), Cy2-conjugated goat anti-rabbit IgG (111-225-144, Jackson ImmunoResearch), and Cy3-conjugated anti-mouse IgG (AP124C, EMD Millipore).

2.8. Plasmid Construction and Transfection. By short hairpin RNA inference, the silenced sh-YAP expression plasmids were purchased from Sigma, with the control group using the nontargeting shRNA expression plasmid (MISSION Plko.1-puro Empty Vector Control Plasmid DNA). The cells were transfected according to standard procedures [25].

2.9. Primary Hepatocyte Isolation. The liver was perfused with an immunoenzyme (10 units) to digest connective tissue [19]. Then, use Percoll gradient to purify primary hepatocytes.

2.10. Hepatic Lymphocyte Isolation. After the liver tissue was gently crushed, the lymphocytes were obtained using percoll gradient purification [19]. Then, the cell suspension was stained for viability analysis, and markers including CD45, CD47, CD172a, CD11c, I-A/I-E, TNF- α , and IL-12 p40 (eBioscience, San Diego, CA).

2.11. T Cell Isolation. CD4⁺ and CD8⁺ T cells were isolated from the spleen of experiment mice by CD4⁺ and CD8⁺ T cell isolation kit II (Miltenyi Biotec, Bergisch Gladbach, Ger-

many) and followed by labeling with CFSE (Invitrogen) according to the manufacturer's instructions [26].

2.12. DC Function Assay. Bone marrow monocytes were obtained from the cell suspension of mouse tibia and femur [27]. To generate bone marrow-derived DC (BMDCs), 10 ng/mL recombinant mouse granulocyte-macrophage colony-stimulating factor (rmGM-CSF) and 1 ng/mL IL-4 (R&D) were added in the medium (Figure S2C). BMDCs were collected after verifying purity (more than 95% CD11c positive) and 1×10^6 /mL cells were incubated under 1 mg/mL LPS stimulation, and the experiment group was supplemented with 30 mg/mL EVs for 24 h, with PBS supplemented as control. To evaluate the antigen-presenting ability of DCs, LPS-stimulated BMDCs were collected and cocultured with CFSE-labeled CD4⁺ and CD8⁺ T cells from BALB/c mouse at a ratio of 1:10 for 96 hours.

2.13. Cytokine ELISA. Both murine serum and culture supernatants from BMDCs were harvested for further cytokine analysis [28]. ELISA kits to measure IL-12 p40, TNF- α , and IL-6 levels individually were purchased and used under the manufacturers' instructions (eBioscience, San Diego, CA).

2.14. Immunogold Electron Microscopy. For immune electron microscopy, we used anti-CD47 antibody (Novus-NBP2-44408) for primary staining and incubated overnight at 4°C. Then, we applied 18 nm colloidal gold-conjugated goat anti-mouse IgG (115-215-166, Jackson ImmunoResearch) as the secondary antibodies. The following steps were performed according to previous reports [24].

2.15. Statistical Analyses. Student's *t*-test was used to analyze statistical comparisons between groups. The resulting *p* value < 0.05 is considered significant statistically.

3. Results

3.1. YAP Silencing during I/R Aggravates Liver Damage While Decreases Serum EV (sEV) Concentration. We first confirmed YAP expression level to be negatively correlated with hepatocellular damage in I/R-stressed human orthotopic liver transplantation (OLT) samples (Supplementary Fig. 1A-C, Supplementary Table 1) [4]. And during hepatic IRI in mice, hepatic YAP protein and YAP mRNA gradually increased over time (Figures 1(a) and 1(b)). Then, hepatocyte-specific YAP knockout (YAP-HKO) mice were constructed to study whether YAP knockout could aggregate hepatic dysfunction in hepatic IRI mice (Supplementary Fig. 1D-E), since the pan-tissue YAP knockout mice are lethal in a fetus. By these YAP-HKO mice with I/R at 24 h, we observed severe hepatic damage by pathological analysis (Figure 1(c)) and measured their serum ALT levels (Figure 1(d)), while there were no obvious differences between YAP-HKO and wild-type (WT) mice under sham operation. Likewise, Suzuki's score indicated significantly increased hepatocellular damage by YAP silencing (Figure 1(e)). These data suggested that YAP silencing can exacerbate hepatic IRI.

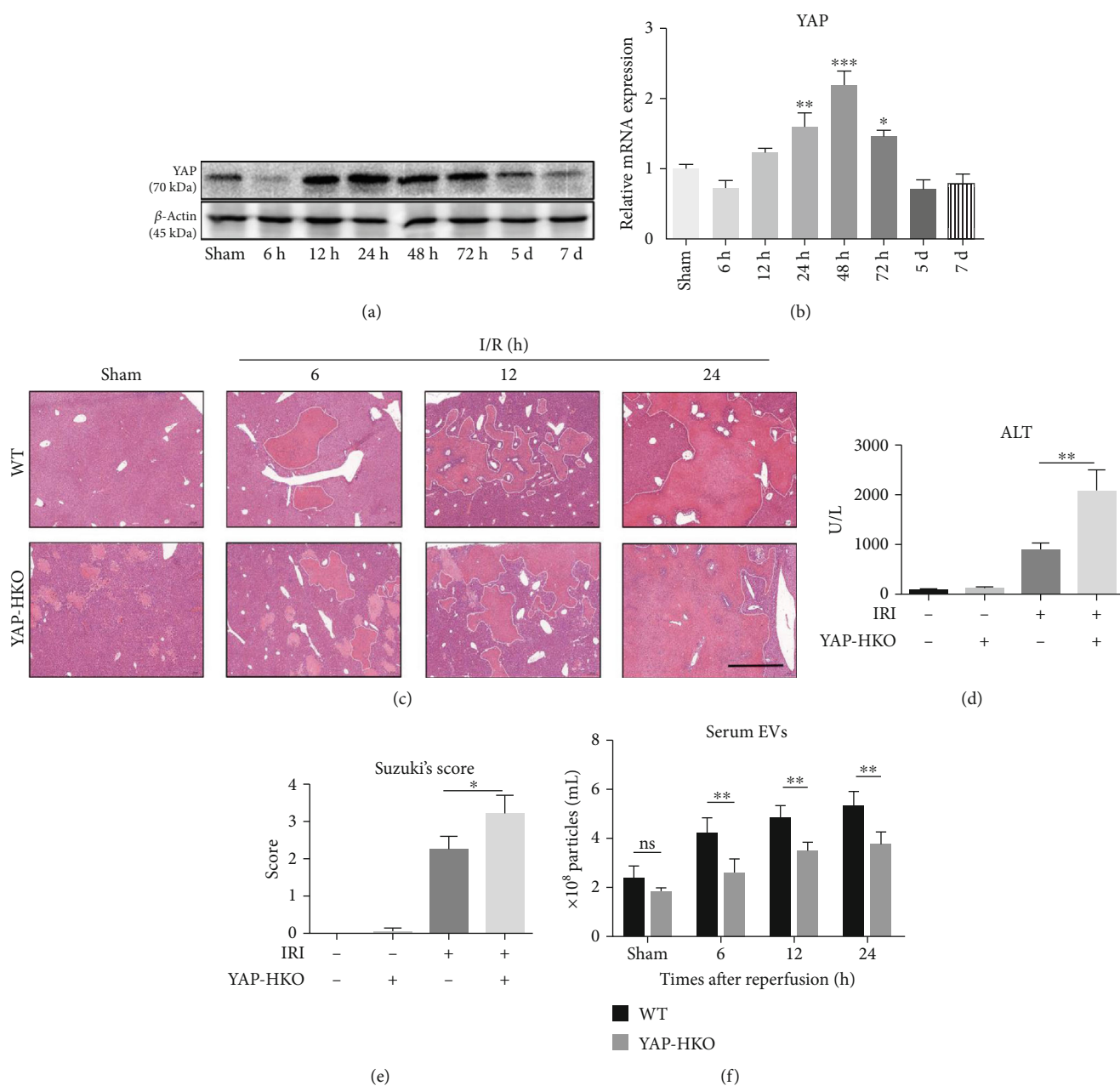


FIGURE 1: Silencing of YAP exacerbates liver injury and decreases sEVs' concentration during IRI. (a) Western blot analysis of hepatic YAP protein levels of IRI mice at different time points; (b) the mRNA levels of hepatic YAP from IRI mouse liver were detected by qPCR at different time points. (c) H&E staining of ischemic livers in WT and YAP-HKO mice showed that the injury increased with reperfusion time and reached the peak at 24 h after reperfusion. Scale bar, 1 mm. (d) Serum ALT levels of YAP-HKO mice were significantly higher than WT mice with I/R at 24 h (2059 ± 214.2 U/L vs. 872.8 ± 76.15 U/L, $**p < 0.01$). (e) Suzuki's histological score of YAP-HKO mice was higher than WT mice with I/R at 24 h (score: 2.25 ± 0.17 vs. score: 3.2 ± 0.25 , $*p < 0.05$). (f) The concentrations of sEVs from WT and YAP-HKO groups at different time points after IRI, as measured by CD81 exosome ELISA kit. $n = 6$ per group. $**p < 0.01$, ns: $p > 0.05$, t -test.

Next, we isolated sEVs from WT mice and YAP-HKO mice after hepatic IRI with a serum EV isolation kit [29]. By CD81 exosome ELISA kit for quantification, we found that sEVs' concentration gradually increased after IRI and reached the peak in 24 hours (Figure 1(f)). This trend was in consistency with the YAP protein expression levels as shown in Figures 1(a) and 1(b). Silencing YAP *in vivo* decreased sEVs' concentration after IRI (Figure 1(f)). sEVs

were verified by transmission electron microscopy (TEM) (Supplementary Fig. 2A). EV markers including CD81, ALIX, and TSG101 were expressed in sEV lysates, but the endoplasmic reticulum marker calnexin was not found in sEVs [30] (Supplementary Fig. 2B). Our *in vivo* observations indicate that sEVs' concentration is affected by YAP expression, and it is necessary to explore the mechanism and effect of YAP regulation on EV secretion.

3.2. YAP Silencing Decreases the Formation of EVs in an F-Actin-Dependent Manner. To explore the effect of YAP on EV secretion from hepatocytes, we first found that lower YAP expression is correlated with smaller amount of secreted EVs from nanoparticle tracking analysis (NTA) and western blot analysis, by comparing EVs from WT and YAP knock-down (YAP-KD) L02 cells (the normal human hepatocyte line) during hypoxia/reoxygenation (Figure 2(a), Supplementary Fig. 2C, and Figure 2(b)). To elucidate the underlying mechanism of EV secretion in hepatocytes, we explored the role of the dynamic actin and branched actin networks in EV secretion under YAP regulation in vitro, which are on the surface of early endosome (EE). These networks are very important for membrane remodeling, which are critical for selective cargo sorting and EE shape control [7]. We found that most of the WT EE (marked by EEA1) were intensively covered by branched actin networks. In YAP-KD L02 cells, the amount of branched actin on EE decreased significantly (Figure 2(c)). Further analysis of YAP-KD L02 cells revealed that the recycling endosome (RE), which was formed by buddings from EE tubules, also decreased significantly as branched actin formation reduced, indicated by the decreased coposition of EE and F-actin on the plasma membrane (yellow). The RE is the main source of endosomal membrane formation. To study the role of F-actin in EV secretion under the regulation by YAP, we used cytochalasin D (CytoD) to induce F-actin depolymerization for 30 minutes. The depolymerized F-actin restored the inhibition of RE under YAP-KD condition, presenting as an increased level of copositioning of EE and F-actin on the plasma membrane (Figures 2(c) and 2(d)). At the same time, CytoD treatment also reversed the inhibitory effect of YAP-KD on EV secretion (Figure 2(e)). These results suggested that YAP might regulate the formation of EVs via F-actin in hepatocytes.

3.3. YAP Expression Is Essential for Inhibiting the Fusion of MVB and Lysosomes. Next, we evaluated whether YAP could induce EV secretion by inhibiting MVB and lysosome degradation. The dense reticulum of F-actin might form organelle traps in cells and slow down lysosome transport through an active F-actin anchoring mechanism [31]. We used late endosomes (LE, labeled with RAB7) to indicate MVE. With increased formation of F-actin patches in YAP-KD (Figure 2(c)), the fusion of lysosome (labeled by LysoTracker Red) with LE significantly increased (Figures 3(a) and 3(b)). When F-actin depolymerization was induced by CytoD, there was no significant difference in the colocalization of LE and lysosomal fluorescence between YAP-KD and WT L02 cells (Figure 3(b)). These results suggested that YAP induced EV secretion through F-actin by increasing membrane formation, as well as inhibiting the fusion of MVB and lysosomes.

3.4. CD47-Enriched EV Inhibits CD172⁺ DC Activation in a YAP-Dependent Manner. To determine the potential effect of YAP-induced EVs on hepatic IRI, we used quantitative mass spectrometry to detect EVs originated from WT L02 and YAP-KD L02 cells. 2883 trusted proteins were retrieved

from the original data of mass spectrometry by Protein Pilot software (Supplementary Table 2, Figures 4(a) and 4(b)). Based on this result, we noticed CD47 was one of the target that highly expressed on hepatocyte-derived EVs in a YAP-dependent manner and then verified its expression on primary mouse hepatocytes (PMH) by western blotting (Supplementary Fig. 2D) and immunogold electron microscopy (Supplementary Fig. 2E). CD47 has been reported to exert its inhibitory effect by binding specifically to the surface receptor CD172 α of myeloid cells [32]. We examined whether CD47-enriched EVs target on the proinflammatory cells during hepatic IRI. By evaluating the inflammatory cytokines IL-12 p40 and TNF- α of CD172⁺ cells in hepatic tissue with I/R at 24h, we found that CD172a⁺ rather than CD172a⁻ cells are the main sources of IL-12 p40 and TNF- α (Figure 4(c)). Compared with the sham operation group, the ratio of CD172a⁺ IL-12 p40⁺ or TNF- α ⁺ cells in the IRI group significantly increased (Figure 4(d)). Furthermore, we found that CD11c expression in hepatic tissues with I/R was limited to the CD172a⁺ cell subset (Figure 4(e)). We next confirmed that among CD172⁺ cells, CD172⁺ CD11c⁺ IA/IE⁺ (MHC II⁺) cells or CD172⁺ DCs represented as the main producers of IL-12 p40 and TNF- α in hepatic IRI. These data suggested that the inflammatory cytokine production is restricted to CD172a⁺ DCs in hepatic IRI. As CD47 is located on the surface of EVs, we used CD47 neutralizing antibodies to neutralize EVs and found that neutralizing of CD47 from PMH-EVs significantly antagonized the ability of these EVs to inhibit the secretion of inflammatory cytokines by bone-marrow-derived dendritic cells (BMDCs) (Figure 4(f)). These results suggested that CD47-enriched EVs could suppress inflammatory responses of CD172⁺ DCs.

To evaluate the antigen-presenting function of DCs, we detected the proliferation of CD4⁺ and CD8⁺ T cells in vitro. In comparison to the YAP-HKO PMH treatment group, we found the proliferation rates were inhibited in BMDCs pretreated by a conditioned medium of WT PMH (Figures 5(a) and 5(b)). Meanwhile, by detecting IL-12 p40, we found LPS-induced-BMDC activation was significantly restrained by a PMH conditioned medium in a YAP-dependent manner (Figure 5(c)). These results implied that, in the absence of YAP, hepatocytes lose their ability to suppress BMDC activation in vitro.

To elucidate that YAP-dependent-DC function was regulated by hepatocyte-released EVs, we isolated EVs by ultracentrifugation from the supernatant of PMH. We found EVs isolated from WT were more potent in inhibiting BMDCs than EVs from YAP-HKO PMH, as evaluated by IL-12 p40 secretion (Figure 5(c)). To distinguish between EVs and other nonmembrane extracellular particles [20], EVs were treated with detergent (Triton X-100) which can destroy the membrane structure and halt the functions of EVs. The particles after detergent treatment failed to inactivate BMDCs (Figure 5(c)). These results indicated that DC activation was inhibited by hepatocyte-released EVs in a YAP-dependent manner.

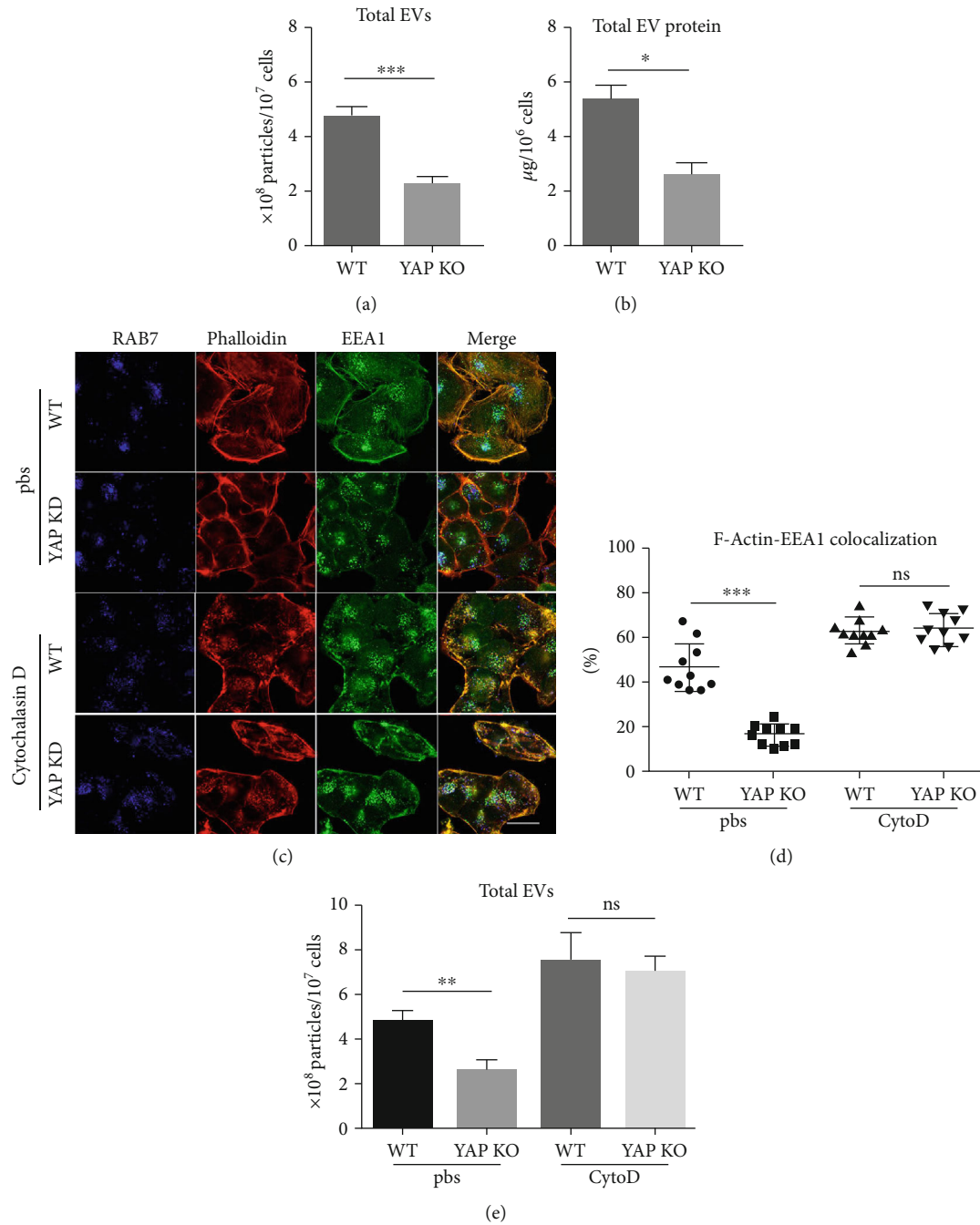


FIGURE 2: Hepatic YAP silence decreases EV formation. (a) EVs extracted from culture medium of WT or YAP-KD L02 cells were subjected to nanoparticle tracking analysis (NanoSight) for quantitative [20]. $n = 3$, $***p < 0.001$, t -test. (b) A BCA Protein Assay Kit was used to detect the protein concentration of EVs. $n = 3$. $*p < 0.05$, t -test. (c) Rhodamine-labeled phalloidin staining (labeling membrane-associated F-actin, red), EEA1 staining (labeling early endosomes, green), and RAB7 staining (labeling late endosomes) for YAP-KD and WT L02 cells under either PBS or cytochalasin stimulation. Scale bar, $10 \mu\text{m}$. (d) Statistical analysis of amounts of EEA1 that colocalized (orange) with F-actin, shown as percentages of the total EEA1, $n = 10$, $***p < 0.001$, ns: $p > 0.05$, t -test. (e) EVs extracted from a culture medium of equal amount of WT or YAP-KD L02 cells with or without CytoD treatment were subjected to NanoSight for quantification. $n = 3$. $**p < 0.01$, ns: $p > 0.05$, t -test.

3.5. CD47⁺ EVs Could Alleviate Hepatic IRI as a Therapeutic Strategy. To investigate whether CD47⁺ EVs have the potential to treat hepatic IRI, we first isolated CD47⁺ EVs and CD47⁻ EVs using nonblocking anti-CD47 Ab (REA170)-FITC and anti-FITC magnetic beads. We then verified the purified CD47⁺ EVs contain CD47 and EVs' label proteins

TSG101 and Alix (Figures 6(a) and 6(b)). Next, we injected CD47⁺ EVs into WT mice to determine whether CD47⁺ EVs have any adverse effect, and we found there was no damage to normal mice without IRI. While in the IRI model, less hepatic damage was observed in the group treated by CD47⁺ EVs (Figures 6(c) and 6(d)). We found the expression of

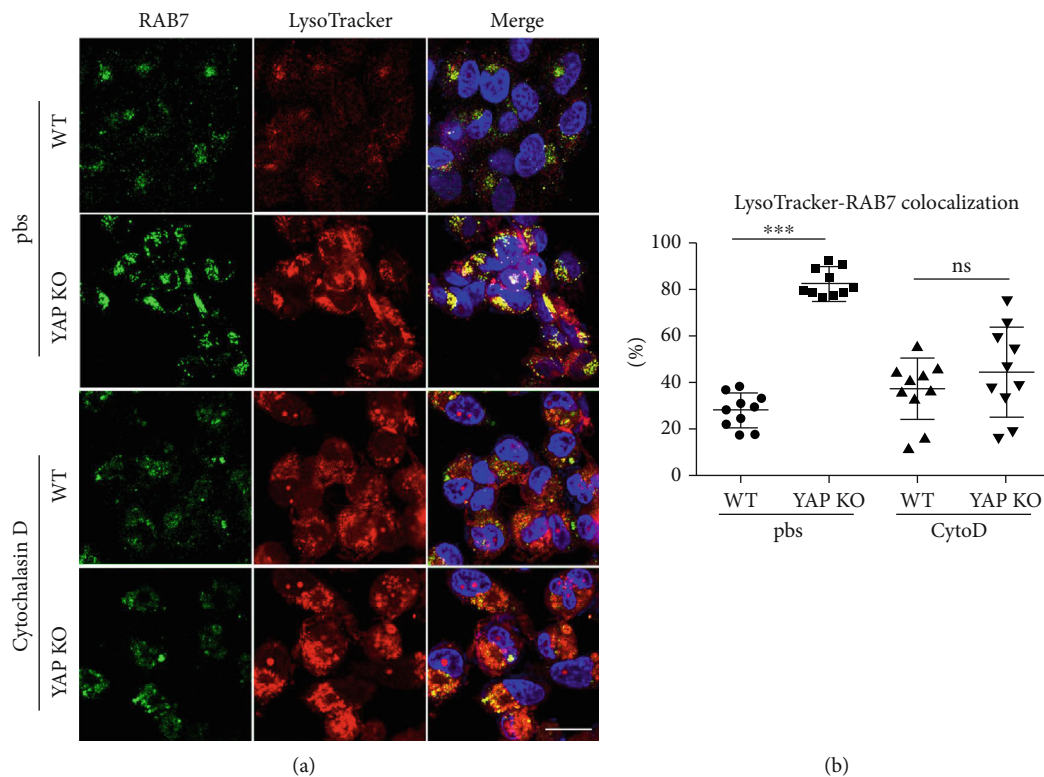


FIGURE 3: YAP expression is required for the fusion of MVB and lysosomes. (a) Representative image of the fusion of lysosome (labeled by LysoTracker staining, red) with late endosomes (labeled by RAB7 staining, green) significantly increased in YAP-KD compared to WT L02 cells with or without CytoD treatment. Scale bar, 10 μm . (b) Statistical analysis of the amounts of RAB7⁺ granules colocalize (orange) with lysosome, $n = 10$, *** $p < 0.001$, ns: $p > 0.05$, t -test.

antioxidative genes increased including thioredoxin-1 (Trx1) and heme oxygenase-1 (HO-1) after CD47⁺ EV treatment. Further, we examined the expression of Cyr61, which has been recognized as a key chemokine controlling liver injury [5]. The mRNA levels of hepatic Cyr61 were reduced after CD47⁺ EV treatment (Supplementary Fig. 2F). As CD47mAb could reverse the protective effects of CD47⁺ EVs, the protection of these EVs on hepatic IRI is possibly mediated by CD47 (Figures 6(c) and 6(d)). In addition, there was no significant amelioration in hepatic damage after I/R in CD11c-DTR mice injected with DT after CD47⁺ EV treatment (Figures 6(c) and 6(d)), suggesting that CD47⁺ EVs alleviate hepatic IRI at least partially depending on DCs. Similarly, CD47⁺ EV injection reduced the serum levels of IL-6 and TNF- α , while this effect was reversed by CD47mAb (Figure 6(e)). These results showed that CD47⁺ EVs may be a potential therapeutic strategy for the treatment of hepatic IRI.

Taken together, our data showed that YAP regulates the secretion of hepatocyte-derived EVs, which can inhibit DC activation through its surface CD47 and contribute to liver protection during hepatic IRI.

4. Discussion

In this study, we identified a novel mechanism that YAP activation affects the release of hepatic EVs, which regulates DC activation through CD47/CD172a axis. CD47-enriched EVs

could be a novel therapeutic strategy for treating hepatic IRI by targeting on CD172a⁺ DCs.

The participation of YAP in IRI has been reported in different studies with controversial effects [4, 5]. In our study, hepatic YAP protein and mRNA were induced in a time-dependent manner in hepatic IRI, demonstrating the requisite role of YAP. This notion was strongly supported by human OLT samples. Further, we reported that conditional knockout YAP in hepatocytes led to severe hepatic damage with IRI, by crossing Albumin-Cre (*Alb-Cre*) mice and *Yap^{flox/flox}* mice [34]. These mice displayed increased serum ALT levels and pathological hepatic changes, indicating YAP silencing played a pivotal role in aggregating hepatic IRI. Then, via serum EV isolation kit, we found in the serum of YAP-HKO mice, the amount of sEVs decreased after IRI. Thus, we further investigated how YAP knockout affects sEV secretion and exacerbates hepatic injuries.

Actually, it has been found that IRI can induce the secretion of EVs [29], but how YAP knockout in IRI decreased EV secretion remains unclear. EVs are formed through direct germination of plasma membrane or germination of endomembrane structure after fusing with late endosomes (LE) or multivesicular body (MVB) and are secreted based on the process that fuses with plasma membrane [35]. During this process, the branched actin network is known to play a key role in endosomal trafficking and EV secretion [36]. YAP can regulate the actin-binding activity of AMOT family members by competing with F-actin for binding to

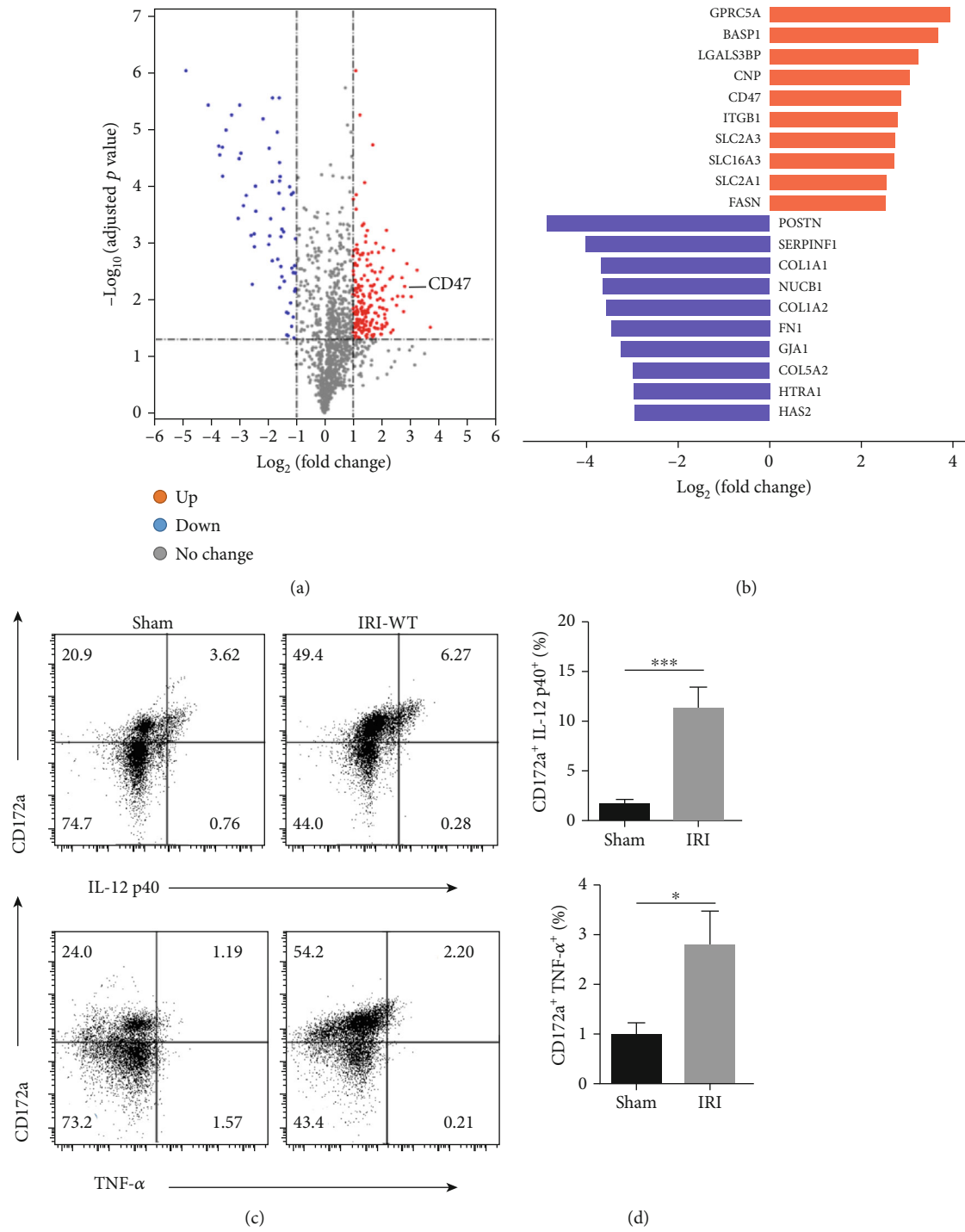
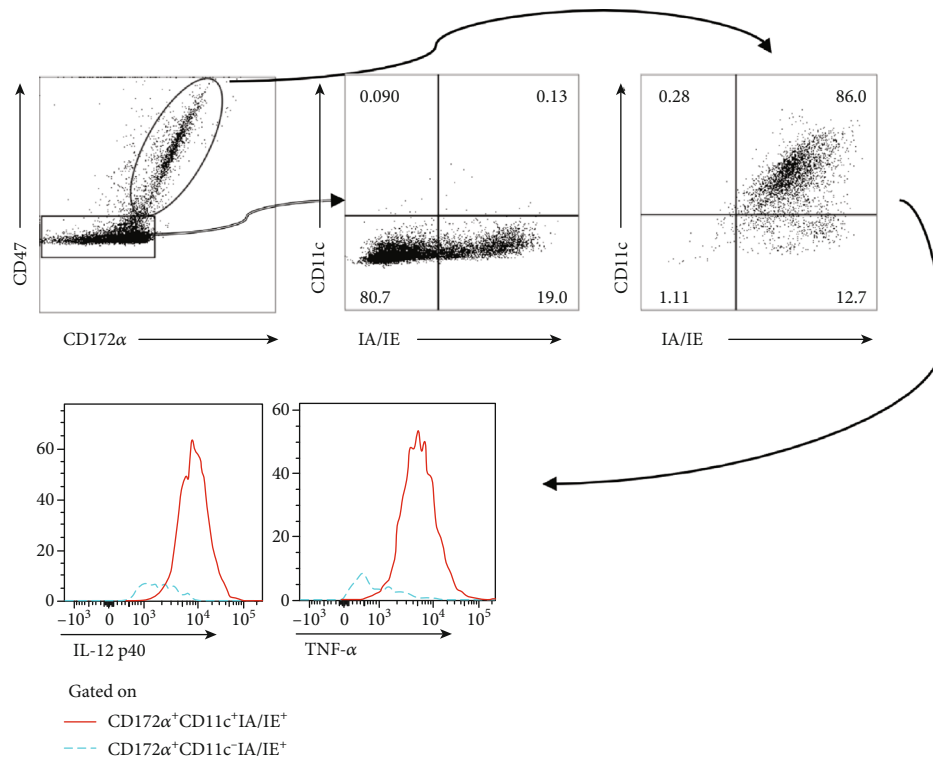
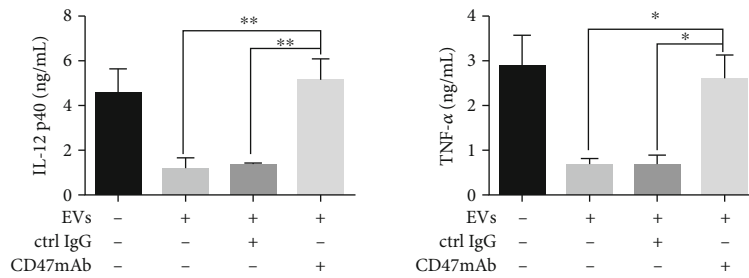


FIGURE 4: Continued.



(e)



(f)

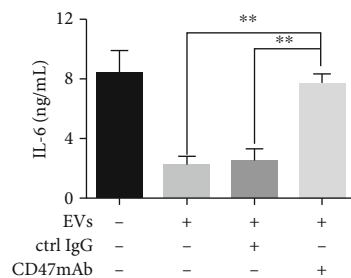
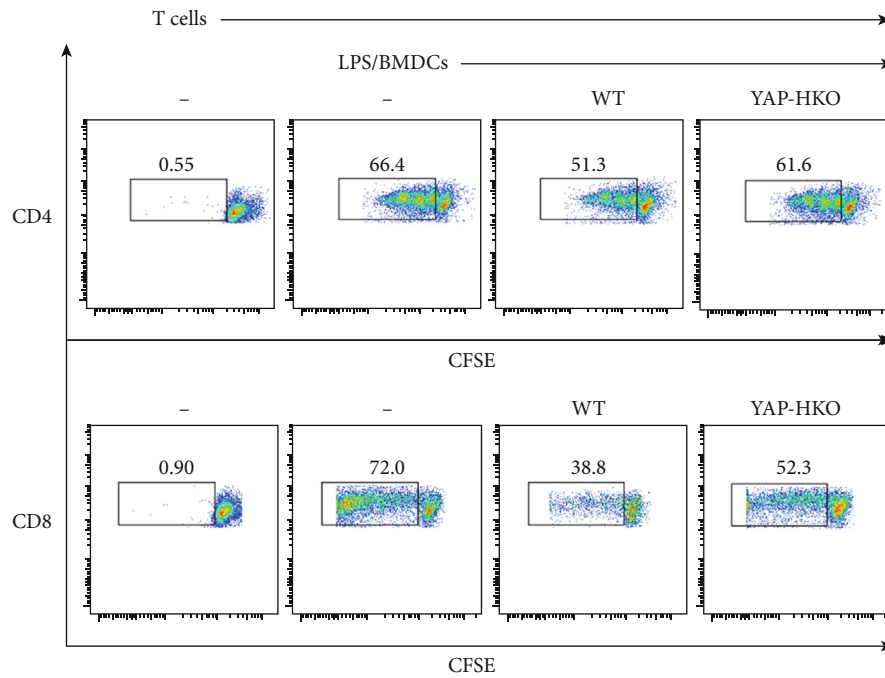
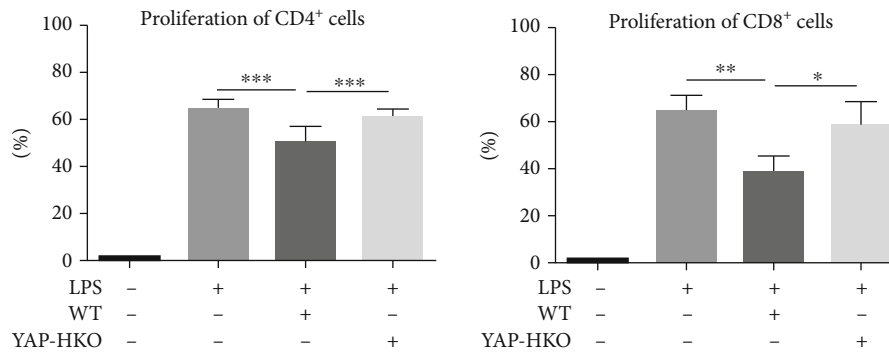


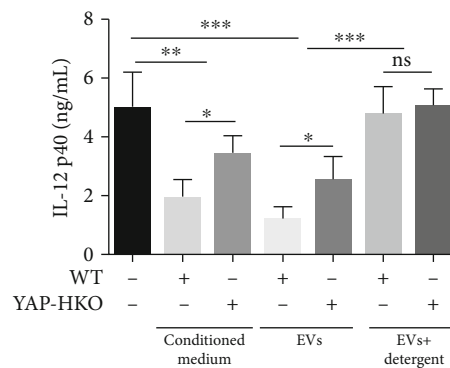
FIGURE 4: CD47-enriched EVs inhibit CD172a⁺ DC activation. (a) Volcano map presenting the 62 downregulated and 277 upregulated proteins in EVs originated from WT L02 and YAP-KD L02 cells by mass spectrometry, in which CD47 were among the upregulated proteins. (b) Bar chart showing the top 10 upregulated and downregulated proteins with CD47 ranked top four. Protein expression (Ex) was converted to log₂(Ex), and the scale represented relative expression [20]. (c) Representative flow cytometry images of CD45⁺ cells stained by CD172a combined with IL-12 p40 or TNF-α in sham or IRI mouse models. (d) The proportion of CD172a⁺ IL-12 p40⁺ or CD172a⁺ TNF-α⁺ cells was shown. Bars represent the subset amounts of CD172a⁺ IL-12 p40⁺ or CD172a⁺ TNF-α⁺ cells (mean ± s.d., n = 4 mice). (e) CD47 and CD172α expressions were analyzed on hepatic immune cell populations. CD172a⁺ cells were further subdivided according to CD11c and IA/IE expressions. Intracellular expression of cytokines (IL-12 p40 and TNF-α) was examined on CD172a⁺ CD11c⁺ (solid red lines) and CD172a⁺ CD11c⁻ (dotted blue lines) gated cells. (f) PMH-derived EVs were treated by CD47 neutralizing antibody or control IgG. qPCR analysis showed a significant increase in inflammatory cytokines including IL-12 p40, TNF-α, and IL-6 after CD47 neutralization. n = 6, *p < 0.05; **p < 0.01; ***p < 0.001.



(a)



(b)



(c)

FIGURE 5: EVs released from hepatocytes inhibit DC activation in a YAP-dependent manner. (a) Primary BMDCs were treated by a conditioned medium from WT or YAP-HKO PMH and were stimulated with LPS. BMDCs were then cocultured with CD4⁺ and CD8⁺ T cells isolated from BALB/c mice at the ratio of 1 : 10. The proliferation of CD4⁺ and CD8⁺ T cells was measured by CFSE-MLR. (b) The extent of T cell proliferation in (a) was analyzed. (c) BMDCs were treated with a conditioned medium or EVs from WT or YAP-HKO PMH culture supernatants, and then, the IL-12 p40 level in the culture medium was determined by ELISA. * $p < 0.05$; ** $p < 0.01$; *** $p < 0.001$. $n = 4$.

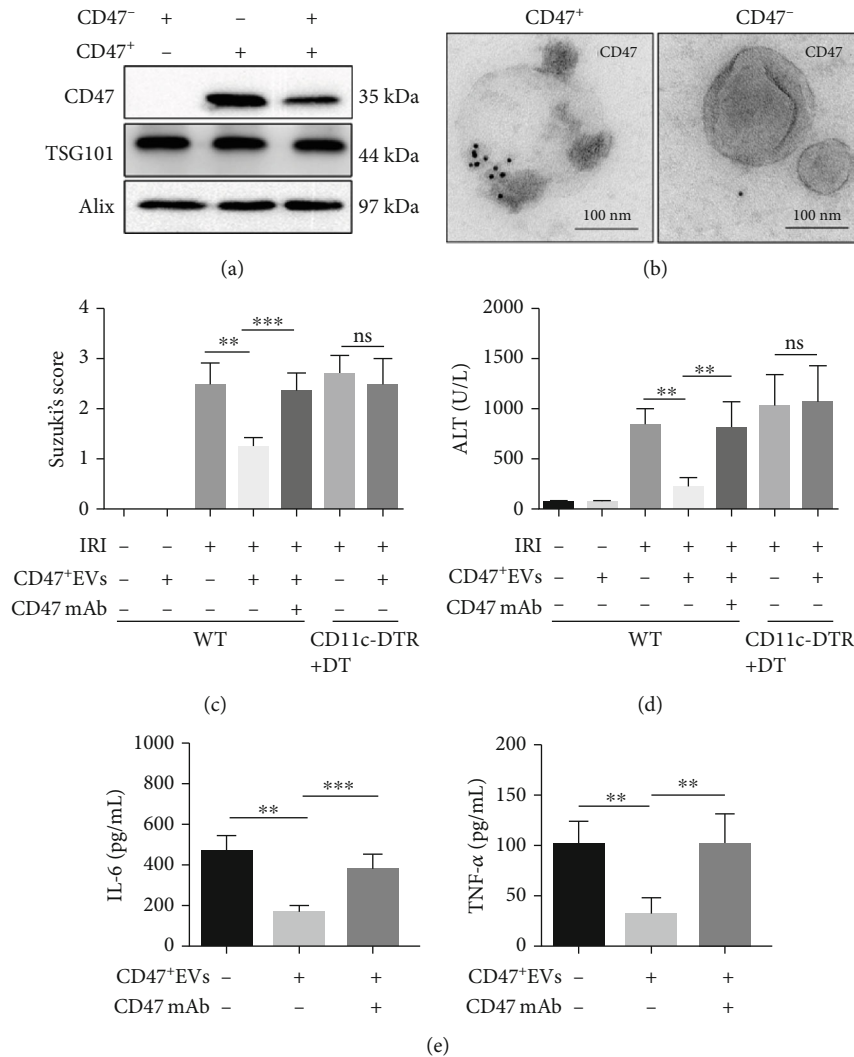


FIGURE 6: CD47⁺ EVs alleviate hepatic IRI in mouse models. (a) CD47⁺ EVs and CD47⁻ EVs were isolated by nonblocking anti-CD47 Ab (REA170)-FITC and anti-FITC magnetic beads. Alix, TSG101, and CD47 in CD47⁺, CD47⁻, and total PMH-EVs were checked by western blot. (b) Immunogold electron microscopy images showed the immunoreactivity for CD47 on CD47⁺ and CD47⁻ EVs. (c) CD11c-DTR were treated with DT (4 mg/kg b.w.) and/or plus with CD47⁺ EVs (100 μg/kg b.w.) on 2 and 0 days before IRI model construction. The severity of hepatic IRI was evaluated by Suzuki's grading [33]. (d) Hepatocellular function was assessed by serum ALT level (U/L). (e) ELISA analysis showed decreased concentrations of IL-6 and TNF-α after CD47⁺ EVs supply without CD47mAb treatment during IRI. *n* = 6, **p* < 0.05; ***p* < 0.01; ****p* < 0.001.

AMOT130 [6]. It is possible that YAP may regulate EV secretion by regulating F-actin. In our study, we investigated the mechanism involved in endosomal trafficking, which involves the Rab family of small GTPases, lysosomes, and remodeled actin [37]. We found that YAP knockdown by lentivirus shRNA significantly reduced EV release, suggesting that YAP participated in EV secretion. By comparing WT and YAP-KD hepatocytes, we found that YAP-KD decreased the formation of branching actin. By limiting the fusion of intraluminal vesicles and cell membranes, it is conducive to the development of RE and further decreases the occurrence of EV membrane [24, 38]. RE is closely related to the generation of EVs [39]. Both dynamic and branched actin could reduce the fusion of LE and lysosome, thereby increasing the secretory MVE as EVs. Therefore, we are the

first to report that YAP from hepatocytes regulate EV secretion through F-actin in hepatic IRI. But our works focused on the role of EVs released from hepatocytes; further studies are needed to explore the effect of EVs from other nonparenchymal cells, such as Kupffer cells, liver sinusoidal endothelial cells, and immune cells. Besides, autophagy has been reported to promote the fusion of MVB and autophagy [40], and YAP is well known to regulate autophagy flux by promoting autolysosome degradation [41]. Whether YAP regulated EV secretion through autophagy requires further study.

Then, to investigate the potential effect and mechanism of EVs in hepatic IRI, we applied mass spectrometry to explore the essential elements. Among the top factors, we found that CD47 exists on the surface of EV membrane.

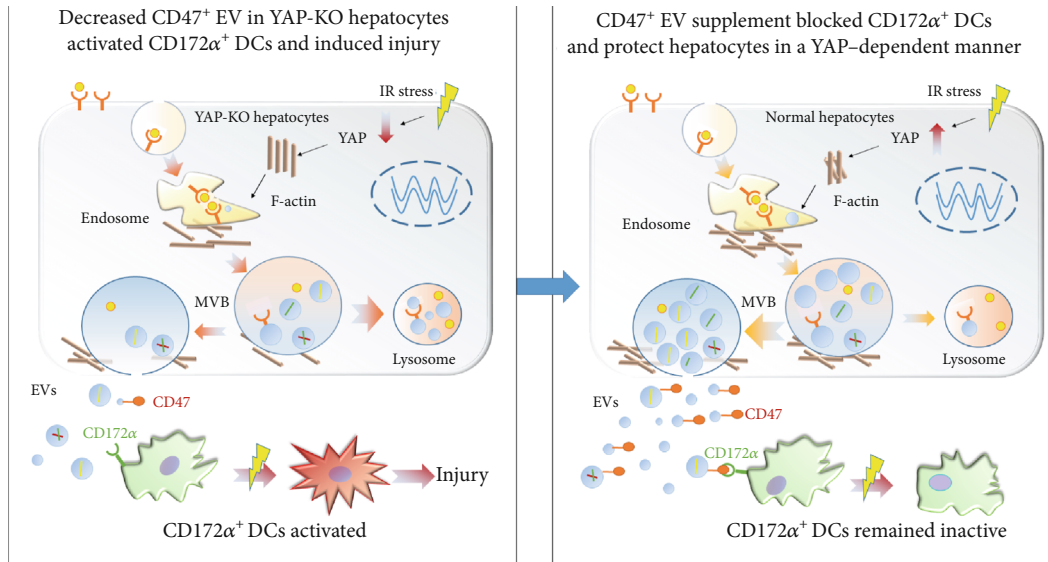


FIGURE 7: Mechanism diagram for the immunosuppression effect of YAP/F-actin/EV-CD47 axis on DCs in hepatic IRI. IR stress stimulated YAP expression in normal hepatocytes and promoted the remodeling of F-actin to form an endosomal trafficking network, which is critical for EV formation. These EVs were rich in CD47, which could bind to CD172a receptor on DCs. In normal conditions, most of the MVB would form into EVs with a little few into lysosome. When YAP expression was knocked down, however, F-actin failed to gather around and form a network report; thus, the amount of EVs decreased with more vesicles engulfed by lysosome. The amount of CD47 was scarce, and CD172⁺ DCs were activated and led to more severe damage. Therefore, EVs lack of CD47⁺ due to YAP knockout in hepatocytes, activated DCs, and aggregated hepatic IRI, while YAP activation induced by hepatic IRI promoted the secretion of CD47-enriched EVs by remodeling of cytoskeleton F-actin, and CD47⁺ EVs induced the immunosuppressive DCs and protected the liver from IRI. CD47⁺ EV supplement could be a novel therapeutic strategy for hepatic IRI treatment.

CD47 is considered to be the self-recognition marker that specially binds CD172 α , which profoundly inhibits the secretion of inflammatory cytokines. The latest tumor research uses CD47 to modify nanoparticles, which reduces the clearance rate of nanoparticles by macrophages [42]. Studies have shown that CD47 not only takes part in autoimmune diseases and tumors but also plays a key role in IRI-related diseases in kidneys and hearts [43, 44]. And CD172 α ⁺ DCs, as target cells of CD47, are the main cells secreting proinflammatory cytokines in hepatic IRI [15]. CD47mAb blockade confirmed that EV-associated CD47 take the immunosuppressive effect on DCs and reduced hepatic IRI. Under normal conditions, DCs remain in an inactivated state. Under inflammation stress, DCs are exposed to foreign antigens, microorganisms, and inflammatory cytokines resulting in activation and then subsequently initiating immune response [28]. Our results highlighted the regulatory role of YAP in the regulation of DC function during hepatic IRI. In this study, we observed that hepatocyte culture medium obviously inhibited LPS-induced IL-12 p40 production and antigen-presenting ability of BMDCs in a YAP-dependent manner. We suspected that under stress, YAP induced EV secretion from hepatocytes, which have the immunosuppressive effect on DCs. Interestingly, we treated EVs with detergent, which destructed the membrane structures of EVs, reversing the inhibitory effect of EVs on DCs. This suggested that YAP induced the secretion of EVs to exert an immunosuppressive effect on DCs. In addition, we found that CD47⁺ EVs can inhibit DC activation and inflammatory responses, which can explain their protective effects on IRI. Together, these data suggest that

CD47-enriched-EVs can inhibit DC activation and decrease subsequent hepatic damage.

Innate immunity is the dominant ingredient of liver IRI, among which dendritic cells, macrophage, and neutrophils are pivotal participants [45]. In comparison with neutrophils and macrophages, DCs are the dominant local immune cells surveilling and maintaining immune homeostasis with less complex phenotype switches [46]. Moreover, DC has been determined as the main contributors in hepatic IRI, affecting the development of adaptive immunity by regulating the initial response and amplifying the innate immune response [11]. The role of other immune cells such as macrophages or neutrophils in hepatic IRI needs further investigation.

EVs have been proved to be ideal cargos for drug delivery, which showed better stability, easier preservation, and more precise targeting in comparison to traditional cell therapy or RNA drugs [47]. The advantages of EVs make them attractive as the potential candidates for treating many diseases. The specific structure of phospholipid bilayer enables EVs to protect their contents from in vivo degradation and the disturbances from inflammatory microenvironment [48]. Besides, EVs could be modified and produced in a standard process. Therefore, CD47-enriched EVs could be engineered by integrating EVs with CD47 loading, which could be manufactured at a large scale independent of the cell origin, which could be the future direction of precise drug development.

In summary, our study reported a novel regulatory mechanism between EVs and DCs depending on YAP activation in hepatic IRI (Figure 7). Specifically, YAP knockout

decreased the release of EVs in hepatocytes by affecting F-actin, which reduced membrane formation and promoted MVB to fuse into lysosomes. The YAP-deficient EVs are lack of CD47, which failed to inactivate CD172 α ⁺ DCs and lead to sustained IRI injury. CD47-enriched EV treatment blocked CD172 α ⁺ DCs and protected IRI mice from hepatic injury. Our findings suggested that the secretion of CD47⁺ EVs depending on YAP activation played a protective role during hepatic IRI, and CD47-enriched EVs could be a novel therapeutic strategy for hepatic IRI treatment.

Abbreviations

ALT:	Alanine aminotransferase
AMOT:	Angiomotin
BM:	Bone marrow
CytoD:	Cytochalasin D
DCs:	Dendritic cells
DT:	Diphtheria toxin
EVs:	Extracellular vesicles
HO-1:	Heme oxygenase-1
I/R:	Ischemia-reperfusion
IRI:	Ischemia-reperfusion injury
LPS:	Lipopolysaccharide
MVB:	Multivesicular body
MLR:	Mixed leukocyte reaction
NanoSight:	Nanoparticle tracking analysis
OLT:	Orthotopic liver transplantation
PMH:	Primary mouse hepatocyte
SIRPa:	Signal-regulated protein alpha
Trx1:	Thioredoxin-1
WT:	Wild-type
YAP:	Yes-associated protein
YAP-HKO:	Hepatocyte-specific YAP knockout.

Data Availability

All data relevant to the study are included in the article or uploaded as supporting information.

Ethical Approval

This study was approved by the ethics institutions of the Third Affiliated Hospital of Sun Yat-sen University, Guangdong Province, China. In detail, the experiments relating to clinical data were approved by the Clinical Ethics Review Board, while all animal procedures were approved by the animal experimental ethics committee.

Consent

All participants agreed on the results in this study and signed informed consent for publication.

Conflicts of Interest

No conflict of interest was declared by all authors.

Authors' Contributions

Zenan Yuan and Hua Li designed the experiments and analyzed the data. Linsen Ye and Xiao Feng performed the surgical procedure. Tian Zhou assisted in analyzing the data and writing the manuscript. Yi Zhou, Shuguang Zhu, and Changchang Jia helped in acquiring data. Haibo Li, Dongbo Qiu, Kun Li, Wei Liu, and Hui Tang assisted in analyzing data. Guoying Wang and Qi Zhang contributed to collecting samples. Li Hua, Guihua Chen, and Yang Yang supervised the study. All authors approved the final manuscript. Zenan Yuan, Linsen Ye, Xiao Feng, and Tian Zhou contributed equally to this work.

Acknowledgments

This study was supported by the National Key R&D Plan (2017YFA0104304), the China Postdoctoral Science Foundation (2020M672980), the National Natural Science Foundation of China (81702393, 81770648, 81802897, 81802897, and 81900886), the National 13th Five-Year Science and Technology Plan Major Projects of China (2017ZX10203205-006-001), the Basic and Applied Basic Research Foundation of Guangdong Province (2021A1515010726), the Key Scientific and Technological Projects of Guangdong Province (2017A030311034), the Guangdong Natural Science Foundation (2017A030310373), the Science and Technology Planning Project of Guangdong Province (2017B030314027, 2017B020209004, 20169013, and 2017A020215178), the Science and Technology Planning Project of Guangzhou (201607010024 and 201604020001), and the Sun Yat-sen University Young Teacher Training Project (17ykpy47 and 17ykzd27).

Supplementary Materials

Supplementary Figure 1: (A) representative images of YAP expression in liver graft by immunohistochemistry (left panel), 37 patients were in the YAP high-expression group and 32 patients were in the YAP low-expression group; representative histology of liver by H&E staining (right panel) from indicated groups. Magnification $\times 200$. (B) Suzuki's histological grading of the YAP high-expression group was significantly lower than the low-expression group (score: 1.60 ± 0.08 vs. score: 2.37 ± 0.13 , $***p < 0.001$). (C) The peak serum ALT within 7 days after transplantation of the high-expression group were significantly lower than the low-expression group (448.4 ± 22.78 U/L vs. 653.9 ± 36.44 U/L, $***p < 0.001$). (D) The schematic diagram of design strategy of YAP-HKO mice, and the plasmid map of the targeting vector used in YAP-HKO mice. YAP-HKO mice were constructed by crossing Albumin-Cre (*Alb-Cre*) mice and *Yap^{flox/flox}* mice. (E) YAP protein levels of the liver from two independent WT and two independent YAP-HKO mice were measured by western blot. Supplementary Figure 2: (A) EVs isolated from mouse serum were visually confirmed by transmission electron microscopy, and (B) subjected to western blot analysis with antibodies to the indicated proteins. (C) WT L02 cells secrete more EVs. EVs isolated from culture

supernatants of WT or YAP knockout (KO) L02 cells were subjected to nanoparticle tracking analysis (NanoSight) to quantify the number and size distribution. (D) A total of 35 μg of EVs isolated from culture supernatants of WT or YAP-HKO PMH were analyzed by western blot using the indicated antibodies. Data are representative of three independent experiments. (E) Immunogold electron microscopy analysis depicts the presence of CD47 on the surface of PMH-derived EVs. (F) Quantitative RT-PCR-assisted detection of Trx1, HO-1, and Cyr61 after CD47⁺ EV treatment during IRI. Supplementary Table 1: demographics, perioperative situation, and laboratory results of liver transplantation surgery patients. Supplementary Table 2: the 62 downregulated and 277 upregulated proteins in EVs originated from WT L02 and YAP-KD L02 cells by mass spectrometry. (*Supplementary Materials*)

References

- [1] M. A. Zimmerman, I. Kam, H. Eltzschig, and A. Grenz, "Biological implications of extracellular adenosine in hepatic ischemia and reperfusion injury," *American Journal of Transplantation*, vol. 13, no. 10, pp. 2524–2529, 2013.
- [2] D. Papadopoulos, T. Siempis, E. Theodorakou, and G. Tsoulfas, "Hepatic ischemia and reperfusion injury and trauma: current concepts," *Arch Trauma Res.*, vol. 2, no. 2, pp. 63–70, 2013.
- [3] J. P. Duffy, K. Kao, C. Y. Ko et al., "Long-term patient outcome and quality of life after liver transplantation: analysis of 20-year survivors," *Annals of Surgery*, vol. 252, no. 4, pp. 652–661, 2010.
- [4] Y. Liu, T. Lu, C. Zhang et al., "Activation of YAP attenuates hepatic damage and fibrosis in liver ischemia-reperfusion injury," *Journal of Hepatology*, vol. 71, no. 4, pp. 719–730, 2019.
- [5] M. Mooring, B. H. Fowl, S. Z. C. Lum et al., "Hepatocyte stress increases expression of yes-associated protein and transcriptional coactivator with PDZ-binding motif in hepatocytes to promote parenchymal inflammation and fibrosis," *Hepatology*, vol. 71, no. 5, pp. 1813–1830, 2020, Epub 2019/09/11.
- [6] S. W. Chan, C. J. Lim, F. S. Guo, I. Tan, T. Leung, and W. J. Hong, "Actin-binding and cell proliferation activities of angiomin family members are regulated by Hippo pathway-mediated phosphorylation*," *Journal of Biological Chemistry*, vol. 288, no. 52, pp. 37296–37307, 2013.
- [7] K. G. Campellone and M. D. Welch, "A nucleator arms race: cellular control of actin assembly," *Nature Reviews. Molecular Cell Biology*, vol. 11, no. 4, pp. 237–251, 2010.
- [8] J. Wolfers, A. Lozier, G. Raposo et al., "Tumor-derived exosomes are a source of shared tumor rejection antigens for CTL cross-priming," *Nature Medicine*, vol. 7, no. 3, pp. 297–303, 2001.
- [9] H. Peinado, M. Alečković, S. Lavotshkin et al., "Melanoma exosomes educate bone marrow progenitor cells toward a pro-metastatic phenotype through MET," *Nature Medicine*, vol. 18, no. 6, pp. 883–891, 2012.
- [10] Y. Zhai, X. D. Shen, R. O'Connell et al., "Cutting edge: TLR4 activation mediates liver ischemia/reperfusion inflammatory response via IFN regulatory factor 3-dependent MyD88-independent pathway," *Journal of Immunology*, vol. 173, no. 12, pp. 7115–7119, 2004.
- [11] T. L. Sumpter, M. Abe, D. Tokita, and A. W. Thomson, "Dendritic cells, the liver, and transplantation," *Hepatology*, vol. 46, no. 6, pp. 2021–2031, 2007.
- [12] R. M. Steinman, "The dendritic cell system and its role in immunogenicity," *Annual Review of Immunology*, vol. 9, no. 1, pp. 271–296, 1991.
- [13] T. Nakao, Y. Ono, H. Dai et al., "DNAX activating protein of 12 kDa/triggering receptor expressed on myeloid cells 2 expression by mouse and human liver dendritic cells: functional implications and regulation of liver ischemia-reperfusion injury," *Hepatology*, vol. 70, no. 2, pp. 696–710, 2019.
- [14] D. J. van Rees, K. Szilagyi, T. W. Kuijpers, H. L. Matlung, and T. K. van den Berg, "Immunoreceptors on neutrophils," *Seminars in Immunology*, vol. 28, no. 2, pp. 94–108, 2016, Epub 2016/03/16.
- [15] A. N. Barclay and T. K. Van den Berg, "The interaction between signal regulatory protein alpha (SIRP α) and CD47: structure, function, and therapeutic target," *Annual Review of Immunology*, vol. 32, no. 1, pp. 25–50, 2014.
- [16] B. Buttari, E. Profumo, B. Cuccu et al., "Erythrocytes from patients with carotid atherosclerosis fail to control dendritic cell maturation," *International Journal of Cardiology*, vol. 155, no. 3, pp. 484–486, 2012.
- [17] Y. Li, D. Y. Ruan, C. C. Jia et al., "Aging aggravates hepatic ischemia-reperfusion injury in mice by impairing mitophagy with the involvement of the EIF2 α -parkin pathway," *Aging (Albany NY)*, vol. 10, no. 8, pp. 1902–1920, 2018, Epub 2018/08/10.
- [18] X. Li, S. Yi, Y. Deng et al., "MiR-124 protects human hepatic L02 cells from H₂O₂-induced apoptosis by targeting Rab38 gene," *Biochemical and Biophysical Research Communications*, vol. 450, no. 1, pp. 148–153, 2014, Epub 2014/05/31.
- [19] V. L. Kolachala, S. Palle, M. Shen, A. Feng, D. Shayakhmetov, and N. A. Gupta, "Loss of L-selectin-guided CD8(+), but not CD4(+), cells protects against ischemia reperfusion injury in a steatotic liver," *Hepatology*, vol. 66, no. 4, pp. 1258–1274, 2017.
- [20] T. Moroishi, T. Hayashi, W. W. Pan et al., "The hippo pathway kinases LATS1/2 suppress cancer immunity," *Cell*, vol. 167, no. 6, pp. 1525–1539.e17, 2016, e17.
- [21] C. Shi, Y. Cai, Y. Li et al., "Yap promotes hepatocellular carcinoma metastasis and mobilization via governing cofilin/F-actin/lamellipodium axis by regulation of JNK/Bnip3/SERCA/CaMKII pathways," *Redox Biology*, vol. 14, pp. 59–71, 2018, Epub 2017/09/05.
- [22] C. L. Da, Y. Xin, J. Zhao, and X. D. Luo, "Significance and relationship between yes-associated protein and survivin expression in gastric carcinoma and precancerous lesions," *World Journal of Gastroenterology*, vol. 15, no. 32, pp. 4055–4061, 2009.
- [23] Y. Xunyi, Y. Zhentao, J. Dandan, and L. Funian, "Clinicopathological significance of PTPN12 expression in human breast cancer," *Revista Brasileira de Pesquisas Médicas e Biológicas*, vol. 45, no. 12, pp. 1334–1340, 2012, Epub 2012/10/10.
- [24] S. Yoon, A. Kovalenko, K. Bogdanov, and D. Wallach, "MLKL, the protein that mediates necroptosis, also regulates endosomal trafficking and extracellular vesicle generation," *Immunity*, vol. 47, no. 1, pp. 51–65.e7, 2017, e7.
- [25] Z. Yuan, J. Zhang, Y. Huang et al., "NRF2 overexpression in mesenchymal stem cells induces stem-cell marker expression

- and enhances osteoblastic differentiation,” *Biochemical and Biophysical Research Communications*, vol. 491, no. 1, pp. 228–235, 2017.
- [26] H. Ji, X. D. Shen, Y. Zhang et al., “Activation of cyclic adenosine monophosphate-dependent protein kinase a signaling prevents liver ischemia/reperfusion injury in mice,” *Liver transplantation : official publication of the American Association for the Study of Liver Diseases and the International Liver Transplantation Society.*, vol. 18, no. 6, pp. 659–670, 2012, Epub 2012/02/01.
- [27] L. Jiang, Y. Shen, D. Guo et al., “EpCAM-dependent extracellular vesicles from intestinal epithelial cells maintain intestinal tract immune balance,” *Nature Communications*, vol. 7, no. 1, p. 13045, 2016, Epub 2016/10/11.
- [28] B. Ke, X. D. Shen, N. Kamo et al., “ β -Catenin regulates innate and adaptive immunity in mouse liver ischemia-reperfusion injury,” *Hepatology*, vol. 57, no. 3, pp. 1203–1214, 2013, Epub 2012/10/20.
- [29] M.-q. Yang, Q. Du, J. Goswami et al., “Interferon regulatory factor 1-Rab27a regulated extracellular vesicles promote liver ischemia/reperfusion injury,” *Hepatology*, vol. 67, pp. 1056–1070, 2018.
- [30] Y. Aoki, R. Manzano, Y. Lee et al., “C9orf72 and RAB7L1 regulate vesicle trafficking in amyotrophic lateral sclerosis and frontotemporal dementia,” *Brain : a journal of neurology.*, vol. 140, no. 4, pp. 887–897, 2017, Epub 2017/03/24.
- [31] B. van Bommel, A. Konietzny, O. Kobler, J. Bar, and M. Mikhaylova, “F-Actin patches associated with glutamatergic synapses control positioning of dendritic lysosomes,” *The EMBO Journal*, vol. 38, no. 15, article e101183, 2019.
- [32] S. Pengam, J. Durand, C. Usal et al., “SIRP α /CD47 axis controls the maintenance of transplant tolerance sustained by myeloid-derived suppressor cells,” *American Journal of Transplantation*, vol. 19, no. 12, pp. 3263–3275, 2019.
- [33] Q. Zhu, C. Li, K. Wang et al., “Phosphatase and tensin homolog- β -catenin signaling modulates regulatory T cells and inflammatory responses in mouse liver ischemia/reperfusion injury,” *Liver transplantation : official publication of the American Association for the Study of Liver Diseases and the International Liver Transplantation Society.*, vol. 23, no. 6, pp. 813–825, 2017, Epub 2017/02/06.
- [34] S. V. Iverson, K. M. Comstock, J. A. Kundert, and E. E. Schmidt, “Contributions of new hepatocyte lineages to liver growth, maintenance, and regeneration in mice,” *Hepatology*, vol. 54, no. 2, pp. 655–663, 2011.
- [35] C. C. Scott, F. Vacca, and J. Gruenberg, “Endosome maturation, transport and functions,” *Seminars in Cell & Developmental Biology*, vol. 31, pp. 2–10, 2014.
- [36] M. A. Puthenveedu, B. Lauffer, P. Temkin et al., “Sequence-dependent sorting of recycling proteins by actin-stabilized endosomal microdomains,” *Cell*, vol. 143, no. 5, pp. 761–773, 2010.
- [37] H. Bai, Q. Zhu, A. Surcel et al., “Yes-associated protein impacts adherens junction assembly through regulating actin cytoskeleton organization,” *American Journal of Physiology. Gastrointestinal and Liver Physiology*, vol. 311, no. 3, pp. G396–G411, 2016.
- [38] A. Akhter, K. Caution, A. Abu Khweek et al., “Caspase-11 promotes the fusion of phagosomes harboring pathogenic bacteria with lysosomes by modulating actin polymerization,” *Immunity*, vol. 37, no. 1, pp. 35–47, 2012.
- [39] S. Lemoinne, D. Thabut, C. Housset et al., “The emerging roles of microvesicles in liver diseases,” *Nature Reviews. Gastroenterology & Hepatology*, vol. 11, no. 6, pp. 350–361, 2014.
- [40] C. M. Fader, D. Sanchez, M. Furlan, and M. I. Colombo, “Induction of autophagy promotes fusion of multivesicular bodies with autophagic vacuoles in k562 cells,” *Traffic*, vol. 9, no. 2, pp. 230–250, 2008.
- [41] Q. Song, B. Mao, J. Cheng et al., “YAP enhances autophagic flux to promote breast cancer cell survival in response to nutrient deprivation,” *PLoS One*, vol. 10, no. 3, article e0120790, 2015.
- [42] Z. Belhadj, B. He, H. L. Deng et al., “A combined “eat me/don't eat me” strategy based on extracellular vesicles for anticancer nanomedicine,” *Journal of Extracellular Vesicles*, vol. 9, no. 1, p. 1806444, 2020.
- [43] X. Wang, M. Xu, J. Jia et al., “CD47 blockade reduces ischemia/reperfusion injury in donation after cardiac death rat kidney transplantation,” *American Journal of Transplantation*, vol. 18, no. 4, pp. 843–854, 2018.
- [44] N. M. Rogers, M. Yao, E. M. Novelli, A. W. Thomson, D. D. Roberts, and J. S. Isenberg, “Activated CD47 regulates multiple vascular and stress responses: implications for acute kidney injury and its management,” *American Journal of Physiology. Renal Physiology*, vol. 303, no. 8, pp. F1117–F1125, 2012.
- [45] Y. Zhai, R. W. Busuttill, and J. W. Kupiec-Weglinski, “Liver ischemia and reperfusion injury: new insights into mechanisms of innate-adaptive immune-mediated tissue inflammation,” *American Journal of Transplantation*, vol. 11, no. 8, pp. 1563–1569, 2011.
- [46] T. Kaisho and S. Akira, “Dendritic-cell function in toll-like receptor- and MyD88-knockout mice,” *Trends in Immunology*, vol. 22, no. 2, pp. 78–83, 2001.
- [47] J. P. Armstrong, M. N. Holme, and M. M. Stevens, “Re-engineering extracellular vesicles as smart nanoscale therapeutics,” *ACS Nano*, vol. 11, no. 1, pp. 69–83, 2017, Epub 2017/01/10.
- [48] L. Han, J. Xu, Q. Xu, B. Zhang, E. W. Lam, and Y. Sun, “Extracellular vesicles in the tumor microenvironment: therapeutic resistance, clinical biomarkers, and targeting strategies,” *Medicinal Research Reviews*, vol. 37, no. 6, pp. 1318–1349, 2017, Epub 2017/06/07.